IAEA TECDOC SERIES

IAEA-TECDOC-1795

IAEA-TECDOC-1795

Volcanic Hazard Assessments for Nuclear Installations: Methods and Examples in Site Evaluation

IAEA
International Atomic Energy Agency

IAEA SAFETY STANDARDS AND RELATED PUBLICATIONS

IAEA SAFETY STANDARDS

Under the terms of Article III of its Statute, the IAEA is authorized to establish or adopt standards of safety for protection of health and minimization of danger to life and property, and to provide for the application of these standards.

The publications by means of which the IAEA establishes standards are issued in the **IAEA Safety Standards Series**. This series covers nuclear safety, radiation safety, transport safety and waste safety. The publication categories in the series are **Safety Fundamentals**, **Safety Requirements** and **Safety Guides**.

Information on the IAEA's safety standards programme is available on the IAEA Internet site

http://www-ns.iaea.org/standards/

The site provides the texts in English of published and draft safety standards. The texts of safety standards issued in Arabic, Chinese, French, Russian and Spanish, the IAEA Safety Glossary and a status report for safety standards under development are also available. For further information, please contact the IAEA at: Vienna International Centre, PO Box 100, 1400 Vienna, Austria.

All users of IAEA safety standards are invited to inform the IAEA of experience in their use (e.g. as a basis for national regulations, for safety reviews and for training courses) for the purpose of ensuring that they continue to meet users' needs. Information may be provided via the IAEA Internet site or by post, as above, or by email to Official.Mail@iaea.org.

RELATED PUBLICATIONS

The IAEA provides for the application of the standards and, under the terms of Articles III and VIII.C of its Statute, makes available and fosters the exchange of information relating to peaceful nuclear activities and serves as an intermediary among its Member States for this purpose.

Reports on safety in nuclear activities are issued as **Safety Reports**, which provide practical examples and detailed methods that can be used in support of the safety standards.

Other safety related IAEA publications are issued as **Emergency Preparedness and Response** publications, **Radiological Assessment Reports**, the International Nuclear Safety Group's **INSAG Reports**, **Technical Reports** and **TECDOCs**. The IAEA also issues reports on radiological accidents, training manuals and practical manuals, and other special safety related publications.

Security related publications are issued in the **IAEA Nuclear Security Series**.

The **IAEA Nuclear Energy Series** comprises informational publications to encourage and assist research on, and the development and practical application of, nuclear energy for peaceful purposes. It includes reports and guides on the status of and advances in technology, and on experience, good practices and practical examples in the areas of nuclear power, the nuclear fuel cycle, radioactive waste management and decommissioning.

VOLCANIC HAZARD ASSESSMENTS FOR NUCLEAR INSTALLATIONS: METHODS AND EXAMPLES IN SITE EVALUATION

The following States are Members of the International Atomic Energy Agency:

AFGHANISTAN
ALBANIA
ALGERIA
ANGOLA
ANTIGUA AND BARBUDA
ARGENTINA
ARMENIA
AUSTRALIA
AUSTRIA
AZERBAIJAN
BAHAMAS
BAHRAIN
BANGLADESH
BARBADOS
BELARUS
BELGIUM
BELIZE
BENIN
BOLIVIA, PLURINATIONAL STATE OF
BOSNIA AND HERZEGOVINA
BOTSWANA
BRAZIL
BRUNEI DARUSSALAM
BULGARIA
BURKINA FASO
BURUNDI
CAMBODIA
CAMEROON
CANADA
CENTRAL AFRICAN REPUBLIC
CHAD
CHILE
CHINA
COLOMBIA
CONGO
COSTA RICA
CÔTE D'IVOIRE
CROATIA
CUBA
CYPRUS
CZECH REPUBLIC
DEMOCRATIC REPUBLIC OF THE CONGO
DENMARK
DJIBOUTI
DOMINICA
DOMINICAN REPUBLIC
ECUADOR
EGYPT
EL SALVADOR
ERITREA
ESTONIA
ETHIOPIA
FIJI
FINLAND
FRANCE
GABON
GEORGIA
GERMANY
GHANA
GREECE
GUATEMALA
GUYANA
HAITI
HOLY SEE
HONDURAS
HUNGARY
ICELAND
INDIA
INDONESIA
IRAN, ISLAMIC REPUBLIC OF
IRAQ
IRELAND
ISRAEL
ITALY
JAMAICA
JAPAN
JORDAN
KAZAKHSTAN
KENYA
KOREA, REPUBLIC OF
KUWAIT
KYRGYZSTAN
LAO PEOPLE'S DEMOCRATIC REPUBLIC
LATVIA
LEBANON
LESOTHO
LIBERIA
LIBYA
LIECHTENSTEIN
LITHUANIA
LUXEMBOURG
MADAGASCAR
MALAWI
MALAYSIA
MALI
MALTA
MARSHALL ISLANDS
MAURITANIA
MAURITIUS
MEXICO
MONACO
MONGOLIA
MONTENEGRO
MOROCCO
MOZAMBIQUE
MYANMAR
NAMIBIA
NEPAL
NETHERLANDS
NEW ZEALAND
NICARAGUA
NIGER
NIGERIA
NORWAY
OMAN
PAKISTAN
PALAU
PANAMA
PAPUA NEW GUINEA
PARAGUAY
PERU
PHILIPPINES
POLAND
PORTUGAL
QATAR
REPUBLIC OF MOLDOVA
ROMANIA
RUSSIAN FEDERATION
RWANDA
SAN MARINO
SAUDI ARABIA
SENEGAL
SERBIA
SEYCHELLES
SIERRA LEONE
SINGAPORE
SLOVAKIA
SLOVENIA
SOUTH AFRICA
SPAIN
SRI LANKA
SUDAN
SWAZILAND
SWEDEN
SWITZERLAND
SYRIAN ARAB REPUBLIC
TAJIKISTAN
THAILAND
THE FORMER YUGOSLAV REPUBLIC OF MACEDONIA
TOGO
TRINIDAD AND TOBAGO
TUNISIA
TURKEY
TURKMENISTAN
UGANDA
UKRAINE
UNITED ARAB EMIRATES
UNITED KINGDOM OF GREAT BRITAIN AND NORTHERN IRELAND
UNITED REPUBLIC OF TANZANIA
UNITED STATES OF AMERICA
URUGUAY
UZBEKISTAN
VANUATU
VENEZUELA, BOLIVARIAN REPUBLIC OF
VIET NAM
YEMEN
ZAMBIA
ZIMBABWE

The Agency's Statute was approved on 23 October 1956 by the Conference on the Statute of the IAEA held at United Nations Headquarters, New York; it entered into force on 29 July 1957. The Headquarters of the Agency are situated in Vienna. Its principal objective is "to accelerate and enlarge the contribution of atomic energy to peace, health and prosperity throughout the world".

IAEA-TECDOC-1795

VOLCANIC HAZARD ASSESSMENTS FOR NUCLEAR INSTALLATIONS: METHODS AND EXAMPLES IN SITE EVALUATION

INTERNATIONAL ATOMIC ENERGY AGENCY
VIENNA, 2016

COPYRIGHT NOTICE

For further information on this publication, please contact:

International Seismic Safety Centre
International Atomic Energy Agency
Vienna International Centre
PO Box 100
1400 Vienna, Austria
Email: Official.Mail@iaea.org

Printed by the IAEA in Austria
July 2016

IAEA Library Cataloguing in Publication Data

Names: International Atomic Energy Agency.
Title: Volcanic hazard assessments for nuclear installations : methods and examples in site evaluation / International Atomic Energy Agency.
Description: Vienna : International Atomic Energy Agency, 2016. | Series: IAEA TECDOC series, ISSN 1011–4289 ; no. 1795 | Includes bibliographical references.
Identifiers: IAEAL 16-01050 | ISBN 978–92–0–104916–2 (paperback : alk. paper)
Subjects: LCSH: Nuclear facilities — Location. | Volcanic hazard analysis. | Nuclear power plants — Safety measures.

FOREWORD

To provide guidance on the protection of nuclear installations against the effects of volcanoes, the IAEA published in 2012 IAEA Safety Standards Series No. SSG-21, Volcanic Hazards in Site Evaluation for Nuclear Installations. SSG-21 addresses hazards relating to volcanic phenomena, and provides recommendations and general guidance for evaluation of these hazards. Unlike seismic hazard assessments, models for volcanic hazard assessment have not undergone decades of review, evaluation and testing for suitability in evaluating hazards at proposed nuclear installations. Currently in volcanology, scientific developments and detailed methodologies to model volcanic phenomena are evolving rapidly.

This publication provides information on detailed methodologies and examples in the application of volcanic hazard assessment to site evaluation for nuclear installations, thereby addressing the recommendations in SSG-21. Although SSG-21 develops a logical framework for conducting a volcanic hazard assessment, this publication demonstrates the practicability of evaluating the recommendations in SSG-21 through a systematic volcanic hazard assessment and examples from Member States. The results of this hazard assessment can be used to derive the appropriate design bases and operational considerations for specific nuclear installations.

The contributions of all those who were involved in the drafting and review of this report are greatly appreciated. The IAEA officer responsible for this publication was K. Watanabe of the Division of Nuclear Installation Safety.

EDITORIAL NOTE

This publication has been prepared from the original material as submitted by the contributors and has not been edited by the editorial staff of the IAEA. The views expressed remain the responsibility of the contributors and do not necessarily represent the views of the IAEA or its Member States.

Neither the IAEA nor its Member States assume any responsibility for consequences which may arise from the use of this publication. This publication does not address questions of responsibility, legal or otherwise, for acts or omissions on the part of any person.

The use of particular designations of countries or territories does not imply any judgement by the publisher, the IAEA, as to the legal status of such countries or territories, of their authorities and institutions or of the delimitation of their boundaries.

The mention of names of specific companies or products (whether or not indicated as registered) does not imply any intention to infringe proprietary rights, nor should it be construed as an endorsement or recommendation on the part of the IAEA.

The IAEA has no responsibility for the persistence or accuracy of URLs for external or third party Internet web sites referred to in this publication and does not guarantee that any content on such web sites is, or will remain, accurate or appropriate.

CONTENTS

1. INTRODUCTION

1.1. BACKGROUND

Approximately 25% of Member States have active volcanoes within their borders and many types of volcanic phenomena have regional effects, extending beyond national borders. Volcanic phenomena include lava flows and pyroclastic density currents that generally constitute site exclusion criteria and widespread phenomena such as tephra falls (i.e. volcanic ash) for which facility design or operational planning might practically mitigate potential hazards.

To provide guidance on protection of nuclear installations against such effects of volcanoes, the IAEA issued Specific Safety Guide No. SSG-21 entitled Volcanic Hazards in Site Evaluation for Nuclear Installations [1] in 2012, pertaining to the safety assessment of nuclear installations in respect of effects of volcanoes.

The SSG-21 addressed hazards relating to volcanic phenomena, and provided recommendations and general guidance for evaluation of these hazards. Unlike seismic hazards assessments, models for volcanic hazards assessment have not undergone decades of review, evaluation, and testing for suitability in evaluating hazards at proposed nuclear installations. Currently in volcanology, scientific developments and detailed methodologies to model volcanic phenomena are evolving rapidly. In addition, any single volcanic eruption can produce a variety of potentially hazardous phenomena, each of which represent complex thermo fluid dynamical processes that are challenging to model. Thus, an IAEA TECDOC is needed to support the practicable application of the requirements in SSG-21.

1.2. OBJECTIVE

The objective of this TECDOC is to provide information on detailed methodologies and examples in the application of volcanic hazard assessment to site evaluation for nuclear installations, thereby addressing the recomendations in SSG-21. Although SSG-21 develops a logical framework for conducting a volcanic hazards assessment, this TECDOC demonstrates the practicability of evaluating the requirements in SSG-21 through a systematic volcanic hazards assessment. The results of this hazard assessment can be used to derive the appropriate design bases and operational considerations for specific nuclear installations. Although detailed design bases for specific installations are not presented in this TECDOC, perspectives are provided on typical installation design capacities.

1.3. SCOPE

The scope of this TECDOC follows the framework for volcanic hazards assessment established in SSG-21. In addition to developing approaches for collecting needed data and assessing volcanic hazards, the TECDOC outlines specific considerations for the siting, design, and operation of nuclear installations. A comprehensive range of volcanic hazards is presented in the TECDOC, which represent phenomena ranging from small volume tephra falls and gas emissions, to large volume pyroclastic eruptions and lava flows. Potential volcanic hazards that can be associated directly or indirectly with a volcanic eruption, such as sector collapse or hydrothermal activity, also are included in this TECDOC.

In addition to the assessment of potentially hazardous phenomena, a section is devoted to a discussion of volcano monitoring. This section is needed because volcano monitoring (as

recommended in SSG-21) is a relatively new concept for assuring the safety of nuclear installations. There are many practical aspects that need to be considered in developing an appropriate monitoring network, if warranted by the conclusions of the hazards assessment.

1.4. STRUCTURE

Section 2 explains the details of a staged approach to the volcanic hazards assessment, such as initial scoping, characterizing volcanic sources and hazard screening. This section uses examples from the Armenian nuclear power plant (ANPP) and other areas, which take into consideration cyclical volcanic activity in different time frames. In addition to the collection of data needed to develop hazards models, Section 3 also discusses the development of a tectono magmatic model to explain the occurrence of volcanic activity, based on local and regional scale geologic and tectonic data. Section 4 presents different approaches to evaluate recurrence rates, including data requirements, calculation methods, and statistical models. Specific examples from volcanic systems in Member States also are provided in this section.

The bulk of the TECDOC is contained in Section 5, which provides evaluation methodologies for the potentially hazardous volcanic phenomena identified in the SSG-21. For each phenomenon, individual sections present an overview of currently available approaches for the evaluation of future hazards, along with examples of hazard assessments that use these approaches. These approaches generally represent a range of model complexities, from simplified physics based conceptual models to highly coupled thermo fluid dynamical approaches. Each of these models depends on input derived from detailed volcanological investigations, such as mapping and stratigraphic correlations discussed in Section 3. In addition, important considerations are identified for the siting, design, and operation of a potential nuclear installation with regards to decisions involving these phenomena. Section 6 presents important considerations for volcano monitoring, such as monitoring types and examples of monitoring used for volcanic hazards forecasting. Concluding remarks are presented in Section 7.

2. STAGED APPROACH

2.1. GENERAL

The SSG-21 [1] recommend a staged approach be taken to the volcanic hazard assessment of any nuclear power plant (NPP) site, with increasing amounts of data and modelling required with increased potential for volcanic hazards. This staged approach is represented schematically in FIG. 1, the volcanic hazard assessment for a site is composed of four stages, with each stage providing more detailed geological information. The information collected over the four stages is accumulated in a database. This data set is used to identify capable volcanoes within the geographic area of interest around the proposed site [1]. A capable volcano or volcano group is one for which both: (i) there is a credible likelihood of a future eruption or other volcano related event (e.g. slope failure on a volcano) (See FIG. 1), and (ii) has the potential to produce volcanic phenomena that may affect the site. A credible likelihood of future volcanic events is one where there is: (i) evidence of current activity; (ii) activity in the Holocene; or (iii) an assessment that indicates recurrence $>10^{-7}$/year or determines that volcanic activity in the past 10 million year is consistent with the current geologic setting of the site. The concept of volcano credibility is discussed further in Section 3.

A comprehensive volcanic hazard assessment is required for capable volcanoes for those phenomena that may impact the site. The purpose of this section is describing the general steps required to identify capable volcanoes in the site geographic region. The methodology for comprehensive volcanic hazard assessment is presented in subsequent sections.

2.2. STAGE 1: INITIAL SCOPING

Stage 1 of the assessment is primarily concerned with defining the geographic region of interest within which sources of volcanic hazards will be assessed, and the collection of evidence for the occurrence of volcanism in the region within the last 10 million year [1]. The geographic region of interest is defined to include all volcanic features that may potentially produce phenomena that may impact the NPP site, including distal volcanic phenomena such as tephra fallout. Stage 1 analyses are completed using scientific literature and field investigations of volcanoes in the region as needed, and are documented using regional scale maps.

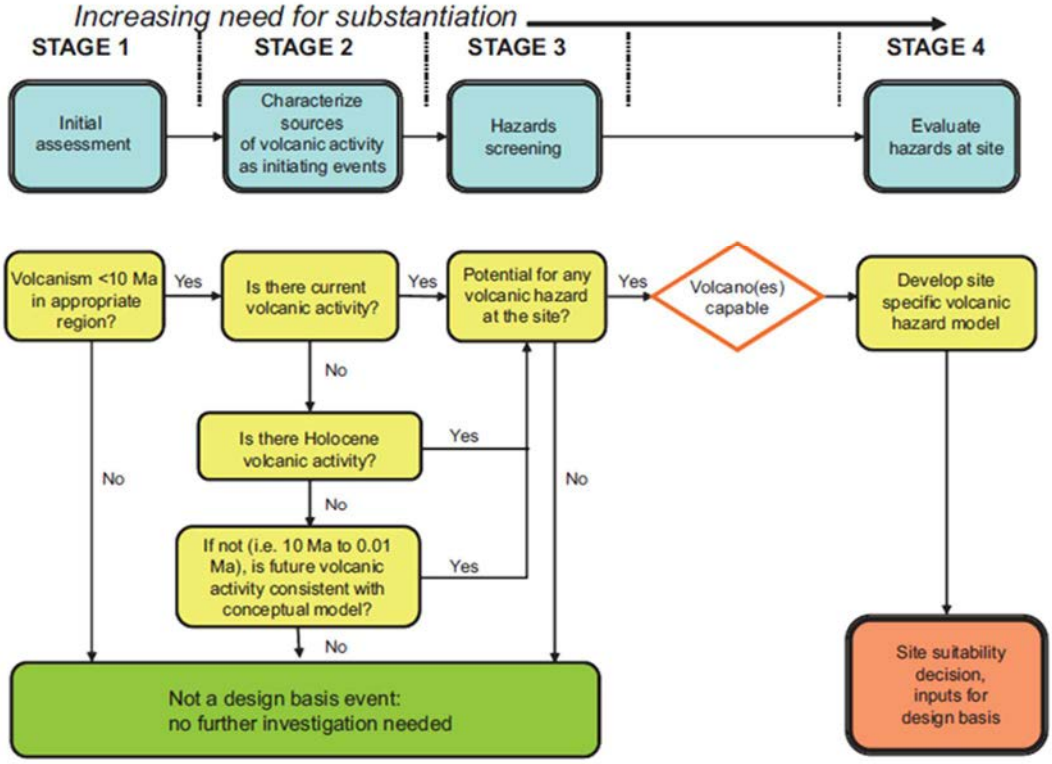

FIG. 1. Staged approach to volcanic hazard assessment recommended by SSG-21 [1]. Also see McBirney and Godoy [2]. This hazard assessment follows the staged approach in defining volcano capability.

Selection of the geographic region of interest depends on the potential areal extent of volcanic phenomena that may affect the site. The geographic region of interest is usually a circular area extending at least 300 km from the site boundary. A distance of 300 km is used because there are documented cases of hazardous volcanic phenomena extending 300 km from source volcanoes. These phenomena include tephra fallout, pyroclastic density currents and associated lahars, and very long lava flows. It is noted, however, that the geographic region of interest need not be symmetric or of predetermined size, but should reflect the tectonic setting and volcanic history of the region. For example, the Sumatra and Java volcanic arcs are characterized by infrequent, extremely violent volcanic eruptions [3]. Such eruptions result in substantial tephra fallout, even 1000 km from the volcano [4]. The geographic region of interest for sites in Southeast Asia might need to extend one thousand kilometres from the site to account for the capability of such volcanic systems. Similarly, eruptions in Japan and southern Europe, such as those associated with Aso caldera [5], the Campi Flegrei volcanic field [6], [7], and Santorini volcano [8], [9] have resulted in substantial tephra fallout at great distances from the caldera. Conversely, in some volcanic regions, a 300 km radius for the geographic region of interest might be adequate.

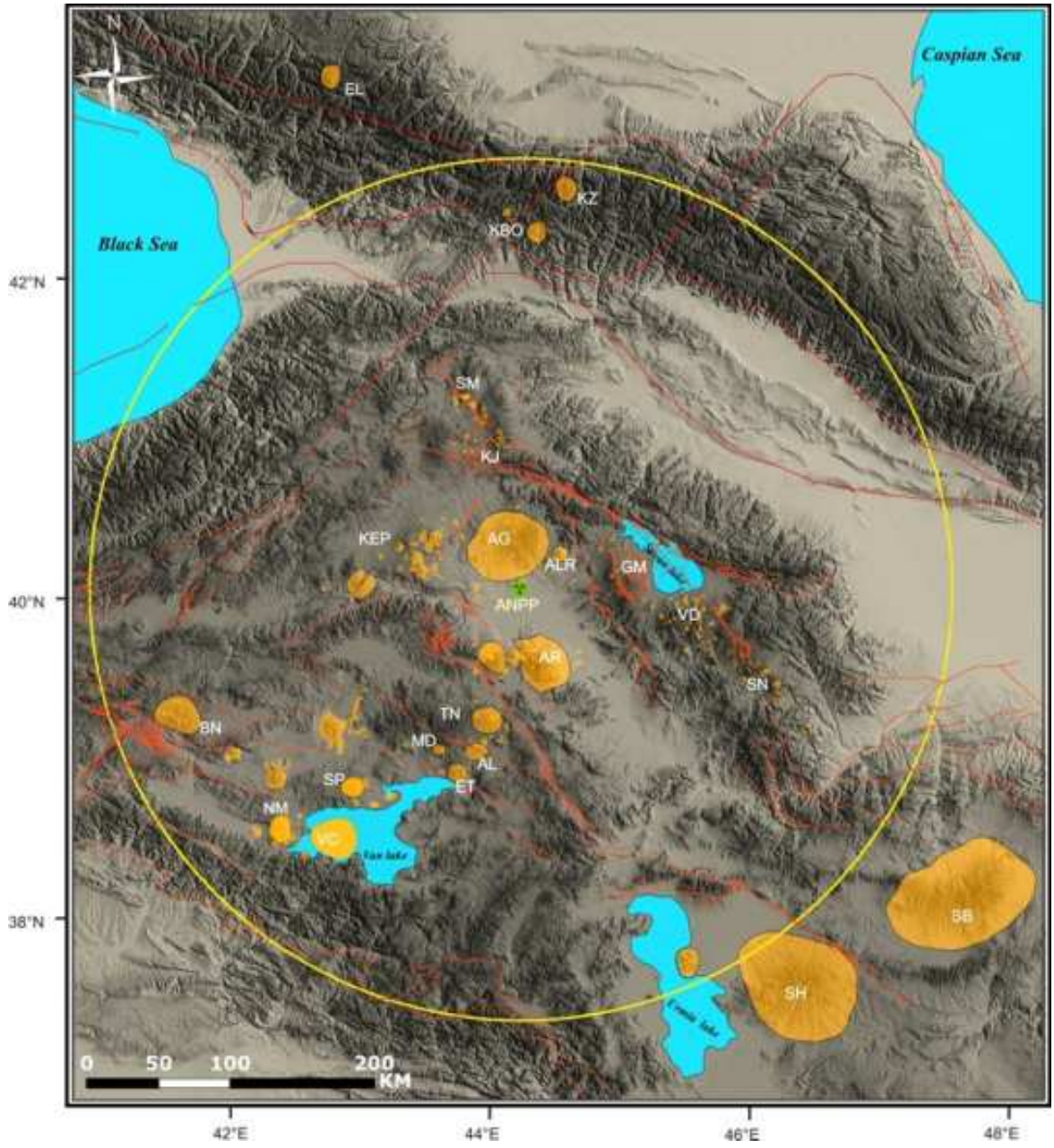

FIG. 2. Distribution and tectonic setting of Quaternary volcanoes within a 300 km zone around the ANPP. Map key: Aragats (AG), Aladag (AL), Arailer (ALR), Ararat (AR), Bingol (BN), Elbrus (EL), Etrusk (ET), Gegham volcanic highland (GM), Kabargin Oth group (KBO), Kars-Erzerum volcanic plateau (KEP), Kechut-Javakhk volcanic plateau (KJ), Kazbek (KZ), Meydan Dag (MD), Nemrut (NM), Sabalan (SB), Sahand (SH), Samsari volcanic field (SM), Syunik volcanic highland (SN), Süphan caldera (SP), Tondrak/Tendurek (TN), Vardenis volcanic highland (VD), Van caldera (VC). Such maps are used in Stage 1 analyses to determine if potential volcanic centres represent sources of credible hazards to facilities located at the site. Reproduced courtesy of the Ministry of Energy and Natural Resources of the Republic of Armenia [10].

An example of a geographic region, FIG. 2 shows the distribution and tectonic setting of all Quaternary volcanoes within a 300 km zone around the ANPP site of a proposed nuclear installation in Armenia. This example is developed to illustrate the initial scoping methodology for the remainder of Section 2.2, based on the hazard study of Connor et al. [10]. The geographic region includes volcanoes and volcanic fields in Armenia, Turkey, Iran, Georgia and Russia/Georgia border (Holocene volcanoes of Great Caucasus ridge). The geographic region includes areas east of the city of Yerevan (the Gegham ridge) and some volcanic centres in Turkey (e.g. Kars plateau, Tendürek, Ararat). That is, the area of geographical interest transcends political boundaries. In the case illustrated, much of the entire region includes volcanoes active in the Quaternary, with some evidence of Holocene volcanic activity at some centres. Thus, this map is a critical document used to assess whether potential volcanic events represent credible hazards to safe operation of the NPP site.

If no volcanoes or volcanic fields younger than 10 Ma are located within the geographic region of interest, then no further investigations are required. That is, potential volcanic events do not represent credible hazards to safe operation of the NPP site. In such cases it is simply necessary to document the data used to make this assessment.

Conversely, if volcanoes or volcanic fields are identified within the region of interest, then Stage 1 efforts require a simple volcanological description of these features. For example, the following description summarizes a Stage 1 analysis conducted for the recognized volcanic centres in Armenia (See FIG. 2).

The closest volcanoes to the ANPP site are volcanoes of the Shamiram plateau, which is located at the southern base of Aragats volcano (See FIG. 2). Geological mapping [11] include at least eight Quaternary monogenetic volcanic centres and 18 vents. All of these volcanoes are located within 10 km of the ANPP site. The occurrence of Quaternary monogenetic volcanoes within the geographic region of interest indicates that further assessment of volcanic hazards is necessary.

The 4090 m summit of Aragats volcano is ≈37 km from the ANPP site (See FIG. 2). Aragats volcano is the source of voluminous Quaternary volcanic products including numerous adventive cones that occur on its flanks, long lava flows, and Quaternary ignimbrites. Although the Smithsonian Institution Global Volcanism Program database lists Aragats as a Holocene volcano, there is no evidence of post glacial volcanic activity on Aragats, and all of the deposits above approximately 3000 m on the volcano have been glaciated. Nevertheless, this Quaternary volcanic system is long lived and the potential for future eruptions cannot be ruled out.

Several volcanoes, volcano alignments, and potential volcanic features are located south and west of the ANPP site within the Yerevan basin. One of these centres is of unknown origin but is potentially a volcanic explosion crater, although pyroclastic deposits have not been identified around the crater margins. Nevertheless, this unconfirmed centre is considered as representative of a potential source of volcanic activity in the site area for the purposes of the volcanic hazard analysis.

All of these volcanic systems represent potential sources of distal and proximal volcanic phenomena. Distal volcanic phenomena include tephra fallout and long run out pyroclastic density currents and related phenomena such as lahars. Proximal phenomena include lava flows, pyroclastic density currents and a range of associated phenomena [1].

In addition to these potential sources of activity there are several additional, more distant volcanoes in the region that warrant consideration for Stage 1 analyses (See FIG. 2). Ararat volcano is a Holocene volcano complex located approximately 55 km southeast of the ANPP site. Ararat is a very large composite volcano, reaching 5100 m in height, and located at the north eastern end of a chain of older composite volcanoes and adventive cinder cones and domes, extending from Nemrut volcano on the north shore of Lake Van (Turkey). Although Ararat volcano is too distant from the ANPP site to present proximal hazards, potential impacts could occur from tephra fallout and from very long run out volcanic debris avalanches from this volcano. Little Ararat volcano is an only slightly smaller composite volcano located on the flanks of Ararat, which has also erupted in the Quaternary and is a potential source of tephra fallout at the site.

The Kars plateau of Eastern Turkey is another potential source of distal volcanic phenomena at the ANPP site. The Kars plateau is a complex of voluminous ignimbrite deposits, cinder cones and domes that lie approximately 70 km west of the ANPP site. As with Ararat volcano, the volcanic centres of the Kars plateau are too far from the site to produce proximal volcanic phenomena with potential to impact the site. Nevertheless, the potential exists for impacts from distal volcanic phenomena, particularly tephra fallout, associated with eruptions of the Kars plateau.

The Gegham ridge is located east of Yerevan and is approximately 70 km from the ANPP site (See FIG. 2). This volcano complex includes numerous Quaternary monogenetic volcanoes. Although some of the volcanic eruptions of the Gegham ridge were energetic, these volcanoes are located too far from the ANPP site to be a significant source of hazard, given the lack of evidence of past voluminous eruptions in this area. Nevertheless, there is potential for tephra fallout from eruptions on the Gegham ridge.

Therefore, it is clear from initial scoping that there are moderately recently active volcanoes in the ANPP region. The geographic region of interest is defined based on the nature of Quaternary volcanism in the region, summarized as follows:

- Volcanoes of the Shamiram plateau are Quaternary in age and the potential for future volcanic activity within this cluster cannot be ruled out. Such volcanic activity might potentially produce proximal volcanic hazards at the ANPP site, including phenomena associated with the opening of new vents, such as volcanic ballistic projectiles and lava flows.

- Aragats volcano also might potentially produce proximal volcanic phenomena that may impact the ANPP site, largely because the site is located near the topographic base of this large volcano complex.

- Monogenetic volcanism is prevalent elsewhere in the Yerevan basin, such as in the areas of Sardarapat and Taqavoranist. Although these volcanoes do not themselves produce volcanic phenomena that may impact the site, they do provide further evidence of the potential for the opening of new vents in the ANPP site vicinity.

- Other volcanic centres might produce some distal volcanic phenomena, especially tephra fallout, which potentially could impact the site. These volcanic centres are the Ararat volcano complex (including Little Ararat), Tendürek volcano, Gegham Ridge, and the Kars plateau.

Therefore, it is clear from initial scoping (Stage 1) that potential sources of volcanic activity exist in the region of the ANPP site.

For the Armenian example, the information presented is sufficient to indicate that the volcanic hazard assessment should proceed to Stage 2. Note that the level of description in this examples based on maps and data that were available in the scientific literature. Site specific data are generally not required for Stage 1 assessments, although these data might be needed for some locations with sparse information on the age and character of Quaternary or older volcanic activity. Additionally, a basic understanding of volcanology is sufficient to recognize that scoria cones on the Shamiram Plateau are located sufficiently close to the site, such that future lava flows and tephra fall might create hazards. In contrast, similar scoria cone volcanoes on the Kars Plateau are located too far from the site to create potential lava flow or tephra fall hazards.

2.3. STAGE 2: VOLCANIC HAZARDS SOURCES - CHARACTERIZATION

Stage 2 of IAEA guidelines [1] is concerned with characterization of potentially active volcanoes. The primary issue is whether volcanoes within the geographic region of interest discussed in Stage 1 are potentially volcanically active in the future, and on what time scales, or with what probability. Stage 2 focuses on understanding the age of past events, because this information often can be derived from existing studies or focused short term investigations. Based on the past patterns of activity, a reasonable projection can be made about the potential for future activity from the volcanic systems of interest.

Evidence of a credible potential for future activity within the geographic region of interest includes evidence of Holocene volcanic eruptions or current manifestations of volcanic activity (i.e. FIG. 1). Returning to the Armenian example, Ararat (See FIG. 3) is one of the most recently active volcanic systems in the geographic region around the ANPP site. Radiometric age determinations of the products of eruptions of Ararat show a range of eruption ages across the entire Quaternary, with dates reported to be as young as 20 ka [12], with much of late stage activity resulting in formation of adventive cones and domes. Karakhanian et al. [13] and Karakhanian et al. [14] recognize even younger volcanic events on Ararat. Ararat appears to have been active during 4500–4400 BP, as pyroclastic flow deposits overlie early Bronze Age artefacts and human remains. Karakhanian et al. [14] describe eyewitness accounts of incandescent clouds accompanying the destruction of Akory Village following the July 1840 tectonic earthquake. Although there is apparently some disagreement about details of these events [15], available data suggest that Ararat experienced Holocene activity and, thus, should be considered a potential source of future volcanic activity within the geographic region of interest about the Armenian nuclear facility.

FIG. 3. Photo of Ararat volcano (background) and monogenetic volcanoes of the Sardarapat area (foreground). View looking SE from vicinity of ANPP. Reproduced courtesy of the Ministry of Energy and Natural Resources of the Republic of Armenia [10].

In addition to recent or Holocene activity, a volcanic system with evidence of Quaternary activity (i.e. in the last 2.6 million year) should be considered at this stage of the hazards assessment as a potential source of future activity [1]. Complex volcanic systems can have gaps in eruptive activity that commonly exceed 10 000 year, thus, an absence of activity during the last 10 000 year (i.e. during the Holocene) is not a robust indicator of a negligible potential for future activity. During the Stage 2 analysis, complete or accurate information typically is not available for the physical and temporal characteristics of complex Quaternary volcanic systems. Although additional, detailed investigations might demonstrate that a Quaternary system is unlikely to create future hazards for the proposed site, these investigations typically are conducted at Stage 4 of the analysis. Thus, evidence of Quaternary volcanic activity should be considered sufficient in Stage 2 analyses to move the hazards analysis forward to the evaluation of potential for hazards to reach the site (i.e. Stage 3).

Using the ANPP site as an example of the types of evaluations used for characterizing Quaternary volcanic activity in Stage 2 analyses, the Shamiram plateau volcanoes form a cluster of monogenetic centres immediately north of the ANPP site (See FIG. 4 and FIG. 5). Three different samples from this group have been previously dated by the University of Bern with a range of 0.76–0.96 Ma [16], [17], although samples analysed by Chernyshev et al. [18] yielded ages of 0.35–0.56 Ma [16]. Recent Ar/Ar age determinations in Connor et al. [10] confirm that most of the Shamiram eruptions occurred before the eruption of the overlying Yerevan Tuff at approximately 0.65 Ma. Lavas of the Dashtakar scoria cones overlie the Yerevan Tuff, but have radiometric ages that are indistinguishable from the age of the Yerevan Tuff [10]. Based on the apparent young geologic age and the proximity of the Shamiram Plateau volcanoes to the ANPP site, it has been previously concluded that these volcanoes are potential sources of future volcanic activity [16], [17], [19].

Additional monogenetic volcanoes also are located in the Yerevan basin south and west of the ANPP site. Radiometric age determinations have confirmed that these volcanoes are Quaternary in age [10]. Greako cinder cone is part of this group and new Ar/Ar age determinations indicate it erupted at 1.32±0.07 Ma. Sardarapat ridge lava in the same area has been dated (Ar/Ar) as 0.902±0.021 Ma. The Quaternary ages of these volcanoes suggest that future volcanic activity related to the opening of new vents should be considered in the detailed hazard assessments (Stages 3 and 4).

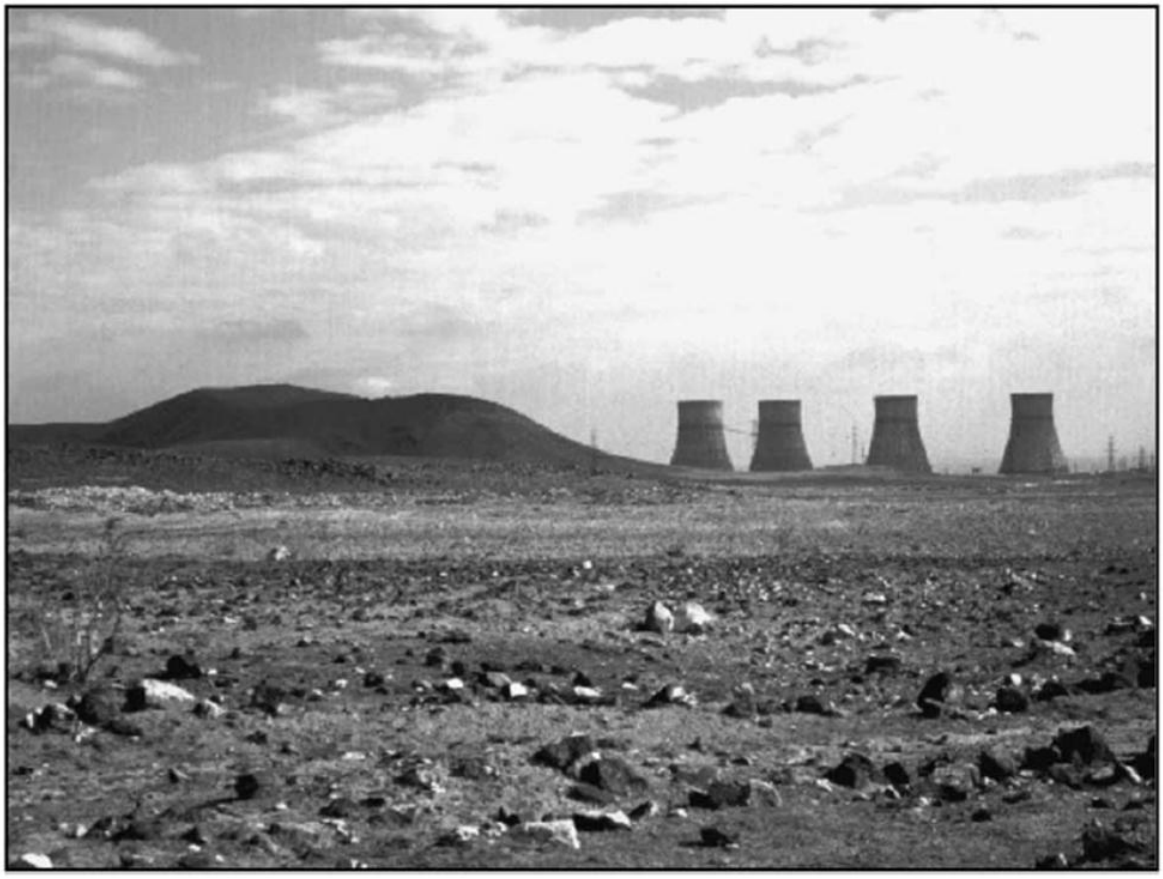

FIG. 4. Atomakhumb cinder cone, with cooling towers for the ANPP site located approximately 1 km in the background. Towers are founded on lava flows from Shamiram Plateau scoria cones. Reproduced courtesy of the Ministry of Energy and Natural Resources of the Republic of Armenia [10].

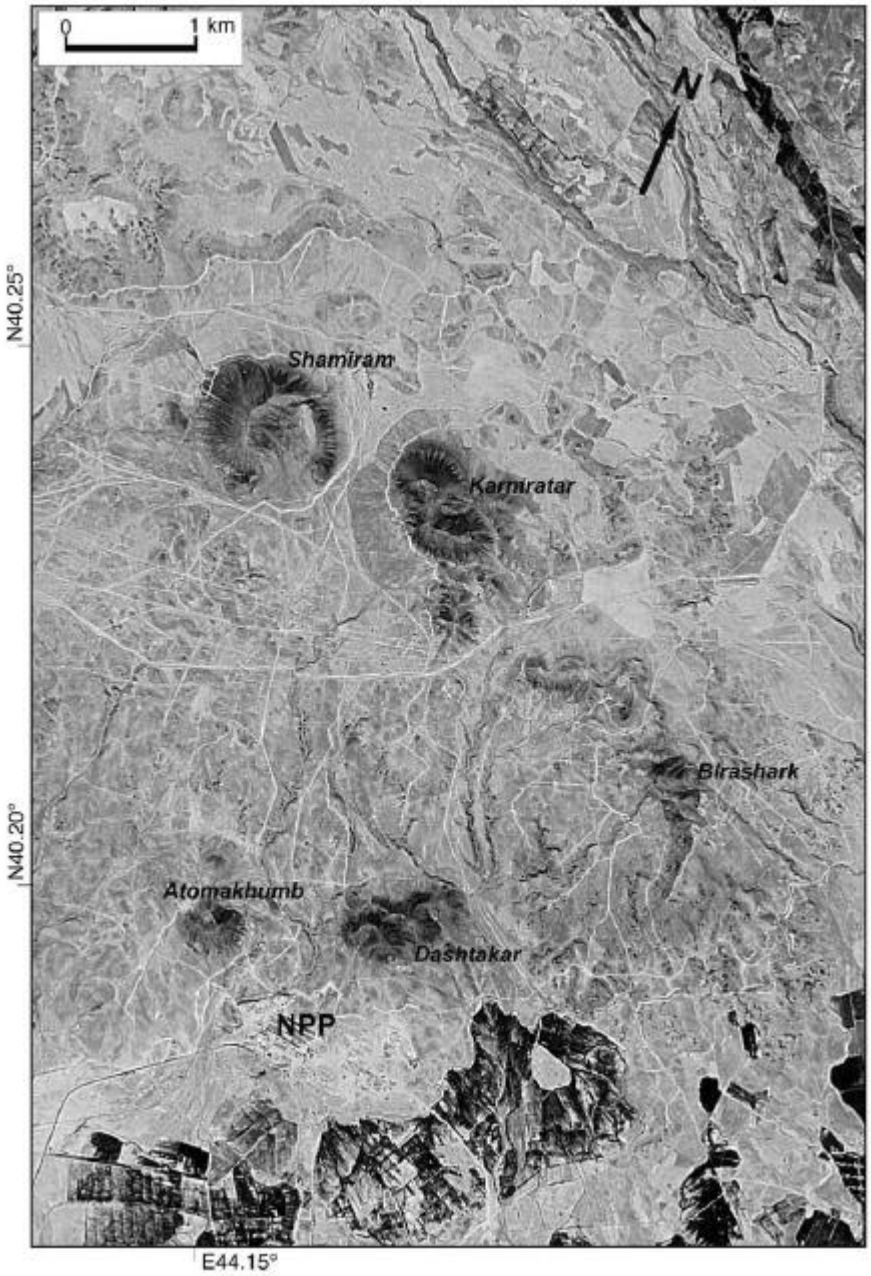

FIG. 5. Satellite image (Corona mission) of volcanic centers on the Shamiram plateau and their relationship to the ANPP site. The image is originally from open source of National Aeronautics and Space Administration.

Aragats volcano was constructed by a tremendous volume of volcanic activity during the late Pliocene and Quaternary [20]. The Ashtarak lava flow, a geomorphologically young lava on the southeast flank of Aragats volcano, was dated as 0.53±0.07 Ma [18]. The Tirinkatar lava flow on the south flank of Aragats was dated radiometrically at the University of Bern, Switzerland [17] at 0.87±0.09 Ma to 0.91±0.03 Ma [21], although other dates have yielded younger ages, comparable to the Ashtarak flow [18]. More recent Ar/Ar age determinations essentially confirm these earlier age determinations. An Ar/Ar age determination on the Tirinkatar lava flow yields an age estimate of 0.614±0.019 Ma [10]. The areally extensive Yerevan tuff is stratigraphically immediately beneath the Tirinkatar lava flow. Two Ar/Ar age determinations on the Yerevan Tuff yield ages of 0.66±0.04 Ma and 0.65±0.04 Ma [10]. Ar/Ar

age determinations on Irind volcano yield an age of 0.49±0.03 Ma and on the Pokr Bogutlu lava of 0.75±0.03 Ma [10]. Although there is an absence of historical or activity younger than 10 ka at Aragats volcano, the extensive record of Quaternary volcanism indicates that Aragats volcano also should be assessed in detail for specific volcanic hazards at the ANPP site (i.e. See FIG. 1).

Within the geographic region of interest for the ANPP site, the Kars plateau includes numerous domes and cones, and regionally extensive ignimbrites thought to have formed 2.5–5 Ma [22]. These deposits include the 3.5 Ma Aladag formation, which is a voluminous ignimbrite sheet extending to the Turkey-Armenia border [22]. Many of the volcanic features of the Kars plateau are not dated directly and have poor geomorphic and stratigraphic age constraints. Nevertheless, some of these volcanic features post date the eruption of the regionally extensive ignimbrites. Thus, the Kars plateau should be included as a source of potential eruptions that might reach the ANPP site.

There is additional evidence that future volcanism is possible in the region around the ANPP site. Karakhanian et al. [13] note numerous examples of Late Pleistocene–Holocene volcanoes in eastern Armenia and the Gegham Ridge region, 50–150 km from the ANPP site. Yilmaz et al. [12] describe historical eruptions of Nemrut, and possible Holocene activity at other volcanoes (Süphan caldera, Tendürek volcano) north of Lake Van, 100–250 km from the ANPP site. Although these volcanoes are too far from the ANPP site to be a source of proximal or significant distal hazardous phenomena, they do indicate that active volcanism continues in the region today, albeit at a very low rate of activity compared with active arcs. This information is relevant to the development of the geologic model for volcanism, which is discussed in Section 3 of this report.

For the ANPP example, the Stage 2 analyses show that volcanoes in the geographic region of interest have the potential for future volcanic activity. These potential sources of future activity include:

- Opening of new vents on the Shamiram plateau or elsewhere in the Yerevan basin, potentially producing proximal volcanic hazards at the ANPP site;
- Reactivation of Aragats volcano, possibly resulting in proximal volcanic hazards at the ANPP site;
- Reactivation of Ararat and/or Little Ararat volcanoes, resulting in potential distal volcanic hazards at the site;
- Reactivation of Tendürek volcano, resulting in potential distal hazards at the site;
- Reactivation of the Kars plateau, resulting in potential distal hazards at the site.

Note that the ANPP example concludes there is some unquantified potential for future activity to occur at each of the volcanic systems identified in Stage 1 analyses. In essence, there is no technical basis available to preclude consideration of future eruptions from these volcanoes. Nevertheless, at this stage of the hazards analysis, there typically is insufficient information to accurately quantify this potential for future hazards. Detailed field, laboratory, and other investigations are necessary before this potential can be accurately quantified. It is sufficient to conclude in the Stage 2 analyses that the potential for future activity from these volcanoes exists, and that the hazards analysis should proceed to Stage 3 for those volcanoes with this potential.

2.4. STAGE 3: HAZARD SCREENING

In the event that future volcanic events within the geographic region about the site are found in Stage 2 to be possible, the analysis proceeds to Stage 3. The goal of Stage 3 is to determine if volcanic hazards associated with possible eruptions from sources identified in Stage 2 represent a potential threat to site suitability or design. As a result of Stage 3 analyses, specific types of phenomena, such as pyroclastic density currents or lava flows, might be screened from further consideration due to the distance of the volcanic source from the site, the topography of the site region, and similar considerations.

The screening distance is an extremely useful concept for determining in Stage 3 if there is a potential for specific volcanic phenomena to reach the site. The screening distance refers to the distance from a volcano beyond which a specific phenomenon will have negligible impact. In general screening distance values are set according to the maximum known run out distances of specific phenomenon, either in general or considering the types of phenomena that occur from a volcanic system. Specific values for screening distances are quite variable, and depend on the phenomena under consideration. For example, for volcanic ballistic projectiles, screening distances on order 10 km are typical. Screening distance values for tephra fallout might be 500–1000 km.

Estimation of screening distance values does not need to include detailed numerical modelling or consideration of site specific topography, wind field, or related site features. If such considerations are warranted, the analysis should proceed to a site specific hazard assessment in Stage 4. Nevertheless, with appropriate documentation, screening distance analyses can provide a technical basis that is sufficient to demonstrate a proposed site is unacceptably close to a potentially active volcano, or that some potentially hazardous phenomena are not capable of reaching the proposed site. In many regulatory frameworks, the level of information needed to support detailed analyses (i.e. Stage 4) is significantly less than the level of information needed to screen a potential hazard from further consideration. Some phenomena clearly can be excluded with basic volcanological information (e.g. ignimbrite eruptions from scoria cones). In contrast, a screening distance value that precludes further consideration of a phenomenon but does not account for uncertainties in the geologic record or available information appears difficult to support.

Returning to the ANPP example, Stage 2 analyses showed future volcanic activity appears to be possible within the geographic region about the ANPP site, and the potential for hazardous phenomena to impact the site should be assessed. In the case of the ANPP site, the most straightforward approach is to characterize the products of Quaternary volcanic eruptions that are found at the site itself. The occurrence of these products indicates that the site is within the screening distance for most volcanic phenomena, and a detailed hazard assessment is

warranted. In the ANPP site case, geological investigations indicate these products are from volcanic eruptions on the Shamiram plateau and from Aragats volcano.

Opening of new vents is generally considered probabilistically. A screening distance value, however, is useful for determining if there is a credible potential for new vents to form at relatively great distances from the existing distribution of vents. In many areas, vents cluster, either near composite volcano or caldera, or within volcanic fields. Often the spacing of vents in such environments is < 10 km, but in rare cases can be much more. Care should be taken to ensure tectonic features that might localize magmatism are accounted for appropriately in the screening analysis for new vents.

In the case of the ANPP site, the site is located close to Quaternary monogenetic volcanoes of the Shamiram plateau and the Yerevan basin. Volcanoes of the Shamiram plateau are distributed over an area ≈100 km^2 and the ANPP site is at the southern edge of this dense cluster of volcanoes. Therefore it appears possible that future eruptions of the Shamiram plateau will directly disrupt the site, and the probability of such events must be evaluated. Monogenetic volcanoes are also widely distributed over an area: 1000 km^2 throughout the Yerevan basin (See FIG. 6). These volcanoes are largely of Early to Middle Pleistocene age. Thus, the distribution and ages of these volcanoes also make it possible that new vents may open in the ANPP site area, or potentially at the site itself. Using a screening distance value of 30 km, both activities associated with the Shamiram Plateau and the Yerevan Basin has a potential for impacting the site.

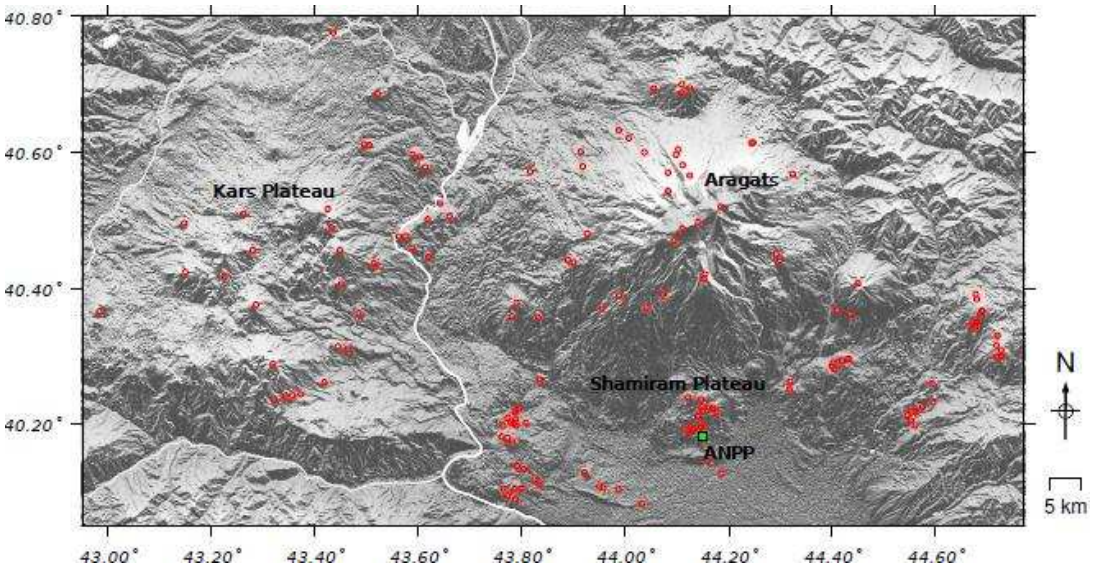

FIG. 6. Quaternary volcanic vents located in the ANPP region (open red circles). Reproduced courtesy of the Ministry of Energy and Natural Resources of the Republic of Armenia [10].

TABLE 1. POTENTIAL SOURCE AREAS AND SCREENING DISTANCES FOR HAZARDOUS VOLCANIC PHENOMENA AT THE ANPP SITE. Reproduced with courtesy of the Ministry of Energy and Natural Resources of the Republic of Armenia [10]

Volcanic phenomena	Potential source(s)	Screening dist. (km)	Evidence
Opening of new vents	Shamiram plateau, Yerevan basin	30	Close proximity of the ANPP site to Quaternary volcanoes of the Shamiram plateau (1.5–8 km) and the Yerevan basin (5–30 km)
Pyroclastic density currents	Aragats volcano, Shamiram plateau, Yerevan basin	50	Occurrence of Yerevan tuff (source Aragats) at the ANPP site; occurrence of other moderately large ignimbrites on Aragats; possibility of surges associated with opening of new vents
Tephra fallout	Shamiram plateau, Aragats volcano, Ararat volcano, Kars plateau	300	Tephra fallout deposit found in borehole at site and in nearby outcrops stratigraphically beneath Yerevan tuff; tephra fallout facies associated with monogenetic centres; thick (>10 m) tephra fallout at east margin of Kars plateau.
Volcano generated missiles	Shamiram plateau, Yerevan basin	10	Pyroclastic cones on the Shamiram plateau and in the Yerevan basin; potential for violent strombolian, vulcanian, and phreatomagmatic eruptions.
Lava flows and domes	Shamiram plateau, Aragats volcano	30	Occurrence of lava flows from Dashtakar and Atomakhumb volcanoes in the site vicinity; occurrence of lavas in borehole at the ANPP site; Occurrence of long lava flows on the flanks of Aragats volcano.
Debris avalanches and sector collapse	Ararat volcano	60	High relief of Ararat edifice; historical accounts of slope instability and magmatism (?) following 1840 tectonic earthquake.
Atmospheric phenomena	Shamiram plateau and Yerevan basin	80	Potential for eruption column to ground lightning strikes during opening of new vents.
Volcanic gases, hydrothermal systems, and ground deformation	Shamiram plateau and Yerevan basin	5	Potential for development of hydrothermal systems, gas emissions, and ground deformation associated with the opening of new vents.
Laharic flows	Aragats volcano	30	Potential for development of debris flows owing a large explosive eruption of Aragats or Ararat, which would produce voluminous tephra fallout or pyroclastic flows.
Volcanic earthquakes and seismic events	Shamiram plateau, Yerevan basin, Aragats volcano	30	Volcanic earthquakes may accompany for opening of new vents or reactivation of Aragats volcano.

Note: the screening distance is variable and different screening distance values should be formulated for different sites.

Pyroclastic density currents (sometimes referred to as pyroclastic flows) and surges may move considerable distances down topographic slopes and inundate the region surrounding volcanoes. A screening distance value of 30–50 km is typical (i.e. TABLE 1). In the case of the ANPP, pyroclastic flows (ignimbrites) are mapped on the Shamiram plateau adjacent to the site and these units are found at shallow depths (< 50 m) in borehole core taken at the site. Pyroclastic units include the Yerevan tuff, a low aspect ratio ignimbrite, which erupted from a source near the present summit of Aragats volcano and inundated an area of 650 km^2, including the ANPP site. This pyroclastic flow is mapped near the tops of several monogenetic volcanoes on the Shamiram plateau, indicating that the flow maintained considerable kinetic energy when it reached the site vicinity. Thus, the ANPP site is within the screening distance from pyroclastic flows associated with the reactivation of Aragats volcano. In addition, pyroclastic flows have erupted from flank vents on Aragats volcano. The most spectacular example is Irind volcano, where near vent Plinian tephra fallout deposits are capped directly by welded pyroclastic flow deposits. In addition, the low lying areas south of the ANPP site are swampy, and thus there is a potential for pyroclastic surges in these areas associated with phreatomagmatic eruptions. Although the area around Echmiadzin Crater is highly disturbed by human activity, it is possible that this crater formed as a result of phreatomagmatic eruptions [10], [17]. Therefore the ANPP site lies within the screening distance for pyroclastic flows and surges associated with eruptions of Aragats volcano and the opening of new vents on the Shamiram plateau and the Yerevan basin.

Tephra fallout may reach 100s to 1000s of kilometres downwind from an erupting volcano, depending on the energy of the eruption, its volume, and the nature of the wind field in the region. There are numerous potential sources for tephra fallout in the geographic region about the ANPP site (See FIG. 2). Thick accumulation of tephra at the site is possible if paroxysmal eruptions occur at Aragats volcano. A thick tephra deposit is found in the ANPP site borehole immediately beneath the Yerevan tuff, attesting to the possibility of Plinian tephra fallout from Aragats volcano. Monogenetic volcanoes on the flanks of Aragats and on the Shamiram plateau may have also produced substantial tephra fallout during violent strombolian or sub plinian style activity. Tephra fallout from future eruptions of Ararat volcano, Tendürek volcano and the Kars plateau are also possible. More distant volcanoes, such as Nemrut and Süphan (Turkey) also have the potential to experience explosive eruptions during the lifetime of the ANPP, and would need to be considered in the detailed hazards assessment (i.e. Stage 4).

Screening distance values for volcano generated missiles (sometimes referred to as ballistic projectiles) are typically 5–10 km. Volcano generated missiles would accompany the opening of new vents on the Shamiram plateau or the Yerevan basin. Thus, the ANPP site is located within the screening distance for missile impacts from these volcanic sources. Other volcanoes, such as Aragats and Ararat are too distant to be potential sources of volcano generated missiles.

Lava flows are quite variable in volume and length. Often, an appropriate screening distance for lava flows can be estimated by considering the dimensions and rheology of past lavas that have erupted in the region of interest. Lava flows were mapped in the ANPP site area and found in substantial thickness in a borehole at the site. Therefore, it is clear that the ANPP site is within the screening distance for lava flows associated with the formation of a new vent on the Shamiram plateau. Long lava flows are also found on Aragats volcano that issued from flank vents. These lava flows include the Tirinkatar, Ashtarak and Cakhkasar lavas. Thus it is possible that future flank eruptions of Aragats volcano may produce lava flows that could

reach the site area. On the other hand, lava flows cannot reach the site from other sources in the region, such as Ararat volcano because the distance from the volcano to the site (≈ 60 km) exceeds lava flow lengths from Ararat or analogous volcanoes. In this example, the site is located outside the screening distance for lava flows associated with Ararat volcano.

Volcanic debris avalanche associated with sector collapse and related phenomena might have long run out distances from the volcano. Depending on edifice volume and geometry, screening distance values of 50–100 km might be appropriate. The edifice of Ararat volcano is high and steep sided, making this volcano a potential source for volcanic debris avalanche and other types of slope failure, such as landslide. Hummocky topography has been mapped on the north flank of Ararat volcano [12], indicating past avalanche events likely occurred and, thus, there is potential for similar large volume collapse events in the future. As volcano debris avalanches can be highly mobile, with very long run out potential, there is a possibility of such flows reaching the ANPP site. Such a hazard was considered physically unrealistic for Aragats volcano because of its low slope [10]. Also note there is an absence of extensive hydrothermal activity or alteration on Aragats, and a low potential for pore water pressure effects that have been recognized to cause large debris avalanches at some other volcanoes (e.g. Elsworth and Voight). Thus, Ararat is the only potential source of such activity in the region.

Like other types of geophysical flows, laharic flows (sometimes referred to as debris flows or lahars) can have very long run out and, therefore, screening distance values on order of 100 km might be appropriate. In the ANPP case, debris flows, lahars and related phenomena appear unlikely to originate on the nearby Shamiram Plateau due to the low topographic relief and lack of soil development on the Shamiram plateau. Furthermore, debris flows are not mapped on Aragats volcano, which has a shallow slope. The Shamiram Plateau also forms a significant topographic obstacle for potential debris flows that might originate on the southern flank of Aragats volcano and travel towards the ANPP site. Debris flows have been mapped on Ararat volcano, but it is not possible for the site to be inundated by such flows from Ararat, given the several hundred meter high site elevation above the Yerevan basin and ≈40 km distance from Ararat. Therefore the only potential for lahars and debris flows affecting the site would result from remobilization of some other deposit, such as a large tephra fallout deposit or pyroclastic flow on Aragats volcano, which would need to have sufficient momentum to overtop the Shamiram Plateau (approximately 125 m relief) and reach the ANPP site. Debris flows are considered in the context of such coupled volcanic events in the Stage 4 analyses.

Atmospheric phenomena are associated with some energetic volcanic eruptions. Unusually high concentrations of eruption column to ground lightning strikes occur during some explosive volcanic eruptions, especially within 5 km of the vent. The ANPP site, therefore, is located within the screening distance value for such phenomena that may occur during the opening of new vents. The site is located beyond the screening distance value for this type of phenomena for other potential sources of activity in the region.

In addition to the direct disruption caused by the formation of the vent itself, the opening of new vents may produce additional phenomena that may impact site suitability or design bases. These phenomena include release of volcanic gases, development of hydrothermal systems, and occurrence of ground or subsurface deformation (either as a result of magma intrusion into the shallow subsurface or change in pore pressure associated with the development of a hydrothermal system). Screening distance for these phenomena, therefore, may be comparable to those associated with the opening of new vents, although some

subsurface phenomena such as dike intrusion could extend farther. In the ANPP example, as such phenomena have the potential to occur during the formation of any new vent, the site lies within the screening distance value of these phenomena. More distant sources would not be a significant source of hazard associated with these phenomena.

Like tephra fallout, tsunami generated by volcanic eruption might have significant impact far from the volcano source. Consequently, screening distance values might be 1000 km or more, for sites located near large bodies of water. However, no significant bodies of water exist in the geographic region of interest about the ANPP site. Therefore there is no potential for tsunami or seiche and these hazards need not be considered further.

Volcanic earthquakes and seismic events may accompany the opening of new vents. Therefore, the ANPP site is located within the screening distance for volcanic seismicity. However, earthquakes associated with volcanic events will be encompassed by the seismic hazard assessment, which has relatively large magnitude seismic sources located within tens of kilometres from the ANPP site [10]. Consequently seismic hazard associated with volcanism is not considered explicitly in the volcanic hazard analysis for the ANPP.

TABLE 2. CAPABILITY OF SPECIFIC VOLCANOES OR VOLCANO GROUPS AND THE HAZARDS OF POTENTIAL CONCERN FOR THE ANPP SITE. Reproduced courtesy of the Ministry of Energy and Natural Resources of the Republic of Armenia [10]

Volcano or Group	Capable	Potential volcano phenomena
Shamiram plateau	Yes	Opening of new vents and associated phenomena including pyroclastic flows and surges, tephra fallout, ballistic projectiles, lava flows, near vent phenomena (atmospheric, gases, hydrothermal anomalies, ground deformation).
Yerevan basin	Yes	Opening of new vents and associated phenomena including pyroclastic flows and surges, tephra fallout, ballistic projectiles, lava flows, near vent phenomena (atmospheric, gases, hydrothermal anomalies, ground deformation).
Aragats volcano	Yes	Pyroclastic flows and surges, tephra fallout, lava flows.
Ararat volcano	Yes	Tephra fallout, volcano debris avalanche
Tendürek	Yes	Tephra fallout
Kars plateau	Yes	Tephra fallout
Gegham Ridge	Yes	Centres too distant for significant hazard; tephra fallout potential accounted for by nearer sources.
Nemrut volcano and Süphan caldera	No	Centres too distant for significant hazard; tephra fallout potential accounted for by nearer sources.

This screening distance information is used initially to assess the capability of volcanoes in the site region, which indicates that potentially hazardous volcanic phenomena have a credible potential for reaching the site. The Armenian example concludes that capable volcanoes exist in the region of the ANPP site because there are potential sources of future volcanic activity and these sources of volcanic activity may produce eruptive phenomena that affect the site, given initial assumptions about the nature of past volcanism (i.e. screening distance analyses). Thus, a comprehensive volcanic hazard assessment (i.e. Stage 4) is required for such capable volcanoes or volcanic groups for those phenomena that might reach the site (See TABLE 2).

2.5. SUMMING UP THE ANPP CASE

The ANPP example illustrates the utility of a screening distance approach for the initial hazards assessment in Stage 3. Volcanic systems in this area were relatively well characterized by previous studies, and screening distances for individual phenomena could be developed with defensible technical bases. There also was confidence that the record of past events was representative of the range of future events, and that there were no significant gaps in the geologic record that would fundamentally affect the screening distance determinations. Not all volcanic terrains will be characterized in sufficient detail to support a robust screening distance approach to Stage 3 analyses. For locations where there are potentially significant uncertainties in the completeness or representativeness of the volcanological record, a deterministic approach to hazards screening (i.e. Stage 3 analyses) may not be justified at this stage of the hazards analysis except for physically unsupportable phenomena (e.g. pyroclastic flows from scoria cones, tsunamis at inland locations). For locations where data uncertainties preclude a robust screening distance analysis, the hazards assessment should proceed to a site specific hazards analysis (i.e. Stage 4), which includes an assessment of relevant uncertainties. Details of the methods used to conduct the site specific hazards analyses in Stage 4 are presented in Section 5 of this report.

3. TECTONO MAGMATIC MODEL OF VOLCANISM

3.1. INTRODUCTION

A critical part of any volcanic hazard assessment is determining if past patterns of activity are consistent with the current and expected future patterns of activity in the volcanic system. In other words, are the geologic conditions that led to the formation of past volcanic events expected to occur in the future, or has the geologic setting changed such that some, or all, past events are not expected to occur in the new geologic setting? The need for this consideration is driven by the uncertainty in extrapolation of recurrence rates based on patterns of past activity. For systems with historical or Holocene activity, this uncertainty might be relatively small, because the likelihood of future events is relatively high. Conversely, for older or longer lived systems, low rates of activity might lead to relatively large uncertainties in extrapolation of past patterns of activity into the future.

To evaluate such uncertainties in the extrapolation of past patterns of activity, a key component of the volcanic hazards assessment is to formulate a robust conceptual model for volcanism in the area of interest (See FIG. 1). Generally, this is a tectono magmatic model that integrates the geologic history of the volcanic system with a regional tectonic framework, to

develop an understanding of the geologic processes that resulted in the occurrence of past events. This model is used to determine if these geologic processes are expected to occur in the future. The conceptual model also can be used to condition the hazards analyses to consider changes in recurrence rates (e.g. a waning volcanic system) or in the characteristics of phenomenon (e.g. increase in frequency of silicic pyroclastic flows, cyclicity in eruptive style).

A tectono magmatic model is needed to determine if future hazards are credible, especially in areas that have experienced low rates of activity in the past. The tectono magmatic model is developed from regional geologic information related to:

1. Spatio temporal patterns of volcanism, including time volume relationships.

2. Geophysical and tectonic setting, including patterns of faulting.

3. Geochemical evolution of magmatic systems.

Several tectono magmatic models are reviewed in this section illustrating their use in hazard assessments on a variety of scales, starting from the most regional, plate tectonic scale and moving toward the scale of individual volcanic systems.

3.2. SPATIO TEMPORAL PATTERNS

Volcanism is a manifestation of heat transfer from the interior to exterior of the Earth by the advection of magmas. These magmas are generally formed within 200 km of the surface by partial melting of mantle in response to plate tectonic processes. Therefore, worldwide, a correlation exists between the distribution of active volcanism and distribution of earthquakes, mostly at plate boundaries (See FIG. 7). Roughly 80 % of the area of Earth's continents is geologically stable, where rates of volcanism and faulting are relatively low. Volcanoes and earthquakes are instead concentrated near plate boundaries, and in diffuse deformation zones, sometimes hundreds of kilometres wide, which extend into continental areas from plate boundaries (See FIG. 8). Numerous authors have commented on the correlation between population growth, and hence the development of nuclear facilities, and plate margins, especially when continental diffuse deformation zones are taken into account (See [23–25], and references therein).

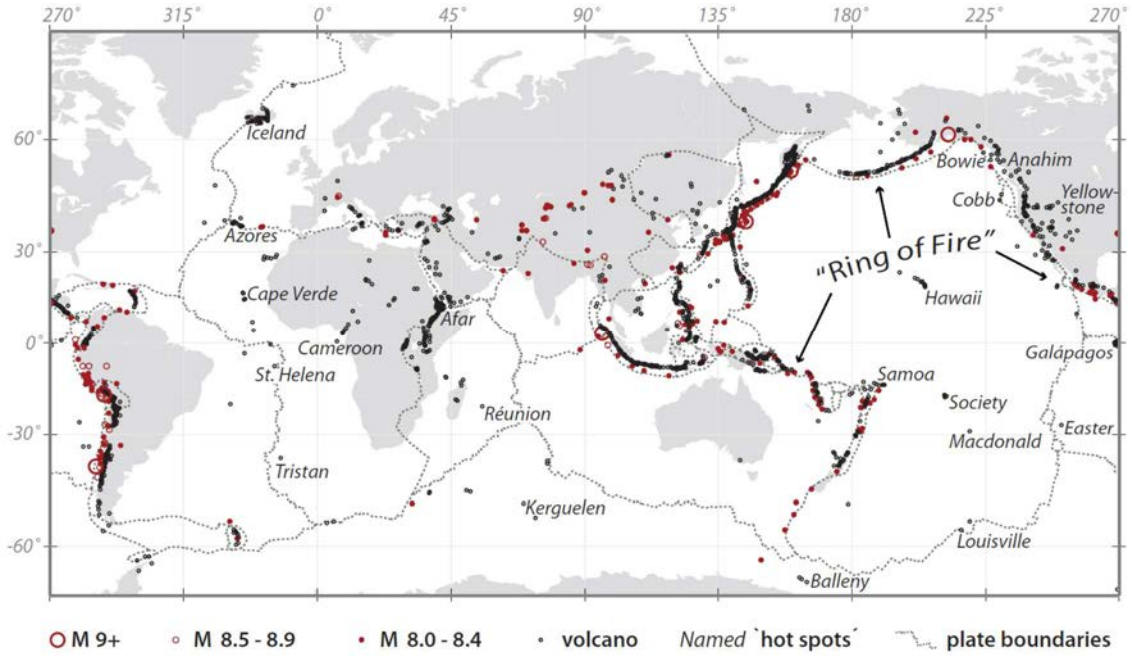

FIG. 7. Map showing the locations of Holocene volcanoes and all large ($M \geq 8$) earthquakes since 1900 A.D. Seismic and volcanic hazards are broadly correlated with the margins of tectonic plates. Most of the volcanic activity and large earthquakes occur around the margins of the Pacific Ocean basin. This concentration of activity is commonly referred to as the "Ring of Fire". This Figure reflects the latest information (version 4.3.0, updated on 3 July 2014) from the Smithsonian Institution's Global Volcanism Program database (http://www.volcano.si.edu/) and supersedes FIG. II-1 in SSG-21 [1].

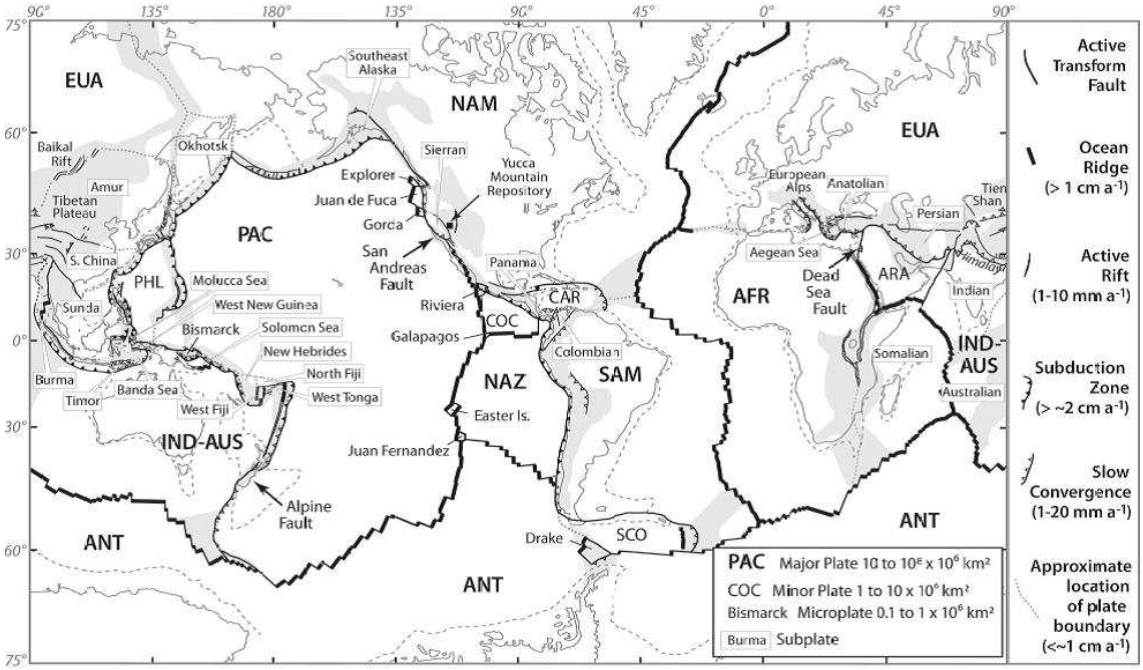

FIG. 8. Map showing the distribution of major and minor plates and diffuse deformation zones (shaded) that occur on the margins of many continents. Volcanism occurs at plate boundaries and is also generally correlated with diffuse deformation zones. Reproduced courtesy of © Cambridge University Press 2009 [24].

Volcanism occurs predominantly in volcanic arcs associated with subduction zones, at divergent plate margins (See FIG. 9), and associated with hot spots. All of these plate tectonic features are reasonably identified and mapped worldwide, on the scale of individual plates, sub plates, and microplates. For the purposes of hazard assessment for nuclear facilities, this global setting provides context and a starting point for volcanic hazard assessments (e.g. Initial scoping, FIG. 1). Volcanism, however, is not limited to the generic tectonic environments of subduction, divergence and hot spots. In western North America, for example, volcanism is widely distributed throughout a diffuse deformation zone known as the Basin and Range. This region is characterized by low volume, infrequent eruptions of basaltic magmas within volcanic fields. Volcanism throughout much of the region is attributed to decompression melting, resulting from extension of the lithosphere of western North America. This partial melting is thought to be enhanced in the region because the area was the location of ancient subduction over a period of tens of millions of years, which chemically modified the mantle and made it more susceptible to partial melting [26]. Nuclear facilities throughout much of the western US, such as the proposed repository at Yucca Mountain, Nevada [27], [28] must take this type of volcanism into account in hazard assessments. Similarly, subduction ceased millions of years ago in the Anatolian region of Turkey, Armenia, and Iran, yet active volcanism persists today in this region [29]. Furthermore, widespread but diffuse volcanism in continental Asia, particularly in China, is not directly related to an active convergent or divergent plate boundary [30].

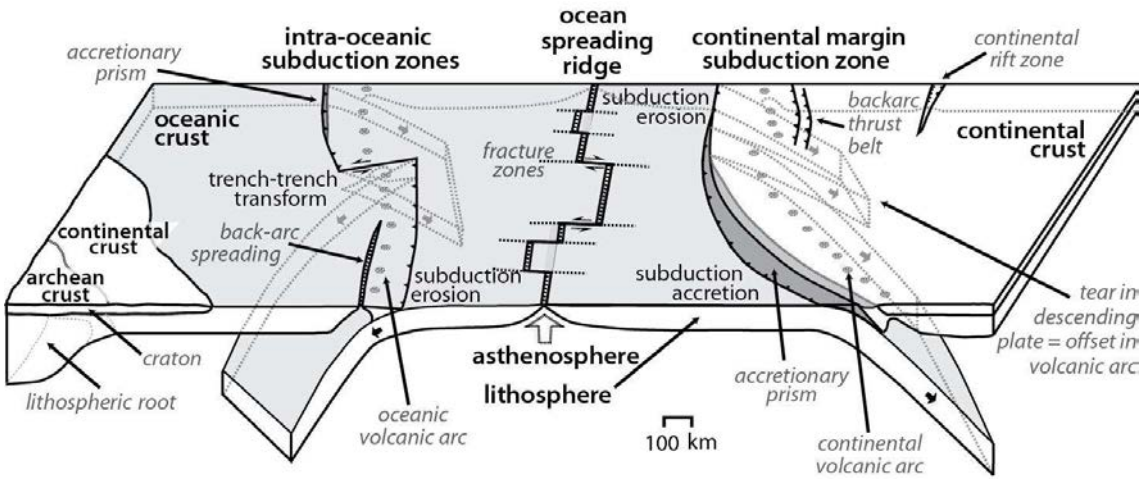

FIG. 9. Schematic illustration of the types of plate margin where volcanism commonly occurs. Divergent plate margins occur where seafloor spreading generates new ocean crust resulting in decompression melting. Incipient divergent plate motion on continents results in rift zones, also the site of volcanism. Subduction zones develop at convergent plate margins where volatiles are introduced into the mantle wedge, resulting in partial melting and the generation of magmas. Ocean trenches and arcs of explosive volcanoes are generated in the process. Transform margins occur without significant divergence or convergence of plates. Mafic volcanic fields can occur associated with transform margins, perhaps because of shear melting of lithospheric mantle. Reproduced courtesy of © Cambridge University Press 2009 [24].

A critical issue is that on the scale of the geographic region of interest, within any one of these plate tectonic settings, the distribution of volcanoes can be quite complex and non uniform. Rates of magmatism, eruption rates, and even the types of eruptions may vary substantially with profound impact on hazard assessments for nuclear facilities.

3.2.1. Tohoku tectono magmatic model

As an example of a regional tectono magmatic model, decades of work by numerous research groups has shown that the Tohoku volcanic arc, northern Honshu, Japan, evolved as a volcanic arc since approximately 14 Ma as a result of subduction of the Pacific plate beneath Japan and opening of the Sea of Japan. Relative to many other volcanic arcs, the Tohoku arc has persisted as a volcanic arc in a stable position with stable rates of eruption since 14 Ma. In assessing volcanic hazards for this region, one might confidently use a tectono magmatic model based on this persistent subduction (e.g. [31]). The classic model of the Tohoku subduction zone related volcanism includes a description of the volcanic front, along which volcanism is maximum, a fore arc that lacks volcanic activity, and a back arc that experiences much lower rates of activity than those associated with the arc. This model emphasizes variation in the rate of volcanism and potential volcanic hazards across the arc. In contrast, relatively little variation in rates occurs along the arc. FIG. 10 illustrates these general geodynamic relationships. A smoothed probability model for the long term potential of volcanism in the arc can be constructed from the distribution of Quaternary volcanoes. Briefly, this probability model is constructed using a kernel density function (See Section 5.2) to estimate the probability of a new volcano forming, given the distribution of existing, mapped Quaternary volcanoes. The kernel density function is estimated using a bandwidth that smoothes volcano distribution. It is assumed in this particular model that a smooth asymptotic mean squared error optimisation algorithm is appropriate. The probability is estimated for a time period of 100 000 year for a new volcano centre forming within a given 25 km^2 area. The potential magnitude of eruptions from newly formed volcanoes is not considered. This smooth model is consistent with a classic model of stable subduction. That is, the probability model has a steep increase in rate of volcanism at the volcanic front, and a gradual decrease in the rate of volcanism in the back arc. Thus, this probability model is consistent with a tectono magmatic model of simple, uniform subduction rate.

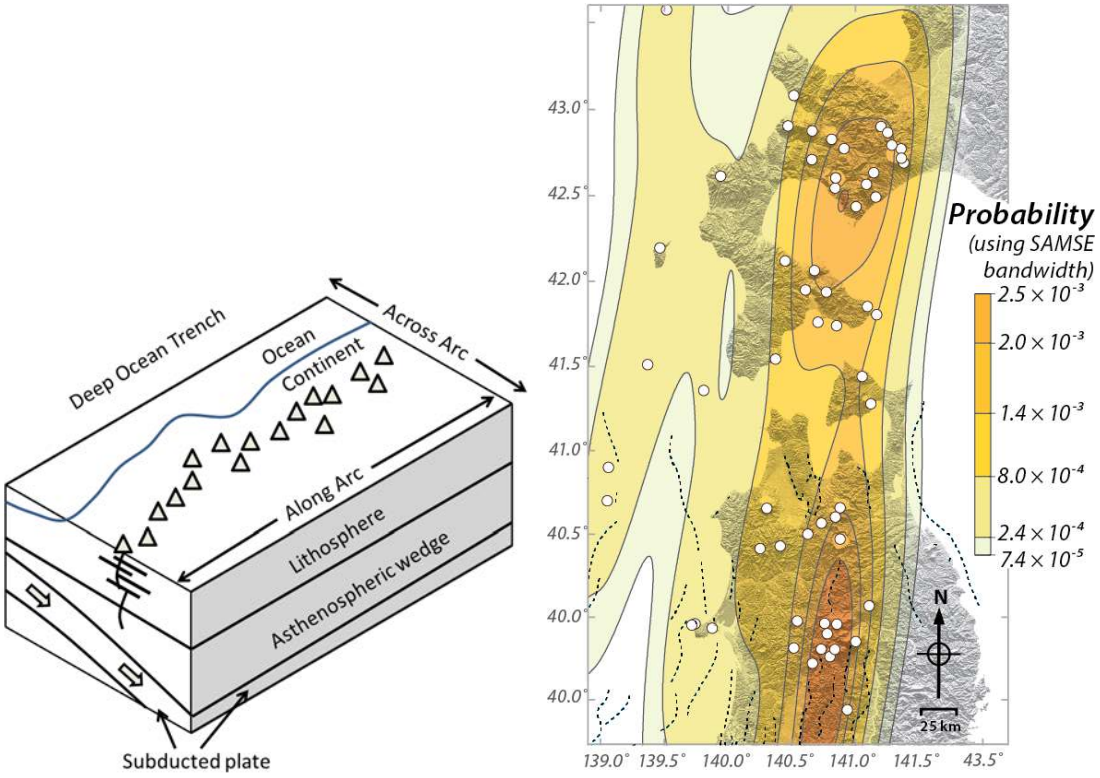

FIG. 10. Left: a classic subduction zone model in which rates of volcanism vary dramatically across the arc but are assumed to be relatively uniform in an along arc direction. Triangles indicate the postions of volcanoes; large arrow indicates the direction of subduction and the direction of flow in the uppermost asthenospheric wedge. Hot zones of partial melting develop beneath volcanoes in the lithosphere with equal probability all along the volcanic arc, providing the potential for future eruptions. Right: A spatial density model illustrating the probability of volcanism along the Tohoku arc. The model is consistent with the classic model of subduction, with little variation in rates of activity along the arc. See Section 5 for discussion of how these types of spatial density probability models are made [32]. Reproduced courtesy of Nuclear Waste Management Organization of Japan [32].

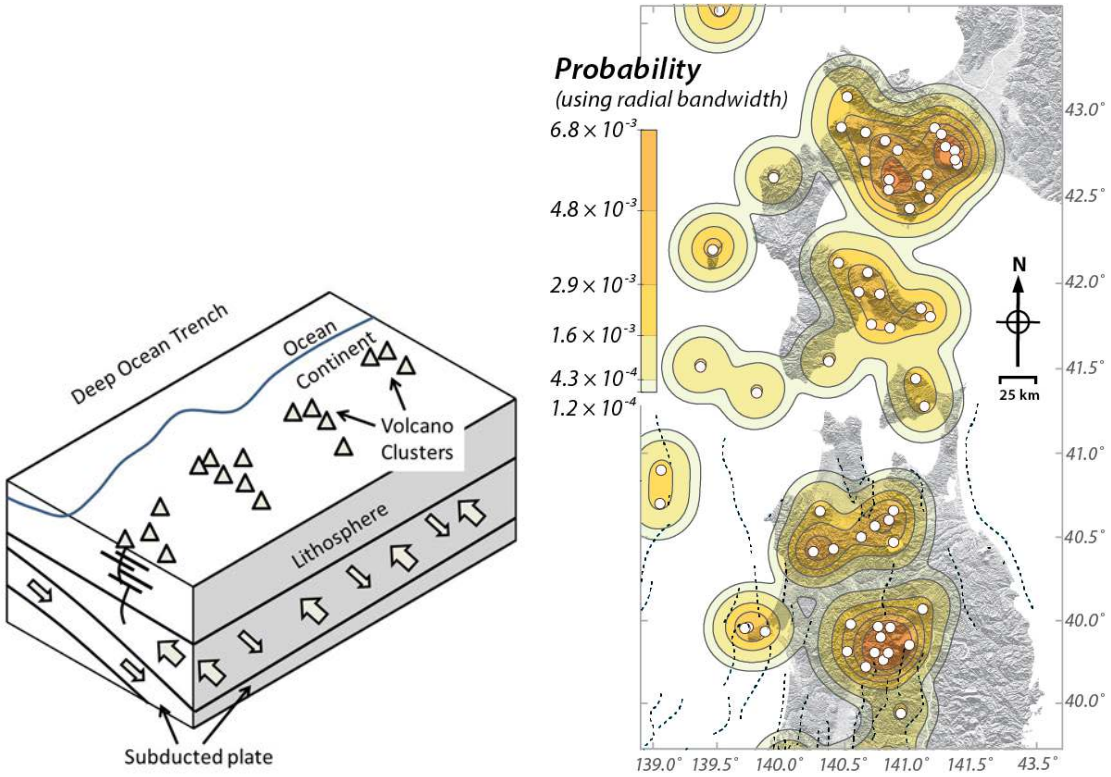

FIG. 11. Left: A schematic illustration of the hot finger model of Tamura et al. [33] emphasizing the clustered nature of volcanism along the arc and its relationship to counter flow in the asthenosphere. Volcano postions are indicated by triabngles; large arrows indicate counterflow in the asthenosphere. Right: Alternative probability models for the future distribution of volcanoes may be constructed that emphasize these alternative geophysical models. The left panel shows regional probability models for Tohoku arc emphasize volcano clustering within the arc and behind the arc. These probability models are most consistent with hot finger model [32]. The right panel shows a regional probability model that emphasizes the classical subduction zone model, with relatively uniform probability all along the arc. See Section 5 for discussion of how these types of spatial density probability models are made [32]. Reproduced courtesy of Nuclear Waste Management Organization of Japan [32].

Alternative models of the Tohoku subduction zone have been developed (e.g. [33]) that emphasize along arc variations in rates of volcanic activity. This model emphasizes the clustering of Q

uaternary volcanoes along the arc, distinct areas within which Quaternary volcanism is much more prevalent, and gaps in activity along the arc, in areas that rates of volcanic activity are very low. Geochemical and geophysical data have also been used to support this clustered model. These data include the presence of regional scale seismic tomographic anomalies and isostatic compensation of the crust resulting in basement uplift within Quaternary clusters and eruption of more highly differentiated magmas. Tamura et al. [33] linked these different observations and developed the 'hot finger' model of volcanism for Tohoku, in which counter flow in the asthenosphere results in zones, or 'fingers', of enhanced partial melting and, therefore, higher rates of volcanism. The hot finger model is not only supported by volcano distribution in Tohoku, but by seismic tomographic anomalies, bedrock uplift and isostatic compensation associated with volcano clusters, and geochemical modelling [34–36]. An alternative probabilistic hazard model can be developed that reflects this tectono magmatic model of the Tohoku arc (See FIG. 11). This alternative probability model make the same assumptions as used in FIG. 10, but uses a different optimisation algorithm, the least squares cross validation method, to estimate the kernel bandwidth. In this model an algorithm is used to estimate the spatial density of volcanism that emphasizes compact clusters of Quaternary volcanism and gaps in activity along the arc.

Comparison of probability maps (See FIG. 11 right) illustrates that the hazard assessment should be sensitive to underlying assumptions about the tectono magmatic setting of volcanism. Using the classic subduction zone model probabilities of volcanism are relatively uniform along the arc. Using the hot finger model, clusters of volcanoes are emphasized and probability of future volcanism is not uniform along the arc. On this scale, alternative models of the tectonic setting of volcanism should be considered and the effects of these alternative models on probabilistic hazards at any particular site should be assessed.

3.2.2. Building a conceptual tectono magmatic model

The Tohoku example illustrates that differences in tectono magmatic models may result in significant differences in probabilistic hazard models developed in site evaluations. On a regional scale, tectono magmatic models are constructed based on geodynamic information, which includes geological, geophysical and geochemical data. It is necessary to gather these data, usually from existing literature, with the purpose of developing one or more tectono magmatic models for the site region. For the Tohoku arc example, these data include:

- Regional distribution of volcanoes, erupted volumes, and ages of their products to understand rates of magmatic processes;
- Use of geophysical data (e.g. seismic tomography, hypocenter distributions, gravity, magnetotelluric soundings) to characterize the regional tectonic setting, especially the nature of the mantle wedge and underplating of the crust;
- Geochemistry and petrography of volcanic products to characterize magma production rates and source region, assimilation, storage, and fractionation processes (e.g. major and trace elements, rare earth elements, isotopic analyses);
- Data showing the relationship between regional and local scale tectonic features and volcanoes, such as distribution of contemporaneous faults or expressions of crustal stress and strain.

Some discussion of specific data gathered in support of these tectono magmatic models is provided in Annex. These data represent the regional geology of the site. They are used specifically in hazard assessment to assure that the hazard models are consistent with observations, and to understand the general geodynamic framework. It is noted that despite years of effort, alternative models for the tectonic setting of volcanism may persist, as illustrated by the Tohoku example. As investigations continue, the collection of additional data can result in the creation of additional alternative models, and rejection of models that are inconsistent with the newer data. Although investigations should attempt to assess the validity of alternative models, it may be necessary to consider these alternative models individually in later steps of the hazard assessment.

For example, there are numerous alternative models of recurrence rate, volume, magnitude, and magnitude frequency relationships that apply well to different types of volcanic systems (e.g. distributed volcanism, open versus closed conduits at composite volcanoes and calderas). The main point is that alternative models be identified and tested using available data (e.g. [37–42]).

Tectono magmatic models also are important to consider on the scale of specific volcanic systems. In the case of individual volcanoes or volcanic systems, it is important to understand how the volcano works in order to make forecasts of future activity. Persistently active volcanoes usually reveal a range of eruptive products and eruption styles through investigation of the recent geological record. For less frequently active, or long dormant volcanic systems, it is more important to develop a tectono magmatic model that informs the hazard assessment. Not only might data about past eruptions be missing from the geologic record, but the eruption products preserved in the record may reflect conditions that no longer exist in the volcanic system. For example, it may be important to investigate whether the tectono magmatic conditions that gave rise to past patterns of activity persist in the present, or whether the tectonic setting of the volcano has changed.

On a more local scale, tectono magmatic models are used to address specific concerns about potentially active volcanic systems, such as:

- How often and how much magma is supplied from depth?
- Where is the magma stored within the volcanic system?
- Is the shallow conduit plugged between eruptions or does it remain open, which affects the degassing and explosive potential? How do volatiles behave in volcanic system?
- Does the eruptive history of the volcano show any progressive changes in the nature of eruptions, eruption rate or cyclicity?
- Is there evidence of abrupt transitions from one style to another, for example from stratovolcano to caldera?

Specific data are required to answer these questions. Description of these data types are provided in SSG-21 [1] and discussed in Annex. Briefly, tectono magmatic models depend on reconstruction of the eruptive history of the volcano. This process begins with detailed stratigraphic analyses, correlation, and geologic mapping to characterize eruptive sequences. Often this process involves characterization of individual eruptions using maps of tephra layers, their temporal relation with pyroclastic flows and similar studies of other phenomena,

such as lava flows and lahars. Standard geologic mapping of the units found at the surface is the first step in developing the eruptive history. Subsequently, stratigraphic columns and correlation are used to constrain recurrence times of various phenomena, geochemical trends within individual eruptions or from one eruption to the next, and the time volume relations of eruptions.

3.2.3. Nejapa-Apoyequetectono magmatic model

The need for a tectono magmatic model on the scale of a volcanic system, and requiring detailed stratigraphic analysis, is illustrated by the Nejapa-Apoyeque volcano alignment located on the west side of the city of Managua, Nicaragua (See FIG. 12). This alignment of Holocene volcanic vents includes craters formed by magmatic, phreatic and phreatomagmatic eruptions. Detailed stratigraphy has revealed that eruptions vary from relatively small volume and low intensity to phreato plinian events of large volume [43], [44]. Detailed stratigraphic studies were required in order to characterize this eruptive sequence.

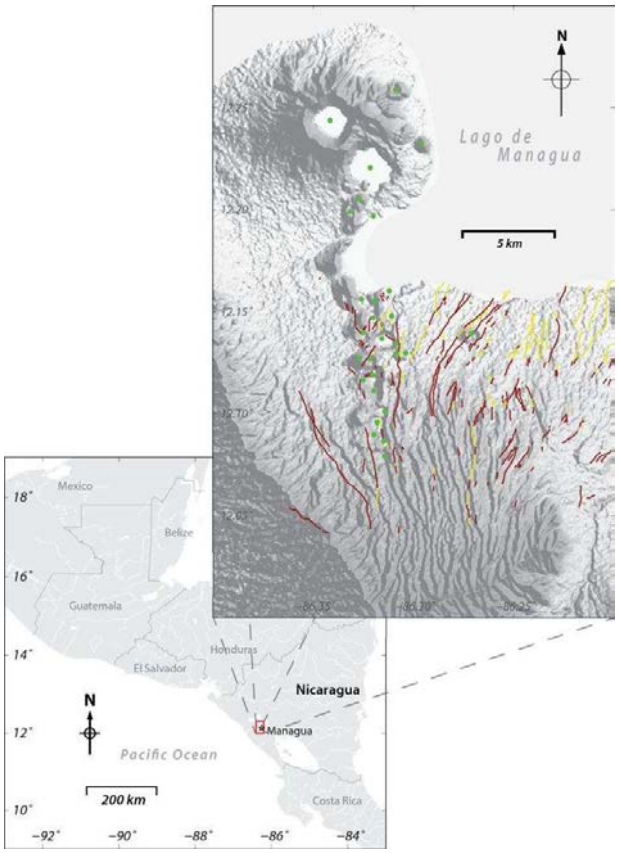

FIG. 12. The Nejapa-Apoyeque alignment located on the west side of the city of Managua, Nicaragua. This volcanic system comprises at least 21 vents (green circles) distributed along an N-S trending alignment. The alignment is located near the western margin of the Nicaraguan depression, and is associated with numerous active faults (red) and inferred faults (yellow). Pacific Ocean bathymetry shown in lower left section of inset.

For these types of volcanic systems where vent locations are spatially distributed, it is often important to identify the relationship between magmatism and tectonic features on the scale of tens of kilometres. The Nejapa-Apoyeque volcano alignment is located in a basin, bounded by a prominent fault to the west. Numerous faults and fault segments are located adjacent to the volcano alignment, and the alignment is oriented perpendicular to the inferred

minimum horizontal compressional stress. FIG. 13 illustrates one model of the geodynamic setting of the Nejapa-Apoyeque alignment and its relationship specifically to the basin bounding fault. This finite element model consists of a 2D section drawn perpendicular to the alignment, and consisting of a layered lithosphere, including brittle crust, ductile lower crust, and mantle. The upper brittle crust is cut by a fault which experiences a dip slip component. The finite element model suggests that the occurrence of this fault localizes extension when the model is subject to extensional strain of approximately 1 mm year^{-1}. The localized strain, in turn results in upwelling in the mantle, which may induce partial melting of basalt due of decompression and/or perturbation of the local geothermal gradient.

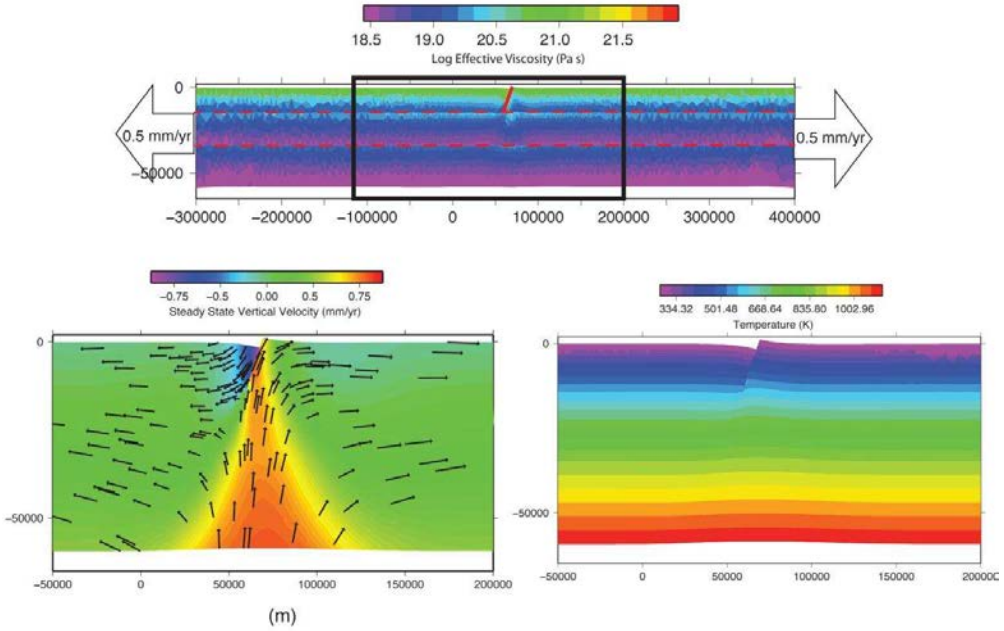

FIG. 13. Finite element model illustrating the tectono magmatic model of the Nejapa-Apoyeque volcano alignment. Upper panel: Essential features of the model include brittle, ductile, and mantle layers (separated by dashed red lines) each with different physical properties. A fault with dip slip component (solid red line) is represented as a dislocation in the model and the entire model experiences extension at a total rate of 1 mm year^{-1}. Left panel: Extension results in upwelling and divergence, focused in the fault region, which moves mantle closer to the surface and perturbs the geothermal gradient (right panel), conditions that can lead to magma generation in some circumstances. Figure courtesy of R. Malservisi.

This tectono magmatic model has implications for the hazard model of the Nejapa-Apoyeque volcano alignment, and of course, for risk to the city of Managua and for critical infrastructure located in this zone. First, the model suggests that future volcanic vents are more likely to form along the N-S trending alignment due to focusing of magmatism along the basin bounding fault system, than elsewhere in the basin. Nevertheless, the finite element model and the geologic record of activity shown by the map distribution of volcanoes (See FIG. 12) suggest formation of new volcanic vents off the alignment is also possible. Second, the recurrence rate of volcanic activity should be linked to the rate of crustal extension. In this model, a constant rate of extension should result in a relatively steady recurrence rate of volcanism. The hazard model (See FIG. 14) reflects these basic features of the tectono magmatic model, which in turn is developed based on a detailed understanding of Holocene activity in this system [43]. The spatial density model (See FIG. 14 left) reflects the overall N-S trend of the alignment, perpendicular to extensional strain, as illustrated in the finite element

model. In this case, an anisotropic spatial density model (See Section 5) is preferred that reflects this strong elongation of the alignment, and the repeated return of volcanic activity to the alignment even over thousands of years. Radiometric age determinations from [43] and references therein are used to develop a model of recurrence rate (See FIG. 14 right). Although not every unit is dated, the available dates and stratigraphic sequence are consistent with steady state volcanism, with a high degree of confidence. In other words, the spatial and temporal hazard models are built on detailed volcano stratigraphic work and are consistent with the tectono magmatic model.

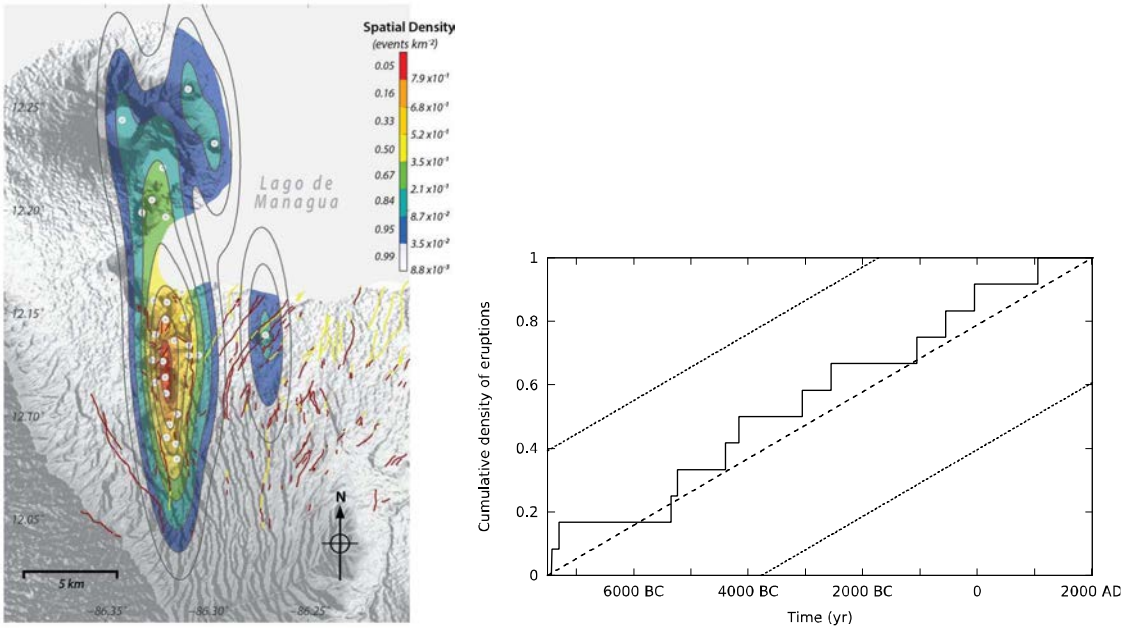

FIG. 14. Hazard model showing, Left: Spatial density map of the Nejapa-Apoyeque alignment, created using an anisotropic kernel density function to be consistent with the tectono magmatic model (See FIG. 13). See Section 5 for details about construction of this type of model. Right: Recurrence rate of volcanism along the Nejapa-Apoyeque alignment based on data from [43]. The observed recurrence rate of events (solid line) matches well with a steady state model of volcanism, and is stationary within uncertainty bounds (fine dashed lines).

3.2.4. Example of a long term petrogenetic trend: the geochemistry of Aragats volcano and adjacent volcanic centres

Once the eruptive history of a volcano has been documented, it becomes possible to use the petrology and geochemistry of eruptive sequences to identify trends or evolution of the magmatic system. These investigations rely on detailed analyses of individual units and their components. The units' petrology and geochemistry may constrain parameters such as the depth of the magma source region, the temperature, rheology and gas content of magmas, rates of magma ascent, and the occurrence of eruptive triggers, such as magma mixing events. The hazard assessment of the ANPP, located low on the flanks of Aragats volcano, provides an example of the use of this information.

Aragats volcano is situated in the NE part of the Anatolian-Armenian-Iranian plateau, an intensely deformed segment of the Alpine-Himalayan belt. The complex geological structure of the region is represented by a mosaic of tectonic blocks comprising fragments of volcanic arcs, continental crust and exhumed oceanic crust. Collision of the Arabian plate with

the Eurasian margin in the early Miocene resulted in orogenic uplift associated with widespread and voluminous volcanism. Aragats (4090 m, 45 km in diameter) is one the largest volcanoes in the entire region and produced central vent (Plinian eruptions of volcano explosivity index (VEI) > 4) and monogenetic flank eruptions and periphery plateaus within a total area >5000 km^2, known as Aragats volcanic province (AVP). The AVP comprises the composite cone of Aragats volcano and dozens of flank vents, scattered monogenetic cinder cones on the adjacent volcanic plateaus, as well as the neighbouring stratovolcano Arailer.

Petrology, geochemistry and volcano stratigraphy of Aragats and nearby volcanic plateaus were studied in the framework of volcanic hazard assessment of ANPP site [10]. K-Ar and $^{40}Ar/^{39}Ar$ age determinations of groundmass and separated plagioclase samples indicate that volcanism at AVP began ~2.5 Ma [10], [45]. The most recent known volcanic activity was 0.49 Ma and produced a Plinian eruption of trachydacites from Irind volcano, a flank vent. Additional activity at approximately that time included basaltic trachyandesite lava flows from Tirinkatar (0.45–0.61 Ma), Kakavasar, (0.52–0.54 Ma) and Ashtarak (0.58 Ma) monogenetic flank centres, as well as trachyandesites of Jrbazhan volcano on the summit plateau of Aragats (0.52 Ma).

The majority of Aragats rocks are of alkaline and subalkaline types. The AVP series of volcanic products encompasses the entire compositional range from trachybasalts to rhyolites, although the majority (86 %) are basaltic trachyandesites, trachyandesites, and trachydacites. The most primitive samples appear to be trachybasalt lavas. The most evolved samples are rhyolites (and their obsidian variety) from the 1.5 Ma Arteni volcanic complex.

Aside from small within suite differences, chondrite normalized rare-earth element (REE) abundances in the entire Aragats region are remarkably similar, indicating origins from a common, long lived magmatic source region. This source region is thought to have experienced nearly identical degrees of mantle melting and very little or no assimilation of xenomorphic materials (rocks or crystals) upon magma ascent from the source to the surface. For all series, significant enrichment of light REE (LREE) and medium REE over high REE (HREE) can be observed (See FIG. 15).

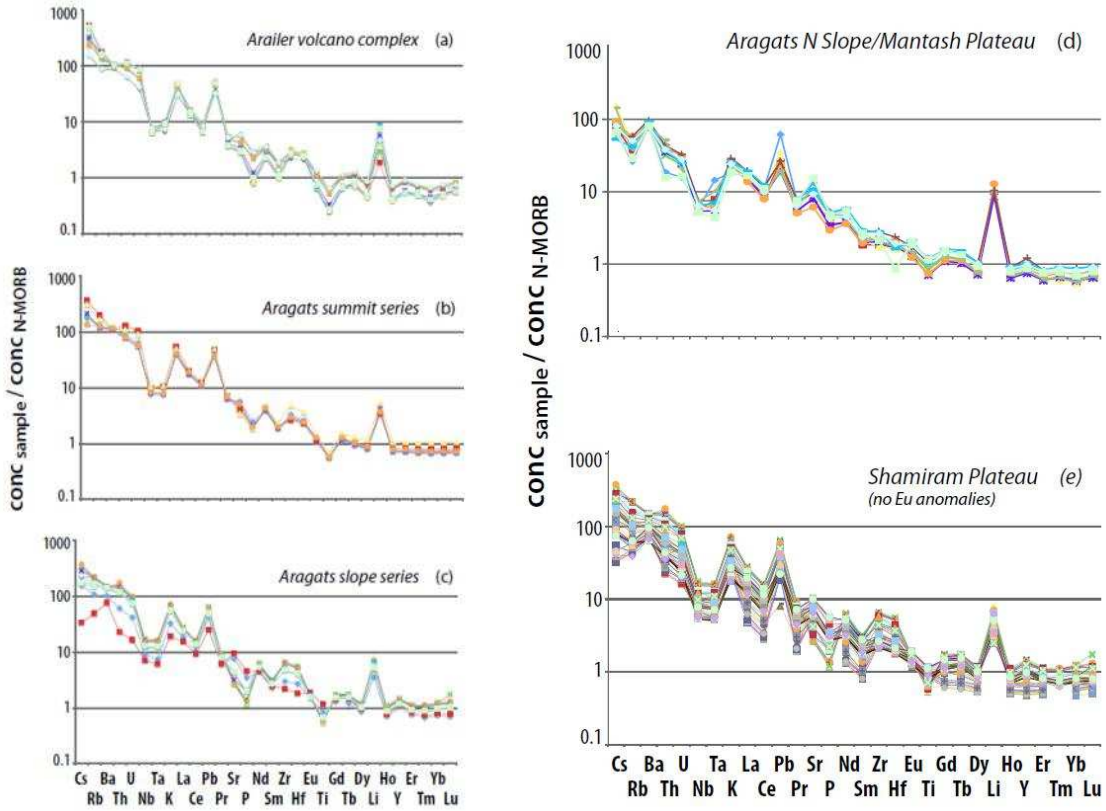

FIG. 15. Normal mid-ocean ridge basalt (N-MORB) normalized trace element spider diagrams for NPP samples, (a) samples from Arailer volcano complex; (b) samples from Aragats summit series; (c) samples from Aragats slope series. N-MORB values from [46]. N-MORB normalized trace element spider diagrams for (d) samples from Aragats north slope/Mantash plateau; (e) samples from Shamiram plateau (with no Eu anomalies). Note the very strong enrichments relative to N-MORBs for the large lithophile elements (Cs, Rb, Ba,), K, Pb, Th, U and the somewhat enriched concentrations relative to N-MORBs for elements like Li, the LREE (La, Ce, Pr, Nd) and Sr. Also note that Ti, Y and HREE are N-MORB like or even more depleted. Reproduced courtesy of the Ministry of Energy and Natural Resources of the Republic of Armenia [10].

Aragats rocks have geochemical features that are typical for active continental margins and island arcs (i.e. [47]). For example, large ion lithophile elements (LILE) and LREE are enriched relative to MORB. Prominent negative anomalies of Nb and Ta occur relative to neighbouring elements of similar incompatibility. Positive anomalies are evident for Pb and Li. The depletion of Nb and Ta is typically ascribed to the retention of these elements in the subducting slab during progressive dehydration, whereas LILE and LREE are transported upward by slab derived fluids and/or melts [48]. The subduction zone signature of Aragats rocks is shared by volcanic rocks the adjacent volcanic regions [12], [22], [49], [50]. Most of the studied volcanic series show homogeneous patterns despite the variety of rock types, and variations observed (e.g. in the Aragats slope series) can be attributed to the overprinting effects of fractional crystallization. This is an important observation for the tectono magmatic model of Aragats volcano and surrounding regions, because it indicates that, although subduction ceased well before the Quaternary (early Miocene?), Quaternary volcanism is geochemically linked to the partial melting of a subduction enriched mantle.

Isotopic analyses provide further insights about magmatism at Aragats. Both the $^{87}Sr/^{86}Sr$ and the $^{143}Nd/^{144}Nd$ isotopes show no significant variation with SiO_2, which indicates a lack of pronounced crustal assimilation. Moreover, all of the studied Sr and Nd isotope ratios are typical of melts originating from moderately depleted mantle source regions. The average $^{143}Nd/^{144}Nd$ in the studied mafic samples is 0.512807 (minimum = 0.512760, maximum = 0.512863). The average $^{87}Sr/^{86}Sr$ ratio of all studied samples (trachybasalt to rhyolite lava flows, tuffs, pumice fragments, ash) is 0.704211 (minimum = 0.704035, maximum = 0.704414). $^{87}Sr/^{86}Sr$ ratios are remarkably similar in all samples collected on Aragats and surrounding areas. This is additional evidence that one magma source region fed all of these volcanic eruptions. The observed overall small variations in both the $^{87}Sr/^{86}Sr$ and the $^{143}Nd/^{144}Nd$ isotope ratios, together with trace element evidence and mineral chemistry insights, reveal that all analysed magmas from the region of Aragats originate from the same mantle source region and that they experienced no significant crustal assimilation processes. Rather, the isotope ratios of the volcanoes of the ANPP area were controlled by processes of simple crystal fractionation (See FIG. 16). No isotopic variations are found with time, from upper Pliocene to Quaternary, within the AVP, which also indicates that parental magmas have not changed, or changed very little, during the history of activity of the volcanic system.

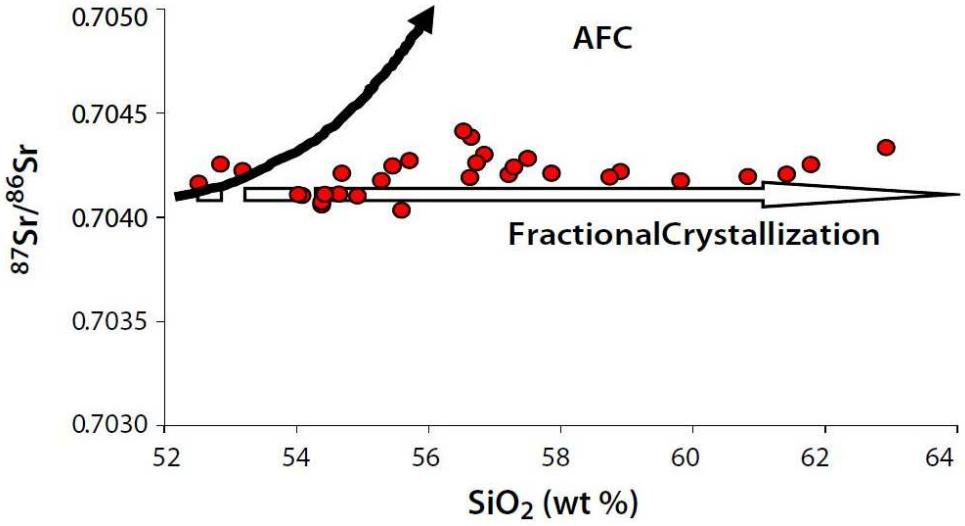

FIG. 16. SiO_2 versus $^{87}Sr/^{86}Sr$ isotope ratio diagram for Aragats lava samples. Noteworthy is alignment of data points along fractional crystallisation trend. Reproduced courtesy of the Ministry of Energy and Natural Resources of the Republic of Armenia [10].

The limited variation in isotope ratios from rocks that record different crystallinity and age supports the eruption of volcanic materials from a relatively well mixed, homogeneous magma source underneath Aragats and adjacent volcanoes. The model of mixed subduction zone and asthenospheric mantle inputs at Aragats is in agreement with the tectono magmatic model of slab break off and asthenospheric flooding of the otherwise subduction modified mantle source region, proposed by Keskin [29]. Based on bulk rock geochemical data (major, minor and low abundance trace elements, Sr and Nd isotopes) and mineral chemistry, it is likely that volcanic rocks of AVP are largely recording a complex mixing between deep asthenospheric mantle and remnants of subduction modified and metasomatically enriched mantle sources, followed by fractionation in large magma chambers [10]. Mineral melt equilibria studies reveal atypically dry (< 1% H_2O) and hot mantle source. Noteworthy are high

eruption temperatures compared to global volcanic arcs, explaining the very long (up to 25 km) and thick (> 200 m) trachydacitic lava flows mapped on Aragats.

The major and trace element geochemical data and Sr and Nd isotopic studies of Aragats lavas demonstrate that the parental magmas do not change spatially or evolve through time in this volcanic system. For instance, 0.71 Ma trachyandesites erupted on the periphery of Shamiram plateau are almost identical to those erupted on the summit plateau at approximately 0.52 Ma. Thus, the magmatic system beneath Aragats is long lived (1.55–0.45 Ma) and produced a large volume of magmas of mafic, intermediate and silicic compositions without distinguishable time scale related petrological and geochemical patterns of parental magmas or their differentiates. It is estimated that Aragats produced about 860 km^3 of lavas and pyroclasts during this period [10].

The major conclusion from this detailed stratigraphic, petrography and geochemical study is that large volume Aragats system is a product of regional, post collisional and long lived magmatism. There is no evidence from the geochemistry to support waning activity in the system. Rather, the volcanism of the Aragats system simply stopped about 0.48–0.45 Ma with eruptions of basaltic trachyandesites, trachyandesites and trachydacites; volcanism elsewhere in the region continued throughout the Upper Pleistocene, and Holocene. Furthermore, the geochemistry indicates that magmas in this system ascended rapidly from depth, erupted at high temperature, low volatile content, and low viscosity, compared to typical arc magmas. In other words, it is not possible to rule out the possibility of persistent mafic melt in the system, especially as large volumes of mafic melt are required to generate the volumes of silicic magmas erupted 0.9–0.4 Ma. Furthermore, it is conceivable that deep magma reservoirs might persist in this system, which trap ascending mafic melts.

There is an absence of petrologic or tectonic information to explain why the Aragats volcanic system hasn't erupted since 0.45 Ma. Although a lack of activity in 0.45 million years has been viewed by some researchers as indicating the Aragats system is extinct, there is significant uncertainty in the current understanding of how long a volcanic system can remain quiescent but still erupt. As a result of this analysis, a probabilistic study of volcanic hazards was conducted for the ANPP site, despite the long apparent hiatus since last eruptive activity. This was done because a credible potential for future eruptions could not be ruled out in light of available information. This consideration also ensures that the safety assessment will not underestimate potential hazards at the ANPP site. Nevertheless, several alternative models for recurrence rate estimates were developed to account for the observed hiatus in activity. These alternative models reflect the possibility that 0.8–0.4 Ma recurrence rates overestimate rates that appropriately represent the near term hazard. The development and analysis of these alternative recurrence rate models is discussed further in Section 4. Additional examples of volcano tectonic models developed for long term investigation and characterization of volcanic systems include [51–54].

3.2.5. Example of a short term petrogenetic trend: the geochemistry and petrology of the most recent lava flows from Volcán de Colima, Mexico

On short timescales, petrologic changes in volcanic systems occur that are potentially indicative of potential changes in eruption intensity. Such trends are important to consider for active volcanoes within the geographic region of interest. In this context, petrological tools are used to study eruptive sequences [55] and to investigate compositional changes that occur in historical eruptions. Compositional changes identified in whole rock analyses might reflect a spectrum of magmatic processes such as modifications of mantle source regions, degrees of partial melting, interaction with the crust and shallow magmatic processes (e.g. differentiation, mixing, mingling, host rock assimilation and interaction with new mafic magma), acting over a range of time periods [56–70].

Such petrologic trends are important to identify, or at least consider, for hazard models related to frequently active volcanoes within the geographic region of interest. Currently, in order to identify systematic changes in whole rock composition requires a high resolution stratigraphic record. Volcán de Colima has had frequent eruptions since 1519–1523 A.D. [71]. The 1913 Plinian eruption has been documented in detail taking into account eyewitness observations, stratigraphic studies, and geochemistry in such a way that the dynamics of this particular eruption has a high level of detail [72]. Luhr and Carmichael [73] proposed that the most recent eruptive history of Volcán de Colima shows two century long cycles of activity: 1818–1913 and 1913 to the present. These eruptive cycles are separated by Plinian eruptions. The petrology and geochemistry of the products before and after these markers are contrasting, for instance, the 1913 scoriae are much more mafic than the andesitic rocks erupted between 1869 and the present [62], [73]. Luhr and Carmichael [73] argue that the current eruptive cycle will end with another Plinian eruption, as occurred in 1818 and 1913. Tephrochronologic data for the last ≈ 10 000 years improves the understanding of explosive behaviour of Volcán de Colima [74]. According to this information the volcano is capable of alternating between different types of magma that enter into the upper conduit system, affecting the dynamics of the emplacement of magma and possibly influencing the shape of the conduit system.

In general, identification of petrographic trends requires detailed analyses. For Volcán de Colima, point counted modes, representative mineral analyses, and whole rock major and trace element compositions were obtained for samples of the andesitic lava flows erupted in 1991 and 1998–1999. Together with published trace element data for other andesites erupted in 1869–1982, this permitted the evaluation of compositional changes during the 1818–1913 and 1913–present cycles.

The eruptive cycles of Volcán de Colima are dominated by andesitic lavas with ~ 61 wt% SiO_2, but end with Plinian eruptions (as occurred in 1818 and 1913), involving relatively mafic andesites with ~ 58% SiO_2. Following eruptions of andesitic lava flows with ~ 61% SiO_2 in 1961–1962 and 1975–1976, a trend toward lower SiO_2 contents began in 1976 and peaked in 1981, probably as a small volume of deeper, more mafic magma ascended into the shallower andesitic reservoir beneath the volcano. Since then, andesitic lavas have become progressively richer in SiO_2 through the 1991 and 1998–1999 eruptions. Andesites erupted between 1961 and 1999 show many subtle but important differences compared to those erupted between 1869 and 1913. Based on rocks of similar SiO_2 content, the 1961–1999 andesites are richer in modal plagioclase and in the elements Y, Nb, Tb, Ho, Er, Yb, and Ta, and they are poorer in modal hornblende and in Ba and Sr.

These petrologic observations are consistent with the interpretation that the magmas of 1961–1999 had significantly lower water contents compared to those erupted in 1869–1913, which diminished the role of hornblende crystallization and enhanced the role of plagioclase crystallization. The relatively lower magmatic water contents for the 1961–1999 andesites imply that the explosive eruption anticipated to end the current eruptive cycle will be less powerful than the 1913 eruption. Of equal importance to this question, however, is the role of magmatic degassing. The relatively higher viscosities of andesitic magmas with ~ 61% SiO_2 likely lead to relatively slow ascent rates and more thorough degassing prior to arrival of the magma at the summit crater and its eruption as block lava. In contrast, the lower viscosities of more mafic andesitic magmas with ~ 58% SiO_2 result in faster ascent and greater retention of volatiles, so that they erupt explosively upon reaching the summit crater.

The 1818 and 1913 eruptions provide good models for the end of the current cycle. The magmas erupted in 1869–1913 show many subtle but important differences compared with those erupted in 1961–1999, all of which however, are consistent with the interpretation that the latter evolved with significantly lower water contents than the former. This fact must be considered in any model of the culminating eruption of the current cycle. Because expansion of steam derived from magmatic water is the main propellant of explosive volcanism, it is logical to conclude that the termination of the current cycle will involve eruptions less violent than the 1913 event.

Recent work by Saucedo et al. [72] indicates that magma mixing triggered the 1913 eruption. The eruption was characterized by a mass eruption rate of $\sim 9 \times 10^7$ kg s^{-1} for a total of produced mass of 1.5×10^{12} kg. They also conclude that the events of 1813 and 1913 are quite similar and petrographic and chemical evidences in eruptive products of both eruptions indicate this mixing of magma.

Equally important to the original magmatic water content, however, is the extent of magmatic degassing during ascent toward the surface [70], [75], [76]. For the relatively mafic andesites that were explosively erupted in 1913 (VEI = 4), little pre-eruptive degassing appears to have taken place, as evidenced by a lack of reaction rims on hornblendes with green brown to yellow brown pleochroic colours. In contrast, the lavas erupted in 1961–1999 and especially the hornblende rich lavas erupted in 1869–1880 must have originally had at least 3% H_2O, necessary to stabilize hornblende phenocrysts, but must have lost virtually all of that water prior to reaching the surface. The degassing history of these magmas is illustrated by hornblende phenocrysts with reaction rim from a non-explosively erupted lava sample.

The petrographic analysis of the recent eruption of Volcán de Colima suggest that models of future potential eruptions can be refined, in that the next eruption might be less explosive than the 1913 eruption. In other words, a hazard analysis that used the complete record of explosive and nonexplosive eruptions from Volcán de Colima might overestimate the hazard of the next eruption being explosive, if the interpreted petrologic trends are supported For volcanoes like Volcán de Colima in a geographic region of interest for a nuclear installation, such petrological approach might be used as an alternative model to condition input parameter distributions in simulations of tephra fallout and related processes, which are discussed in Section 5. In many safety assessments, however, models that result in lower estimates of hazard require significant levels of support to ensure that the hazard to a nuclear installation has not been underestimated.

3.3. CONCLUSIONS

Establishing and using alternative tectono magmatic models on a variety of scales is crucial for hazard assessments for nuclear facilities. This step is particularly important for characterization of those volcanic systems that have not been active historically or in the Holocene, because the geologic record in such systems is usually sparse and uncertainty in hazard estimates is high. These models are needed to understand and refine hazards models for volcanic systems nearby a nuclear installation and for far field volcanoes whose products may potentially affect a site. In this section, a range of tectono magmatic models have been presented with the goal of illustrating how such models are used in hazard assessments. Nevertheless, it is emphasized that volcanic systems are complex and varied, and a much broader range of activity is extant worldwide, than is illustrated by these few specific examples. The volcanological literature is replete with additional examples, see [42], [77–79] as starting points.

The data needed for construction of the tectono magmatic model is fundamental, starting from current models of the volcano tectonic setting of the geographic region of interest, which are extant for most potential sites. Refining these models requires detailed volcano stratigraphy, geophysical, geochronological and geochemical data, as described in SSG-21 [1], which can only be acquired through dedicated study.

The phrase “the past is a key to the future” is of particular relevance for diagnostic and forecasting purposes. It is crucial to determine that past patterns of activity are likely to persist into the future or not. This can be accomplished on a variety of scales using diverse methods, as illustrated by the examples used in this section. That said, often alternative models cannot be discounted, and uncertainty about a particular tectono magmatic framework remains. In such cases, successful hazard models will clearly reflect these alternative models of volcanic systems.

4. RECURRENCE RATES

4.1. GENERAL

A probabilistic volcanic hazard assessment requires estimation of the recurrence rate of volcanic activity, here defined as the expected number of volcanic events for a given time interval. Recurrence rate estimates of volcanic events are most often based upon the frequency with which these events (eruptions or other evidence of volcanic unrest) occurred in the past for a specific volcanic system. These estimates are then used to forecast future recurrence rate. For example, shorter term recurrence rates of volcanic activity have been quantified for many volcanic systems [80–85]. Other studies have inferred recurrence rate for longer time periods and sometimes overbroad areas (e.g. [19], [35], [86–92]).

In addition to a probabilistic approach, SSG-21 [1] recognizes that deterministic methods could also be used to assess the potential for future activity from a volcanic system. Deterministic methods normally involve the assumption that future events will occur in the time period of performance of the facility and assess the potential consequences of such events. Empirical methods, sometimes referred to a deterministic, may evaluate the cumulative volume of magma erupted by a volcanic system through time and assume this rate of activity will occur in the future. Time volume trends from these data are used to assess the potential for

future activity from the volcanic system, or to consider the possibility of renewed activity in the future (e.g. [93]), which is an empirical approach without characterization using a probability model. Nevertheless, parameter uncertainty should be evaluated as part of any deterministic assessment.

In all of these cases, a key component of hazard assessment is the estimation of recurrence rates from past activity with the assumption that future rates of activity will reflect this past rate, at least throughout some time scale of interest, such as the performance period of the installation. In other cases, the primary concern is the duration of quiescence, or lack of activity, over a prolonged period of time. Some volcanic systems can be argued to be 'extinct'. That is, there is no credible potential for future eruptions from the volcanic system. Although specific volcanoes certainly go extinct, it is often quite ambiguous whether the system is truly extinct, or merely experiencing a prolonged period of inactivity. Data on the timing of past volcanic events are required and statistical models must be developed in order to assess recurrence rate of activity on anytime scale. This section is concerned with the development of recurrence rate models and the assessment of credible potential for future volcanic activity for volcanoes and volcanic systems within the geographic region of interest.

In the context of site evaluation for nuclear installations, the 'credibility' of a future event often is expressed as the likelihood of occurrence of the event, or the likelihood of an event exceeding some physical characteristic such as magnitude of ground acceleration or flow thickness. Although there is no generally accepted metric for an event likelihood being credible or incredible, many IAEA member states use a likelihood of 10^{-7} year^{-1} as a threshold for considering events with the potential to result in unacceptable radiological releases [1], [94]. Accordingly, probability estimates for volcanic hazards will need to evaluate the recurrence rate of what commonly are referred to as 'rare', 'very infrequent', or 'extremely infrequent' events.

Adopting the nomenclature of [95], consider a sequence of volcanic events (i.e. eruptive events) associated with a volcanic system. An estimation of the current recurrence rate, $\lambda(S,T)$, is derived from the history of the volcano, between times S and T. S might be defined as the age of the oldest event in the entire volcanic system, or the time of onset of some recent episode of activity. T is the time of the youngest event in the sequence, or perhaps the present time. The number of events known to have occurred during the interval between S and T is denoted $N(S,T)$. Assuming the events are independent and that the size of the event is not considered, the probability of renewed eruptions during some time period, u (e.g. the performance period of the nuclear facility) is:

$$\Pr[N(T, t+u) \geq 1] = 1 - exp\left[-\int_T^{T+u} \lambda(t)\, dt\right] \quad (1)$$

Then the probabilistic analysis becomes a matter of estimating the recurrence rate, $\lambda(t)$ at time T. $\lambda(t)$ is also referred to as the intensity of volcanism, or the instantaneous recurrence rate. Most generally, the recurrence rate depends on the history of the volcanic system, H_t [95]:

$$\lambda(t|H_t) = \lim_{t\to\infty} \frac{Pr\big(N(t,t+\Delta t)\big)=1|H_t}{\Delta t} \quad (2)$$

where the history H_t is deduced from the onset times of a sequence of eruptive events t_0, t_1, t_2…, t_n. Alternatively, the history of the volcano can be considered in terms of repose intervals, defined as $r_i = t_i - t_{i-1}$ for $i = 1, 2, \ldots n$. These events may also be considered in terms of eruption

volume, v_i, eruption magnitude or explosivity, m_i, or composition, x_i. Consideration of volume eruption rate is important because some volcanic systems follow a volume time predictable model [81], [93], [96]. Long term trends or cycles in eruption magnitude are also inferred for many volcanic systems [97], [98]. Compositional trends and cycles are also observed in volcanic systems. For example, volcanoes may trend from mafic to silicic compositions through time [99], or show cyclic variations in a narrower range, likely related to long term magma injection [100].

Although this general model structure is straightforward, there is nearly always ambiguity in how events, t_i, and the onset of activity, S, are defined. Historically, the timing of the onset of eruptions is usually reported, but the duration of eruptions is often not reported. This becomes problematic, for instance, when the repose interval between eruptions is short compared to the duration of eruptions. To address this problem, and to attempt to clarify the nature of events, volcanologists use terms such as eruptive phase, to characterize and differentiate one part of an eruptive sequence from another. Eruptive episodes are sometimes defined as sequences of eruptions that are relatively closely spaced in time. In the geological record, it is often difficult to distinguish eruptive phases, eruptions, or eruptive episodes without very high precision geochronology. Often, eruptions are defined in the geological record in terms of mappable units [101]. In practice, it is most important to use a consistent definition of terms such as eruption, eruptive episode, and events when estimating recurrence rate for a volcanic system. The basis for this definition should be clearly established early in the hazards analysis and in supporting documentation.

4.2. DATA REQUIREMENTS FOR ESTIMATING RECURRENCE RATES

Determining the recurrence rate of volcanic activity for a specific volcanic system requires detailed study. The most fundamental data required are geologic maps and stratigraphic studies that may be used to delineate the sequence of eruptive events in the volcanic system. Stratigraphic relationships are often quite complex and ambiguous. Mapping efforts must focus on the identification of individual eruptive units and their stratigraphic relationships.

There are numerous factors to consider at the outset of data collection for recurrence rate estimates:

- For some volcanic systems within the geographic region of interest, particularly those located comparatively far from the site, it may be sufficient adopt a deterministic approach to assume that that eruptions will occur within these systems during the performance period of the facility and to assess the potential magnitude of these eruptions, based on the geologic record and the potential for products of these eruptions to impact the site. This assumption is useful because considerable expense and effort is involved in estimating the recurrence rate of volcanic eruptions. Furthermore, the recurrence rate estimates, even after detailed study, may have considerable uncertainty. There is usually less uncertainty involved in constraining the potential magnitudes of eruptions of a volcanic system and the potential impacts of these hazards. Distant volcanoes, for example, might be screened from further consideration for specific eruptive products, such as pyroclastic density currents or lava flows that occur close to the vent. These volcanoes would be assessed only for tephra fall hazards, which are the most common hazard at distances beyond several tens of kilometres from the vent.

- Similarly, for volcanic systems within the geographic region of interest that have erupted historically, in the Holocene, or show signs of unrest (such as an active hydrothermal system), it may be appropriate to make the assumption that eruptions will occur from that volcanic system during the performance period of the site.

- For many volcanic systems only the most recent volcanic events are known with any degree of certainty. In some cases the timing of these events is known from historical accounts of eruptive activity. For many volcanoes, the most recent eruptive events are the best known, simply because the products of these eruptions mantle the topography and comprise the most accessible rock outcrops. As a result, in the geological literature and volcano databases, often only the ages of the most recent activity have been reported. Conversely, the oldest volcanic units are often not exposed or are unrecognized, so the onset of activity, *S*, and the total duration of volcanic activity are often uncertain and difficult to constrain without subsurface investigations.

- Eruptive data tends to be biased toward the largest eruptive events, simply because these large eruptions leave copious deposits with a greater chance of being preserved and correlated in the rock stratigraphic record. It is often unclear if the youngest ages for volcanic systems are associated with the largest recent eruptions or are significantly younger, as the record of smaller eruptions may go unmapped or may be completely removed by erosion. In addition, some types of large explosive eruptions (e.g. directed blasts) can produce thin, poorly preserved deposits (e.g. [102], [103]), and can also erode underlying deposits. For example, in the characterization of the Bataan NPP site, original dating of deposits of Mt. Natib volcano identified the most recent activity at approximately 60 ka [104]. Later detailed study offshore the NPP site identified much younger primary volcanic units associated with eruptive activity of Mt. Natib at 27–63 ka based on radiocarbon age determinations, and possibly 11.3–18 ka, based on stratigraphic relationships [105]. Discovery of much younger deposits long after initial site characterization led to re-evaluation of volcanic hazards for this facility [106], [107].

- Overall, the number of eruptions identified in the geological record decreases with age. For example, Kiyosugi et al. [108] compiled a database of 696 explosive volcanic eruptions in Japan known to have occurred since 2 Ma. The number of known eruptions of a given magnitude decreases exponentially with age (See FIG. 17). In fact, for this data set, 50% of the total known eruptions occurred since 65 ka. The trend for VEI 4 eruptions indicates that 97% of these eruptions older than 200 ka are missing from the geologic record (i.e. eroded or unrecognized). This same trend exists for even the largest eruptions (i.e. VEI 6 and 7). As the tephra stratigraphy for Japan is among the best known in the world, these figures are a clear indication that recurrence rate estimates based on known events appear biased toward lower rates. Such biases must be accounted for in the hazards analyses, for example by considering a limited time range over which the record may be more complete for eruptions of a given magnitude for frequently active volcanoes in the geographic region of interest.

- Sequences of volcanic eruptions often are, or appear to be, episodic on widely varying time scales [40], [109], [110]. Periods of activity in the volcanic system may persist for tens to thousands of years, with periods of inactivity between episodes of thousands, or even tens of thousands of years' duration. Even longer periods of inactivity appear possible based on the history of some Quaternary central vent systems, however,

erosion and burial of older units make this hypothesis difficult to test. At this time, it does not appear possible to conclude with confidence that a period of inactivity on order of a hundred thousand years reliably predicts the extinction of a longer lived volcanic system. In some distributed mafic vent systems, periods of inactivity between eruptive episode shave persisted for hundreds of thousands of years, or, in some instances, for millions of years. Due to these common gaps in activity, the recurrence rate of eruptions during episodes of increased activity is often much greater than the average recurrence rate (e.g. [93]). Especially for volcanoes that appear to be in prolonged periods of inactivity, analyses may need to consider the likelihood of renewed episodes of volcanic activity, rather than recurrence rate of individual eruptions based on long term averages [93].

- Volcanic systems can have nonstationary recurrence rates. There are documented cases of volcanic systems increasing recurrence rate by one order of magnitude or more. Similarly, volcanic systems may decrease in rate of activity over time (e.g. [101]) in response to regional scale tectonic or magmatic processes.

- Some individual volcanoes or volcanic regions appear to exhibit a frequency magnitude relationship for volcanic eruptions. Large volume eruptions are much less frequent that small volume eruptions in many volcanic systems [85], [111], [112]. These relationships, however, only can be established following detailed investigation of the volcanic system. It currently is not possible to simply estimate or constrain the recurrence of large magnitude volcanic events at a volcano from the general distribution of more frequent, smaller events. Similarly, recurrence rate of the largest magnitude events, in isolation, does not constrain the frequency of smaller magnitude events. This is an important distinction between volcanic hazards and seismic hazards, where Gutenburg-Richter magnitude relationships can help constrain the recurrence of larger events.

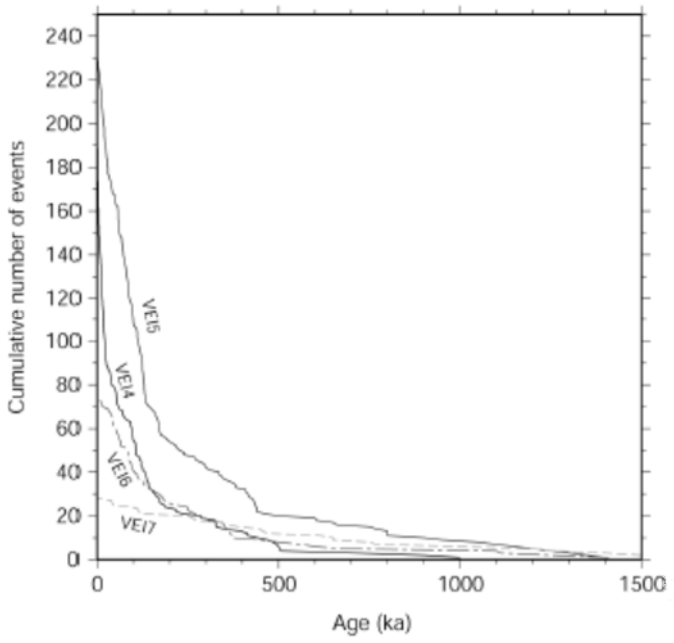

FIG. 17. The number of explosive volcanic eruptions known to have occurred in Japan since 2 Ma, shown by volcano explosivity index, VEI. Assuming stationarity, the decrease in frequency of explosive eruptions within increasing time into the past indicates that many

eruptions are missing from the geologic record. Note particularly that VEI 5 eruption deposits in the stratigraphic record are more commonly identified than VEI 4 eruption deposits. This feature of the database suggests that either eruptive deposits, particularly the smaller volume VEI 4 deposits, are eroded away, are unrecognized, or are misclassified as larger magnitude events. This creates bias in recurrence rate estimates.

Given these realities, even with the most detailed mapping, the stratigraphic sequence of activity at volcanoes is generally incompletely known. This leads to uncertainty in recurrence rate estimates of volcanic activity which may span several orders of magnitude. This incomplete record biases the recurrence rate estimate to lower values, as undetected events have not been included. It is a typical experience that long term, detailed study of volcanic systems reveals additional evidence of the frequency of volcanic eruptions, which invariably increases the estimated recurrence rate of events. For example, prior to the 2008 eruption of Chaitén volcano, Chile, this volcanic systems was considered to be long dormant, perhaps not having erupted since 9 ka. Following the 2008 eruption there was renewed interest in stratigraphic studies of the volcano, which revealed more frequent Holocene activity than known previously [4], [113], [114].

4.3. STEPS IN RECURRENCE RATE ESTIMATION

Given the complexities of recurrence rate estimation, the following steps are suggested in determining the recurrence rate of activity for volcanic systems.

4.3.1. Step 1

Identify, to the extent possible, all eruptive units in the volcanic system. This may include mapped units and additional units identified through stratigraphic studies. In some cases, drilling the stratigraphic section in key areas is warranted as a means of identifying a more comprehensive range of activity. Lacustrine and ocean drilling studies often complement the subareal eruption record, particularly for volcanic islands where much of the eruptive products have been deposited offshore (e.g. [115]). A crucial task is to differentiate between products of eruptions that are widely separated in time, versus those representing a single eruptive event.

For many models, volumetric information is needed. These volume estimates typically involve interpolation of eroded units between characterized stratigraphic sections. A critical point in this analysis is quantification of uncertainty in these volume estimates, particularly for pyroclastic deposits and for older deposits that are buried and not readily expressed at the surface. These uncertainties might be small for the youngest, best preserved deposits, whereas volume uncertainties might be appreciable for older units. The uncertainty analysis should account for preservational bias in the geologic record.

4.3.2. Step 2

Identify or infer the total duration of volcanic activity within the volcanic system, through recognition of the oldest and youngest stratigraphic units.

4.3.3. Step 3

Determine all stratigraphic relationships possible. Essentially, for each known unit, several states may exist. The unit may be:

1. Bounded stratigraphically by older and younger units or unconformities (e.g. presence of soil horizons, erosional surfaces, or non volcanic deposits).

2. Not bounded stratigraphically. That is, the stratigraphic relationship between the mapped unit and any other unit cannot be determined.

3. Stratigraphically bounded only by a younger or older unit.

In additional to these stratigraphic relationships, additional data should be gathered including rock magnetic data for comparison with the magnetic polarity time scale, and morphological information, for example, through identification of glacially eroded units. Particular attention is needed in incised terranes, where younger units might occur at lower elevations than older units.

4.3.4. Step 4

Age determinations for specific eruptive units are identified from the literature or samples for new age determinations gathered and analysed. A variety of age determination methods might be used, depending on the inferred age and composition of samples. These include, but are not limited to, radiometric age determinations such as ^{14}C, Ar/Ar, and K/Ar. These methods yield mean age determinations and reported analytical uncertainty in age determinations. Age determinations are often made on bounding units, such as charcoal age determinations in paleosols bounding the eruptive unit. If data are used from the literature then it is essential that the exact eruptive unit, sample location and analytical method and uncertainty be known and reported. Care must be taken to ensure that the analytical date represents the geologic age of the event (e.g. presence of inherited material; [116]).

In general, it is useful to radiometrically date as many stratigraphic units as possible. This may involve tens to hundreds of radiometric age determinations, a process that may require several years' effort because of the considerable laboratory time required to date individual samples. Of course, the stratigraphic relationships identified in Step 3 are very useful in prioritizing age determinations. In particular, stratigraphically youngest and oldest units generally receive high priority. Care should be taken to appropriately characterize the period of eruptive activity that will be used to develop or constrain the recurrence rate models. Due consideration should be given to characterize occurrences of eruptive phases, episodes, or apparent changes in the character of eruptive activity through time. Units bounding specific stratigraphic packages of eruptive vents may also receive high priority, while stratigraphically bounded units may receive lower priority. Units that are not bounded stratigraphically should receive high priority, particularly if these units are not modified by erosion and are of normal magnetic polarity.

4.3.5. Step 5

The inferred stratigraphic sequence and age determinations are verified. This might be achieved through development of age charts, showing the ages of units and their stratigraphic and paleostratigraphic relationships (See FIG. 18). The goal of this verification process is to identify and resolve ambiguities in the stratigraphic sequence and potential range of ages of individual events. This may involve the development of statistical models of ages for individual units. For example, radiometric age determinations generally have Gaussian uncertainty associated with the analytical method. Units bounded by two dated units might be assigned an age according to a uniform random distribution, bounded by the ages and

associated uncertainties of the two dated units. Nondated units with no known stratigraphic relationship could have any age (again a uniform random distribution) bounded by the oldest possible age of the volcanic system and the youngest possible age of such an eruption (e.g. the beginning of the historical record in the region).

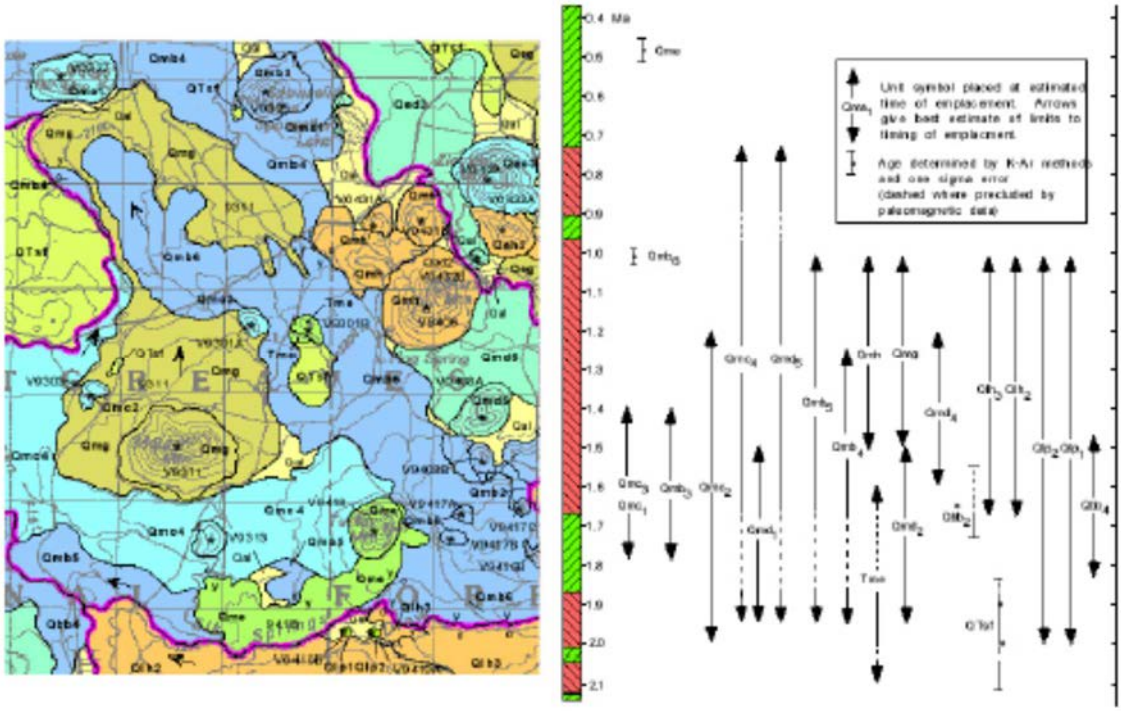

FIG. 18. Age chart of timing of mapped eruptive events in the Springerville volcanic field, Arizona (from [101]). The geologic map relationships, stratigraphic relationships, radiometric age determinations, and paleomagnetic stratigraphy are used to constrain the ages of each known eruptive unit, to illustrate the uncertainty in these ages. Reproduced courtesy of the Geological Society of America [101].

Of course, at any stage in this five step process it may be necessary to return to an earlier step and gather additional data or re-evaluate the data based on new information. Development of the stratigraphic sequence for a volcano is usually a highly iterative process.

Always, in addition to the analytical uncertainty associated with the dates, ambiguity will remain in terms of the sequence of events and the timing of these events. This means that different sets, t_0, t_1, …, t_n can be developed for the same volcanic system, and use of these alternative sets will result in variation in the recurrence rate estimate, $\lambda(t)$ (EQ. (1)). It is critical to consider the impact of these alternative sets of sequences of events on the recurrence rate estimate, which is often more substantial than the impact of choice of a statistical model of recurrence rate. One approach is to consider extreme values of the timing of sequence of events, another is to sample alternative sequences of events using Monte Carlo methods [92], [117].

Once these steps are accomplished, and a set or sets of potential eruption sequences (t_0, t_1, …, t_n) are defined it is possible to make recurrence rate estimates using a variety of statistical approaches, as summarized in the following.

4.4. STATIONARITY

Whether or not some statistical models (e.g. Poisson, Pareto, Weibull, Log-logistic) can be applied to estimate recurrence rate and probability of eruption within a given time period for a given set of eruption sequences depends on determining if this sequence is stationary or nonstationary. Often stationarity may be present in eruption sequence data over some time period, say the Holocene record, and the same data set may appear to be non stationary over a longer time period. Nonstationarity may reflect sampling bias, as described previously, or may reflect the episodic nature of volcanic eruptions in some systems. Bebbington [95] defines eruption regimes to distinguish between long term episodic behaviour and changes in rate of eruptions over the long term.

Bebbington [95] recommends the Kolmogorov-Smirnov test for stationarity, because usually there are few events comprising the eruption sequence and because the test is simple. For the cumulative number of volcanic events in the sequence:

$$F_n(t) = \frac{\#(t_i \leq t)}{n}, i = 1 \ldots n, s < t < T \quad (3)$$

then the Kolmogorov-Smirnov test statistic is:

$$D_n = \max_{t \in [S,T]} \left[\left| F_n(t) - \frac{t-S}{T-S} \right| \right] \quad (4)$$

In other words, in the Kolmogorov-Smirnov test statistic, the maximum deviation from the expected frequency of events determines whether the process is stationary or not. For relatively few events, almost always the circumstances in volcano repose interval estimates, the 95% confidence bounds are given as $1.36/\sqrt{N(S,T)}$

Consider the history of eruptions at Cerro Negro volcano, Nicaragua, since its formation in 1850 [81]. The cumulative distribution function for Cerro Negro eruptions shows statistically significant nonstationarity, barely, based on the Kolmogorov-Smirnov test at the 95% confidence level (See FIG. 19). Eruptions prior to approximately 1947 occurred at a significantly lower rate than subsequent eruptions. This suggests that a change in eruptive regime occurred at Cerro Negro at approximately this time, and a different recurrence rate applies to these two different regimes. However, time volume relationships at Cerro Negro remained steady state throughout most of the eruptive history [81]. Even for a historically active volcano such as Cerro Negro, small eruptions that didn't produce tephra falls on surrounding farms were likely underreported prior to the large 1947 eruption. Subsequent interest in Cerro Negro eruptions increased efforts to monitor the volcano more closely, which likely leads to the apparent bias in the distribution of 29 reported events.

4.5. STATISTICAL MODELS

Numerous statistical models have been applied to describe patterns of volcanic activity through time. These models include classic Poisson models, Weibull, Pareto and others where volcanism can be described as steady state. More complex models are invoked to describe waxing or waning rates of volcanism, which are observed in many well studied volcanic systems [101], [118]. The Weibull-Poisson model and Weibull renewal model have been applied [82], [84], [86] where waxing or waning volcanic activity is particularly important. For example, Ho [83] analysed cyclic temporal patterns of some volcanic events of Avachinsky volcano (Russia) with time series analysis techniques and forecast the number of new events

for the next 25 years. This approach is similar to time series analysis methods applied by Varley et al. [119] to time series of volcanic events at Colima (Mexico), Karymsky, (Russia), Erebus (Antarctica), and Tungurahua (Ecuador) volcanoes. Alternative parametric models have been applied to a number of volcanic systems. These include modelling series of eruptive events using log logistic model [97], [120] and Pareto model [121]. Turner et al. [84] used nonparametric kernel estimates to estimate the recurrence rate of volcanic activity for Mount Taranaki, New Zealand. Similarly, variogram methods have been used to identify statistical structure in time series of volcanic events, thereby improving recurrence rate estimates for short term (e.g. [122]) and long term [123] hazard assessments. See [95] for a review of the statistical basis for many of these recurrence rate models.

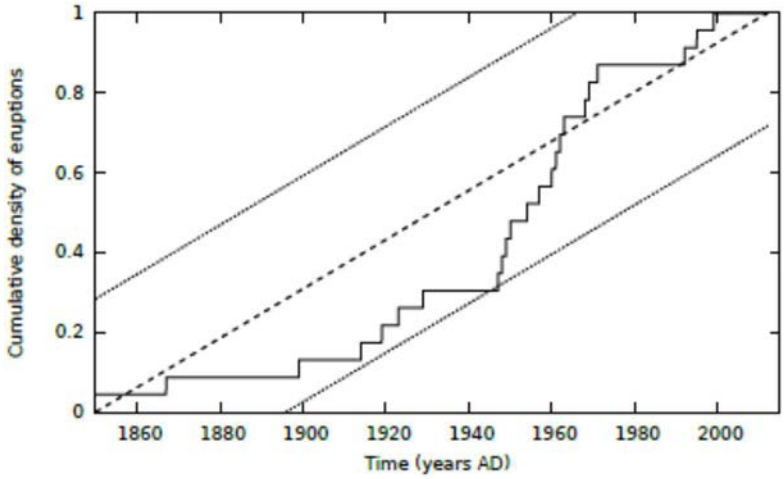

FIG. 19. Cumulative distribution function for eruptions of Cerro Negro volcano, Nicaragua, since its formation in 1850 (solid line). The dashed line indicates a steady state temporal model with the confidence interval for this steady state model shown by finer dashed lines. The Kolmogorov-Smirnov test indicates that this series is nonstationary, with eruptions occurring (or being reported) at a significantly increased frequency after approximately 1947. For this series, $\boldsymbol{N(S,T)}$ *= 23, and* D_n *= 0.29.*

Although recurrence rate is basically estimated using the number of volcanic events in a specific time range, some alternative calculation methods have been proposed. The simplest approach is to average the number of events that have occurred during some arbitrary time period [86], or between the oldest and youngest events in an eruptive episode. For example, Martin et al. [35] used the number of Quaternary volcanoes located in the Tohoku volcanic arc to estimate the long term hazard of new volcano formation within that arc. An alternative approach, especially appropriate when the total number of known events is small, is to calculate recurrence rate using the repose time method, in which the time range is restricted by the estimated ages of youngest and oldest events [86]:

$$\widehat{\lambda_t} = \frac{N-1}{S-T} \qquad (5)$$

where $\widehat{\lambda_t}$ is the recurrence rate, N is the number of events, occurring between S, the age of the first (oldest) event, and T, the age of the most recent (youngest) event. To use this approach, however, there must be a high degree of confidence that the youngest and oldest events are known. If a subset of the geologic record is used, justification is required to ensure that the selection of the time interval is reasonable and appropriately captures the range of eruptive behaviour that is thought to represent potential future events. Arbitrary time periods, or periods selected solely because of data availability, often bias the recurrence rate estimate.

If the distribution of repose intervals in a volcanic system shows Poisson behaviour, then the probability of a given number of events, k in some time interval u is:

$$P_r[N(t+u) - N(t) = k] = \frac{e^{-\lambda_t u}(\lambda_t u)^k}{k!}, k = 1 \dots n \quad (6)$$

and the probability of zero events in the time interval, u, is:

$$P_r[N(t) = 0] = e^{-\lambda_t u} \quad (7)$$

indicating that repose intervals between eruptive events have an exponential distribution, a fact useful in testing whether an eruption sequence is Poissonian or not.

If the eruption sequence can be described as Poissonian, then the constant recurrence rate, λ_t or the mean repose interval, $\mu = 1/\lambda_t$, can be estimated from the sequence of known eruptions, The 90 % confidence interval of the repose interval of a sequence of eruptions is:

$$P_r\left\{\frac{2\sum_{i=1}^{N} r_i}{x^2_{2\,N,\alpha=0.95}} < \mu < \frac{2\sum_{i=1}^{N} r_i}{x^2_{2\,N,\alpha=0.05}}\right\} = 0.90 \quad (8)$$

which states that the mean repose interval has a probability, P_r, of occurring within some interval, based on a x^2 distribution with $2N$ degrees of freedom, at a given confidence level, α, and μ is the mean repose interval. N is the total number of units sorted by age. γ_i is the repose interval before i^{th} unit [25].

In a nonhomogeneous Poissonian model, the recurrence rate is allowed to vary with time, $\lambda_t(t)$.

$$\lambda_t(t) = M(t) \quad (9)$$

so that:

$$P_r[N(t+u) - N(t) = k] = \frac{e^{-M(t)u}(M(t)u)^k}{k!}, k = 1, \dots, n \quad (10)$$

For a nonhomogeneous Poisson model with a power law distribution:

$$M(t) = \alpha t^{\beta} \quad (11)$$

and the probability is:

$$P_r[N(t+u) - N(t) = k] = \frac{e^{-\alpha t^{\beta} u}(\alpha t^{\beta} u)^k}{k}, k = 1, \dots, n \quad (12)$$

In this case the parameters α and β must be estimated in order to use the distribution, usually using iterative fitting techniques.

Given this framework, alternative statistical models can be constructed to account for alternative interpretations of recurrence rate for an eruption sequence, *t*, or repose intervals, *r*. In the case where *t* is defined as the time elapsed since the last eruption, the recurrence rate $\lambda_t(t)$ is equivalent to the hazard function. For example, for a log logistic model [120]:

$$F(t) = \frac{1}{1+(t/\alpha)^{\beta}} \; t > 0, \alpha > 0, \beta > 0 \tag{13}$$

$$f(t) = \frac{(\beta/\alpha)(t/\alpha)^{\beta-1}}{\left(1+(t/\alpha)^{\beta}\right)^2} \tag{14}$$

$$\lambda_t(t) = \frac{f(t)}{1-F(t)} = \frac{(\beta/\alpha)(t/\alpha)^{\beta-1}}{1+(t/\alpha)^{\beta}} \tag{15}$$

Similarly, for a Weibull statistical model:

$$\lambda_t(t) = \alpha\beta(\alpha t)^{\beta-1} \; t > 0, \alpha > 0, \beta > 0 \tag{16}$$

and for compound exponential:

$$\lambda_t(t) = \frac{\beta}{t+(\beta/\alpha)} \; t > 0, \alpha > 0, \beta > 0 \tag{17}$$

Numerous other distributions can be defined. Dzierma and Wehrmann [110] and Bebbington [95] recommend comparing models using the Akaike Information Criterion. This is extremely useful for comparing different statistical models when the eruption sequence is precisely known, or can be rigorously sampled. In practice, there may be insufficient information available to distinguish among these different statistical models. Usually a simpler (e.g. one parameter) model is justified over more complex (e.g. two parameter) models if the major uncertainties are geological, and lie with the determination of the eruption sequence.

4.6. EXAMPLE FROM THE YUCCA MOUNTAIN VICINITY, NEVADA, USA

The recurrence rate of volcanic activity in the Yucca Mountain vicinity of Southern Nevada, the proposed site of a high level radioactive waste geological repository, provides an example of hazard estimation where many radiometric age determinations are reported. Basaltic rocks of Pliocene and Quaternary age erupted briefly and sporadically in the Yucca Mountain vicinity, generally as volumetrically minor flows and cinder cones [124]. Larger volumes of similar composition basalt also erupted between 5–10 Ma, following a period of silicic caldera activity. A total of 223 dates for approximately 10 volcanoes are available in the Yucca Mountain region for Plio-Quaternary volcanoes with surface expression, including K/Ar dates [124], Ar/Ar dates [125–128], U-series isochron ages [127], ^{3}He surface exposure ages [129] and ^{36}Cl surface exposure ages [130] (See FIG. 20 a – FIG. 20 c). Thus, many volcanoes have multiple reported radiometric age determinations. For example, 76 radiometric age determinations are reported for Lathrop Wells volcano alone.

Several different interpretations are possible in defining what feature constitutes a volcano in this long lived system. Although individual vents can be readily determined, erosion and burial has obscured many important field relationships that would help determine if

multiple basaltic vents formed during a single eruptive episode, or were the product of temporally distinct eruptions. A simple vent count, for example, could yield at least 16 individual vents that might represent discrete eruptions (cf. [124]). In addition, 5 Pliocene vents are buried beneath alluvium in the southern part of the field and are poorly characterized. For the purposes of their analyses, Kiyosugi and Connor [117] interpreted 10 individual volcanoes as independent eruptive events.

In addition, basaltic systems typically form alignments of scoria cones during a single eruptive event. In the Yucca Mountain vicinity, Quaternary volcanoes in Crater Flat form an alignment that might represent a single volcanic event. In one model of recurrence rate, Kiyosugi and Connor [117] considered these scoria cones as a single, contemporaneous event, leaving a total of six Plio-Quaternary events for their analyses (See FIG. 20 d – FIG. 20 f).

The large number of radiometric age determinations, and their analytical uncertainties, create alternative eruption sequences for Plio-Quaternary events (that is, 5.3 Ma to the present). The timing of eruptions within these sequences is further constrained by paleomagnetic stratigraphy [125], [126]. Kiyosugi and Connor [117] studied the impact of these alternative data sets on estimates of recurrence rate, using a simple model for the local recurrence rate. Each eruptive unit, *e*, is assigned a cumulative number (1,2,3, …, $N(S,T)$), where *N* is the total number of units sorted by age. Recurrence rate λ_t at the time period of interest between i_{th} and $(i+1)_{th}$ units is calculated with the oldest and the youngest ages of arbitrary number of *n* events around that time, with *n* assigned to be an even number:

$$\lambda_t = \frac{e_{i+(n/2)} - e_{i-(n/2)+1}}{T_{i-(n/2)+1} - T_{i+(n/2)}} \tag{18}$$

where $T_{i-(n/2)+1}$and $T_{i+(n/2)}$ are the oldest and youngest ages of *n* events and $e_{i+(n/2)}$ and $e_{i-(n/2)+1}$ are their cumulative number of events. In this approach, *n* is a local window, corresponding to a time during which the recurrence rate is considered to be constant.

For the Yucca Mountain region, the estimated recurrence rate changes with the number of independent events (6 or 10) and the local window, *n*, used to estimate recurrence rate. With a small local window, $n = 2$, a peak in recurrence rate occurs between 3–6 Ma, followed by a minimum in recurrence rate around 2 Ma. These fluctuations are averaged and disappear with a larger local window ($n = 4$, See FIG. 20 b). In addition, another higher peak in recurrence rate occurs since about 1 Ma. This peak is visible for all calculations using N ($S = 5.3$ Ma, $T = 0$ Ma) = 10, and for N ($S = 5.3$ Ma, $T = 0$ Ma) = 6 using a small local window, $n = 2$ (See FIG. 20 a – FIG. 20 d). For $N = 6$ events and larger local windows, this peak in recurrence rate after1 Ma is averaged out and disappears ($n = 4$, See FIG. 20 e). These results suggest that the local window, *n*, and the number of independent events, *N*, influence recurrence rate estimates.

Current cross section of recurrence rate of small volume basaltic volcanism is estimated as an example of uncertainty of recurrence rate at a specific time period. Based on the results of the Monte Carlo simulation and using a local window of $n = 4$, the current recurrence rate of the Yucca Mountain vicinity is 3.2–6.4 events/million year (5–95th percentile) using $N = 10$ independent events, and 0.9–1.2 events/million year (5–95th percentile) using 6 independent events [117]. For smaller local windows there is more fluctuation and much greater uncertainty. A larger local window reduces the uncertainty and greatly smooths the change in recurrence rate with time. In the Yucca Mountain vicinity, because there are relatively few events, uncertainties are relatively small for individual models (See FIG. 20 a, FIG. 20 b, FIG.

20 d and FIG. 20 e). Nevertheless, there is significant model uncertainty, resulting in a broad range of recurrence rates when models that make different assumptions about the local window, n, and the number of independent events, $N(S,T)$, are compared.

The significance of these variations in recurrence rate can be assessed using a X^2 test. In this case, the X^2 test suggests sampled eruption sequences are reasonably explained by a homogeneous Poisson behaviour. This means that the apparent variations in recurrence rate can be explained as random variation around a mean recurrence rate. Therefore, the current recurrence rate can be estimated from the confidence interval of mean repose interval of data set sampled in each sequence of eruptions (See EQ. (8)). The upper and lower boundaries of confidence interval for recurrence rate for a total of 10 000 eruption sequences are: For 10 events, lower = 0.5–1.2 events/million year and upper = 1.5–3.8 events/million year; for 6 events, lower = 0.3–0.5 events/million year and upper = 1.3–2.5 events/million year (See FIG. 20 c and FIG. 20 f). The mean confidence interval of recurrence rate ranges 1.0–3.2 events/million year using $N = 10$ independent events and 0.4–2.0 events/million year using $N = 6$ independent events. There is no evidence that volcanism has ceased in the Yucca Mountain vicinity. Rather, it appears to persist at a low rate, which can be modeled as constant during the Quaternary [117].

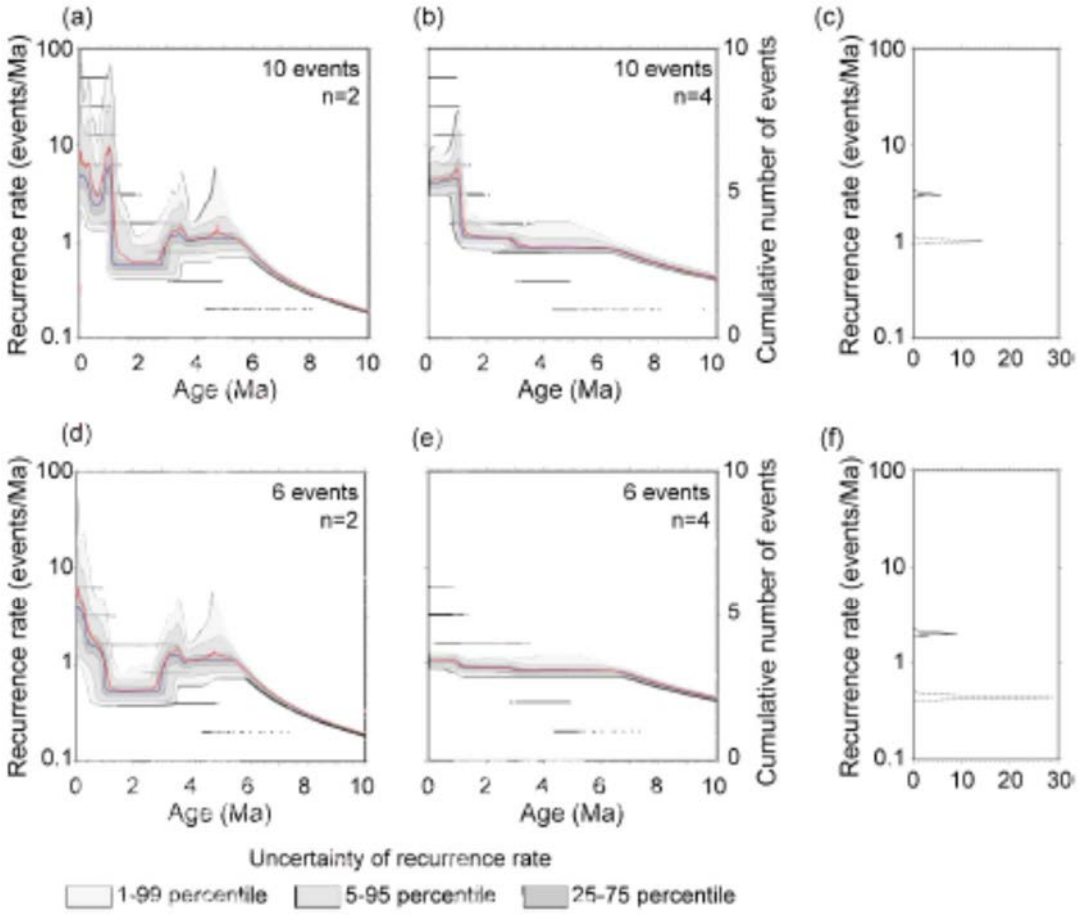

FIG. 20. Result of 10 000 recurrence rate simulations for the Yucca Mountain region, from [117]. Black dots show sampled ages for the sets of eruption sequences. Shaded areas show 1–99th, 5–99th and 25–75th percentile range of the calculated recurrence rate. Red and blue solid lines show mean and median recurrence rates respectively. (a) N (S = 5.3 Ma, T = 0 Ma) = 10 events, n = 2, (b) 10 events, n = 4, (c) Probability distributions of upper (solid line) and lower (dashed line) boundaries of 90 % confidence interval for 10 000 eruption sequences calculated with 10 events, (d) 6 events, n = 2, (e) 6 events, n = 4, (f) Probability distributions of upper (solid line) and lower (dashed line) boundaries of 90% confidence interval for 10 000 eruption sequences calculated with 6 events.

4.7. EXAMPLE FROM VOLCANIC ACTIVITY IN THE ARAGATS VOLCANIC SYSTEM, ARMENIA

Volcanic hazard estimates for the ANPP involve assessment of the probability of future eruptions from the long dormant Aragats volcano, a large volume volcano complex located within the geographic region of interest about the ANPP site. Based on development of a conceptual model of volcanism at Aragats and the surrounding region, several features salient to the volcanic hazard assessment for the ANPP site emerge. First, although rates of volcanic activity in the region are low compared to active arcs around the world, there is no basis for assuming that volcanism could not occur in the future within the region. Over the last ≈ 1 Ma (which covers the periods of activity and inactivity at Aragats), there is no evidence from geochemical or tectonic data and models of any significant shift in the nature of magmatism.

Rather, the region is characterized by infrequent eruptions of relatively volatile poor hot magmas. Second, although there are differences in the details of the magma geochemistry among eruptive units across the region and through time, basically, all of the region analysed can be characterized in terms of a single magma source region. This suggests that the types of eruptions that have occurred in the early Middle Pleistocene, including summit eruptions of Aragats, flank eruptions, and eruptions of monogenetic volcanoes in the Shamiram plateau, are all conceivable in the future. In the parlance of the IAEA guidelines on volcanic hazard assessment, the Aragats volcanic system, including monogenetic vents of the Ararat Depression, is considered to be capable of future volcanic activity, although the probability of such activity during the lifetime of the ANPP is low.

The stratigraphy of Aragats suggests that activity in the Aragats system has waned since approximately 490–800 ka, which is bracketed by the eruptions of two flank vents, Pokr Bogutlu and Irind, respectively. Volume time relationships (i.e. the estimated volume of magma erupted over a period of time) can be used to frame arguments about the potential for future eruptions, given this observed change in recurrence rate. For example, Chernyshev et al. [18], [131] suggested that Aragats volcano is extinct because of the lack of known activity in the Late Pleistocene and Holocene. Their conclusion, however, appears to be at odds with the lack of geochemical variation in the system or explanation as to where magmatism shifted given the lack of change in the overall tectonic setting. Volume time relationships are considered in the following discussion, in light of new radiometric age determinations, volume estimates for significant episodes of volcanism, and basic probability models.

A significant difficulty in analysing volume time relationships is that much of the record is inaccessible, buried by subsequent volcanic activity. This is the case at Aragats, where most of the surface is covered by the products of Middle Pleistocene eruptions. Therefore, estimation of eruptive volumes is restricted to Middle Pleistocene units. TABLE 3 shows the ages and volumes of known episodes of volcanism during the Middle Pleistocene.

Episodes of volcanic activity are defined here for the purpose of characterizing volume time relationships instead of individual eruptions, because of the high uncertainty about the timing of many individual eruptions. Episodes comprise geological units that are described the geologic map of the volcano. Volumes of these episodes are determined by interpolating the areas and thickness of geological units from outcrop distribution. Even for well exposed units, this interpolation may lead to errors of 50 % or more.

Irind is the youngest known eruptive episode of the Aragats system and included the eruption of ignimbrites and lavas. This volume represents the volume of lavas, as the ignimbrites are completely eroded except where they are welded in the near vent region or preserved beneath the lava flow. Summit plateau andesite includes the stratigraphically highest map units, which have been K/Ar dated. The volume of older Middle Pleistocene lavas that erupted in the summit region is uncertain, but these may be substantially larger in volume than the younger summit lavas. The volumes of the Artik and Yerevan tuffs are estimated by interpolation between widely separated outcrops. Lavas of the Shamiram plateau are considered as a single unit, using the age of Shamiram volcano, although this monogenetic cluster formed from dispersed eruptive activity over an extended period of time (> 600 ka, based on the age of dated lava flows near Echmiadzin crater). All of the youngest cinder cones and lava flows on the Shamiram plateau are older than the Yerevan tuff, with the exception of Dashtakar (volume of 0.03 km^3), which is radiometrically dated as the same age as the Yerevan tuff, within uncertainty. The Paros episode includes several lava flows on the north and

northwest flank of Aragats erupted from four flank vents. These events are K/Ar dated to be 740 ka or older. Thus, there is considerable uncertainty about the volume and timing of episodes, but these estimates broadly describe voluminous Middle Pleistocene activity.

TABLE 3. DATA USED TO ESTIMATE TIME VOLUME RELATIONSHIPS IN THE ARAGATS SYSTEM (800 ka–present) Reproduced courtesy of the Ministry of Energy and Natural Resources of the Republic of Armenia [10]

Episode	Volume (km^3)	Age (ka)	Description
Irind pyroclastic eruption and lava flow	3.6	490	Ar/Ar age determination, dacite
Ashtarak lava flow	0.5	500	K/Ar age determination, trachybasalt
Andesites of summit plateau	0.21	530	K/Ar age determinations, andesite trachyandesite
Artik tuff	0.80	600	Approximate age based on stratigraphic position (between Yerevan tuff and Ashtarak flow), trachydacite
Tirinkatar lava flow	0.58	614	Ar/Ar age determination, trachyandesite
Yerevan tuff	5.3	650	two Ar/Ar age determinations, volume extrapolated from mapped deposit
Shamiram Plateau	23.7	640–870	Ar/Ar and K/Ar age determinations on Shamiram plateau volcanoes
Paros	1.3	740	lava flows on N-NW Aragats (Arich, Barcradir, Mets Mantash, Paros), K/Ar determination and stratigraphy, trachyandesite
Cakhkasar flow (Pokr Bogutlu)	18.2	750	Ar/Ar age determination, trachydacite

FIG. 21 plots the variation in erupted volume with time, separating episodes that are dominantly trachybasalts andesites from trachydacites. From the available data, a clear change in eruption rate occurred after approximately 500 ka, with a total of nine episodes known to have occurred between 800 ka and 490 ka, and no known eruptions since that time. Conversely, no clear trend in volume is apparent in eruptive activity between 800 ka and 490 ka. The Cakhkasar flow from Pokr Bogutlu is the largest volume trachydacite episode and the oldest, but the Yerevan tuff and Irind episodes are of comparable volume.

Similarly, the Ashtarak and Tirinkatar lava flows are comparatively young, large volume events. Presumably, a large number of radiometric age determinations on lavas of the Shamiram plateau would distribute the volume of this volcanic cluster over a period of several hundred thousand years.

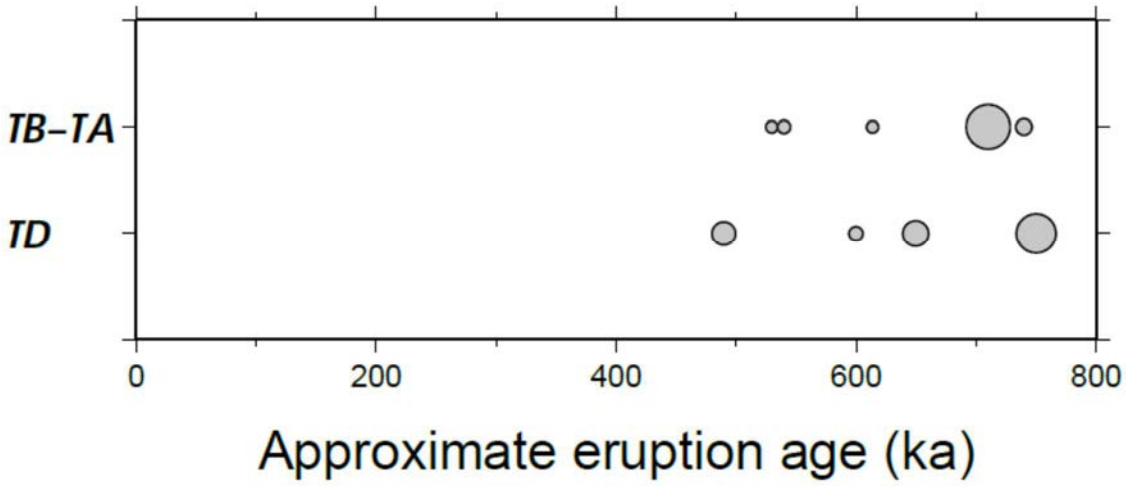

FIG. 21. Volume time relationships for erupted trachybasalts andesites (TB-TA) and trachydacites (TD) in the Aragats volcanic system, 800 ka to present. Circles represent eruptive episodes (See TABLE 3); circle diameter is directly proportional to the cube root of estimated volume. Reproduced courtesy of the Ministry of Energy and Natural Resources of the Republic of Armenia [10].

Using the data shown in TABLE 3, eruptive episodes in the Aragats volcanic system appeared to be well described as a stationary process between approximately 490 ka and 800 ka. Since that time, there appears to have been a change in eruptive regime, with no known eruptions since approximately 490 ka (See FIG. 22). A conceptual model of volcanism must reconcile the lack of significant eruptive volume since 490 ka (perhaps lack of any eruptive activity whatsoever) with the lack of geochemical indicators of a waning system in Middle Pleistocene eruptive products, continued activity in nearby volcanic systems, and absence of discernible changes in either the local or regional tectonic setting. Connor et al. [10] concluded that these features indicated that future eruptions from the Aragats volcanic system could not be precluded, and that recurrence rate models should be developed to account for this potential. Furthermore, given the recognition of Pliocene and early Pleistocene stages of volcanism, albeit very poorly resolved, Connor et al. [10] determined that comparable gaps in activity might have occurred in the volcanic system in the past, and that the system could be currently experiencing such a gap.

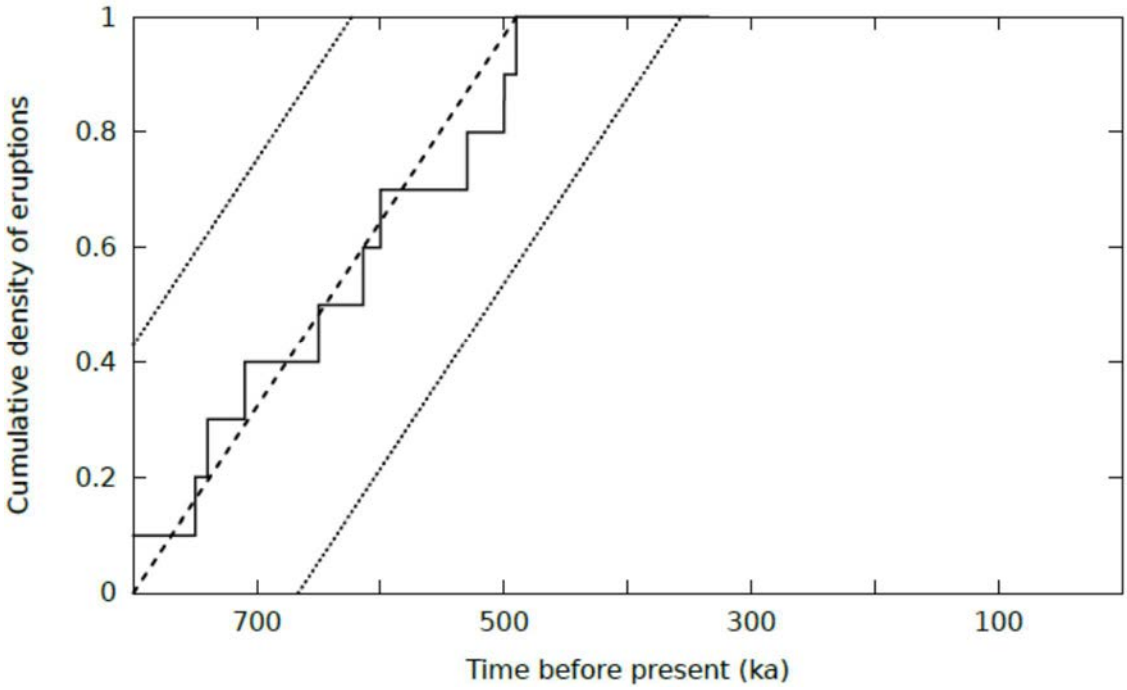

FIG. 22. Cumulative density function for eruptive episodes at Aragats volcano (solid line), shown with steady state model for volcanism from approximately 800 ka to 490 ka (dashed line), with uncertainty bounds based on the Kolmogorov-Smirnov statistic. The lack of known activity since 490 ka indicates a change in the eruptive regime, with > 95 % confidence. Reproduced courtesy of the Ministry of Energy and Natural Resources of the Republic of Armenia [10].

If one considers the episodes of volcanism illustrated in FIG. 21 and described in TABLE 3 to be realizations of a random process, then the maximum likelihood estimate of recurrence rate, $\hat{\lambda}$, for episodes of volcanism using a homogeneous model is

$$\hat{\lambda} = \frac{N-1}{S-T} \tag{19}$$

where N is the number of episodes, S is the age of the oldest episode, and T is the age of the youngest episode. During the time period 490–800 ka, the estimated recurrence rate for trachydacite episodes is calculated to be $\hat{\lambda} = 1 \times 10^{-5}$ episodes per year, for trachybasalts andesites, $\hat{\lambda} = 2 \times 10^{-5}$ episodes per year, and for all episodes combined, $\hat{\lambda} = 3 \times 10^{-5}$ episodes per year.

Consequently, assuming a Poisson probability distribution and given a Middle Pleistocene recurrence rate of $\hat{\lambda} = 3 \times 10^{-5}$ episodes per year for all episodes combined, what is the probability that no volcanic events would have occurred since 490 ka? The probability of no events during this time period is given by:

$$P[N = 0] = exp\left[-\hat{\lambda}\Delta t\right] \tag{20}$$

with Δt = 490 000 year and $\hat{\lambda} = 3 \times 10^{-5}$ episodes per year. This yields a probabilityof no events since 490 ka, of $\hat{\lambda} = 2 \times 10^{-7}$. This probability is so small that, if these episodes are indeed independent, the recurrence rate of volcanism must have decreased significantly since 490 ka, confirming results of the Kolmogorov-Smirnov test. Alternatively, the geochemical

model of the Aragats system suggests that there are no major differences in the source regions of lavas and ignimbrites, and that trachydacitic magmas evolve from more mafic magmas by fractional crystallization. Therefore, episodes of activity may be better represented by the comparatively voluminous eruptions of trachydacites alone, with trachybasalt andesite eruptions occurring as part of this same sequence of activity, rather than trachybasalt andesite eruptions occurring as independent events. Reducing the total number of episodes to four, yields a probability of no events since 490 ka, of $\hat{\lambda} = 3 \times 10^{-2}$. As a result, one can conclude with some confidence that the recurrencerate of volcanism has changed since 490 ka, but the dramatic change in probability reveals the sensitivity of this analysis to assumptions about the independence of events.

Given that a change in recurrence rate occurred at approximately 490 ka, what then, is a reasonable estimate of the present recurrence rate? One model is that the present recurrence rate is zero, that the volcanic system is extinct. On the other hand, an alternative conceptual model is that future volcanism is possible, but the recurrence rate of activity is lower than the rate from approximately 490 ka to 800 ka. One generally accepted approach to evaluate alternative conceptual models is by using a logic tree, where each alternative model is weighed by the likelihood that this model accurately represents the process being modelled. The weighing scheme and appropriate number of conceptual models to use in the logic tree depends heavily on expert judgment. Nevertheless, the logic tree approach provides a traceable methodology to consider alternative conceptual models in the hazards analysis and to document the rationale for significant parameters. Here, a logic tree approach (e.g. [132], [133]) is developed for the Aragats system (See FIG. 23) to evaluate the recurrence rate since 490 ka.

In this logic tree, node N_1 represents the present state of the magmatic system. The transition, w_1, gives the weight assigned to the model that the Aragats volcanic system is extinct, in other words, that future eruptions of the volcanic system are impossible at any time in the future. This transition leads to node, $N_{2,2}$, representing the extinct state of the magmatic system. Node, $N_{2,1}$ represents the non extinct state of the magmatic system, with transition $1–w_1$, giving the weight assigned to the model that the Aragats volcanic system is not extinct.

Four possible recurrence rates of volcanic activity in the Aragats system are considered or the non extinct state ($N_{2,1}$), based on alternative interpretations of the Aragats eruptive history. Node $N_{3,1}$ represents the most active state, with recurrence rates of volcanism estimated as $> 5 \times 10^{-5}$ year^{-1}. Even though a recurrence rate this high exceeds the Middle Pleistocene recurrence rate, it would allow for a period of enhanced activity comparable to the rates of activity at many Holocene volcanoes. Nevertheless, the transition $w_{2,1}$, gives the weight assigned to this high recurrence rate model, and is considered to be vanishingly small. If the recurrence rate of volcanic activity is 5×10^{-5} year^{-1} the probability of no events occurring since 490 ka is approximately 2×10^{-11} (See EQ. (20)). Because this value is so low, zero weight is given to this high recurrence rate model ($w_{2,1} = 0$). In other words, an assumption is made that there is no possibility of the recurrence rate of volcanism exceeding 5×10^{-5} year^{-1}, because of the absence of volcanic episodes in the geologic record since 490 ka.

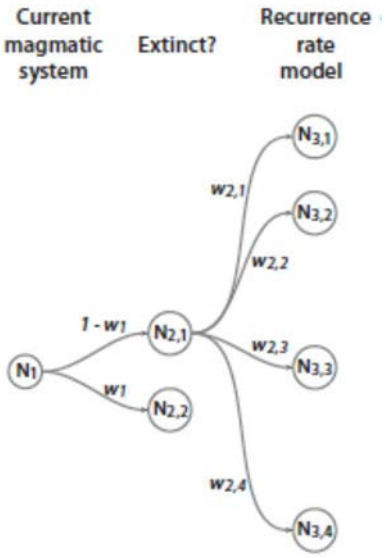

FIG. 23. Logic tree for the recurrence rate of volcanic activity in the Aragats volcanic system. Node N_1 represents the present state of the magmatic system; node $N_{2,1}$ (not extinct) represents the possibility of future eruptions; node $N_{2,2}$ (extinct) considers the possibility that future eruptions are impossible. Nodes $N_{3,1}$–$N_{3,4}$ represent alternative recurrence rate models and are discussed in the text. The text fully defines each node and discusses the weights, w_1–$w_{2,4}$, assigned to different models. Reproduced courtesy of the Ministry of Energy and Natural Resources of the Republic of Armenia [10].

Node $N_{3,2}$ represents a recurrence rate of volcanic activity within the range 5×10^{-6} year^{-1} to 5×10^{-5} year^{-1}. The absence of known events since 490 ka suggests a recurrence rate of $< 5 \times 10^{-6}$ year^{-1} with 90 % confidence. That is, if the recurrence rate of volcanism exceeds5 $\times 10^{-6}$ year^{-1} there is some chance (approximately 10 %) that no events would be observed since the eruption of Irind at 490 ka. Therefore, $w_{2,2}$ is the weight given to model of the volcanic system with recurrence rate that falls within this range ($w_{2,2} = 0.1$).

Node $N_{3,3}$ represents a recurrence rate of volcanic activity within the range 9×10^{-7} year^{-1} to 5×10^{-6} year^{-1}. Based on equation 4.20, for Δt = 490 000 year and $\hat{\lambda} = 1.3 \times 10^{-6}$ year^{-1}, the probability of no events, $P[N = 0] = 0.5$. In other words, if the recurrence rate of volcanism is between 9×10^{-7} year^{-1} and 5×10^{-6} year^{-1}, there is a reasonable chance that no event would be observed since the eruption of Irind volcano. Similarly, node $N_{3,4}$ represents a lower recurrence rate $< 9 \times 10^{-7}$ year^{-1}. For Δt =490 000 year and $\hat{\lambda} = 9 \times 10^{-7}$ year^{-1}, the probability of no events, $P[N = 0] = 0.65$. Consequently, there is no criterion for weighting recurrence rates of 9×10^{-7} year^{-1} to 5×10^{-6} year^{-1} differently from recurrence rates of $< 9 \times 10^{-7}$ year^{-1}. Thus, as a matter of judgment, the boundary between states $N_{3,3}$ and $N_{3,4}$ is chosen so that the weights given to each model are equal ($w_{2,3} = w_{2,4} = 0.45$).

Although statistical arguments have been made about the values of weights $w_{2,1}$–$w_{2,4}$ given to recurrence rate models, no statistical argument can be made for the weight w_1 given to the model that the Aragats volcanic system is extinct. The long absence of episodes is the primary justification for suggesting that the volcano is extinct. On the other hand, as previously discussed, there is no indication in the geochemistry of eruptive products that the volcanic system is waning (e.g. change in eruptive temperature, geobarometry, or degree of partial melting). Other regional volcanoes remain active, precluding a fundamental change in the regional conditions that give rise to volcanism. There is a suggestion of a hiatus before the

Middle Pleistocene stage of volcanism at Aragats, and therefore the volcanic system may be quiescent between stages of activity. Therefore, because there is extremely high uncertainty about the possibility that Aragats may be extinct, the weight given to this model is $w_1 = 0$, and is assumed that future eruptions in the volcanic system are possible, noting that the possibility of effectively no credible likelihood of future eruptions is included in the high weight, $w_{2,4} = 0.45$, given to very low recurrence rate models, which assume a recurrence rate $< 9 \times 10^{-7}$ year^{-1}.

4.8. RECURRENCE RATES BASED ON THE ERUPTIVE HISTORY: EXAMPLE OF TEQUILA VOLCANIC FIELD

An important question in hazards assessment concerns the notion of whether a volcano is 'extinct' or not. In risk assessment, this question should be rephrased as whether there is a potential for future activity, or that such potential is so low as to be negligible. There needs to be a significant level of information to support a determination that a volcanic system is incapable of producing future activity. Because volcanoes can remain active for long periods of time (hundreds of thousands of years), patterns in activity can change through time. Understanding these trends is an important component of the hazards assessment, for both estimating the likelihood of future events and evaluating the characteristics of potentially hazardous phenomena. This understanding, in turn, hinges on understanding the tectonic and magmatic processes that led to volcanic activity.

Although activity in the Holocene provides confidence that there is a potential for future eruptions, a lack of Holocene activity does not provide a robust argument for a negligible potential of future activity. For example, some well studied volcanoes such as Tequila volcano in Mexico (Lewis-Kennedi et al. 2004) show periods of inactivity of tens of thousands of years or longer, followed by periods of activity.

The eruptive history of the Tequila volcanic field (1600 km^2) in the western Trans-Mexican Volcanic Belt is based on 40Ar/39Ar chronology and volume estimates for eruptive units younger than 1 Ma [134]. Ages for 49 volcanic units were performed, including Volcán Tequila (an andesitic stratovolcano) and peripheral domes, flows, and scoria cones. Volumes of volcanic units $\leq$ 1 Ma were obtained with the aid of field mapping, orthophotographs, digital elevation models (DEMs), and ArcGIS software.

Between 1120 and 200 ka, a bimodal distribution of rhyolite ($\sim$ 35 km^3) and high Ti basalt ($\approx$ 39 km^3) dominated the volcanic field. Between 685 and 225 ka, less than 3 km^3 of andesite and dacite erupted from more than 15 isolated vents; these lavas are crystal poor and show little evidence of storage in an upper crustal chamber. At approximately 200 ka, $\sim$ 31 km^3 of andesite erupted to form the stratocone of Volcán Tequila. The phenocryst assemblage of these lavas suggests storage within a chamber at $\approx$ 2–3 km depth. After a hiatus of $\approx$ 110 000 years, $\approx$ 15 km^3 of andesite erupted along the W and SE flanks of Volcán Tequila at $\approx$ 90 ka, most likely from a second, discrete magma chamber located at $\approx$ 5–6 km depth. The youngest volcanic feature ($\approx$ 60 ka) is the small andesitic volcano Cerro Tomasillo ($\approx$ 2 km^3). Since 1 Ma, a total of 128 $\pm$ 22 km^3 of lava erupted in the Tequila volcanic field, leading to an average eruption rate of $\approx$ 0.13 km^3/thousand year. This volume erupted over $\approx$ 1600 km^2, leading to an average lava accumulation rate of $\approx$ 8 cm/thousand year. The relative proportions of lava types are $\approx$ 22–43 % basalt, $\approx$ 0.4–1 % basaltic andesite, $\approx$ 29–54 % andesite, $\approx$ 2–3 % dacite, and $\approx$ 18–40 % rhyolite.

On the basis of eruptive sequence, proportions of lava types, phenocryst assemblages, textures, and chemical composition, the lavas reflect the differentiation of multiple parental liquids in a long lived magma chamber. The rhyolites are geochemically diverse and were likely formed by episodic partial melting of upper crustal rocks in response to emplacement of basalts. There are no examples of mingled rhyolitic and basaltic magmas. Whatever mechanism is invoked to explain the generation of andesite at the Tequila volcanic field, it must be consistent with a dominantly bimodal distribution of high Ti basalt and rhyolite for an 800 thousand year interval beginning ≈ 1 Ma, which abruptly switched to punctuated bursts of predominantly andesitic volcanism over the last 200 thousand year.

In terms of hazards assessment related to the activity of Tequila volcanic field, it is clear that provided the large gaps in eruptive activity (25 to 110 thousand year), there exists a possibility to have another eruption after 90 thousand year of dormancy, in spite of Tequila volcanic field being considered an extinct volcano. In the case of NPP sites, volcanoes with long repose periods, future activity have also to be evaluated even though the volcanoes do not fit the classical definition of an active volcano.

4.9. CONCLUSION

It cannot be emphasized enough that a robust recurrence rate is derived from a robust data set that accurately describes the eruptive history of the capable volcano. Although much attention is placed on determining the age of the youngest events, the methods discussed in this section rely heavily on the volcano's history and geologic setting. A sparse data set effectively restricts the analyst to simple models, which must rely on general assumptions regarding temporal and spatial stationarity. However, a reasonably representative data set of eruption ages, compositions and volumes, when coupled with a knowledgeable understanding of the volcano's geologic setting, can justify the use of advanced statistical models that account for nonstationary processes. Although expert judgment is an inherent component of any recurrence rate analysis, this judgment is not an effective substitute for readily obtainable data. Nevertheless, erosion and burial processes will have to be evaluated in nearly every volcanic system, and the resulting uncertainties in spatio temporal patterns will need to be addressed in the recurrence rate calculations.

An important distinction to recall is that the methods in this section focus on determining the likelihood of a volcanic event occurring in the future, regardless of the magnitude or character of the event. This approach contrasts with seismic hazards assessment, which focuses on determining the likelihood of future seismic events exceeding a given magnitude. This distinction is important because seismic events show a distinctive scaling relationship between event frequency and magnitude, whereas volcanic events generally lack such scaling relationships. For example, thousands of small magnitude eruptions have occurred at Stromboli volcano in Italy. The recurrence rate of these small eruptions, however, does not constrain the recurrence rate of large magnitude eruptions from Stromboli.

Unlike earthquakes, volcanic events also are relatively infrequent in human history and have not, to date, severely affected an operating nuclear installation. This also limits the utility of the historical record in constraining the recurrence of past volcanic events, because the period of historical observation is too short to capture many potential events. Conversely, the historical record often helps constrain the recurrence of past seismic events, because such events occur more frequently than volcanic events.

There is, however, an emerging awareness that rare natural events can indeed happen in our lifetimes or in the service life of longer lived installations, even if such events are unprecedented in recorded history. The methods presented in this section provide transparent and traceable bases to address the challenge of determining recurrence rates for infrequent or rare volcanic events.

5. SPECIFIC PHENOMENA

5.1. GENERAL

The geologic record presents an incomplete eruptive history of a volcanic system. In all but the most extraordinary of circumstances, a volcanic hazards assessment must use numerical models to supplement the geologic record, to better account for uncertainties inherent in the geologic record, and to calculate reliable forecasts of potential future hazards at a site. Over the past decades, many individuals or small teams have developed a variety of numerical models to simulate potentially hazardous phenomena. These researchers have been diligent in publishing, reviewing, and improving these models. Most notably, the multinational EXPLORIS project (2002–2006) helped advance approaches for modeling and model testing for some explosive volcanic hazards [135]. Nevertheless, in spite of such largely individual efforts, no model of volcanic phenomena can be viewed today as generally accepted or inherently suitable for a hazards assessment at a potential nuclear installation.

The seismologic hazards community faced a similar modeling challenge several decades ago, and embarked on an extensive program of international working groups, multinational testing programs, engineering standards development, and extensive peer review of seismic data and models. As a result of this effort, current seismic hazards analyses for nuclear installations commonly use hazards models that have been thoroughly reviewed to a level of general acceptance by the technical community, with multiple models often being implemented through a structured approach (e.g. [136–138]).

To bridge this gap between seismic and volcanic model acceptance, this TECDOC strives to serve as a foundation for building an international consensus on models and methods that appear generally acceptable for use in volcanic hazards assessments at potential nuclear installations. The purpose of this section is to provide an overview of methods that have been used to evaluate specific volcanic phenomena. However, many additional models for volcanic phenomena are available in the literature than can be discussed in this section. The discussions herein are designed to provide a useful synopsis of the types of modeling approaches that have been applied to published assessments of volcanic hazards. We have endeavoured to represent broad classes of models, ranging from basic to complex numerical abstractions, to provide a sense of the types of analyses that appear practicable for hazards assessments at potential nuclear installations. Models that are not discussed in this section also may be practicable for

such hazards assessments, and the analyst is encouraged to consider alternative models that might provide additional insights on potentially hazardous volcanic phenomena at a specific site.

Although the models discussed in this section have had some degree of testing and been used for hazards analyses, none of these models has undergone a formal validation process supporting its use in all potential conditions. Because volcanic processes have large variations in physical characteristics and many 'unknowable' components, strict validation of volcanic hazards models might not be achievable in the same way as possible for many nuclear physics models (e.g. [139]). Nevertheless, a formal program of model testing and confirmation appears achievable, but, to date, has not been accomplished for volcanic hazards codes. Thus, any model discussed in this section should not be misconstrued as 'accepted' or 'approved' for site evaluations. Instead, these models represent a snapshot of the current state-of-the-science in practicable volcanic hazards assessment. If any of these models is used in a safety assessment for a potential nuclear installation, the installation's proponents would need to justify and support the use of the selected models. Nevertheless, compared to the current state-of-practice in seismic hazards assessment, volcanic hazards assessment clearly would benefit from similar programmes to systematically review and evaluate the performance of promising models.

In the context of the SSG-21 [1], the goal of modeling specific phenomenon is to determine if the potential hazard at the site represents either a site exclusion phenomena or a consideration in the design and operation of the proposed nuclear installation. For some volcanic flow or deformation phenomena, transient and sustained thermal, mechanical, and perhaps chemical loads apparently exceed the basis routinely used to design a nuclear installation against external hazards. Thus, a credible potential for these flow phenomena (See TABLE 4) to occur at the proposed site generally indicates that the site is unsuitable for a nuclear installation [1]. Nevertheless, detailed analyses have not been conducted to establish if a specific facility design has sufficient capacity to withstand some, or all, of the demands generated by these volcanic flow or deformation phenomena. The practicability of conducting, and defending, such analyses rest ultimately on the judgment of a facility's proponents.

Although ground deformation and volcanic earthquakes are identified in the SSG-21 [1] as potential volcanic hazards, explicit modeling of these phenomena is not addressed in this TECDOC. Ground deformation is considered as a hazardous process with the opening of new vents, and should be included in developing parameters on the areas affected by the opening of new vents. Conversely, all nuclear installations have requirements for seismic hazards assessments. If the seismic hazard assessment is conducted in a region that has capable volcanoes, this assessment should consider the hazard contribution from volcanic sources in addition to tectonic sources.

For many of the volcanic phenomena listed in TABLE 4, some magnitude of hazard appears practicable to mitigate through appropriate design or operational procedures at the installation (e.g. emergency planning, enhanced inspection and maintenance). The details of the design and mitigation requirements, however, will depend on the specifics of the installation's design and siting characteristics. Although general guidance is provided in the SSG-21 [1] regarding apparent practicability of hazard mitigation, detailed modeling might reveal that the magnitude of hazard at a specific site exceeds the ability to successfully mitigate adverse impacts through design or operation of the installation. Discussions in this section provide additional considerations for potential mitigation of specific volcanic phenomena, which can help inform decisions on possible mitigation strategies or siting decisions. Although

nuclear installations have not experienced significant damage from volcanic phenomena, many volcanic eruptions have had catastrophic impacts on people and facilities around the world. Many sources of information exist showing the damage caused by volcanic eruptions, including videos produced by the International Association of Volcanology and Chemistry of the Earth's Interior (IAVCEI) at www.iavcei.org.

TABLE 4. VOLCANIC PHENOMENA AND ASSOCIATED CHARACTERISTICS THAT COULD AFFECT NUCLEAR INSTALLATIONS, WITH IMPLICATIONS FOR SITE SELECTION AND EVALUATION AND DESIGN [1]

Phenomena	Potentially adverse characteristics for nuclear installations	Considered as exclusion condition at site selection stage?	Can effects be mitigated by means of design[1] and operation?
1. Opening of new vents	Dynamic physical loads, ground deformation, volcanic earthquakes	Yes	No
2. Volcano generated missiles	Particle impacts, static physical loads, abrasive particles in water	Yes	Yes
3. Tephra fallout	Static physical loads, abrasive and corrosive particles in air and water	No	Yes
4. Atmospheric phenomena	Dynamic overpressures, lightning strikes, downburst winds	No	Yes
5. Hydrothermal activity	Thermal water, corrosive water, water contamination, inundation or upwelling, hydrothermal alteration, landslides, modification of karst and thermokarst, abrupt change in hydraulic pressure	Yes	Yes
6. Volcanic gases	Toxic and corrosive gases, acid rain, gas charged lakes, water contamination	No	Yes
7. Lava flows and domes	Dynamic physical loads, floods and water impoundments, temperatures > 700 °C	Yes	No
8. Pyroclastic density currents	Dynamic physical loads, atmospheric overpressures, projectile impacts, temperatures >300 °C, abrasive particles, toxic gases	Yes	No

Phenomena	Potentially adverse characteristics for nuclear installations	Considered as exclusion condition at site selection stage?	Can effects be mitigated by means of design[11] and operation?
9. Laharic flows	Dynamic physical loads, water impoundments and floods, suspended particulates in water	Yes	Yes
10. Debris avalanches and sector collapse	Dynamic physical loads, atmospheric overpressures, projectile impacts, water impoundments and floods	Yes	No
11. Volcanic tsunamis	Water inundation, dynamic loads from fluid flow.	Yes	Yes
12. Ground deformation	Ground displacements, subsidence or uplift, tilting, landslides	Yes	No
13. Volcanic earthquakes and related hazards	Continuous tremor, multiple shocks, usually Earthquake Magnitude M < 5	No	Yes

Note: A 'Yes' in the site selection stage column indicates that the presence of a significant hazard from this phenomenon in the site vicinity generallyconstitutes a site exclusion criterion, i.e. the site is not suitable for a nuclear installation. The design and operation column indicates the generalpracticality of mitigating the potential hazard associated with particular phenomena, by either facility design or operational planning. A 'Yes' in bothcolumns indicates that, in principle, this phenomenon constitutes a site exclusion criterion, although for some cases a design basis may be achievable.

[1] Design also includes the design of site protection measures for some of the hazards.

5.2. OPENING OF NEW VENTS

5.2.1. Physical characteristics

The opening of new vents is a geologically rare phenomenon, but one that can produce significant deleterious effects at the site of a nuclear installation. These effects include the formation of lava flows, pyroclastic fall and flow, ballistic, and ground deformation hazards for a nuclear installation located close to the site of a new volcano (e.g. scoria cone, lava dome). IAEA guidelines indicate that the formation of a new vent at or close to a nuclear installation is beyond the design basis of the facility [1], [2], [140]. Opening of a new vent is a site suitability decision because the opening of a new vent is a major geologic event, expected to completely destroy the area around the new vent by ground deformation and the eruption of volcanic material. In addition, the opening of new vents far from the location of the site (several to tens of kilometres) may also have adverse effects (e.g. produce tephra fallout) and therefore opening of new vents is also important in the assessment of these hazards that impact design basis (See FIG. 24). In the event of the opening of new vents, ground deformation of large magnitude (e.g. metres), volcanic seismicity and gas flux may occur in the site vicinity. During many volcanic eruptions, the formation of a new vent may involve phreatic or phreatomagmatic activity, which is generally highly explosive. In such circumstances the opening of a new vent in water or shallow groundwater systems may result in a significantly more explosive eruption than represented by the products of past eruptions.

Eruptions at new vents vary in magnitude and character through time, with different types of new vents (e.g. scoria cone, tuff ring, maar, fissure, and dome) capable of producing a wide range of eruptive products. Total volume of eruptive products from new vents varies from < 0.01 km^3 to > 1 km^3. In general, the opening of a new vent directly impacts an area of 1–5 km from the centre of the activity, with the formation of the new volcano edifice, tephra emission, pyroclastic density currents and transport of ballistic projectiles. Tephra columns associated with the opening of new vents are commonly 5–8 km in height, but also new vents have sustained eruptions with much higher column heights, 15–20 km. This tephra may impact areas far downrange of the new vent. New vents may produce lava flows that are commonly 2–10 km long, but occasionally inundate areas > 20 km from the new vent. Overall, new vents are commonly formed during eruptions classified as VEI 0–4. Such eruptions from new vents may last as little time as a few days, but new vents are often active for years or decades. Eruptive vents can occur as isolated features (scoria cones, maars) or as a series of aligned or *en echelon* vents that may propagate further as the eruption proceeds and new magma rises to the surface in dykes.

5.2.2. Potential effects for nuclear installation

The opening of new vents is a geological phenomenon that can produce significant flow, tephra fallout, eruption propelled missiles and ground deformation hazards for a nuclear power plant. In the near vent region (1–5 km), devastation is often complete, as substantial volumes of tephra, lava and related eruptive products accumulate in a very short period of time. Lava flows and tephra fallout may inundate areas substantial distances from the new vent.

5.2.2.1.Consideration for siting

The effects from opening of new vents should be considered as part of the exclusion criteria of the site, since these effects cannot be mitigated by means of appropriate design and operation measures if they occur at the site vicinity or they affect directly the site.

5.2.2.2. Consideration for operations and emergency planning

Opening of new vents is considered a beyond design basis event. It is not viewed as practicable to mitigate effects through facility design although detailed analyses of potential impacts have not been undertaken. Because of the potential for relatively voluminous tephra fallout and long lava flows extending from the vent, it is recognized that the opening of a new vent might occur some distance from the controlled area of a facility, but yet could impact operations and infrastructure. Impacts include blockage of surface water systems (e.g. natural dams), disruption of water supply systems outside controlled area, significant disruption of offsite power supply systems, restricted access by roads and airspace, reduced emergency response times for offsite personnel.

FIG. 24. A new vent forming. The 1975 eruption of Tolbachik volcano is one example of a large scoria cone built by eruptive activity in a period of several weeks. Here, tephra fallout is spreading far downrange from the new vent. Photo courtesy of N.P. Smelov. Reproduced courtesy of Nauke [141].

5.2.3. How to evaluate effects

Over the last several decades, considerable experience has been gained in evaluation of these geologic hazards in siting nuclear facilities [2]. Such assessments have been conducted at Yucca Mountain, Nevada, USA [142], [143], the Muria Peninsula, Indonesia [98], for an operating nuclear power plant in Armenia [11], [16], for the Idaho National Laboratory facility on the Eastern Snake River Plain, USA (e.g. [144], [145]), and in Japan [35]. A central issue in all of these assessments is the likelihood of a new volcano forming by eruptions in close proximity to the facility or to the proposed facility. At some facilities, hazards with probabilities on the order of 10^{-6} to 10^{-8} per year might need to be considered in the safety assessment [35], [90] because overall the risks associated with such facilities must be very low and because new vents opening even tens of kilometres from a site may result in hazardous phenomena, such as lava flows, pyroclastic density currents, or tephra fallout.

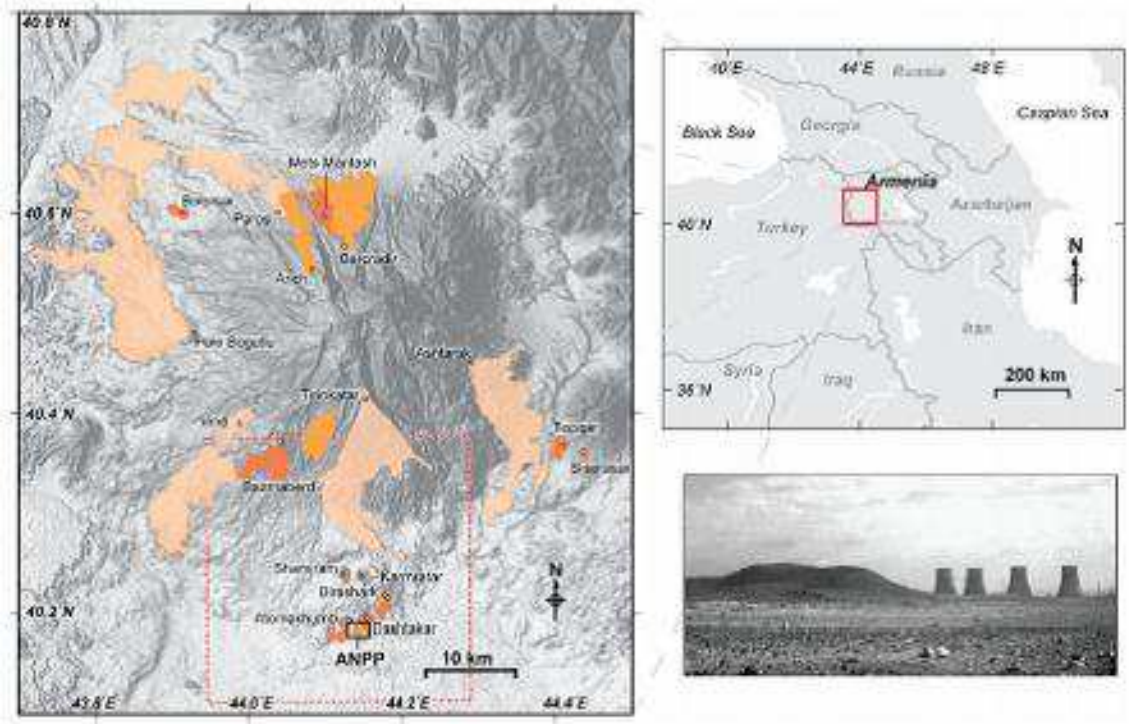

FIG. 25. Location of study area in Armenia. The study area, outlined by a red box on the location map, is located in SW Armenia. The more detailed view shows the areal extent and location of effusion limited (lighter colored) and volume limited (darker colored) lava flows located around Aragats volcano. The dashed red box identifies the boundaries of the lava flow simulation area. The Shamiram Plateau is an elevated region (within the central portion of the lava flow simulation area) comprising lava flows from Shamiram, Atomakhumb, Dashtakar, Blrashark, and Karmratar volcanoes. The ANPP site (black box) is located on the Shamiram Plateau. Photo shows the ANPP site and Atomakhumb volcano. Reproduced courtesy of Journal of Applied Volcanology [11].

Hazards associated with the opening of new vents may be exacerbated by the topography around volcanoes, which is often complex and characterized by steep slopes. For example, small variations in vent location may cause lava to flow in a completely different direction down the flanks of a volcano. Thus, probabilistic models of lava flow inundation, for example, are quite sensitive to models of vent location. Furthermore, many volcanic systems

are distributed. Examples include monogenetic volcanic fields (e.g. the Michoacan-Guanajuato volcanic field, Mexico), distributed composite volcanoes which lack a central crater (e.g. Kirishima volcano, Japan), and volcanoes with significant flank activity (e.g. Mt. Etna, Italy, Mt Aragats, Armenia, FIG. 25). Spatial density estimates are also needed to forecast potential vent locations within such distributed volcanic systems (e.g. [146]). In addition, loci of activity may wax and wane with time, such that past vent patterns may not accurately forecast future volcano locations [101]. It is important to determine if temporal patterns are present in the distribution of past events, so that an appropriate time interval can be selected for the analysis (i.e. use only those vents that represent likely future patterns of activity, not patterns that represent older volcano distributions). Furthermore, additional factors, such as the stress state of the crust, change with time and may influence the probable locations of new vents especially on the flanks of larger composite or shield volcanoes (e.g. [147]).

5.2.3.1.Existing modelling approaches

Hazards associated with new vent or volcano formation place a high priority on statistical model development. Geological hazard assessments for volcano and volcanic vent distributions should present robust estimates of hazard rates, based on the spatial density and frequency of past events formed by geological processes that are expected to persist and continue during the future time period of interest. The challenge presented by these hazards is that observed spatial distribution of volcanoes is only one realization of the potential distribution of volcanoes. The processes controlling the spatial distribution of volcanoes, such as the generation and ascent of magma, are unobserved. Hence it appears unreasonable to forecast the future distribution of vents deterministically, and statistical models of vent distribution should be developed. Sometimes empirical models are developed, such as those that argue for a deterministic offset from existing volcanoes [31], but these models are not appropriate for estimating eruption potential at a specific site, but only in a site selection stage as site screening criteria. Similarly, source zone models are sometimes used in volcanology and seismic hazard assessment, but these source zone models are not recommended because they rely on a deterministic view of the site geologic setting and because the boundaries of source zones create unrealistic steps (discontinuous and non differentiable) in probability.

The spatial distribution of volcanoes is dictated by processes of magma generation within the Earth's mantle and magma ascent through the mantle, ductile lower crust, and brittle upper crust. Each of these processes is understood currently through inferences drawn from the geochemistry of volcanic rocks, the presence and distribution of geophysical anomalies, such as slow seismic wave propagation in areas enriched in magma [148], and geologic features, such as igneous plutons and dykes, that indicate styles of magma transport, and which have been exhumed by deformation and erosion [149]. These observations have helped geologists construct physical models of magma generation and ascent in a variety of tectonic settings (e.g. [33], [150], [151]). Conversely, studies of the spatial distributions of volcanoes have been used to elucidate the geologic processes [152], [153].

Magma generation is not uniform throughout the Earth's mantle, but rather, occurs under a limited set of circumstances. For example, subduction at some plate margins changes the chemical composition of the mantle, particularly, by introducing volatiles, and alters the thermal structure of the mantle, resulting in convection. These physical changes result in partial melting of the mantle to produce magma, which rises buoyantly toward the surface. In other tectonic settings, the development of thermal plumes, or decompression of the mantle through crustal extension, results in partial melting of the mantle, and generation of magmas. On a

smaller scale, gravitational instability in melt regions, density stratification of the crust, differential stress in the crust, distribution of fractures, faults or rift zones, and similar processes further influence magma ascent. Magma generation and the 'plumbing' of the volcanic system are not directly observed in a given area of active volcanism, but, at best, inferred from geophysical and geochemical data, and physical models of magmatism (e.g. [29], [150], [154]).

The frequency with which new volcanoes or volcanic vents form is controlled by the rates of these underlying processes. For example, the rate of subduction of oceanic lithosphere at plate boundaries may play a role in the rate of volcanism in an overlying volcanic arc [154]. In some extensional tectonic settings, such as the Basin and Range of the western United States, the rate of crustal extension may exert a leading order control of the rate of formation of cinder cones (e.g. [96]) and other types of volcanic vents.

The observed spatial distribution of volcanoes is just one sample of an underlying and unobserved distribution of the likelihood of volcano formation in time and space. This underlying distribution is a function of various physical properties, such as variation in chemical composition of the mantle, distribution of heat and heat flow, and nature of the crust. This underlying distribution is continuous, as these physical variations in the mantle and crust are continuous. The fact that these geologic observations and geological models are based on poorly resolved physical processes suggests statistical models that can be used to forecast the process of volcano formation. In this sense, the spatial distribution of volcanoes can be thought of as a point process. A point process is a theoretical construction for generating random events according to some probability model. The observed spatial distribution of volcanoes in any particular region is a single realization of this point process. Because this realization is comprised of a limited number of volcanoes, it may or may not provide a complete picture of the underlying distribution of the likelihood of volcano formation in time and space.

Spatial density estimates

The physics of magma generation and ascent suggest that the long term distribution of volcanic events in monogenetic volcanic fields can be represented by a Poisson process. Each event, the formation of a new volcano, is discrete in time and space. The probability of a new volcano forming at a particular time and place is not in any way influenced by the formation of other volcanoes in the past, but rather is only a function of the underlying processes that influence magma generation and ascent. In other words, a batch of magma that ascends to the surface and forms a new volcano does not itself make it more or less likely that another batch of mafic magma will ascend in another location and form a new volcano. This assumption is valid because mafic magmas, erupted at monogenetic volcanoes, almost always are small volume fraction partial melts, their volume is very small compared to the total volume of mantle which can potentially produce mafic magma. In other words, eruptions are so rare that the mantle is not depleted by previous eruptions.

A Poisson model may not be appropriate for all cases of new vent formation. The formation of parasitic cones (small vents on the flanks of a larger volcano) is not independent of the formation of the central vent. Also, in extreme cases of the largest volume silicic calderas, non refractory elements in the mantle may actually be depleted to the extent that future patterns of volcanism are influenced by the silicic eruption itself.

For a spatial Poisson process, the probability of a new event occurring in a small area within a much larger region is related only to the spatial intensity, the expected mean number of

events per unit area defined at a point [155–157]. Suppose there exists a set of events (e.g. vent locations) that occur within a given region, *R*. These events can be designated as

$$\{X_1, X_2, X_3, \cdots X_N\} \in R \tag{21}$$

where *N* is the total number of events and X_N is a 1×2 matrix whose elements are *x* and *y*, the location of the N^{th} event (possibly given in Easting and Northing coordinates, or, latitude and longitude). These events are realizations of a random variable, *X*, a function that describes the set of all possible realizations. *X* is the distribution of potential volcanic events, from which a set of observed realizations (e.g. those found on a geologic map) are drawn. The spatial intensity is [157]

$$\lambda(s) = \lim_{ds \to 0} \left\{ \frac{E(X)}{ds} \right\} \tag{22}$$

where *E(X)* is the expected number of events that fall within a small area, *ds,* about the point *s* (hence, if the location, *s*, is given as Easting and Northing with units of meters, then the units of $\lambda(s)$ are m^{-2}). The stochastic process that governs the formation of volcanoes is not known, so the true value of the local spatial intensity, $\lambda(s)$, is also unknown. That is, the observed distribution of events is only one realization of the underlying process that gives rise to these events. This distribution may accurately reflect the potential distribution of future events, or not, say if a significant fraction of past events are not mapped (buried by subsequent events) or the volcanic system has changed. Our goal is to find an estimate of the spatial intensity, $\hat{\lambda}(s)$, that approximates the true but unknown value of spatial intensity, $\lambda(s)$.

Often we consider spatial intensity in terms of the probable location of some future event, given that one event occurs within our region of interest. This conditional probability can be estimated by dividing the local spatial intensity by the number of events used to calculate the spatial intensity estimate,

$$\hat{f}(s) = \frac{\hat{\lambda}(s)}{N} \tag{23}$$

Integrating $\hat{f}(s)$ across the region of interest, *R*, gives unity, if *R* is sufficiently large. Since all values of $\hat{f}(s)$ within this region are greater than or equal to zero, this makes $\hat{f}(s)$ a probability density function and this function may be used in probabilistic hazard models. $\hat{f}(s)$ is referred to as one estimate of the spatial density. Note that integrating the spatial intensity, $\hat{\lambda}(s)$, across *R* yields *N*, the total number of events in the region

Assumptions behind spatial density estimates

How does one develop a best estimate of spatial density or spatial intensity of volcanic events? This process starts by first clearly stating several assumptions. The reliance on the distribution of past events implies that these realizations are representations of the underlying random variable, *X*, that will govern the distribution of potential events in the future. This assumption immediately raises a fundamental question. Is the record of past events sufficient to develop the spatial intensity estimate, $\hat{\lambda}(s)$, and density, $\hat{f}(s)$. Event datasets used to estimate the spatial density of future events need to be consistent with several features of geological processes.

First, any spatial intensity function for a geologic process must change with time. On time scales of tens of millions of years, plate boundaries change, volcanic arcs wax, wane, and migrate. On much shorter time scales, the stress state of the volcanic system may change, or rates of magma output may change, that may cause fundamental shifts in the locus of volcanic activity. For processes like volcanism, where a geologic record of past events usually persists for tens of millions of years, consideration needs to be given to which events best represent the distribution of future volcanism. For example, the distribution of Miocene events in a given area might be much less relevant than the distribution of Pliocene and Quaternary volcanoes. Thus, in order to develop an estimate of the spatial intensity, a model of the geologic evolution of the system is required. This conceptual geological model is used to justify the inclusion of some geological features in the event dataset, and the exclusion of others.

Second, it is necessary to assess the completeness of the geologic record. Some past events might be missed in initial geological investigations, as volcanic vents might be buried by subsequent volcanic activity or by sediment. Some volcanoes are particularly susceptible to erosion by a variety of geologic processes, including subsequent volcanic activity. This may lead to bias in the geologic record (e.g. [145], [158]).

Third, geological events, even when they are all identified, may be so rare as to present an incomplete picture of the underlying process. Consider a volcanic vent to be a single event, X_N , one realization of the random variable, X. If, for example, X has a uniform random distribution, then it is likely that the observed set of realizations will have a spatially random distribution within the region of interest, R. However, the underlying density often has additional structure, causing independent realizations to cluster. For example, volcanoes cluster above zones of partial melting in the mantle on one scale, and vents may cluster along rift zones on another scale. For random variables with a great deal of statistical structure, such as many modes in spatial intensity, a great number of events might be required to identify the statistical structure of the random variable. In other words, if the density estimate is based on few events, then the model may be overly smooth.

Fourth, it is critical to ascertain which geologic features are actually independent events. The true statistical structure of the random variable, X, might be obscured if some events included in the event dataset are not independent. The spatial distribution of polygenetic volcanoes reflects processes of magma generation and rise through the crust. The distribution of small vents (sometimes referred to as parasitic or adventive cones) does not necessarily reflect the distribution of polygenetic volcanoes, so a spatial intensity estimate that includes all vents as events would not correctly model the underlying random variable. Furthermore, in monogenetic volcanic fields alignments of volcanic cones develop in response to single magmatic events, episodes of magma rise through the shallow crust. This is because single igneous dikes ascending through the crust might form segments and rotate within the shallow crust, each segment feeding a separate vent and each building a volcanic cone. If the goal of analysis is to forecast the distribution of future magmatic events, each of which might produce more than one monogenetic volcano, geological data must be gathered and volcanoes formed by the same magmatic event must be somehow grouped as single events.

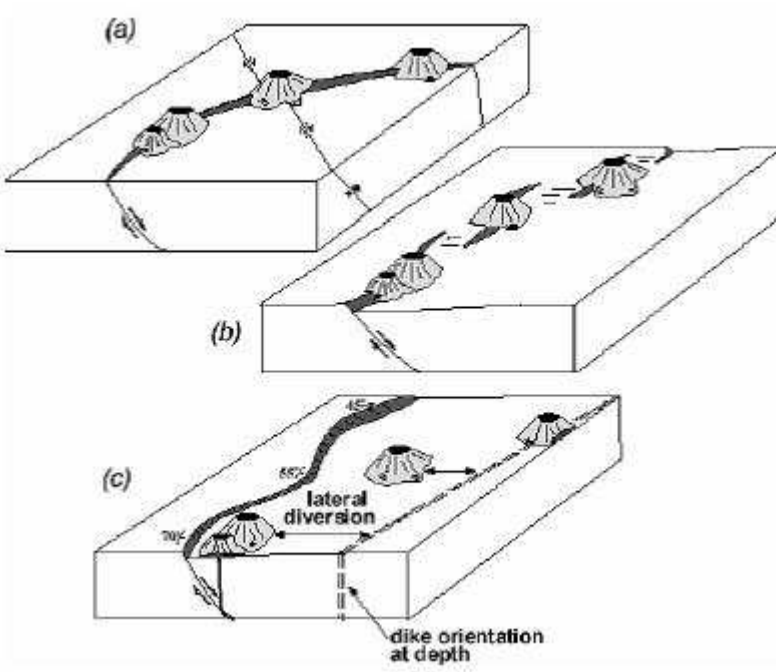

FIG. 26. Scoria cone alignments can form along faults in a variety of geometries. (a) cones can be aligned along the fault trace or at the intersections of two faults; (b) cones can form an en echelon array along the fault trace; (c) cones can be offset laterally from the fault as a function of fault dip, which controls the distance from the fault trace the ascending dike will break out of the fault zone. In such circumstances it is often poorly known if the magmatic events that built these cones are independent.

Independence of events is not necessarily easy to determine. Rather than simply counting volcanoes on a geologic map, one must make a geologic assessment of the independence of these data. This is generally accomplished through detailed analyses of radiometric age determinations, stratigraphic correlations, and related geologic data. Often, even detailed analyses do not resolve whether or not specific features should be grouped as single events or treated as separate, independent events (See FIG. 26). Consequently, a major task in preparing a spatial intensity estimate for volcanic hazard assessment is defining the dataset of events to be used. Hazard assessments often consider alternative event datasets and account for the effect of these varying datasets on spatial density estimates.

Estimating spatial intensity with kernel methods

A nonparametric approach for estimating the spatial intensity involves kernel density estimation [155], [159–161]. With this technique, the observed event locations are used to estimate the spatial intensity at any point in the region using a kernel function. For example,

$$\hat{\lambda}(s) = \frac{1}{2\pi h^2}\sum_{i=1}^{N} exp\left[-\frac{1}{2}\left(\frac{d_i}{h}\right)^2\right] \qquad (24)$$

is a two dimensional radially symmetric kernel function where the spatial intensity decreases with distance from events based on a bivariate Gaussian function. The local spatial intensity estimate, $\hat{\lambda}(s)$, depends on its distance, d_i to each event location, and the smoothing bandwidth, h. The rate of change in spatial intensity with distance from events depends on the size of the bandwidth, which, in the case of a Gaussian kernel function, is equivalent to the variance of the

kernel. In this example, the kernel is radially symmetric, that is, h is constant in all directions (See FIG. 27). Nearly all kernel estimators used in geologic hazard assessments have been of this type (e.g. [90], [101], [162], [163]). The bandwidth is selected using some criterion, often visual smoothness of the resulting spatial intensity plots, or interpretations of the underlying crustal structure. The spatial intensity function is then calculated using this bandwidth. Alternatively, an adaptive kernel function can be used, in which the spatial intensity varies as a function of event spatial intensity (e.g. [19], [163]).

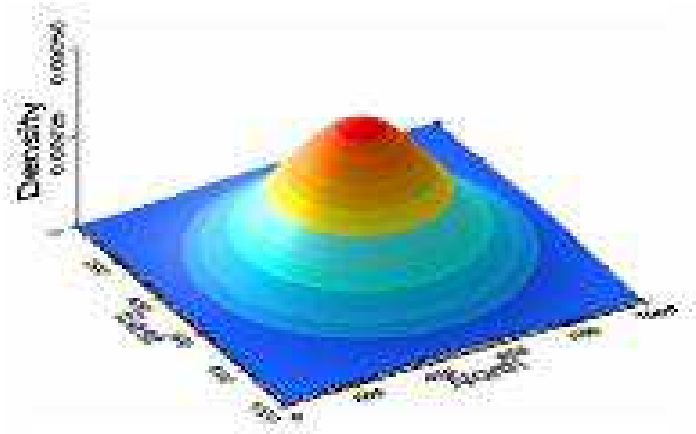

FIG. 27. An isotropic bivariate Gaussian kernel function of the type used in EQ. (24). A vent or volcano is located at the centre of the kernel. Probability of a new vent decreased exponentially away from the location of this older vent.

The simplest implementation of kernel methods to estimate spatial density is to use EQ. (24) and to assume a value for the smoothing bandwidth, h. Using this value of h and the distribution of passed volcanic events, the spatial density can be estimated using EQ. (24) at any map point. Often it is advantageous to calculate the spatial density on a map grid to facilitate contouring. Consider the implementation of EQ. (24) in pseudo code:

```
for (each map point in the north direction) {
  sumn=0 (initialize the summation for each map point)
  for (each volcanic event) {
    find the distance, dist1, between the map
    point and the volcanic event
    use dist1 and h to calculate the kernel:
    kernel = 1/(2*pi) * exp(-0.5*dist1^2/h^2);

    Sum the kernels for all volcanic events
    sumn = sumn + 1/(h^2) * kernel

  }

  spatial intensity at the map point = sumn
  spatial density at the map point = sumn / number
  of volcanic events

 }
}
```

A more general expression can also be used to estimate density with kernel functions in which the kernel is anisotropic. This is particularly useful in areas where directionality exists in the distribution of features, such as the distribution of volcanic vents in rift zones. A two dimensional elliptical kernel with a direction varying bandwidth is given by [161],

$$\hat{\lambda}(s) = \frac{1}{2\pi\sqrt{|H|}} \sum_{i=1}^{N} exp\left[-\frac{1}{2} b^T b\right] \quad (25)$$

where,

$$b = H^{-\frac{1}{2}} x$$

The bandwidth, H, is 2×2 element matrix that is positive and definite (important because the matrix must have a square root), $|H|$ is the determinant of this matrix and $H^{-\frac{1}{2}}$ is the inverse of its square root. x is a 1×2 distance matrix (i.e. the x distance and y distance from s to an event), b is the cross product of x and $H^{-\frac{1}{2}}$, and b^T is its transform. The resulting spatial intensity at each point location, s, is usually distributed on a grid defined as the region, R. For elliptical kernels, all elements of the bandwidth matrix must be estimated. Several methods have been developed for estimating an optimal bandwidth matrix based on the locations of the event data [161], most recently summarized in the statistics literature by Duong [164]. Here we utilize two techniques, a modified asymptotic mean integrated squared error (AMISE) method, developed by Duong and Hazelton [165], called the SAMSE pilot bandwidth selector, and the smoothed cross validation (SCV) method of Hall et al. [166], to optimally estimate the smoothing bandwidth for our Gaussian kernel function. These bandwidth estimators are found in the freely available R Statistical Package [164], [167]. Different bandwidth optimization algorithms yield different spatial intensity and density estimates. It is often useful to use different optimization algorithms to explore their impact on the spatial model.

5.2.3.2.Examples of evaluating potential hazards

Consider the application of the symmetric Gaussian kernel function (See EQ. (24)) to the distribution of volcanoes formed during the Miocene-Quaternary in the volcanic field near Yucca Mountain, Nevada (See FIG. 28). This is an area of distributed monogenetic volcanism since approximately 8 Ma. As a result, each 'event' represents the formation of one or more new volcanic vents. The first step in preparing such a contour map is identification of the past distribution of volcanoes. In this case, past volcanic events are limited to those mapped in the geologic record or identified through interpretation of geophysical anomalies to be volcanic vents buried subsequent to their formation in alluvium.

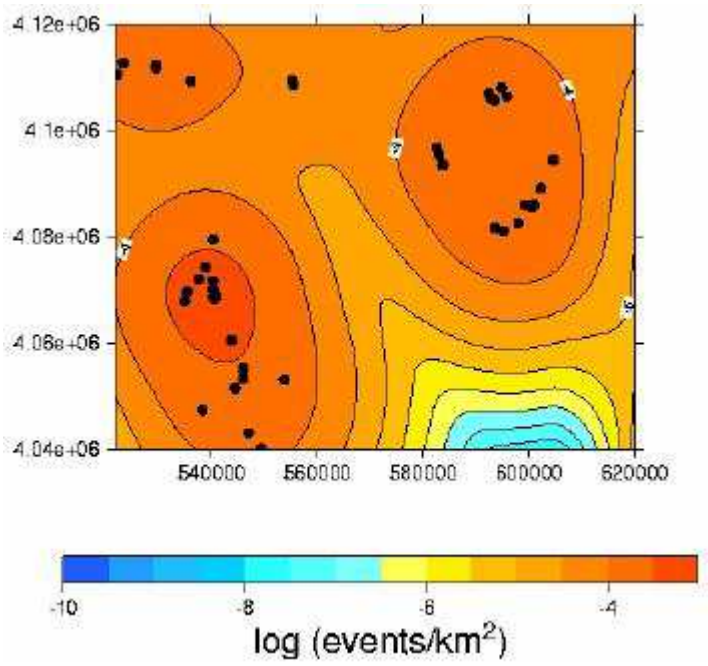

FIG. 28. A spatial density map created by applying EQ. (24) to a dataset of vent locations near Yucca Mountain, Nevada. Probability decreases with distance from distinctive vent clusters formed in the region over a period of approximately 8 million year. The bandwidth, h, controls the smoothness of the spatial density map and must be estimated using geological evidence, from the vent distribution, or assessed independently by calculating hazard using multiple values of h. Reproduced courtesy of © Cambridge University Press 2009 [168].

The bandwidth, *h,* is chosen either subjectively using geological evidence, or may be estimated from the distribution of vents themselves using statistical algorithms [161]. For this map (See FIG. 28) the bandwidth emphasizes the distribution of volcanoes in several clusters.

Consider a second example, where vents are distributed in a volcanic alignment. FIG. 29 shows the distribution of volcanic vents along the Nejapa-Apoyoque volcano alignment on the western margin of the city of Managua, Nicaragua. Radiometric age determinations have shown that at least 22 of these vents have formed in the Holocene, with the most recent vent forming approximately 1000 years ago. Given that future vents may form in the future, what is a reasonable model of the potential vent distribution?

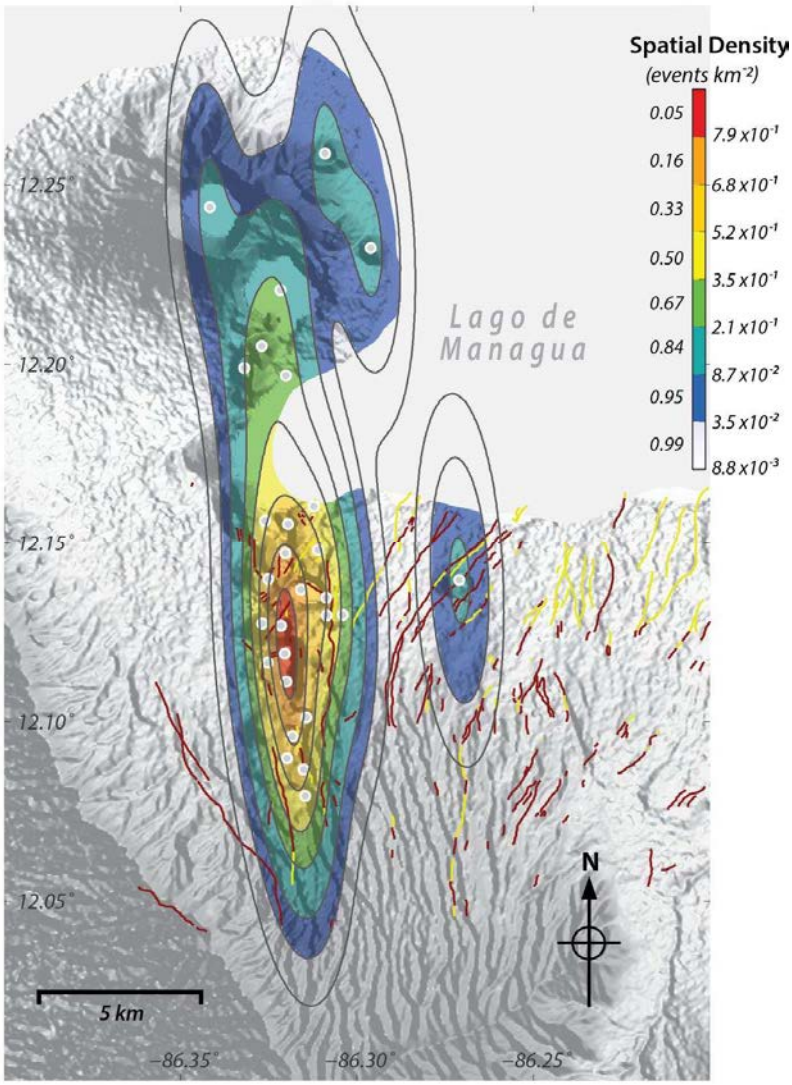

FIG. 29. Spatial density map for the probability of opening of new vents along the Nejapa-Apoyeque volcano alignment in Nicaragua. Dots represent vent locations, contours show the probability density function found using the anisotropic kernel density function with bandwidth calculated using the smoothed asymptotic mean squared error method. The alignment and spatial density are elongated N-S, parallel to the margin of the Managua graben and to many active faults in the area.

In this case, an anisotropic kernel density function (See EQ. (25)) is fit to the data using an optimization algorithm based on the past distribution of vents. This kernel function is elongate in an N-S direction, mirroring the orientation of the alignment and faults distributed throughout this part of Managua graben. Contouring the distribution illustrates the probability of new vent formation within the alignment.

Both maps (See FIG. 28 and FIG. 29) illustrate the probability of new vent formation in a specific small region, given that a new vent forms. These are the types of basic models for the opening of new vents, required in many volcanic hazard assessments. These models require knowledge of the spatial distribution of past events, derived from geological and geophysical studies. An important assumption in these examples is that this conditional probability can be evaluated independently of temporal recurrence rate of new vent formation. A spatio temporal

analysis for the likelihood of new vent formation would need to evaluate the temporal recurrence rate, in addition to the spatial recurrence rate (e.g. [169]). Additional geochronological information is needed for spatio temporal recurrence rate models, in which the spatial distribution and frequency of vent formation is not considered to be independent.

A large number of alternative spatial density models for new vent formation might be estimated using different kernel density functions [90], or other nonparametric statistical methods, such as the Cox process model [123]. A more complex model could take a Bayesian approach, and integrate geologic/process information into the prior conditioning of the spatial distribution model. Such models require the abstraction of more complex geologic information into the prior functions [35], [143].

5.2.4. Summary

Renewed eruptive activity in volcanic systems often involves the formation of a new vent or several vents. Formation of a new vent within the perimeter of a nuclear facility is considered to be beyond design basis. Therefore the probability of new vent formation must be assessed as part of site volcanic hazard assessment. In addition, opening of new vents results in eruption products, such as tephra fallout and lava flows, which affect areas well beyond the immediate vicinity of the new vent. Therefore the probability of opening of new vents is considered when assessing these hazards (e.g. [16]). A variety of methods exist to assess the probability of opening of new vents, such as kernel density methods, Cox process methods, and Bayesian methods such as those used to weight nonparametric models using geophysical data [35], [143]. In general, a series of models can be constructed to bound uncertainty in the probabilistic assessment of opening of new vents.

5.3. VOLCANO GENERATED MISSILES

5.3.1. Physical characteristics

One of the hazards associated with explosive eruptions is the ejection and subsequent emplacement of large rock and lava fragments that follow nearly parabolic trajectories from the vent to the ground. Such fragments can be formed during lava bubble bursting as in Strombolian type eruptions or, for more explosive eruptions, during the fragmentation and/or reworking of deposits in the conduit. These particles are commonly referred to as volcanic ballistic projectiles in the scientific literature, however are here referred to as volcano generated missiles for internal consistency.

Volcano generated missiles are propelled by high pressure gas and have velocities in the range of 50–300 m s^{-1}. The distance travelled is a function of initial velocity, ejection angle, particle size, gravity, and aerodynamic drag, which can be reduced behind the shock waves produced by large eruptions. Collisions with other volcano generated missles may also significantly change distance travelled. Diameters can range from > 6 cm to several meters. Drag forces significantly decelerate small particles, however have less influence on large (> 1 m) blocks and bombs. Large particles are primarily decelerated by the influence of gravity. These factors mean that even large, dense particles can travel kilometers from the volcanic vent.

Studies based on field observations [169–173], experiments [174], [175], and theory [176], [177] all indicate that ballistic projectiles may have kinetic energy in excess of 10^6 J. The impact energy of projectiles is enough to penetrate common building materials including

wood, concrete, and steel [178], [179]. Additionally, projectiles formed from fresh lava can retain high temperatures on impact. These temperatures are typically above the ignition point for vegetation and other common objects. Casualties, damage to infrastructure, and fire ignition resulting from volcanic ballistic projectile impact have been reported at Sakurajima in Japan [180], Stromboli in Italy [181], Masaya in Nicaragua [182], Popocatépetl [183] and Colima in Mexico [184], and other locations [178].

Volcano generated missiles can be associated with a wide variety of eruptions, but are especially notable products of Strombolian and Vulcanian style eruptions, and thus with eruptions at composite, shield, and monogenetic volcanoes. Ejection of missiles nearly always accompanies the opening of new vents and secondary vents associated with lava flows and pyroclastic flows.

5.3.2. Potential effects for nuclear installation

Volcanic ballistic projectiles can cause extreme damage to man made structures. For example, during the 1994–1998 explosions at Popocatépetl volcano, ballistic projectiles damaged power supply systems at seismic stations [183]. At Stromboli volcano, the explosion of 5 April 2003 launched projectiles that produced damages at the small town of Ginostra, affecting buildings and other infrastructure [181]. The potential for impact depends primarily on the initial ejection conditions (e.g. launch angle, ejection velocity, and particle size) and the local environmental conditions (e.g. topography between ejection site and impact site, and atmospheric density). The impact energy, temperature, and frequency of impacts will each contribute to the severity of damage resulting from impact.

During the 27 May 2010 eruption of Volcán Pacaya, Guatemala, the 18 MW Amatitlán geothermal plant, located 3 km north of the active vent, received ballistic bombs and blocks, up to 25 cm diameter (long axis) and an estimated 20 cm of coarse tephra (0.5–50 mm) [185]. Upward facing uncovered steam condenser fans and roofs were dented and bent from falling blocks and heavily abraded by coarse tephra, rendering the units nonoperational and the plant remained offline for three weeks while cleaning and repairs were carried out. Intake and outlet pipe cladding was also dented, although no pipes required replacement or repair and no reduction in thermal efficiency was observed [185].

5.3.2.1.Consideration for siting

As indicated in TABLE 4, the effects from volcano generated missiles should be considered, in principle, one of the exclusion criteria for the site. The range of possible energies of impacting particles can be compared with impacts due to tornado borne projectiles. For example, NPPs in the United States consider the potential impacts of tornado generated projectiles ranging from a 2.5 cm diameter steel sphere traveling at ~8 m s^{-1} to an automobile traveling at ~ 40 m s^{-1} [186]. Nevertheless, such tornado generated impacts occur as transient events at ambient temperatures. Volcano generated missiles can occur at high temperatures with the potential for multiple impacts in a single eruption, which are significantly more severe conditions than envisioned for impacts from tornado generated projectiles. Nevertheless, if the frequency of impacts is low, risks associated from volcanic missile hazards might be reducible to acceptable levels by means of site and plant layout, design, operation and site protective measures.

Although the range of volcano generated missiles increases with increasing eruption explosivity (i.e. missiles generated by Strombolian style activity cannot travel as far as those

generated by Plinian style activity), in practice these missiles rarely travel more than 10 km from the vent. It is therefore unlikely that a proposed site would be located close enough to an existing vent for ballistic projectiles to be of potential hazard. Thus, the analysis would need to focus on ballistic projectiles arising from the opening of new vents if the potential for new vent formation is credible in the site area.

5.3.2.2.Consideration for operations and emergency planning

The surrounding critical infrastructure, including roads, electricity transmission lines, telecommunications and water systems servicing the facility, also are vulnerable to damage from impacting volcanic ballistic projectiles. The ignition of vegetation could result in fires that inhibit access to the site and/or disrupt other services into the site (e.g. power supply, water supply, telecommunications, etc.). Electrical and water supplies could be interrupted for prolonged periods by ballistic impacts, potentially leading to a system blackout condition. The probability of ballistic impact due to new vent formation in the region around the site, in addition to the probability of impact due to the eruption of existing vents, should be considered in the analysis.

5.3.3. How to evaluate effects

For hazard estimates for each capable volcano, it is necessary to estimate the source locations, potential magnitude, and frequency of future explosive eruptions. Threshold values for the maximum distance and maximum impact force that volcano generated projectiles can attain should be determined using information on the maximum distance and maximum size of projectiles produced in previous explosive eruptions from analogous volcanoes. Transport models can be used to determine screening distance as a function of exit speed, particle density, launch angle, and wind field parameters. The analysis should consider the effect of topographic barriers between the nuclear power plant and the vent and the possibility of the generation of projectiles from secondary vents. Impacts due to the possibility of new vent formation should be incorporated into the analysis for locations where new vent formation is a credible hazard.

5.3.3.1.Ballistic models

Several models have been developed to correlate the ejection velocity at the vent of the gas pyroclast mixture to the range reached by the volcanic ballistic projectile during explosive eruptions. Basic models account for the mechanics of particle flight [170–172], [187], [188], atmospheric drag [173], [176], drag reduction in the near vent region due to explosion dynamics [177], [189], additional atmospheric and conduit conditions [174], and multiphase flow in the atmosphere [190]. The factors output from ballistic models that are most relevant to hazard analysis at nuclear facilities are the maximum range and impact energy of projectiles.

During flight, volcano generated missiles are subject to gravity and drag forces. The ballistic equations describing the trajectory of ballistic particles can be expressed as [173], [174], [188]:

$$\frac{dv_x}{dt} = -\frac{AC_d\rho_a(z)(v_x-u_x)|v-u|}{2m} \quad (26)$$

$$\frac{dv_z}{dt} = -\frac{AC_d\rho_a(z)v_z|v-u|}{2m} - g \quad (27)$$

where x and z are the horizontal and vertical position coordinates respectively, $v = (v_x, v_z)$ is the velocity vector of the projectile, t is time, A and m are the cross sectional area and mass of the VBP, respectively, C_d is the drag coefficient, $\rho_a(z)$ is air density as a function of altitude, $u = (u_x, 0)$ is wind velocity (considering only tailwind velocity u_x), $|u - v| = \sqrt{(v_x - u_x)^2 + v_z^2}$ and g is gravitational acceleration. For ellipsoidal particles the ratio $\frac{A}{m} = \frac{3}{(2\rho_b D)}$ where ρ_b is the ballistic density and D is the geometric mean of three perpendicular diameters. Air density decreases with the altitude and can be described as a quadratic function fitting published altitude density data [173]. EQ. (26) and EQ. (27) can be solved numerically [188].

The drag coefficient C_d plays a key role in the trajectory of the VBP. It depends on shape, orientation and roughness of the VBP and on the Reynolds and Mach numbers, which indicate the flow regime. Drag coefficient values typically vary from 0.5 to 1.0 [174]. Most ballistic models assume that particles are ejected into still air from the moment they leave the vent and that their travel from this point onward is unimpeded by interactions with other particles such that their ejection results in 'purely' ballistic trajectories. However, observations indicate that the situation for actual particles is often more complicated. For example, missiles may be ejected into an expanding gas cloud, which reduces the drag force near the vent significantly [176], [177], [190]. In other cases, interactions between particles can result in changes to particle trajectories, significantly increasing or decreasing the maximum range attainable by any given particle [191].

In order to account for reduced drag in the near vent region, Fagents and Wilson (1993) assume that the ejected material accelerates to a maximum velocity (v_o) at some distance (R_o) and time (t_o) from its initial position, and then decelerates at the rate:

$$v = v_o \left(\frac{R_o}{R}\right)^2 \exp(-t/\tau) \tag{28}$$

where the time constant τ is related to the ratio of initial gas pressure (P_g) to atmospheric pressure (P_a):

$$\tau = \frac{P_g}{P_a} t_o \tag{29}$$

Similarly, Mastin [189] incorporate an arbitrary distance from the vent over which the drag coefficient is reduced. In these approaches it is assumed that the volcano generated missiles are launched into the surrounding atmosphere from a fixed position and with a chosen velocity and angle.

The kinetic energy of the volcanic ballistic projectile at impact is calculated using

$$KE_f = \frac{1}{2} m v_f^2 \tag{30}$$

The force of the impact of pyroclasts on engineered structures is calculated from Newton's law, $F_{impact} = ma$, where m is the mass of the pyroclast and a is its acceleration. For theoretical purely elastic collision, the acceleration is $\frac{\Delta v_f}{\Delta t}$, where v_f is the speed of the pyroclast immediately before impact and Δt is the duration of the impact. The speed of sound in

a pyroclast, σ, $\sigma = \sqrt{\frac{E}{\rho}}$ where E is the elasticity (Young's modulus) of the pyroclast and ρ is its density. The duration of the collision is $\Delta t = 2L\sigma$ where L is the length of the block (perpendicular to the impacted surface). If the collision is purely elastic, so that after the bounce the upward speed of the pyroclast is also v_f, the change in momentum is $2mv_f$, and the impact force is:

$$F_{impact} = \frac{mv_f}{\Delta t} = mv_f \frac{\sigma}{L} \quad (31)$$

which yields a maximum impact force, as the change in momentum is likely much less than estimated for the purely elastic case. A typical value for the speed of sound in a solid dense pyroclast is 5000 m s^{-1}. High pyroclast porosity and/or temperature will reduce this impact force. Alternatively, a stopping distance may be used to estimate impact force for an inelastic case:

$$F_{impact} = \frac{mv_f^2}{d} \quad (32)$$

where d is the stopping distance, evident in the field as the displacement in the underlying unit resulting from impact.

5.3.3.2.Explosive scenario definitions

In order to determine the hazard posed by volcano generated missile impact during volcanic explosions in a realistic and comprehensive manner, it is necessary to establish the different explosion scenarios that can occur at each potential vent location. This may include existing vents, in which case the scenario(s) may be defined given the volcano's past activity, and/or impacts due to new vent formation, in which case scenarios may be defined given information from analogous eruptions. The determination of explosive scenario(s) that may be capable of impacting the site and surrounding infrastructure should be based on the geology of capable volcanoes within the region, including the probability of new vent formation. Once these scenarios are defined, the appropriate model to use for range considerations and impact energies (as well as the corresponding input parameters to these models) may be determined.

Examples of different explosive scenarios to consider might include (a) new vent formation near the site characterized by normal Strombolian activity resulting in rapid accumulation of high temperature pyroclasts and/or (b) higher energy violent Strombolian or Vulcanian activity occurring at greater distance from the nuclear power plant yet impacting a larger area.

Major differences between explosive scenarios include the anticipated kinetic energies, particle sizes and densities, and the parameterization of particle drag. Whether particles are erupted into a still atmosphere (i.e. constant or variable drag) or propelled within an expanding gas region (i.e. no drag) can dramatically alter the anticipated range of projectiles (See FIG. 30).

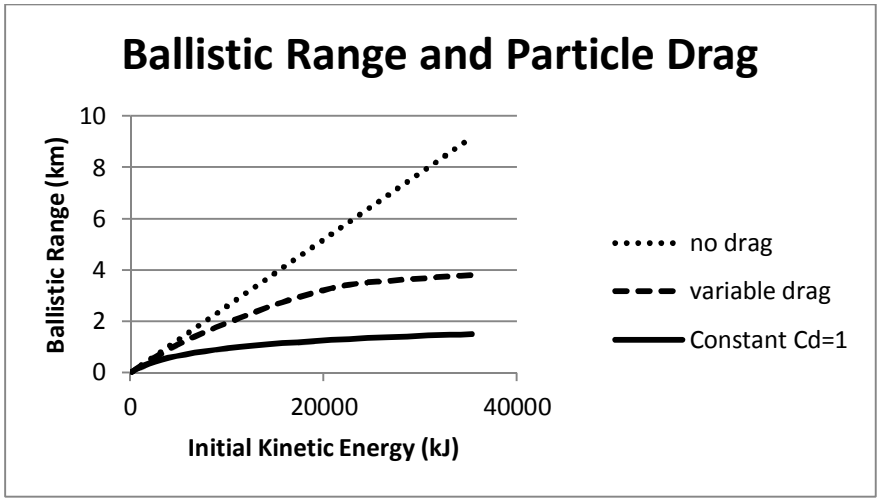

FIG. 30. Ballistic range as a function of initial kinetic energy for multiple particle drag parameterizations. Particle density = 1500 kg m^{-2}, diameter = 0.5 m, launch angle = 45 deg, ejection altitude = landing altitude. Calculated with Eject! Ballistic calculator [189].

5.3.3.3.Maximum range and Strombolian eruptions

The maximum range of ballistic projectiles can be estimated for a range of initial ejection velocities, particle sizes, and particle densities. Care should be taken in the parameterization of particle drag, with higher energy eruptions typically resulting in less atmospheric drag as particles are carried farther within the expanding gas region. The initial kinetic energies of projectiles correspond to the anticipated explosivity of eruption. Normal Strombolian eruptions generate projectiles that typically do not travel more than a few kilometers from the site while higher energy eruptions, including violent Strombolian and Vulcanian eruptions, can result in particles impacting up to 10 km from the site. The goal for hazard analysis is to utilize EQ. (26), EQ. (27) and EQ. (31) to determine the effective upper limit of the range and impact energy of projectiles in order to determine both the probability of impact and the likely effect that impacting volcano generated missiles may have on the facility.

5.3.3.4.Coupling Maximum range and Vulcanian eruptions

In the case of a Vulcanian explosion, EQ. (26) through EQ. (30) may be used with higher ejection velocities (up to ≈ 300 m s^{-1}). Alternatively a model such as that proposed by Alatorre-Ibarbuenrgoitia and Delgado-Granados [174], in which the fragmentation energy of the initial caprock is used to determine the initial conditions of ballistic projectiles, may be utilized. In this model, the effective pressure (P_{ef}) available for particle ejection is given by:

$$P_{ef} = P_o - P_{th} \tag{33}$$

where P_o is the initial gas pressure and P_{th} is the fragmentation threshold of the magma, defined as the minimum pressure differential that leads to complete fragmentation of the pressurized porous magma [192]. The ejection velocity of the particles thereby depends on the surplus kinetic energy available after fragmentation. The equation of motion of the caprock propelled by the expansion of the gas–particle mixture is [193]:

$$\frac{dV_c}{dt} = \frac{A_c}{m_c}\left\{P_{ef}\left[1 - \frac{1}{2}(\gamma - 1)\frac{V}{\sqrt{n\gamma R_g T_o}}\right]^{\frac{2\gamma}{\gamma-1}} - P_{ext}\right\} - g \quad (34)$$

where V_c, m_c, and A_c represent the velocity, mass, and cross sectional area of the caprock, respectively, γ is the specific heat capacity ratio of the mixture considering only the fraction of particles in thermal equilibrium with gas, n is the mass fraction of gas, R_g is the gas constant, T_o is the initial temperature, and P_{ext} is the pressure above the caprock. This equation can be solved numerically to obtain the caprock velocity as a function of time, provided the flow remains one dimensional.

This model can be used together with the normal ballistic model to estimate the range of the volcano generated missile given the initial magma conditions of Vulcanian eruptions: The former model is used to estimate the ejection velocity of the caprock, which is then used as the launching velocity of the volcanic ballistic projectile. This method helps to account for the drag reduction near the vent using the simple approach proposed by Fagents and Wilson [176] given by EQ. (28).

5.3.3.5.Coupling Maximum range with the probability of opening of new vents

Given that the most likely scenario in which a facility is directly impacted by volcanic ballistic projectiles is in the case of the opening of new vents, it may be necessary to couple the probability of new vent formation, described in Section 5.2, with the maximum range calculation. Once the maximum range has been determined, the probability of volcanic ballistic projectiles impacting the site is estimated by integrating the probability of opening of new vents over the area within this distance of the site.

The likelihood of inundation by a large number of high temperature particles, a potential site exclusion criterion, can be determined by considering only the probability of new vents in close proximity to the site. To include impacts from higher energy eruptions (i.e. violent Strombolian, Vulcanian), the probability of vent formation over an area given by the expected range of particles from these types of eruptions must be considered.

Additionally, to consider the potential impact of volcanic ballistic projectiles from the opening of new vents on infrastructure critical to the nuclear power plant (electrical and water transmission lines, roads, etc.), the probability of vent formation over a much wider area should be considered.

5.3.3.6.Probabilistic Models

Unlike many other phenomena, computational models designed to sample the parameter space of possible initial conditions to determine the probability of volcano generated missiles impacting a site given an eruption have not generally employed. Instead, investigators tend to determine either a maximum attainable distance (e.g. [10]) or utilize multiple hazard scenarios corresponding to a variety of distance estimates (e.g. [174], [175]). Where probabilistic methods have been employed [175], they involve investigations of the likelihood of the occurrence of various eruptive scenarios (e.g. VEI 2, VEI 4) rather than the likelihood of the occurrence of specific initial conditions (e.g. ejection angle, initial velocity).

For example, by assuming an inverse relationship between eruption magnitude and occurrence rate, Alatorre-Ibargüengoitia et al. [175] were able to categorize eruptive scenarios by eruption magnitude. This enabled a probabilistic analysis of the volcanic hazard posed by volcano generated missiles at Popocatépetl volcano, Mexico.

5.3.3.7.Examples of evaluating potential hazards

As a practical example of volcanic ballistic projectile hazard assessment at a nuclear power plant site, we will summarize the work of Connor et al. [10] for the volcanic Hazard Assessment of the ANPP Site.

The Armenia site is located on the Shamiram Plateau where the probability of volcanic ballistic projectiles impacting the site is tied to the probability of opening of new monogenetic vents. For this assessment, the potential range, velocity, and impact force of ballistic projectiles is calculated assuming initial conditions designed to provide the maximum ranges and energies expected from new vent formation in the region. Ejection velocity is varied to determine the likely maximum range and impact energy of volcanic ballistic projectiles (See FIG. 31).

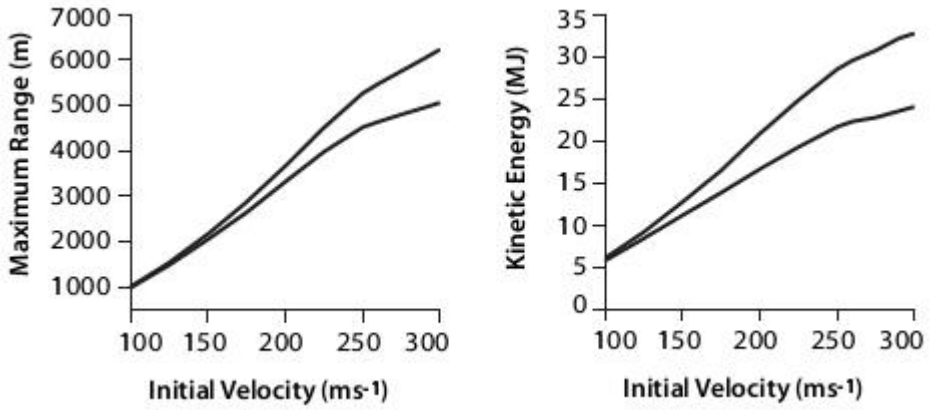

FIG. 31. Maximum range and impacting kinetic energy calculated for spherical particles of 1 m diameter ejected at a launch angle of 45 degrees with variable drag and a reduced drag region extending 500 m from the vent. Particle densities of 2200 kg m^{-3} and 1200 kg m^{-3}, representing dense lithic and dense pumice clasts respectively, were considered. Reproduced courtesy of the Ministry of Energy and Natural Resources of the Republic of Armenia [10].

Ranges corresponding to the approximate upper bound of velocities generated by Strombolian eruptions (~ 150 m s^{-1}) and higher energy violent Strombolian and Vulcanian eruptions (~ 300 m s^{-1}) were determined. These maximum ranges (2 and 6 km, respectively) were then used as the bounds over which to consider the probability of the opening of new vents. That is, to determine the probability of inundation by an abundance of hot volcanic clasts, the probability of opening new vents was integrated over an area extending 2 km radially from the site. To determine the probability of volcanic ballistic projectile impact from higher energy eruptions, the probability of opening of new vents was integrated over an area extending 6 km from the volcano.

5.3.4. Summary

Volcanic projectiles are pyroclastic particles, often of large size, that are forcefully ejected as a result of explosive activity at volcanic vents and which subsequently fall under gravity subject to atmospheric drag. Impacts from volcanic projectiles can result in damage, including penetration, to wood, concrete, and steel structures. Although nuclear facilities typically are designed against impacts from tornado generated projectiles, impact energies associated with single volcanic projectiles might exceed typical design bases. In addition, volcanic events have the potential to create many (hundreds to possibly thousands) of impacts, which might occur at significantly elevated projectile temperatures. The temperature of juvenile objects can ignite vegetation and/or man made objects on contact. As indicated in TABLE 4, the effects from volcanic projectiles usually are considered an exclusion criterion for the site. Nevertheless, if the frequency of potential impacts is low, risks associated from volcanic projectile hazards might be reducible to acceptable levels by means of site and plant layout, design, operation and site protective measures. Modeling of volcanic projectiles requires outlining hazard scenarios that define the range of energies, sizes, and parameterization of atmospheric drag. Once these features are defined, models can be used to determine the maximum range and impact energy of volcanic projectiles given each eruption scenario.

5.4. TEPHRA FALLOUT

5.4.1. Physical characteristics

The fall and deposition of pyroclastic material such as ash, pumice and scoria occur when these particles (generally called tephra) are lifted by an explosive eruption to altitudes of several kilometers to tens of kilometers (generally < 50 km above sea level). Tephra particles (micron to decimeter in diameter) carried aloft in volcanic plumes are advected by the wind, and sediment on to the surrounding areas. On falling, pyroclasts typically reach a constant velocity (the so called terminal velocity), which is determined by the size, shape and density of the falling particle, air density and air viscosity. Their dispersal is governed by wind velocity and direction and by the nature of the eruption column. The thickness and thus loading of tephra fallout varies widely with distance from the source and the intensity of the volcanic eruption (from few mm to several metres). The most intense volcanic eruptions can generate tephra fallout that exceeds 1000 kg m^{-2} in areas located within a few tens of kilometers of the volcano. Small eruptions result in tephra fallout of 10 kg m^{-2} at a few kilometers from the volcanic vent. The thickness and mass per unit area of tephra deposited generally decrease with distance from the volcano, each in a roughly exponential manner. Deposit density range from less than 500 up to more than 1500 kg m^{-3}. When wet, tephra loads of thick deposits may be up to double these values [194].

Tephra falls have created airborne particle concentrations of up to 9 g m^{-3} [195], which are several orders of magnitude higher than those experienced in dust and sandstorms. Tephra particles have unique physical and chemical properties, which may vary widely at different locations during and between eruptions. Tephra is made up of various proportions of vitric (glassy, non crystalline), crystalline and lithic (non magmatic) particles. Vitric particles are typically vesicular and have extremely high surface area to volume ratios. Tephra particles can have irregular particle morphologies and composition which makes them hard and highly abrasive. The variable density and particle shape of tephra particles means their settling behaviour does not typically follow Stokes Law. Exsolved magmatic gases condense onto

tephra particle surfaces while they are in the conduit and eruption plume [196]. While some 55 ionic species have been reported in fresh tephra leachates, the major species found are the cations Na^+, K^+, $Ca^{2+}$and Mg^{2+} and the anions Cl^-, F^- and SO_4^{2-} [197], [198]. The pH of fresh tephra leachates has also been found to be highly variable [197]. Tephra surface coating contains salts and sometimes also acidic gas condensates. These salts are very readily soluble and may deliquesce if relative humidity is high. These properties give tephra a high potential to chemically enrich receiving waters, to be corrosive and of low electrical resistance, when wet [199].

5.4.2. Potential effects for nuclear installation

Tephra fallout is the most widespread hazardous phenomenon from volcanoes. Even minimal tephra accumulation has the potential to disrupt normal operations at a nuclear power plant. Thick tephra accumulation might render a site temporarily inoperable. Possible impacts of tephra fall are listed below:

- The most common disruption of electrical generation and transmission facilities by tephra fall are flashovers (the unintended disruptive electric discharge over or around the insulator) caused by tephra contamination of substation and line insulators, causing disruption to transmission and distribution networks [200]. This could disrupt power supply to the NPP. When wetted, the resistivity of tephra drops significantly due to the small particle size efficiently collecting a water film and the presence of the soluble salts on the particle surface [199]. Cleaning of tephra contaminated insulation and conductors may also require controlled outages;

- Tephra fall or remobilized tephra deposits may disrupt back up power generation units, due to blockage of air intakes or contamination of fuel lines. No empirical observations of this exist from known tephra falls, but it should be considered possible. If back up power generation is disrupted and the main transmission line has been disrupted, it has implications for a NPP's ability to shut downsafely;

- Air heating, ventilation and air conditioning (HVAC) systems may be disrupted by tephra ingress during tephra falls or during remobilization of tephra deposits. External condenser units may be vulnerable to blockage by tephra, especially if wetted [201]. Tephra ingress into air handling systems (e.g. HVAC) can block intakes reducing system performance, resulting in knock on effects to dependent systems. If the system is not split (with separate condenser and air handler units) tephra may be blown into the facility, contaminating the interior atmosphere and causing damage to sensitive equipment. HVAC systems are also vulnerable to abrasion and corrosion when exposed to tephra;

- Surface water supplies (i.e. used for cooling or drinking) are vulnerable to contamination. Tephra suspended in water will increase turbidity in raw water sources. Very fine tephra may settle slowly and residual turbidity may remain in standing water bodies. Tephra accumulation may be sufficient to clog water cooling systems, filters and pipes. Tephra is abrasive to mechanical parts, pipes, blades, potentially causing failure of pumps, In tributary rivers, tephra may continue to be remobilised by rainfall events, and may generate potentially damaging lahars. Fresh tephra has a surface coating of soluble salts that are rapidly released on contact with water, although most natural waters have sufficient alkalinity to make pH changes unlikely [202].

Compositional changes depend on the tephra surface chemistry, the amount of tephra fall and the dilution volume. The potential exists for tephra and associated products to accelerate corrosion.

- Tephra may create loads on structures, particularly when it is wet static loads may increase by up to 100% [194]. Long span, low pitched roofs are typically the most vulnerable [203];

- Conductor (line) breakage, bridged phases, and damage to towers and poles due to tephra loading, both directly onto the structures and by causing vegetation fall onto lines. Precipitation (especially snow and ice accumulation on lines and vegetation) will exacerbate the risk tephra by increasing tephra density [199].

- The deposition of moistened tephra on gravel ballast (substrate) in substation and electrical yards, which is of known resistivity to provide a safe environment for substation workers, could potentially reduce resistivity and increase the possibility of an electrocution hazard [199]. Tephra clouds experience electrical charge separation, so the potential for lightning strikes increases during tephra deposition.

- Tephra accumulation at a nuclear installation will require site cleanup. Tephra cleanup operations can be time and resource consuming, so require adequate planning [201].

- Tephra can be hazardous to people. Direct exposure may cause irritation in the respiratory tract, particularly for people with pre-existing respiratory conditions (e.g. asthma). Direct exposure and irritate eyes and skin. Contamination of water and food supplies may also occur in extreme cases. Disruption of electricity and water supplies from tephra may also have public health consequences.

5.4.2.1.Consideration for siting

Tephra fallout is generally not a site suitability issue unless the volcano is within several tens of kilometres. IAEA guidelines indicate that potential tephra fallout should be assessed as a design basis event.

5.4.2.2.Consideration for design basis

The effects of tephra fallout are not generally considered as part of the exclusion criteria of the site, since these effects usually can be mitigated by means of appropriate design and operation measures.

There are few examples of design criteria for mitigating against tephra fall, however field observations and limited laboratory testing has given some insights (e.g. [201]). Tephra load on structures is possible to mitigate by design, such as by strengthening or increased roof pitch. Design of transmission facilities should consider increasing insulation and other anti pollution strategies to mitigate flashover caused by tephra contamination. The design of backup power supply systems should consider adequate filtration of air supply and cooling systems for very high suspended particle concentrations and a well sealed compartment for the generator set. Horizontally orientated, split (i.e. separate condenser and air handler) HVAC systems are most resilient to tephra fall [201]. Shielding from tephra ingress and filtration should be considered where tephra hazard is high.

Exposed surface water supplies are vulnerable to tephra fall contamination. Settling reservoirs or ponds may allow most tephra to settle, however, coagulation and flocculation may be necessary if low turbidity is required. Appropriate siting and design of intake structures will also increase resiliency. For example, drawing water from several metres below the surface will avoid floating pumice rafts. Clean up methods (i.e. for power systems and general site) typically use large volumes of water, if wet methods are used. Stored water supplies for extensive cleaning operations might need to be isolated from tephra contamination.

5.4.2.3.Consideration for operations and emergency planning

Even minimal tephra accumulation has the potential to disrupt normal operations at a nuclear power plant.

Tephra accumulation at a nuclear installation will require site cleanup. Tephra cleanup operations can be time and resource consuming [201], so requires adequate planning. Wet cleanup methods may exhaust water supplies and lead to tephra accumulating in the waste water system, potentially causing blockages [201]. Dry cleanup methods therefore should be considered. Tephra dumps sites should be carefully selected and capped (i.e. with soil) to avoid on going remobilization [201]. Cleaning tephra from on top of structures is an effective way to reduce the static load. Following a tephra fall, cleaning of contaminated electrical systems (e.g. insulators and conductors) is typically required. Appropriate equipment and safety precautions need to be taken, as slips and falls are very common from surfaces made slippery by tephra [185]. Backup power generators and HVAC systems may be required additional shielding, filtration, maintenance and servicing. If turbidity exceeds normal operating range of water supplies systems for flood flows, suspended tephra may penetrate further into the plant and block filtration equipment. Tephra is highly abrasive and likely to cause accelerated wear on pump impellers. Tephra can penetrate bearings and seals and overload motors. However, previous documented examples for water treatment plants suggests a tephra fall is unlikely to cause service interruptions, although increased maintenance can be expected [201]. Where a high standard of water quality is required, monitoring of ionic concentrations may be required.

Tephra can be hazardous to people. Direct exposure may affect the respiratory tract, and irritate eyes and skin (e.g. [204], [205]), requiring the provision of protective equipment. These hazards might persist for years to decades after the tephra fall occurs, depending on deposit thickness and erosion or stabilization rates. Some circumstances may also lead to tephra contamination of water and food supplies, requiring planning consideration.

Long term exposure to tephra fall or remobilized tephra may create abrasion and corrosion hazards for sensitive components.

Tephra falls can be highly disruptive over a regional scale, which may cause indirect impacts to a NPP. Disruption to external services, such as power supply, water supplies and transportation linkages are common [201]. In particular, electricity supply (previously discussed) and site access may be compromised by disrupted transportation networks due to poor traction or visibility from falling and remobilized tephra. Modern telecommunications systems have not been reported disrupted by tephra fall, but are commonly disrupted by network overloading or loss of electricity supply [201]. Other sensing systems, such as radar, are potentially disrupted by tephra clouds.

5.4.2.4.Examples of evaluating potential hazards

Suspension of tephra in storage dams can lead to abrasion of turbines. During the October 1995 Ruapehu eruption, 7.6 million cubic metres of coarse basaltic andesite tephra was deposited into the Tongariro river catchment, leading to high levels of suspended sediment. This catchment feeds the Rangipo power station (120 MW), which has an intake to the underground headrace tunnel 20 km from Ruapehu volcano. The tephra was composed of varying mixtures of volcanic glass, plagioclase, orthopyroxene and clinopyroxene; there were also minor components of lithic or country rock fragments and spheroids of elemental sulphur [206]. Management elected to continue generation throughout the eruptive episode. However, during inspections in April 1996 it was discovered that significant wear had occurred to the two Francis turbines and all auxiliary components that had been in contact with the suspended tephra. Over a six month period the components suffered the equivalent of 16 years' abrasion damage [207].

In contrast, turbine damage did not appear to be a feature of the impacts of the May 2008 eruption of Chaitén volcano, Chile, on the 448 MW Futaleufú hydro dam, located approximately 90 km SE of the volcano in Chubut province, Argentina. A direct tephra fall of between 50 and 100 mm of fine grained rhyolitic tephra was received at the hydro dam, although greater thicknesses were received across the storage lake and catchment. Due to its fine grain size and high pumice content, tephra remained suspended in the lake for over eight weeks, during which time the dam continued to generate electricity. In February 2009, engineers reported that there had been no drop in generation efficiency, suggesting that turbines had not been damaged by abrasion [201]. However, no inspection was made at the time. The Fuataleufú dam did suffer other problems as a consequence of the tephra fall. Electricity transmission was disrupted by tephra accumulating on vertical transformer insulators in the step up substation which induced a significant flashover fault. The substation connects the dam to the Chubut province power grid, a 240 kV high voltage transmission system. The fault occurred in early May following light misty rain (approx. 2 mm/h) which wetted the tephra, but did not wash it off surfaces. Flashovers also occurred on the 240 kV high voltage Chubut transmission lines. Following this major fault, the dam, substation and transmission lines were cleaned every 10 days for several months as a precaution, due to ongoing light tephra falls and wind remobilised tephra. The tephra was difficult to remove even with a high pressure hose, as it had 'cemented' to the insulators. In some cases crews had to chip tephra off the insulators with a screwdriver. The heavy tephra falls also blocked rain gauges in the dam's catchment. This was a major safety concern for the dam as the tephra fall occurred during the rainy season when high rainfall events could lead to rapid lake rises. The dam management also developed strict building entry exit protocols to limit tephra ingress into buildings, particularly to avoid contamination in the powerhouse and control rooms. This included taping plastic sheeting around windows, doors and HVAC ducts; installing sticky floor mats to collect tephra off footwear; and instigating double door entry. Cleaning up the dam site was a major task. Over 180 t of tephra was removed from the powerhouse roof and substation area (approximately 1500 m^2). There were also difficulties with access to the site due to the poor visibility and traction problems caused by tephra falls on roads [201].

5.4.3. How to evaluate effects

A significant difficulty in the assessment of tephra fallout hazards is that many Quaternary tephra fallout deposits are not preserved in the geologic record. These unconsolidated deposits erode rapidly. Therefore, tephra fallout hazard, while in part developed from an understanding of the volcanic history of the area, often has to rely heavily on simulation of potential eruptions to account for past events that were not preserved in the geologic record (See also discussion in Section 4).

Modeling and forecasting of tephra fallout is crucial to public safety. Empirical, analytical and numerical models have been developed during the last two decades to allow quantitative interpretation and description of tephra deposits. Dedicated analytical and numerical models have also been produced, providing long term assessments for land use planning and a rapid response during volcanic crises. Model testing has shown a reasonable agreement with field data and airborne observations, which supports the use of these models for hazard applications.

5.4.3.1.Existing modeling approaches

Most models for tephra dispersal are based on the mass conservation equation with different degrees of simplicity, following either Eulerian or Lagrangian formulations. The Eulerian approach describes changes in the fluid as they occur at a fixed point, whereas the Lagrangian approach describes changes occurring by as following a fluid particle along its trajectory. Each approach is useful for different applications. For example, weather forecasting is based on the Eulerian approach (fixed measurement system) because it uses data from fixed stations all over the world. The Lagrangian approach is more useful when describing the evolution of a given material as it moves within a certain fluid (e.g. chemical modeling). Tephra dispersal is often described using both approaches and different degrees of approximation ranging from simple empirical to analytical and numerical models.

Basic models

Empirical models

Different empirical methods describing thinning of tephra deposit with distance have been proposed. They range from models based on the exponential and power law thinning on a semilog plot (e.g. [208–211]) to the description of the deposit thinning through a Weibull distribution [212]. Regardless of their strong dependence on tephra deposit exposure and distribution of isomass or isopach contours, empirical integrations of deposit thinning trends have limitations. The exponential method is mainly sensitive to the number and the choice of straight segments, whereas the power law method can better reproduce the natural thinning of tephra deposits but is strongly sensitive to the proximal or distal extreme of integration. However, when data are not well distributed or only a few isopach contours are available, uncertainties are typically large. Data fitting with one or more exponential segments on a semilog plot is straightforward but requires an arbitrary choice of segments and can often underestimate the volume by a factor of 2.5 when proximal or distal data are missing (e.g. [210], [212], [213]). The power law fit can better reproduce the natural thinning of tephra deposits, but cannot be integrated between zero and infinity and can significantly overestimate the volume (up to a factor of 5–6) when proximal or distal data are missing [212]. The Weibull method shows a better agreement with observed data (up to a factor of 2–3), reconciling the debate on the use of the exponential versus power law method. Using this kind of an approach typical thinning parameters can be estimated for different eruption styles and an order of magnitude distance can be estimated for tephra thicknesses that represent potential hazards [211], [212].

Intermediate models

Analytical models

Depending on the application, when some approximations hold (e.g. horizontally uniform wind field, constant diffusion coefficient, negligible vertical motion and diffusion, far enough from the vent where we can neglect expansion rate of an umbrella cloud), the mass conservation equation for tephra particles can be simplified and solved analytically (e.g. [214–219]):

$$\frac{\partial C_j}{\partial t} + U\frac{\partial C_j}{\partial x} + V\frac{\partial C_j}{\partial y} - \frac{\partial (V_{S,j}C_j)}{\partial z} = K\frac{\partial^2 C_j}{\partial x^2} + K\frac{\partial^2 C_j}{\partial y^2} + S_j \qquad (35)$$

where C_j is the average concentration of particle class j, (U,V) are the horizontal wind velocity components, $V_{S,j}$ is the terminal velocity of a particle class j (a particle class is generally identified by particle diameter, density, and shape), and K is a turbulent diffusion coefficient.The first term on the left hand side of the EQ. (35) represents the time rate of change of the average concentration, whereas the second and third terms represent advection (i.e. wind transport) and the forth term represents sedimentation; the first two terms on the right hand side of EQ. (35) represent the diffusive transport due to the atmospheric turbulence (i.e. the simplest approach to describe turbulent fluxes consists of expressing turbulent fluxes as proportional to the gradient of average concentration), the last term, S_j, denotes the source (i.e. the mass flux of particle class j injected per unit volume and unit time). In these models the particle source, which is the eruption column, is typically described as a line source that can be characterized by various mass distribution functions ranging from point source to uniform to exponential. A solution of EQ. (35) is given by a Gaussian distribution (e.g. [214]). The total mass on the

ground is computed as the sum of the contributions of each of the point sources distributed above the ground and of each particle class (e.g. [219]).

Commonly, advection diffusion sedimentation (ADS) models are based on empirical parameters, such as the diffusion coefficient K and column shape parameters introduced for describing the term S. As a result, they must be verified and calibrated with field data of specific eruptions before they can be used for a reliable hazard assessment. Moreover as they are based on a passive transport assumption, their use in the proximal regions (of the order of the column height) is not justified as plume spreading at the neutral buoyancy level as a gravity current (e.g. [220]) can be a dominant transport mechanism in proximal regions. The good performance of these models even when extrapolated in the proximal region is due to the fact they use an effective diffusion coefficient that mimics some of the plume spreading effects. The advantage of these models is the simplicity of the physical parameterization and, therefore, the high computation speed, which allows for a comprehensive probabilistic analysis of the associated inputs and outputs and the solution of inverse problems for the estimation of eruptive parameters, such as total erupted mass and column height, crucial for the definition of eruption scenarios. Pivotal results include the fact that ADS models are very sensitive to both erupted mass and column height, which justifies the use of inversion solutions for estimating these parameters (e.g. [221–223]).

Complex models

Numerical models

When the simplifying assumptions made to derive EQ. (35) are no longer valid, or when there is a need to describe the three dimensional dispersion of the volcanic clouds within the atmosphere, fully numerical models are adopted. For instance, one case is when most of the transport occurs within the Atmospheric Boundary Layer (ABL), i.e. the part of the troposphere that is directly influenced by the presence of the Earth's surface, and responds to surface forcing with a time scale of an hour or less. In fact, due to both topographic effects and rapid temporal variations of wind and temperature field, wind fields and turbulent tensor components are significantly more complex in the ABL than in the higher atmosphere (i.e. free atmosphere). Such considerations might be important in understanding tephra dispersal from weak or low altitude (several kilometers high) plumes. Another case is when the dispersal covers very large regions where the wind field cannot be assumed to be uniform and representatively described by a simple vertical wind profile. Another case requiring a numerical approach is the tracking of volcanic ash clouds for diversion of aircraft flight path and grounding routinely performed by the Volcanic Ash Advisory Centers (VAAC) [224].

However, depending on the application, to make the problem tractable for practical purposes, several simplifying assumptions are introduced even in this category of models. For example, particle tracking models are mainly used to describe the atmospheric transport of volcanic ash for aviation safety, but, except for a few cases [225], they are not used to calculate ground deposition. Several Volcanic Ash Transport and Dispersal Models (VATDM) are routinely used by VAACs to forecast ash cloud location and issue periodic Volcanic Ash Advisories in order to mitigate the associated risks. Other VATDM are used to describe ash ground deposits especially in highly urbanized areas near volcanoes (e.g. Catania, Italy, [226]). The London VAAC, responsible for the Icelandic volcanoes, uses the U.K. Met Office's Lagrangian Numerical Atmospheric dispersion Modeling Environment (NAME) model [227], [228]. The adjacent Toulouse and Montreal VAACs use MOCAGE [229] and MLDP0 [230]

respectively. Other models used at other VAACs or to support national decision makers in different countries include CMAQ [231], EURAD [232], FALL3D [233], [234], FLEXPART [235], HYSPLIT [236], PUFF [237], and REMOTE [238]. For a review of the existing VATDMs as of 2011, see [239]. Additional models, such as Ash3D [240] and VOL-CALPUFF [241], [242] have been developed and also might be considered for use in these assessments. The main difficulties to model transport of volcanic ash are given by the quantification of the source term (i.e. mass eruption rate, column height, total grain size distribution), the possible occurrence of ash aggregation in the atmosphere that alters particle settling time, and the properties of ash particles themselves that can vary notably in shape and size (from sub microns to millimeters).

Among VATDMs, FALL3D [233], [234] is a Eulerian model for transport and deposition of volcanic ash particles used routinely at various institutes (e.g. Istituto Nazionale di Geofisica e Vulcanologia (INGV), Buenos Aires VAAC, etc.). The model solves a set of ADS equations (one equation for each particle class) similar to, but more general than Eq. (35) (e.g. [233]):

$$\frac{\partial C_i}{\partial t} + U\frac{\partial C_j}{\partial x} + V\frac{\partial C_j}{\partial y} + W\frac{\partial C_j}{\partial z} - V_{s,j}\frac{\partial C_i}{\partial z} =$$

$$\frac{\partial}{\partial x}\left(K_H\frac{\partial}{\partial x}C_j\right) + \frac{\partial}{\partial y}\left(K_H\frac{\partial}{\partial y}C_j\right) + \frac{\partial}{\partial z}\left(K_V\frac{\partial}{\partial z}C_j\right) + C_j\frac{\partial V_{s,j}}{\partial z} - C_j\nabla\cdot\vec{u} + S_j \qquad (36)$$

Where C_j is the average concentration of particle class j, $\vec{u} = (U,V,W)$ is the wind velocity vector, and $V_{s,,j}$ is the terminal velocity of a particle class j (a particle class is identified by particle diameter, density, and shape), the coefficients K_H and K_V denote the horizontal and vertical component of the turbulent diffusion tensor (typically in the free atmosphere $K_V/K_H << 1$), S_j, denotes the source (i.e. the mass flux of particle class j injected per unit volume and unit time). When particle aggregation needs to be described a loss term for finer classes has to be also considered.Each particle class is characterized by particle diameter, density and shape. The model deals simultaneously with a wide spectrum of particle sizes (i.e. from lapilli to fine ash) and trace gas components (e.g. H_2O). Particle aggregation can be accounted for using the wet aggregation model described in [243] but the model has no wet deposition mechanisms yet. The FALL3D model follows an off line strategy, that is, independent mesoscale meteorological models provide the meteorological fields *a priori*. The main volcanological model inputs are mass eruption rate (MER), total grain size distribution (TGSD), and height and shape of eruption column. The eruption column height and shape and the mass distribution within the column (i.e. source term) can be described using either a 1D Buoyant Plume Theory (BPT) model based on that of [244] or an empirical relationship based on [214]. The BPT option can provide the MER and the vertical distribution of mass given a column height. The empirical relationship option requires an independent assessment of MER, for example, by using the MER versus column height fits [220], [245]. Primary FALL3D model outputs are the time dependent deposit load and airborne mass concentration for each particle class. However, other physical and optical properties of ash clouds, such as particle number concentration, optical depth and extinction coefficients at 0.5 mm, are also computed [246]. FALL3D has already been tested against several tephra deposit data and space based ash cloud observations from different eruptions [226], [233], [234], [246–249].

5.4.3.2.Probabilistic assessment

First, all the potential sources that have the potential to produce tephra fallout at the proposed site should be carefully characterized defining all the credible eruption scenarios and estimating their probability of occurrence on the basis of the past activity of the volcano. These potential sources include very distant volcanoes capable of producing large explosive eruptions (> VEI 6) that can lead to accumulation of tephra of a few millimeters to centimeters at distances greater than 500 km from the source (e.g. 1815 A.D. Tambora eruption [250–252] and the major Samalas-Rinjani VEI 7 eruption in 1257 A.D. [253]). To define the eruption scenarios and their frequencies, it is necessary to characterize the past explosive activity of a volcano, which includes low volume events that are typically not preserved in sub aerial exposures. In addition to careful examination of the historical record, sedimentary deposits should be examined in detail (e.g. microtephra) for evidence of past tephra fall eruptions, because ash from small volume eruptions is typically best preserved in sedimentary basins.

One difficulty in the assessment of tephra fallout hazards is that many Quaternary tephra fallout deposits are not preserved in the geologic record. These unconsolidated deposits erode rapidly. Therefore, tephra fallout hazard, while in part developed from an understanding of the volcanic history of the area, often has to rely heavily on simulation of potential eruptions and information from analogous volcanoes, to account for past events that are not preserved in the geological region (See Section 4).

After data on past eruptions in the region is collected, these data are used to estimate parameter distributions for inputs to numerical models of tephra fallout. Using these parameter distributions, the conditional probability of tephra accumulation at the proposed site from all possible sources, given the potential range of eruption conditions and wind velocities in the region, should be completed.

Using a Monte Carlo simulation or other similar techniques, tephra fallout from each capable volcano should be conducted, accounting for variation in eruption volume, eruption column height, TGSD, wind velocity distribution in the region and related parameters. Such models lead to a frequency distribution of tephra accumulation, commonly presented as frequency of exceedance curve for the hazard (or 'hazard curve'). A hazard curve should be calculated independently for each volcano, and then a cumulative curve for all capable volcanoes should be considered. If uncertainty in the resulting hazard curves is expressed by confidence bounds, the basis for the selection of the reported confidence levels should be documented.

The hazard assessment for tephra fallout for each capable volcano should consider:

1. Vent locations, including the potential for the formation of new vents;

2. The magnitudes of potential tephra producing volcanic eruptions and the physical characteristics of these eruptions;

3. Meteorological conditions between source regions and the site that will affect transport and deposition of tephra;

4. Secondary effects of tephra eruptions, such as increased likelihood of lahars, potential for pollution and chemical corrosion, which may have adverse effects on the safe operation of a nuclear power plant.

Potential tephra fallout at nuclear installation sites can be assessed applying analytical models (e.g. TEPHRA2 [218], HAZMAP [219]) accounting for a wide range of potential eruption conditions, and using reanalysis wind data for the region (e.g. [254] or ECMWF ERA-40 reanalysis). If the capable volcano is located at distances larger than several hundreds kilometers (i.e. assumption of uniform wind does not hold on the entire domain) then a numerical 3D model should be used. Where relevant, ash aggregation processes should be considered as these aggregation processes may cause dramatic change in tephra accumulation at great distances from the vent.

Typical sources of uncertainty that need to be accounted for are related to the choice of physical parameters (e.g. total mass, column height, TGSD) and physical processes taken in account (e.g. ash aggregation). Pivotal data needed to model tephra fallout dispersal are total erupted mass, column height, wind, and total grain size distribution (particle diameter, density and shape). These data are usually estimated from past eruptions through the collection of deposit thicknesses and granulometric analysis. When needed parameters are not available data from the geographic region of interest, analogue eruption data should be used. Possible occurrence of ash aggregation should be considered in the analysis (e.g. [255]). Concerning differences due to the use of different models, there are parametric and comparative studies showing that output of the models can be strongly sensitive to the uncertainties and assumptions associated with constructing input parameter distributions (e.g. mass eruption rate, column height, distribution of the mass along the column, bulk grain size distribution), whereas differences between models are often lower than those due to the uncertainties of input parameters [248]. Thus the choice of the model mainly depends on the kind of application such as the need to simulate the evolution of volcanic clouds in the atmosphere.

5.4.3.3.Deterministic assessment

If a deterministic approach is used then a range of eruption scenarios (e.g. a mean and a maximum expected eruption) should be analysed and uncertainties related with the choice of the scenarios and other sources should be properly incorporated in such an analysis. The reference scenario should be chosen to reflect the preserved geological records or from model results, and the realistic meteorological conditions should be considered to the extent possible. Confidence must be assessed that the geological record, or reference scenarios used, appropriately bounds future eruptions.

5.4.3.4.Examples of evaluating potential hazards

As a practical example of tephra fallout hazard assessment here wesummarize the study carried out by Volentik et al. [106] to estimate volcanic hazard at the Bataan nuclear power plant (BNPP) site. BNPP is located on Napot Point on the west coast of the Bataan Peninsula, Western Luzon Peninsula, Philippines. The site may be exposed to both proximal and distal effects of volcanic eruptions from Mt. Natib, and to far field effects from Mt. Pinatubo and Mt. Mariveles volcanoes (See FIG. 32). For example, during the 1991 eruption of Mt. Pinatubo, the BNPP site experienced approximately 6 cm of tephra fall.

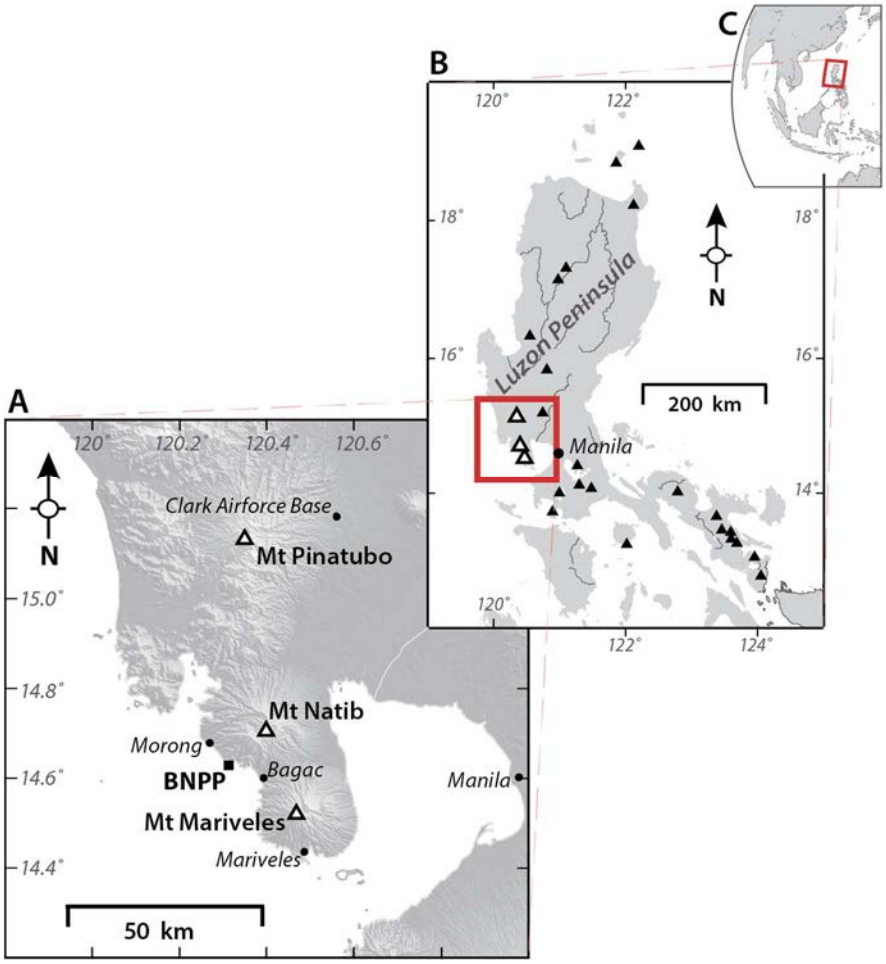

FIG. 32. The Bataan Peninsula (map A enclosed in red on map B), forms the southern part of the Luzon Peninsula (map B enclosed in red on map C) within the Philippines archipelago (map C). Black triangles indicate active volcanoes; larger white triangles indicate the active volcanoes, Mt. Pinatubo, Mt. Natib, and Mt. Mariveles that are closest to the BNPP. The location of the BNPP is marked with a black square.

Volentik et al. [106] carried out both a deterministic and a probabilistic analysis. Deterministic assessments can be useful for estimating potential tephra accumulation resulting from eruptions of a specific size (i.e. a large volume, explosive eruption) using conservative meteorological conditions (i.e. assuming wind always directed from the volcano towards the NPP). For their analyses Volentik et al. [106] used the TEPHRA2 model [218] that is an analytical model for tephra deposits (See Section 5.4.3.1). Such deterministic calculations are useful for estimating screening distances and may provide useful infomation for the

interpretation of probabilistic assessments. As input parameters, TEPHRA2 needs the vent location, column height, total erupted mass and grain size distribution, together with the meteorological parameters (i.e. wind direction and speed as a function of elevation in the atmosphere). Five deterministic scenarios were analysed: eruptions span VEI 3–7 with associated maximum column heights (H_{max}) of 8, 14, 25, 35 and 45 km, respectively [256]. An 8 km high erupting column was used for a small VEI 3 eruption. A 14 km high column represents the approximate boundary between VEI 3 and VEI 4 eruptions. A 25 km column was selected to match the maximum column height of a VEI 5 eruption [257]. The 35 km column height reflects the 1991 eruption (VEI 6) of Mt. Pinatubo, and 45 km represents an upper limit scenario based on the historical eruption (VEI 7) of Tambora in 1815 [252]. In order to maintain consistency among parameters, eruption duration, T, and maximum column height, H_{max}, were used to calculate the total erupted mass for each scenario. Assuming steady state conditions, the mass discharge rate of an eruption is empirically related to the column height [220]:

$$H_{max} = 1.67Q^{0.259} \tag{37}$$

where Q is the magma discharge rate ($m^3\ s^{-1}$). From the density of the deposit (ρ_{dep}) and the duration of the eruption (T), the mean magma discharge rate (Q) is:

$$Q = \frac{M_0}{T\rho_{dep}} \tag{38}$$

where M_o is the total mass of the deposit in kilograms. The bulk density of the deposit, ρ_{dep} (kg m^{-3}), is assumed to be 1000 kg m^{-3}, similar to the average density of the 1991 of Mt. Pinatubo deposits [65], and in good agreement with the typical range, 500–1500 kg m^{-3}, of the bulk density of Plinian deposits [220]. Finally the total mass is related to eruption column height and eruption duration by:

$$M_0 \approx T\rho_{dep}\left(\frac{H_{max}}{1.67}\right)^4 \tag{39}$$

Thus, assuming maximum eruption column heights, total eruption duration (based on analogue eruptions), and deposit density, total eruption mass is calculated for each scenario. TABLE 5 shows the column heights and mass used by each scenario to estimate tephra accumulation at the BNPP site.

TABLE 5. ERUPTION COLUMN HEIGHT AND TOTAL MASS INPUTS FOR DETERMINISTIC TEPHRA MODELS ARE BASED ON ANALOG ERUPTIONS AND VEI

Parameter	VEI 3	VEI 4	VEI 5	VEI 6	VEI 7
Column Height (km)	8	12	25	35	45
Total Mass (kg)	5.7×10^9	5.3×10^{10}	5.4×10^{11}	2.1×10^{12}	5.7×10^{12}

Tephra dispersion also depends on the size distribution of particles (grain size distribution) erupted from the volcano. Complete and reliable total grain size distribution data for explosive volcanic eruptions are difficult to establish from field data and are rarely reported

[210]. Based on estimation of the total grain size distribution by [258], Volentik et al. [106] used a median diameter of volcanic clasts of 1.35 Φ ($\Phi = -\log_2(d)$ with d being the particle diameter in millimeters) and a sorting $\sigma_\Phi = 1.16\ \Phi$ for all simulations in the deterministic analysis of tephra fallout.

Tephra accumulation at a site strongly depends on wind speed and direction during the eruption. Two different wind estimates were used for each scenario. The first one used wind velocities averaged for the year 2006 based on reanalysis data from the National Center for Environmental Prediction Reanalysis project [254]. The second one assumed the wind to blow toward the BNPP with a speed, at each level, similar to the average wind speeds from the reanalysis data for 2006. Actually in order to capture better meteorological variations, a more representative analysis should consider a longer meteorological period on order of decades [259], or the so called typical meteorological year [260]. Wind conditions, very similar to this upper limit estimate, occurred in 2006 $\approx$3% of the time for Mt. Pinatubo, < 9% of the time for Mt. Natib and < 11% of the time for Mt. Mariveles.

TABLE 6. TEPHRA FALLOUT THICKNESS (CM) AT THE BNPP SITE FOR EACH ERUPTION SCENARIO IN THE DETERMINISTIC ANALYSIS

Volcano	Wind (2006)	VEI 3	VEI 4	VEI 5	VEI 6	VEI 7
Mt. Natib	mean[1]	1.000	6.70	39.00	100.0	180.0
	mean (toward)[2]	1.600	12.00	74.00	190.0	360.0
Mt. Mariveles	mean[1]	0.001	0.01	0.03	0.1	0.7
	mean (toward)[2]	0.400	5.30	36.00	98.0	200.0
Mt. Pinatubo	mean[1]	0.005	0.30	4.70	13.0	30.0
	mean (toward)[2]	0.010	5.50	8.00	26.0	58.0

1: mean wind velocity (speed and direction) in 2006

2: mean wind speed in 2006 for winds blowing toward the BNPP site

Results of the different deterministic scenarios are given in TABLE 6. Estimated potential accumulation at the BNPP site varies from trace amounts to 3.6 m for a VEI 7 eruption at Mt. Natib with wind blowing toward the site. These thicknesses correspond to a range in dry tephra load of about 0.01 kg m^{-2} to 3600 kg m^{-2}. Rainfall saturates tephra deposits and may almost double these estimated loads [194], [178]. Isomass map are shown in FIG. 33. For Mt. Pinatubo the model predicts a tephra fallout thickness at the site of $\approx$13 cm, roughly double the observed accumulation during the eruption of Mt. Pinatubo, owing to the difference in wind direction. Comparison of the eruption and the simulations suggest that had the wind blown toward the site on June 15th, 1991, the BNPP might have experienced tephra fallout as thick as $\approx$25 cm (See TABLE 6). Although average wind conditions for 2006 closely mimics the shape of the tephra deposit of the 1991 eruption of Mt. Pinatubo [261], [262], these conditions poorly estimate extreme events. As an example, a VEI 6 from Mt. Mariveles will deposit only 1 mm of tephra with the average wind conditions, while with the wind blowing toward the site, the tephra thickness could reach 1 m, corresponding to about 1000 kg m^{-2} (See TABLE 6). This scenario (wind blowing toward the site) occurs $\approx$11% of the time for Mt. Mariveles. The average wind conditions happen to deposit tephra away from the BNPP, but a large fraction of individual wind fields actually blows closer to the BNPP area. The isomass maps reported in FIG. 33 also point to the possibility that secondary phenomena resulting from

tephra fallout could potentially affect the site area. Although tephra accumulations at the BNPP site are not significant (e.g. not exceeding 10 cm) for many scenarios with < VEI 6, lower explosivity eruptions of Mt. Natib may result in significant tephra accumulations up slope from the site (> 1000 kg m^{-2}). Such deposits would likely remobilize and form lahars that could possibly affect the site.

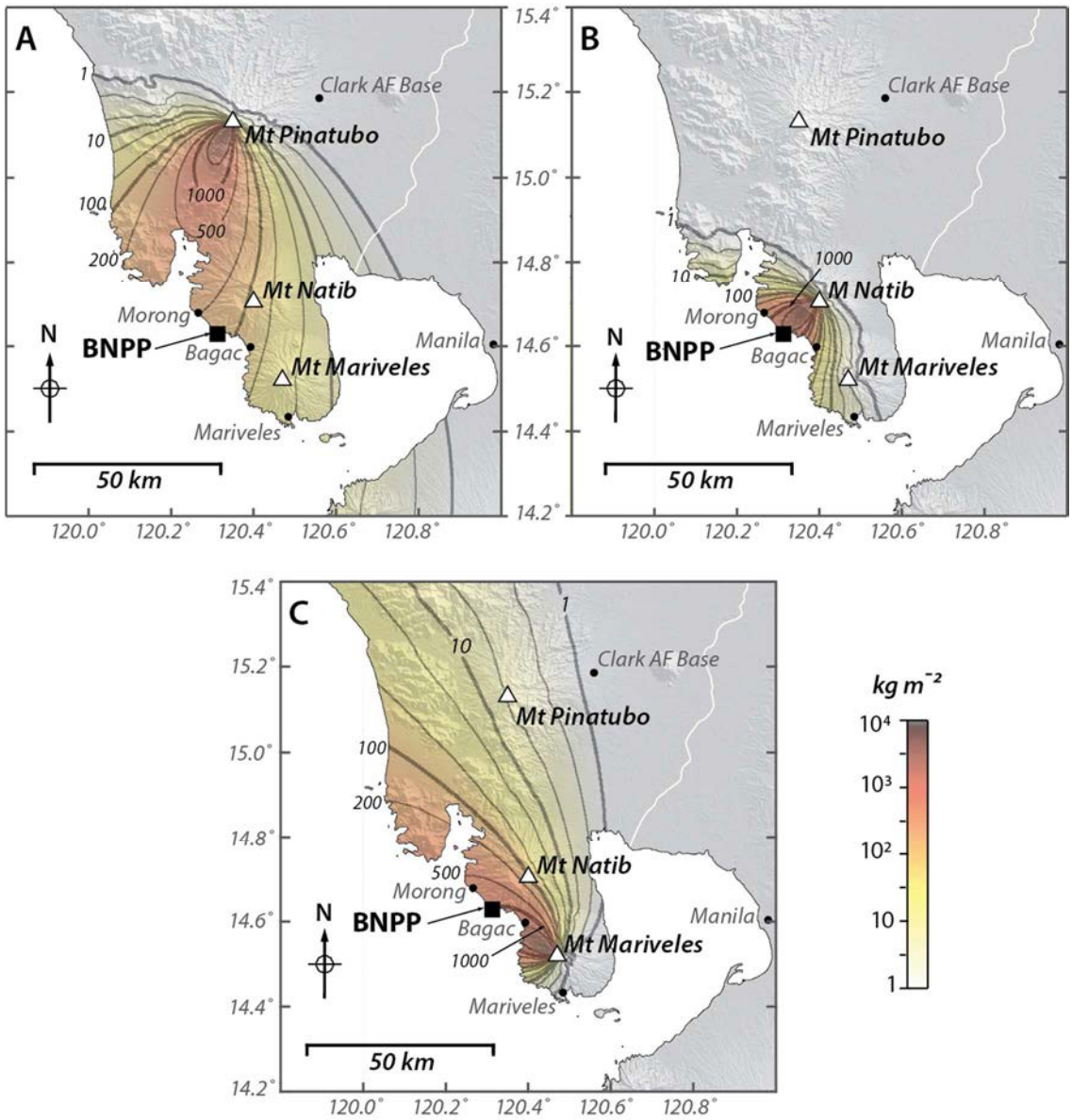

FIG. 33. Isomass maps for explosive eruptions of various magnitudes and wind conditions of (a) Mt. Pinatubo, (b) Mt. Natib, and (c) Mt. Mariveles volcanoes obtained using TEPHRA2 model.

Probabilistic methods more thoroughly assess the effects of random variation in eruption parameters and meteorological conditions on assessing tephra accumulation. For the probabilistic analysis Volentik et al. [106] used TEPHRA2 to calculate the distribution of tephra accumulation at the BNPP site for potentially explosive eruptions of Mt. Natib, Mt. Mariveles, and Mt. Pinatubo volcanoes. For each of the three volcanoes, a Monte Carlo analysis consisting of 1000 simulations was carried out. Eruption column height was randomly sampled from a log uniform distribution of range 14–40 km, which truncated possible values at

the lower limit of credible column heights for small explosive eruptions near the boundary between VEI 3–4 eruptions. The upper bound of the range also has practical significance. Although higher columns may be possible, the properties of the atmosphere at these altitudes are such that higher columns would have little additional impact on the dispersion of tephra particles. The use of a logarithmic function reflects the higher frequency of lower altitude volcanic plumes [263]. The total erupted mass of tephra was calculated using EQ. (39) as explained above. Duration was randomly sampled from a uniform distribution of range 1–9 hours, consistent with eruption durations reported for VEI 4–6 eruptions. No correlation was assumed between eruption column height and eruption duration for the purpose of estimating total eruption mass. The resulting distribution of total eruption mass is log normally distributed, emphasizing the higher probability of smaller eruptions [263]. Large variation in grain size distribution appears possible for different types of Plinian eruptions from similar volcanoes. Given the high uncertainty, $Md\Phi$ and σ_Φ were sampled from uniform distributions with ranges of -1Φ to 5Φ, and 2Φ to 3Φ, respectively. No correlation is assumed between these grain size distribution parameters and column height or eruption mass. Reanalysis data were used to describe the variation in wind velocity with height; a set of 1460 wind profiles (acquired each 6 hours, 4 times daily during 2006 [254]) were randomly sampled, using only one randomly selected profile even per simulation of eruption duration may be longer than 6 hours. As noted above, in order to capture better meteorological variations, a longer meteorological period (e.g. decades [259]) or a typical meteorological year [260] should be considered.

Results indicate that tephra accumulation at the BNPP site from possible eruptions of Mt. Natib and Mt. Mariveles would likely exceed tephra accumulation from possible eruptions of Mt. Pinatubo, by approximately one order of magnitude (See FIG. 34). The results of probabilistic analyses can also be represented as probability maps showing the probability of exceeding a given threshold of tephra accumulation over an area of interest. Thresholds of tephra accumulation can be chosen to reflect potential damage to buildings (i.e. tephra load leading to partial or complete roof collapse) in the area, potential accumulation that might lead to lahar formation, or reflect design factors for NPP structures (See Section 5.4.2.2). Given that an eruption occurs at Mt. Natib, the probability of tephra accumulation exceeding 100 kg m^{-2} (dry accumulation, $\approx$10 cm in thickness) in the region around the BNPP is shown in FIG. 34 and is $\approx$55% near the BNPP site. The probability map indicates that widespread damage to community infrastructure in the region of the NPP is likely in the event of an eruption of significant intensity (e.g. $\geq$ VEI 4). Such conditions are important to consider in site suitability assessment and design [140]. The probability map also indicates that the central part of Mt. Natib, and the W and SW flanks of the volcano, are the most likely areas to be subjected to tephra fallout. This indicates that in the event of an explosive eruption, lahars would likely occur, potentially over widespread areas, on these flanks of the volcano. These lahars could impact community infrastructure and possibly directly impact the BNPP site area.

In summary, the Volentik et al. [106] analysis indicates that the BNPP site is located within the screening distance for tephra fallout from both Mt. Natib and Mt. Mariveles. A screening threshold of approximately 10 cm tephra accumulation is used, based on a damage threshold commonly observed for residential and commercial buildings. A different screening threshold might be desirable for nuclear facilities, which might have greater resiliency for roof loads, but might be more sensitive to particulates affecting water and electrical systems (See Section 5.4.2.2).

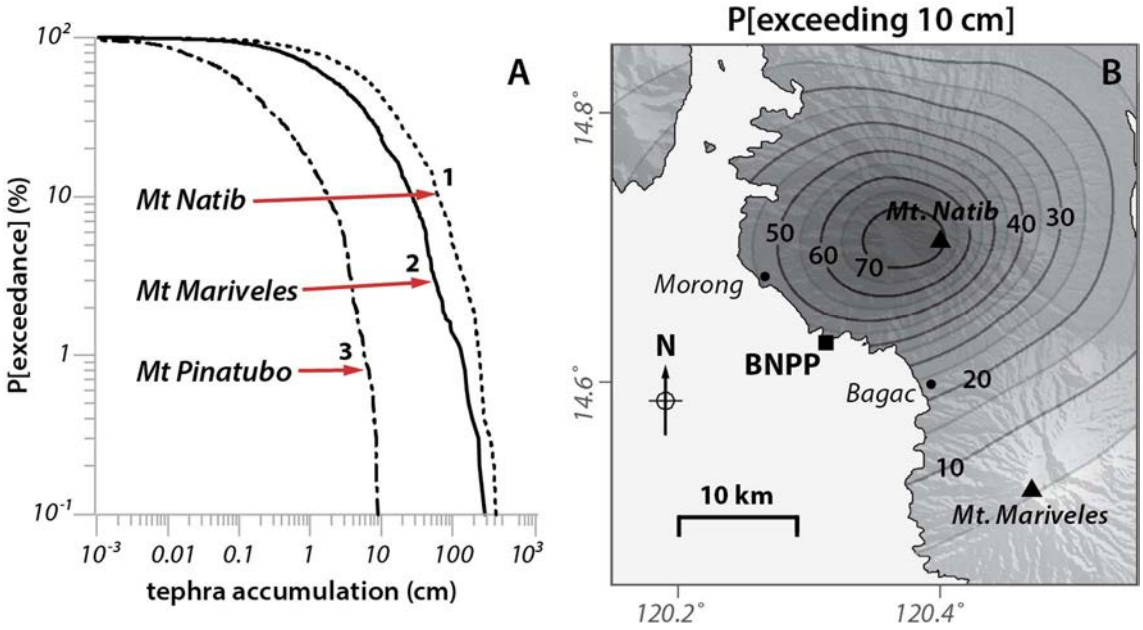

FIG. 34. Hazard curves show the conditional probability of exceeding different thicknesses of tephra at the location of the BNPP, given a volcanic eruption. Graph on the left compares tephra thicknesses modeled for Mt. Natib (1), Mt. Mariveles (2), and Mt. Pinatubo (3). For a given eruption, tephra accumulation at the BNPP from eruptions of Mt. Natib and Mt. Mariveles are similar, and would likely exceed tephra accumulations associated with a Mt. Pinatubo eruption by one order of magnitude. Map on the right shows the probability contours of tephra accumulation exceeding 10 cm (100 kg m^{-2}), given an explosive eruption of Mt. Natib (contours have a 5% interval).

5.4.4. Summary

Tephra fallout is the most widespread hazardous phenomenon from volcanoes. Even minimal tephra accumulation has the potential to disrupt normal operations at a nuclear installation. The thickness and loading of tephra fallout varies widely with distance from the source and the intensity of the volcanic eruption, ranging from a few millimeters to several metres. In some cases, as indicated in TABLE 4, the effects from tephra fallout may be mitigated by appropriate design of many structures, systems, and components that are important to safety. Considerable progress has been made in the understanding of the physics of tephra dispersal and several approaches, ranging from simple empirical to more complex numerical models, have been proposed and satisfactorily applied for hazard assessment and risk mitigation. However, awareness of model uncertainty arising from poor parameter estimation or physical understanding of some processes is critical to determine the appropriateness of these models for use in hazard assessment and estimation of uncertainties.

5.5. ATMOSPHERIC PHENOMENA

5.5.1. Physical characteristics

Explosive volcanic eruptions, such as vulcanian or phreatic explosions, can generate air pressure waves powerful enough to break windows at distances of several kilometers. Peak reduced pressures (i.e. normalized to 1 km) of up to 3050 Pa have been recorded in infrasound data [264–266] although smaller values are more common. Air shocks may accompany lateral volcanic blasts, and thus may affect areas tens of kilometers from the volcano, depending on the interaction of the blast and the topography. They are accompanied by projection of bombs and blocks, but the radius of the shock wave effects may be greater than that of the projected material.

Locally violent weather may accompany the development of explosive eruption columns, as ash particles in the atmosphere cause sudden nucleation of raindrops. Heavy rainfall during tephra fallout may result in the generation of lahars. Downbursts (i.e. locally very strong winds) can occur as a result of explosive columns or of the emplacement of hot lava flows. These winds may cause damage beyond the extent of the lava flows themselves.

5.5.1.1.Lightning

Lightning often accompanies many types of volcanic eruptions, and may involve hundreds to thousands of intra cloud (IC) and cloud to ground (CG) strikes. Small scale lightning is most common near the vent, and larger flashes usually begin several minutes after eruption onset and occur kilometers to tens of kilometers downwind in the ash plume depending on wind speed. In some cases, lightning and high static charges occur up to 80 kilometers from the erupting volcano (e.g. [267]). Lightning is especially common when the eruption column is over 10 km high and ice forms in the upper, cooler parts of the rising ash cloud. Although such atmospheric phenomena may occur during any volcanic eruption, they are most commonly associated with large explosive eruptions.

Volcanic lightning is the result of potential gradients exceeding the electrical breakdown strength of the atmosphere. James et al. [268] provide a contemporary review of volcanic lightning, mainly focused on dry silicate processes. Volcanic plumes generate large perturbations in the surface atmospheric electric potential gradient and high charge densities have been measured on falling volcanic ash particles. The complex nature of volcanic plumes, which contain gases, solid particles, and liquid drops, provides several possible charging mechanisms. For plumes rich in solid silicate particles, fracto emission (i.e. the ejection of ions and atomic particles during fracture events) and triboelectric charging (i.e. from particles interacting) are likely the dominant sources of charge generation. In other plumes, such as those created when lava enters the sea, different mechanisms, such as boiling, may be important. Typically volcanic plumes show a dominant bipolar perturbation that is interpreted as indicating a dipole charge structure with, in most cases, a net positive charge in the higher portions of the plume and a net negative charge in the lower regions. In plumes being dispersed by atmospheric winds, the higher regions of the plumes will usually be advected faster than the lower regions, producing ground level potential gradients. The dipole model has been used to explain data collected at Sakurajima volcano in Japan [269–271] and from plumes rising above pyroclastic flows at Unzen, Japan [272]. Most plumes are thought to contain at least two vertically separated regions of opposite charges, with potential gradient data suggesting space charge densities, ρ_c, of order 10^{-10} to 10^{-9} C m^{-3} and charge magnitudes up to 10 C [270]. Thus, the characteristics of volcanically induced lightning are generally comparable to lightning from

ordinary thunderstorms. This macro scale charge distribution results from the gravitational separation of plume components; lower regions will have larger particles than the upper regions and the upper regions will have more aerosol and finer particles than lower regions. The charge distribution may indicate polarity differences between the net charges held on either particles of different sizes or, alternatively, on different phases (i.e. a net negative charge on the solid silicate particles and a net positive charge on the volcanic gases and aerosols [269]). However, whatever the initial charge distribution, subsequent scavenging processes will inevitably modify the charge distribution and are very likely to produce polarity differences as a function of particle size. Some atmospheric potential gradient data recorded during eruptions showed rapid step like changes that have been attributed to lightning discharges. Many such changes were recorded during the eruption of Mount St. Helens, USA, in 1980 [268]. Within 60 km of the mountain, the potential gradient was generally negative, with a maximum magnitude of 3.5 kV m^{-1}, and changes were predominantly positive (i.e. from 5 to 6 kV m^{-1}, equivalent to lowering negative charge to the ground), indicative of negative charge close to the ground. Farther from the mountain, the potential gradient was generally positive (i.e. up to about 10 kV m^{-1}) with less frequent, smaller amplitude and predominantly negative (i.e. equivalent to lowering positive charge to the ground) changes, indicative of positive charge close to the ground. Potential gradient polarities can be explained in terms of the fallout of net negatively charged 'heavy ash particles' close to the volcano and net positively charged 'lighter ash particles' at greater distances, an interpretation in line with a positive above negative charge distribution model for the plume. This model characterizes lower regions of the plume initially dominated by the charge on larger particles, and the upper regions by charge on smaller particles or aerosols. As well as visual observations and the effect of discharges on potential gradient data, lightning has also been detected by standard detection systems, demonstrating that at least some volcanic lightning has a similar radio signature to that of meteorological lightning [273–275].

The presence of abundant water in volcanic ash columns greatly influences electrification processes [276], [277]. Ice or ice coated ash particles that form high in the cooler (-10 to -20 ºC) portions of the ash cloud tend to have positive charge. This is because ice is the most electro positive substance known. Larger and wetter particles that are not ice tend to have negative charge in the lower parts of the clouds. Thus the polarity and mechanism of charges in ash clouds is quite similar to that in thunderstorms; in fact, some authors have referred to volcanic ash clouds as 'dirty thunderstorms' [273], [276]. Recent data from Redoubt volcano, Alaska, show thousands of flashes in ash clouds that are > 10 km high [267]. The lightning is concentrated above the vent at first, then flashes become longer, stronger, and less frequent as the ash cloud drifts downwind. Individual flashes are quite similar to those observed during ordinary thunderstorms [267].

Basaltic volcanoes generally do not produce large silicate rich plumes because their lower viscosity magmas allow exsolving gases to escape much more freely and less explosively. However, violently explosive basaltic eruptions can occur, particularly when ascending magma encounters significant volumes of water, for example the sea, a groundwater aquifer, or meltwater produced during eruptions through icesheets. Such phreato magmatic eruptions generate significant electrification, not only by increasing the amount of brittle failure (e.g. due to steam expansion increasing strain rates and water cooling the magma surfaces [278]), but also by involving additional water boiling mechanisms. Generally less is known about the electrification of silicate poor plumes, with only those produced by lava flows entering the sea having been studied in detail until recently. These plumes are dominated by condensing steam (from boiled seawater) and entrained atmospheric air, but also contain salt

particles produced during the boiling process, and generally small amounts of silicate material spalled from rapidly quenched lava. Such plumes appear to hold a net positive charge and, during the eruption of Surtsey, Iceland, in 1963, potential gradient data suggested charge densities of up to 10^{-7} C m^{-3} [279]. Similar data were collected during the 1973 eruption of the Icelandic volcano Heimaey, with perturbations of the surface potential gradient in excess of +7 kV m^{-1}, including rapid changes correlated with lightning events [280]. Recent eruptions of Eyjafjallajokull and Grimsvotn, Iceland showed abundant lightning in the ash columns especially when the tops of the plumes were above heights corresponding to -10 ºC, hence conducive to ice formation [281].

Large lightning strikes from large volcanic clouds, very similar to those seen from thunderstorms, pose a potentially fatal hazard similar to lightning from other meteorological phenomena. Lightning is a frequent phenomenon associated with tephra columns formed by explosive volcanic eruption. The likelihood for ground strikes is high, especially in regions of high topography, and may exceed the strike rate for extreme meteorological conditions. A deterministic hazard assessment for volcanically induced lightning strikes should consider use of the screening criteria used in hazard assessments of rare atmospheric phenomena but particular considerations should be given to the fact that there is a potential for a large number of cloud to ground lightning strikes during an explosive eruption.

5.5.1.2.Infrasound and Pressure Waves

Other atmospheric phenomena of interest include infrasound (< 20 Hz) waves. Infrasound data are becoming more abundant for monitoring eruptions [265], [282]. Typically the infrasound signal begins as soon as there is a flux of gases and tephra into the atmosphere. Depending on the pressure, infrasound may propagate as a shock wave at first, with velocity faster than sound speed, then degrade into an acoustic wave as it spreads out geometrically. Acoustic speed in air is 331.4 m sec^{-1} at STP, increasing 0.59 m sec^{-1} per degree C increase. The peak infrasound pressure often occurs near the beginning of eruptions, and the rise time (i.e. first ¼ wavelength) is of the order of seconds for large signals for which the full period is 5–10 seconds. The duration of the infrasound signal is consistent with the eruption duration, typically tens of seconds to tens of minutes based on recent well recorded cases such as Augustine in 2006 [283], Okmok and Kasatochi [284], and Redoubt in 2009 [266].

Atmospheric pressure waves can blow out windows, as happened recently during the March 2013 meteorite fall in Russia. There are documented cases of volcanic explosions causing similar damage [178]. In general, pressures decay as $1/r$ away from the source vent within 100 km. The peak reduced pressures (i.e. normalized to pressure at 1 km) are known for many eruptions (See TABLE 7), and range from a few Pa to > 3000 Pa. From these data, pressures at greater distance are calculated by dividing the pressure by distance in kilometers. Structures subject to damage from infrasound waves would typically be large planar structures (e.g. walls or windows) that are normal to the propagating wave. Structures with a natural period similar to the infrasound waves may suffer greater effects because of resonance. Infrasound waves may travel great distances (i.e. thousands of kilometers) by ducting in the stratosphere. These waves are readily observable on sensitive equipment but are unlikely to cause any damage.

TABLE 7. PEAK REDUCED PRESSURES FOR VOLCANIC ERUPTIONS WITH INFRASOUND DATA

Volcano	Chemistry	Associated Activity	Reference	Year	Pa[a]
Arenal	andesite	Strombolian/Vulcanian activity	[285]	1997	100
Augustine	andesite	Vulcanian explosions	[283]	2006	336
Erebus	phonolite	infrequent large bubble bursts from lava lake	[286]	1997–98	200
Fuego	basaltic andesite	discrete Vulcanian explosions	[265]	2003	100
Karymsky	andesite	discrete Strombolian explosions	[287]	1997–99	10
Kasatochi	Dacite	Plinian eruption	[284]	2008	2500
Klyuchevskoi	basalt	fissure and summit eruptions	[288]	1983,1987	25
Okmok	basalt	vigorous phreatomagmatic eruptions	[284]	2008	85
Redoubt	dacite	Vulcanian to sub plinian eruptions	[266]	2009	3050
Sakurajima	andesite	Vulcanian activity/vigorous explosions	[289]	1985–88	40
Sangay	andesite	discrete Strombolian explosions	[290]	1998	20
Santiaguito	dacite	pyroclastic eruptions from dome	[265]	2003	2
Shishaldin	basalt	vigorous Strombolian activity	[291]	1999	422
Stromboli	basalt	discrete explosions/persistent degassing	[292]	1999,1992	25
Tolbachik	basalt	fissure eruption	[288]	1975–76	200
Unzen	dacite	domeexhalations/pyroclastic flows	[293]	1992	2
Villarrica	basalt	persistent degassing from lava lake	[265]	2002	20

[a]Maximum peak excess pressures in the near infrasound bandwidth as cited in reference. For comparative purposes these pressures have been reduced here to 1 km (i.e. peak reduced pressure), assuming an inverse pressure decrease with radial distance from vent. Most data taken from this link: http://www.knmi.nl/~evers/infrasound/events/010729/etna.html.

5.5.2. Potential effects for nuclear installation

5.5.2.1.Consideration for siting

Nuclear installations routinely consider atmospheric phenomena from meteorological events as design bases, and the potential for atmospheric phenomena from volcanic events is also considered within the facility's design basis rather than as a site exclusion phenomena.

Pressure transients from volcanic events are analogous to dynamic pressures that occur from human induced blasts or explosions, which are considered routinely in a nuclear facility's design basis. For example, peak positive overpressures of > 7 kPa ($\approx$ 1 atm) from potential explosions occurring near United States nuclear power plants must be analysed in detail if the likelihood of such overpressures occurring is > 10^{-7} per year [294]. Structures, systems and components must be able to maintain their safety functions if such overpressures have the credible potential to reach the installation.

Nuclear installations typically protect sensitive equipment with lightning protection systems, which generally consist of air termination (i.e. lightning rods), down conductors, and an earth grounding system. Individual buildings with electronic equipment commonly require an internal grounding system that accounts for cable routing and grounding at key locations [294].

5.5.2.2.Consideration for operations and emergency planning

Atmospheric phenomena from meteorological events are routinely considered in the operations and emergency planning for nuclear installations. Typical effects of these phenomena include loss of offsite power, reactor trip, electrical equipment damage, and voltage transients that may trigger or disable automatic protection systems such as fire suppression [294]. Because some volcanically induced lightning strikes might have higher charge magnitudes than meteorologically induced lightning, the potential for volcanically induced lightning strike could increase the frequency or possibly the severity of damage to electrically sensitive equipment and components.

5.5.3. Approach to use for hazard assessment at NPP

Such atmospheric phenomena should be considered in derivation of the design basis for a nuclear power plant. Because probabilistic approaches have not been developed for these phenomena, hazard assessment should be carried out using a deterministic approach to model the maximum hazard for each atmospheric phenomenon associated with a potential volcanic eruption. For volcanic blasts and shocks, a typical analysis would consider the potential for dynamic pressures arising from capable volcanic sources and determine if such pressures were within the existing design basis for the facility.

Lightning accompanies most volcanic eruptions that produce significant tephra plumes. Lightning associated with volcanic activity has many of the same characteristics as lightning associated with normal meteorological activity, but may occur in much greater intensity and is generally located within or adjacent to the ash columns. The hazard analysis generally would consider the likelihood of a tephra plume occurring at the site, from a capable source that is located at a distance where an increase in lightning strikes has been observed from analogous eruptions. Typical wind speeds and directions should also be considered.

This information would be compared with the facility's design basis for severe weather phenomena, to determine if the potential increase in the frequency and severity of lightning strikes can be accommodated within the current design.

5.5.4. Summary

Common atmospheric hazards from volcanic eruptions are locally violent weather (wind and rain), pressure waves and lightning. The latter two have been systematically studied. Pressure waves may be as high as 3050 Pa at a distance of 1 km from the vent and the pressure decreases with distance. The strongest part of the signal generally occurs early in an eruptive event and the total durations are typically several minutes. Periods of the infrasound waves are from tenths of seconds to about 10 seconds. Lightning may occur in the ash columns of eruptions. Electrical activity is continuous directly above the vent while the eruption is in progress. Short scale length lightning (i.e. 100 m to 3 km) occurs at low rates near the vent within a few minutes of eruption. Large scale plume lightning, with flashes of 10 km length or more, commonly starts 4–12 minutes after eruption onset and may include hundreds to thousands of flashes. Initial lightning is near the vent but lightning moves downwind with the drifting ash column. As time goes by the rate of flashes decreases but the average size increases; strong flashes have been observed 80 km from the vent. The effects of both pressure waves and lightning need to be considered in NPP hazard mitigation plans.

5.6. HYDROTHERMAL ACTIVITY

5.6.1. Physical characteristics

Active hydrothermal systems and groundwater perturbations due to volcanic events at capable volcanic sources can create conditions that result in steam explosions, lahar formation, ground subsidence and slope instabilities [1]. Hydrothermal systems may be present both on volcanoes and in volcanic zones, typically as geothermal fields. Related hazards include:

1. Geyser eruptions: some hot springs (e.g. geysers) occasionally erupt a mixture of steam and boiling water into the air. Many hot springs erupt very infrequently and unexpectedly. Hydrothermal water contains silica, which sticks to glass surfaces causing permanent damage;

2. Hydrothermal explosions: natural hydrothermal explosions are caused by hot water rapidly changing to steam underground. They are due to the same instability as geysers, but are so violent that rocks and mud are expelled along with water and steam. Hydrothermal explosions may occur where shallow interconnected reservoirs of hot water, typically at temperatures of 200–300 °C, reaches critical pressure conditions for different causes, including self sealing of hydrothermal channels, the input from depth of fluids at higher temperatures, and sudden reduction in pressure which provokes a rapid phase transition from liquid to steam, resulting in an explosion of water and rock debris. Causes able to trigger hydrothermal explosions are seismic activity, erosion, or hydraulic fracturing. During the last Ice Age, many hydrothermal explosions were triggered by the release of pressure as glaciers retreated. Hydrothermal explosions often occur without warning. These eruptions can be violent enough to threaten people's lives. Hydrothermal eruption can also occur as a result of altering the amount of ground water in a hydrothermal area (for example land drainage);

3. Boiling mud and mud volcanism: like many other hydrothermal features, boiling mud pools are often unpredictable. A larger than normal eruption can suddenly occur, sending mud further than expected. The mud is boiling hot and can burn clothing and skin. The term mud volcano refers to formations that erupt from depth (up to a few kms) mixtures of water, fine sediment and gases. The associated eruption rates and temperatures are typically considerably lower than those of magmatic volcanoes and hazard is mainly local. However in some cases, similar phenomena can also occur in sedimentary basins characterized by much lower temperatures than hydrothermal systems. In these cases the engine of the process is the high pressure of confined gases, mainly hydrocarbons. An example of these manifestations is the Lusi mud volcano, Indonesia. Lusi has erupted from May 2006 until present, with peak discharge of 180 000 m^3/day [295], inundated over 6.4 km^2, causing the displacement of more than 40 000 people, and economic losses that may exceed 4 billion US dollars [296]. It is expected to continue erupting for years to decades [297], [298];

4. Hydrothermal contamination of water: Hydrothermal waters contain minerals including arsenic and mercury, which are toxic, making hydrothermal water undrinkable or unsuitable for industrial processes. They can also contaminate streams and lakes and get into the food chain. Some hydrothermal water may be either very acidic or very alkaline, and may irritate the skin and corrode clothing. Hydrothermal systems may heat ground and surface waters, potentially reducing water quality (e.g. this may be reduce efficiency of NPP cooling systems);

5. Steam and other gases: in hydrothermal areas, steam can rise from holes in the ground called fumaroles. Steam may be sufficiently hot and voluminous to burn unprotected humans or cause damage to NPP facilities. Hydrothermal areas also produce toxic gases, including H_2S and traces of mercury. Hydrogen sulphide is one of the major hydrothermal gases, often present in CO_2 gas plumes, which because heavier than air, can accumulate in topographic depressions where may reach lethal concentrations;

6. Hydrothermally altered ground and landslides: Hydrothermal systems can also alter rock to clays and other minerals, which may be at risk from subsidence (including formation of sinkholes) and landslides, particularly after heavy rain or earthquakes;

7. Amoebic meningitis: in some areas, hot lakes and springs can contain microscopic organisms (amoebas) that cause the disease amoebic meningitis (e.g. [299]). They may be found in some hydrothermal water that has come in contact with soil, and are a danger if the water is not adequately chlorinated.

5.6.2. How to evaluate effects

Nowadays there are a few well established numerical models for fluid circulation within hydrothermal systems (e.g. [300]) owing from their relevance to geothermal energy exploitation. These models are based on the solutions of the equations describing fluid and heat flows of multiphase (i.e. gas and liquid) and multicomponent (e.g. water and carbon dioxide) fluid mixtures within a porous medium (e.g. TOUGH2 model [301]). However the main difficulty of applying these models is the poor characterization of many volcanic systems. Each case needs to be studied specifically, depending on the particular geological settings, in order to gain insights into the evolution of the specific system. Because of the complexity of the processes involved, data (e.g. gas flux, temperature, composition) derived from monitoring are essential to inform models (e.g. [302–305]).

5.6.3. Potential effects for nuclear installation

5.6.3.1.Consideration for siting and design basis

The occurrence of a hydrothermal system or the potential for such a system to develop within several kilometers of the site should be considered as an exclusion criterion for the site [1]. The indirect impacts of nearby hydrothermal systems, such as effects on groundwater circulation or dispersal of potentially corrosive gases, might need to be considered in developing the design basis of the facility. For sites located in areas where past hydrothermal activity might have occurred in the near surface, particular attention should be given to the potential for increased instability of near surface substrate due to pervasive alteration of rock and soil. Such alteration should be readily apparent in geotechnical investigations for preliminary foundation and site preparation analyses.

Currently, it is difficult to determine the likelihood for steam explosions to occur at specific locations within most hydrothermal systems. Hazards associated with specific phenomena, such as the development of fumaroles or the opening of new vents during steam explosions, are less important to consider explicitly than the development and lateral extent of the hydrothermal system itself. The effects of groundwater anomalies on the potential for lahars, debris flows, ground subsidence and slope stability should be assessed as part of analyses of those phenomena. Factors that should be considered in evaluating the development and possible impacts of hydrothermal systems include:

1. The lateral extent and nature of active hydrothermal systems associated with capable volcanoes;

2. The patterns of groundwater circulation that may give rise to hydrothermal systems;

3. The distribution of features, such as faults, that may influence the location and development of hydrothermal systems.

The assessment (either deterministic or a probabilistic) should identify a threshold value for the distance from an existing hydrothermal system beyond which the hydrothermal system would not expand, and beyond which the probability of a new hydrothermal system developing is negligible. Determination of this threshold value should consider the lateral extent and nature of hydrothermal systems at each capable volcano, the lateral extent of hydrothermal systems at analogous volcanoes, and the hydrogeology of the site and surrounding area. The uncertainties in the various parameters should be properly taken into account.

5.6.3.2.Consideration for operations and emergency planning

Hydrothermal systems are considered a site exclusion criterion. However, the indirect impacts of nearby hydrothermal systems, such as effects on groundwater circulation or dispersal of potentially corrosive gases, might need to be considered in developing operational and emergency plans.

5.6.4. Summary

Hydrothermal systems can generate steam explosions ejecting rock fragments to distances of several kilometres, can create craters up to hundreds of metres, and also can alter rock to clays and other minerals that may lead to unstable ground and landslides. For these reasons, the occurrence of a hydrothermal system and the potential for such a system to develop should be considered as a site exclusion criterion (See TABLE 4). Currently, potential hazards from hydrothermal systems are considered based on field evidence supported by models. Although stochastic assessments for hydrothermal hazards have yet to be conducted, a probabilistic assessment could consider numerical models for the development of hydrothermal systems in specific geologic settings. Alternatively, a deterministic assessment could identify a threshold value for the distance from an existing hydrothermal system beyond which the hydrothermal system would not expand, and beyond which the possibility of a new hydrothermal system developing is deemed negligible. Such models can be informed by information from analogous volcanoes. The uncertainties in the various parameters should be properly taken into account.

5.7. VOLCANIC GASES

5.7.1. Physical characteristics

Volcanic gases make up a significant fraction of the total mass of material emitted by volcanoes. Gases exhaled from volcanic vents, fumaroles, solfataras, mofettes and hydrothermal systems may be highly reactive and hazardous to humans and property. Although volcanic gases consist mainly of H_2O, they also include CO_2, SO_2, H_2S, CO, HCl and HF and form low pH condensates. Typically the most hazardous are CO_2, H_2S, SO_2, and HF. Gases may be discharged in large quantities either from established vents or from new fissures unrelated to established vents, or through diffuse degassing from soils on volcanoes, well before, during and/or after an eruption. Duration and volume of gas emission can be highly variable and episodic, creating short and long term hazards. For example, CO_2 (or SO_2) release on a volcano not undergoing eruption may be on the order a few tons per day to a few thousand tons per day and can be transported by the wind for distances of the order of several kms with concentrations of a few hundreds ppm higher than background [306]. In extreme situations the release of millions of tonnes of volcanic gases can occur over periods of months. The 1783–1784 Laki flood lava eruption in Iceland emitted an estimated 122 megatons (Mt) SO_2 into the atmosphere and maintained a sulfuric aerosol veil that remained over the Northern Hemisphere for > 5 months, leading to significant air pollution and regional climate effects [307].

Volcanic gases can cause a range of health effects to humans, ranging from nuisance to life threatening. Acute and chronic exposure to volcanic gases may lead to corrosion of and mineralization (i.e. deposition of metals from volcanic gas plumes) forming on NPP facilities, ranging from nuisance to highly disruptive or structurally damaging.

Sulfur dioxide gas reacts chemically with sunlight, oxygen, dust particles, and water to form volcanic air pollution, known as vog. Sulfur dioxide chiefly affects upper respiratory tract and bronchi and can irritate skin and the eyes [308]. The interaction of volcanic gases with water in the atmosphere can also produce acidic species, such as H_2SO_4 and HCl, which may precipitate out of the plume, falling as acid rain or as acidic salt particulates [308]. This can have public health effects (e.g. direct exposure and contamination of exposed water and food supplies) and can have corrosive and mineralization effects to sensitive components of the built

environment. However, this phenomenon has not been systematically studied and limited empirical data are available.

Large quantities of volcanic gases, especially CO_2, may also be released suddenly from lakes in volcanic craters and tectonic rifts. Because CO_2 is heavier than air, dense flows of CO_2 gas may follow drainage systems and collect in topographical depressions, displacing air and causing asphyxiation. One of the most tragic examples was the degassing of Lake Nyos, Cameroon in 1986 when a dense cloud of carbon dioxide hugging the ground suffocated more than 1700 people in one night up to several kms from the lake [309], [310].

Volcanic gas emission may occur also from lava flows during volcanic eruptions, as these lava flows continue to cool and crystallize as they flow across the Earth's surface. Changes in hydrothermal systems may result in increases or decreases in volcanic gas emissions. Investigation of the state of the hydrothermal system of the volcano may provide important information about the potential for volcanic gas emissions. Persistent widespread diffuse gas emissions are common at calderas, composite volcanoes, and also occur in areas not characterized by active volcanism (e.g. central Italy).

5.7.2. Potential effects for nuclear installation

The effects from volcanic gases are not considered as part of the exclusion criteria if these effects can be mitigated by means of appropriate design and operation measures. An extensive analysis should be considered in deriving the design basis and in making judgements on site suitability in relation to volcanic gases. Results of this analysis should consider the hazard from direct degassing from volcanic vents and eruptive plumes as well as from indirect passive degassing of erupted products, through the ground, the hydrothermal system and crater lakes, including potential for catastrophic degassing of gas charged (e.g. CO_2, CH_4) water bodies.

5.7.2.1. Consideration for siting

The effects from volcanic gases are generally not considered as part of the exclusion criteria of the site, since these effects can be typically mitigated by means of appropriate design and operation measures. However, extreme events involving the sudden release of huge amounts of volcanic gas creating toxic concentrations at the NPP, such as Lake Nyos 1986 [309], should be considered as part of exclusion criteria.

5.7.2.2. Consideration for design basis

The effects of volcanic gases on mechanical systems and personnel should be coped with by means of appropriate design and operation measures and should be taken account of in derivation of the design basis.

Acute and chronic exposure to volcanic gases may lead to corrosion of and mineral precipitates forming on NPP facilities. The type and severity of corrosion and or mineralization will depend on the composition and concentration of volcanic gases, local atmospheric conditions (e.g. humidity, temperature, wind, etc.) and the exposed materials of the NPP [311]. Corrosion may lead to structural and functional degradation of components and mineralization may disrupt function of components. Although in both instances, corrosion and mineralization processes typically take months to years to manifest.

Volcanic gas will be harmful for occupants at NPP sites in sufficient concentrations. Very high concentrations may be fatal or cause varying degrees of respiratory, gastrointestinal, skin and eye irritation [308]. Air handling systems, which are required to provide air of a stable and or safe quality, may be adversely affected by high concentrations of volcanic gases. For example, back up diesel generation system operation will be disrupted by high gas levels that displace oxygen (e.g. CO_2 plumes).

Indirect effects of volcanic gas may affect systems off site, such as contamination of water supplies, disruption of electric transmission systems (e.g. contamination of insulators) and visibility.

5.7.2.3.Consideration for operations and emergency planning

Corrosion and mineralization issues associated with volcanic gas may require a more frequent maintenance schedule, focusing on vulnerable components. Additional or more frequently serviced filtration may be required to avoid shut down of the system. Volcanic gases can be harmful to NPP facility occupants when present in sufficient concentrations. Appropriate preparedness steps should be undertaken to allow safe function, including controlled shut down, of the NPP during a period of volcanic gas exposure, such as provision of and training with breathing and protective clothing. Where NPP may be exposed to volcanic gas hazards, development of a gas monitoring system may be appropriate to give gas exposure and warning information for the NPP facility (See Section 6).

Volcanic gas plumes may also create indirect effects for the NPP site, such as disruption of transportation systems (e.g. reduced visibility), contamination of water supplies, electricity supplies and even public health concerns for worker's families.

5.7.3. How to evaluate effects

Even though from a theoretical point of view, gas dispersion can be fully studied by solving the complete equations system for mass, momentum and energy transport, in actual practice, modeling and forecasting of gas dispersion can be performed using two different simplified approaches depending on the dispersion regime.The cloud dispersion of gases denser than air released from a volcanic source (e.g. CO_2) is governed by the gravity and by the effects of lateral eddies, which increase the mixing with air around the edges of the plume, decreasing density. In the initial phase the negative buoyancy controls the gas dispersion and the gas cloud follows the ground (i.e. gravitational phase). In this phase, the dispersion of heavy gas is markedly different from that of a diluted gas or from a positively buoyant gas. For diluted gas, when the density contrast is not important, gas dispersion is basically governed by the wind and atmospheric turbulence (i.e. passive dispersion). Models testing have shown a reasonable agreement with observations, which supports the use of these models for hazard applications.

5.7.3.1. Existing modeling approaches

Gas dispersion models range from the simplest analytical Gaussian models to the more complex Computational Fluid Dynamics (CFD) models.

Basic models

Analytical and similarity models

Gaussian plume models assume that the crosswind concentration has a Gaussian profile with the standard deviation that is a function of the downwind distance from the source and of the atmospheric conditions. A Gaussian plume profile is also assumed in the 'puff' models but the release is divided into a number of different puffs and each puff is independently modelled. The final concentration at any point is found by a superposition of all puffs. Although these models are frequently used, several studies have shown that their validity is limited (e.g. [312–314]) and, for example, other analytical non Gaussian solutions are in better agreement with the observed data (e.g. [315], [316]).

Although not a 'puff' model, safety assessments for U.S. nuclear power plants calculate downwind concentrations of gaseous releases using an essentially Gaussian plume approach [317]. This approach considers plume meander, directional dependence of dispersion conditions, and wind frequencies around the facility of interest. However, the emphasis of this approach is to calculate gas concentrations at limited distances away from the release point, to ensure that maximum concentration levels are not exceeded outside of the controlled area of the installation.

Another popular approach is given by the Box (or Similarity) models that describe the integral properties of the plume. A set of differential 1D equations for averaged mass, momentum and energy balance is solved along the plume using different simplifying similarity assumptions using semi-empirical relations whose coefficients are tuned on field test data (e.g. [318]), SLAB [319], HEGADAS [320] and DEGADIS [321]) are examples of this type of model used in safety engineering applications.

Intermediate models

When the gas plume is sufficiently diluted (i.e. its average density is near to that of the surrounding air) a *passive gas dispersion model* can be adequately used to describe gas transport from diffuse volcanic sources typically emitting hot gases like CO_2 [306], [322]. For some gas species, like H_2S and SO_2, chemical reactions with background and other plume gas should be considered.

The shallow layer approach is used to model dense gas plumes. Shallow layer models use depth averaged variables to describe the flow behavior [323–326] and represent good a compromise between the complexity of CFD models and the simpler analytical models.These models have been used to describe gravity driven flows of dense volcanic gas (such as CO_2) over complex topography (See FIG. 35).

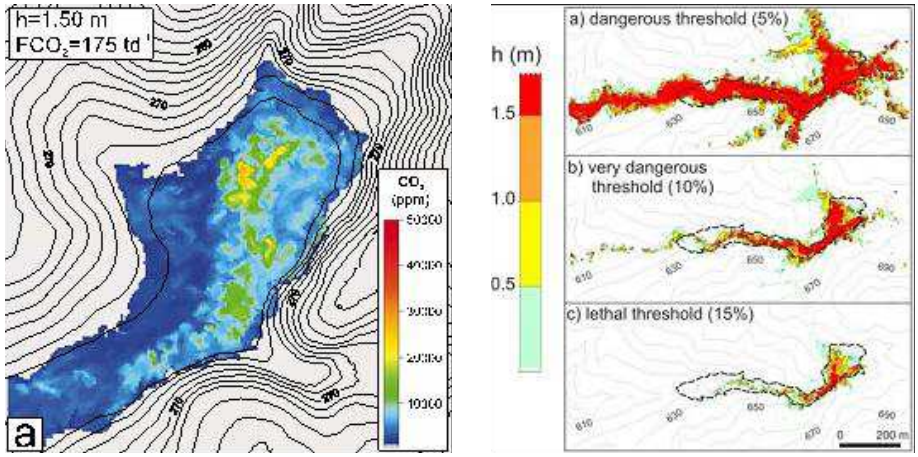

FIG. 35. Left: Gas concentration maps at Caldara di Manziana, Italy, at heights of 1.5 m and assuming very low wind stable conditions for a nighttime emission duration of 10 hours. Right: Simulations of maximum elevation of selected CO_2 thresholds for different wind velocities and directions at Mefite d'Ansanto. Italy, the largest natural emission of low temperature CO_2 rich gases, from non volcanic environment, ever measured in the Earth. Dashed line delimitate the area characterized by absent or damaged vegetation. Reproduced courtesy of American Geophysical Union [327], [328].

Shallow layer models for heavy gas dispersion

In shallow layer models, equations are obtained by integrating mass, density and momentum balance equations over the fluid depth, from the bottom up to the free surface. This approach describes the cloud as a function of time and of the ground position in terms of four variables: cloud depth, two depth averaged horizontal velocities, and depth averaged cloud concentration. Although the formulation is quite general, here we describe the variables and equation used by the TWODEE-2 model [327–329] that have been used for simulating dispersion of volcanic gases (See FIG. 35).

Differently from liquids gas clouds do not have a definite upper surface, and as a consequence, it is necessary to define the cloud depth, h, in terms of the vertical concentration distribution $\rho(z)$. The actual vertical concentration profile is not uniform as for liquids, but it is rather characterized by an exponential decay [323–325]:

$$\rho(z) - \rho_a = (\bar{\rho} - \rho_a)\frac{1}{S_1} exp\left(-\frac{1}{S_1}\frac{z}{h}\right) \tag{40}$$

where $\bar{\rho}$ is the average gas density, and S_1 an empirical parameter. Depth averaged values of gas density ρ and velocities $(u; v)$ are therefore defined in terms of their vertical distributions $\rho(z)$, $u(z)$, and $v(z)$. Defining the gas cloud depth, h, as:

$$\int_{z=0}^{h} g\big(\rho(z) - \rho_a\big)\, dz \equiv \alpha \int_{z=0}^{\infty} g\big(\rho(z) - \rho_a\big)\, dz \tag{41}$$

where α is an empirical constant with a value of about 0.95 (ρ_a is the air density, and g stands for gravity acceleration), and assuming a vertical concentration profile, such as an exponential decay with height [323], [327], [329], all the depth averaged variables can be described. For example the depth averaged density is given by:

$$h(\bar{\rho} - \rho_a) \equiv \int_{z=0}^{\infty} (\rho(z) - \rho_a)\, dz \qquad (42)$$

and, in a similar way, the other depth averaged variables (e.g. momentum, energy) can be defined. Knowing the variation of gas density with height, the gas concentration profile $c(z)$ can be estimated as:

$$c(z) = c_b + \frac{\rho(z) - \rho_a}{\rho_g - \rho_a}(10^6 - c_b) \qquad (43)$$

where c is expressed in parts per million (ppm) and c_b is the background concentration [327], [329]. Gas transport is described by solving the system of equations based on the depth averaged variables (See Appendix) describing the conservation of gas volume, mass, and momentum in accord to the shallow layer approach.

Passive dispersion models

As mentioned previously, when the gas plume is sufficiently dilute, that is when its average density is similar to that of the surrounding air, a passive gas dispersion model can be used to describe gas transport. In this case gas dispersion is mainly controlled by atmospheric conditions, and models are based on the solution of the equation expressing mass conservation of the gas [306], [322] that, from a mathematical point of view, is similar to the advection diffusion EQ. (36) described for tephra dispersal problems.

In particular, the model DISGAS [306], [322] is an example of this category of models. As mentioned above, it is based on the solution of a mass conservation equation similar to EQ. (36):

$$\frac{\partial C}{\partial t} + U\frac{\partial C}{\partial x} + V\frac{\partial C}{\partial y} + W\frac{\partial C}{\partial z_*} = \frac{\partial}{\partial x}\left(K_h \frac{\partial C}{\partial x}\right) + \frac{\partial}{\partial y}\left(K_h \frac{\partial C}{\partial y}\right) + \frac{\partial}{\partial z_*}\left(K_z \frac{\partial C}{\partial z_*}\right) + Q_* \qquad (44)$$

where t is time, (U, V, W) are the scaled wind speeds, K_h and K_z are the diagonal scaled diffusion coefficients and Q_* the source term in the generalized coordinate. In DISGAS the wind field (U, V, W) can be estimated using the mass consistent Diagnostic Wind Model (DWM [330]) for describing the wind fields over complex terrains. The model was applied to simulate CO_2 dispersion from La Solfatara Volcano, Naples, and results have been successfully compared against experimental field data [306], [322].

Complex models

Release of hazardous materials in urban areas is a major concern in industrial risk assessment. In order to simulate gas dispersion over complex urban geometries or large obstacles, and to analyse the effect of large obstacles on gas dispersion, full three dimensional analysis based on fluid dynamics methods able to describe small scale turbulence and predict gas velocity, temperature and concentration fields are used. Thanks to increasing CPU power, CFD codes have been applied in the last decade (e.g. [331], [332]). This approach is able to simulate dispersion of both dilute and heavy gases accounting for obstacles and topographic effects, variation of atmospheric conditions and wind direction, and additional variables and model parameters. Results of this kind of simulations have been successfully validated against experimental field data [333], lab scale trials [334] and in urban canyons [335].

However, these complex models are computationally very expensive. Applications on complex terrain and large domains, such as those for volcanic gas hazard assessment, are commonly prohibitive and they have not been applied to investigate their potential use for describing dispersion of volcanic gas under general conditions.

5.7.3.2. Probabilistic assessment

Either deterministic or probabilistic assessments should be considered in deriving the design basis and in making judgments on site suitability in relation to volcanic gases. Results of this analysis are generally expressed in terms of the expected atmospheric concentration of volcanic gases. Analyses should consider the hazard from direct degassing from volcanic vents and eruptive plumes as well as from passive diffuse degassing through the ground, the hydrothermal system and volcanic lakes. The analysis should also evaluate the potential for catastrophic degassing of gas charged (e.g. CO_2, CH_4) water bodies (e.g. crater or fault bounded lakes) or hydrothermal systems to affect the site. The hazard assessment for volcanic gas for each capable volcano should consider:

1. Potential sources of volcanic gas, including possibilities of limnic eruptions (i.e. when a gas suddenly erupts from deep lake water);

2. Assessing probability and possible concentrations of volcanic gases at the NPP under different source conditions;

3. Meteorological conditions and topography between source regions and the site that will affect transport of gas;

4. Secondary effects of gas release, such as potential for pollution and chemical corrosion, which may have adverse effects on the safe operation of a nuclear power plant.

Concerning the probabilistic approach, first, all the potential sources of gas emission in the region around the site must be identified. Second, the sources that have the potential to produce significant gas dispersion at the site have to been carefully characterized, defining all possible gas flux scenarios and estimating their probability of occurrence. Then an analysis is designed and carried out to estimate the probability of gas concentration at the site from the possible sources, given the potential range of flux conditions and wind velocities in the region. An analysis based on Monte Carlo simulations or similar techniques should be completed to estimate gas hazard from each capable source, accounting for variation in gas fluxes, gas properties, wind velocity distribution in the region and related parameters. Such models lead to a frequency distribution of gas concentration. Uncertainty in the resulting hazard curves should be expressed by confidence bounds, and the basis for the selection of the reported confidence levels should be documented. All the uncertainties need to be properly considered in order to be confident that gas hazard is not underestimated.

5.7.3.3.Deterministic assessment

If a deterministic approach is used, then a range of gas emission scenarios (e.g. finite duration vs. persistent, maximum and mean fluxes, etc.) should be analysed. The most adverse meteorological conditions should be considered. Uncertainty related with the choice of the scenarios, together with other sources of uncertainty, should be properly incorporated in such an analysis.

5.7.4. Summary

Volcanic gases emitted by volcanoes may be highly reactive and hazardous to humans and infrastructures. Gases may be discharged in large quantities either from established vents and fissures or through diffuse degassing from soils on volcanoes. Large quantities of magmatic gases, such as CO_2, may also be released suddenly from lakes in volcanic craters and tectonic rifts. Dense flows of CO_2 gas may follow drainage systems and collect in topographical depressions, displacing air and causing asphyxiation. The interaction of volcanic gases with water in the atmosphere can also result in acid rain, and pollution of surface water. Persistent widespread diffuse gas emissions are common at calderas, composite volcanoes, and in areas not characterized by active volcanism, like central Italy. As indicated in TABLE 4, the effects from gases may be accounted for within the design basis of many structures, systems, and components that are important to safety. Considerable progress has been made in the understanding of the physics of gas dispersal and several approaches, ranging from simple Gaussian or puff models to more complex three dimensional numerical models, have been proposed and applied for hazard assessment and risk mitigation. However, awareness of model uncertainty arising from poor parameter estimation or physical understanding of some processes is critical to determine the appropriateness of these models for use in hazard assessment and estimation of uncertainties.

5.8. LAVA FLOWS AND DOMES

5.8.1. Physical characteristics

Lava flows are driven by gravity along topographic gradients. Lavas are viscous, dense ($\approx$2000–2500 kg m^{-3}) fluids, and flow at speeds from less than $\approx$1 m s^{-1} to $\approx$20 m s^{-1} in extreme cases, such as at Mount Nyiragongo [336]. The morphology and velocity of lava flows depend on the eruption rate, viscosity (which varies strongly with temperature, composition, and crystal content), vent geometry and topography. Thick lava flows can inundate and change topography enabling the lava to invade new areas initially not connected to the lava source. Lava temperature can range from 1200 °C to around 800 °C or less, depending on magma composition. Lava viscosity can range from 10 Pa s (basaltic) to 10^{12} Pa s (rhyolite) depending on magma composition, temperature and crystal content. Lava flows can travel tens of kilometers from the vent, and in unusual cases up to several hundred kilometers, and range in thickness from less than one meter to more than 100 meters. Flow lengths for open channel flows are mainly controlled by effusion rates [337], whereas lengths of strongly insulated flows are controlled by eruptive volume. Slope and viscosity can also influence flow length, in fact steeper slopes and lower viscosities can promote longer but thinner flows. In the case of short duration lava emissions further complications are due to volume limits and insulation [338]. Lava may erupt from the main volcanic conduit, or from multiple vents or fissures located on the flanks of volcanoes, up to tens of kilometers from the location of the main vent. Effusive activity from a single vent can sometimes continue unabated for several years. Lava flows typically inundate areas of 0.1 km^2 to 1000 km^2. Flowage of low viscosity lava over dense vegetation will likely ignite vegetation and can trigger explosion from trapped gases such as CO_2 and CH_4 [336]. In heavily forested areas, this secondary hazard might be significant. Explosive activity and degassing is possible upon entry of lava flows into water bodies or the sea. Eruption of lava under snow or ice can generate massive floods, such as happens in Iceland (i.e. jökulhlaups). The extrusion of very viscous lavas can last a few days to years or decades, leading to formation of lava domes. Lava dome eruptions on volcano summits or steep slopes typically produce voluminous pyroclastic material from the gravitational collapse and

explosive disintegration of the lava dome or lava flows. This material is emplaced at the base and on the volcano where it can be remobilized (i.e. lahars) for many years to decades after cessation of the eruption.

5.8.2. Potential effects for nuclear installation

Lava flows commonly destroy or bury engineered structures in their path. The impact of lava and the length of lava flows depend primarily on three factors: (i) the discharge rate and duration of the eruption, (ii) the physical characteristics of the lava (e.g. rheological properties, temperature), and (iii) the morphology of the vent and the topography across which lava flows move. Lava flows have a direct impact owing to their dynamic and static loads, flow thickness and their high temperature (up to 1200 °C). Lava domes not entirely degassed may be subject to gravitational collapse and occasionally explode, generating hazardous pyroclastic density currents (See Section 5.9).

5.8.2.1.Consideration for siting

The physical conditions of lava flows appear to exceed many design bases for nuclear safety systems [1], although detail analyses of lava flow impacts on system performance have not been conducted. In addition, lava flows have the potential to create prolonged disruptions in critical infrastructure such as offsite power supply, water circulation systems, and site access. Thus, lava flows should be considered as an exclusion criterion for the site [1]. However knowledge of likely path and front velocity of lava flow is very important for evaluating potential impacts to the site and the surrounding area. A hazard map should contain quantitative information on the probability that a site or its environs may be inundated by a lava flow under a set of several conditions, such as different effusion rate, vent location, lava viscosity, and related parameters.

5.8.2.2.Consideration for operations and emergency planning

Lava flows are massive phenomena that inundate areas at high temperature (typically > 800 °C), destroying structures or entombing them in meters of rock. For these reasons IAEA guidelines [1] indicate that lava flows are generally considered to be beyond the design basis of facilities and usually are considered as part of the exclusion criteria of the site, since their impacts on facility design and operation have not been analysed at a level commensurate with a nuclear safety analysis.

Although the potential for lava flow inundation is considered a site exclusion criterion, lava flows also have the potential to affect facility operations from impacts on critical infrastructure located away from the site. For example, lava flows might affect the offsite electrical supply for the facility if transmission lines or switchyards are impacted, leading to a potential for a prolonged station blackout condition. Lava flows might create water impoundments that disrupt water flow to the facility cooling system, or interact with ice and snow fields to create floods. In addition, the presence of lava flows near the site might restrict access of critical personnel to the facility.

In the western United States, the proposed Idaho Spent Fuel Facility (i.e. interim spent fuel storage facility) had an estimated likelihood of lava flow inundation of approximately 5×10^{-6}/year. Emergency procedures were proposed to mitigate the impacts of any potential lava flow through the construction of earthern barriers and flow front cooling with on site water [339]. The low topographic gradient in the area and ready access to heavy construction

equipment and water supply systems at the surrounding Idaho National Laboratory supported the conclusion that diversion efforts likely would be successful, and the risks from potential lava flows was judged acceptable by the NRC [339].

5.8.3. How to evaluate effects

Lavas can show a complex flow behavior due to (1) a non Newtonian rheology; (2) formation of crust, levèes, and tunnels; (3) transitions between different flow regimes, such as pahoehoe, 'aa', and blocky lava; (5) change in the topography over which the flow moves; (6) formation of ephemeral boccas; (7) flow bifurcations; (8) surmounting of natural (or artificial) barriers, and similar factors. Lava cooling is governed by the coupling of energy transport in the flowing lava with heat transfer from lava surface into the atmosphere by convection and radiation, and into the underlying material by conduction [338], [340]. Moreover, kinematics and dynamic behavior of lava flows may dramatically change with lava temperature variations because of the strong temperature dependence of viscosity [341], [342].

At present a complete simulation of all these phenomena, although possible in principle, does not exist.

5.8.3.1.Existing modeling approaches

Modelling approaches discussed here represent a hierarchy of complexity, which reflects increasing requirements for well characterized data in order to produce a broader range of output information. In selecting lava flow models for the hazard analysis, the user needs to carefully consider the question that needs to be answered by the models. If the site analysis requires an understanding of the rates of potential inundation or flow temperatures, then a relatively complex model would have to be used in the analysis, with associated burdens of thorough data characterization. In contrast, a determination of flow inundation potential, without rate or characteristics, might be met by a basic flow model using topography and characteristic volumes and thicknesses.

Basic models

Models based on maximum slope

Models based on maximum slope [343] assume that topography plays the major role in controlling lava flow path. The identification of the different zones that can be potentially invaded by a lava flow is computed probabilistically using a Monte Carlo algorithm. The flow is allowed to propagate along random paths starting from a source point on a topographic map by following a set of probabilistic propagation rules: i) the paths cannot propagate upward, whereas ii) the down flow paths are more probable along the maximum slope direction. Due to the probabilistic character of the propagation rules, the paths may propagate also on a noisy topography with small morphologic barriers. When several paths are generated, areas with greater probability are crossed many times, whereas areas with lower probability are crossed very seldom. The flow paths have no lateral dimensions and cannot fill basins; when many paths enter a basin, they randomly propagate and spread until they touch the walls of the basin and stop. Therefore, a basin behaves as a sink for the flow paths, and this allows an easy recognition of these potentially hazardous areas. Flow rate cannot be specified in the source points and the program does not account for time evolution. The model simply shows which paths are more likely when lava exits from source points. It must be noted that this program does not solve any physical equations and, for this reason, it allows a very fast computation of

the areas that can be potentially flooded by lava. However, since the results are only the probabilities of fluid invasion, without knowing the rheological properties of the fluid, the main application of this model is generating hazard maps when eruption rate and lava property are unknown. The program was used to evaluate the eruptions of Mt. Etna of 1983, 1985, 1987, and 1989 and to evaluate a hazard map for Mt. Etna [343] by using data on the spatial distribution of historic eruptive vents and structural data from [344] and [345]. This computer program was utilized during the 1991–1993 Etna eruption by [346–348], providing in a short time a hazard map of the potentially impacted areas [346], [348]. Favalli et al. [349], [350] used a very similar approach, stochastically perturbing the topographic morphology with a random length of the order of the lava thickness in order to describe better lava spreading.

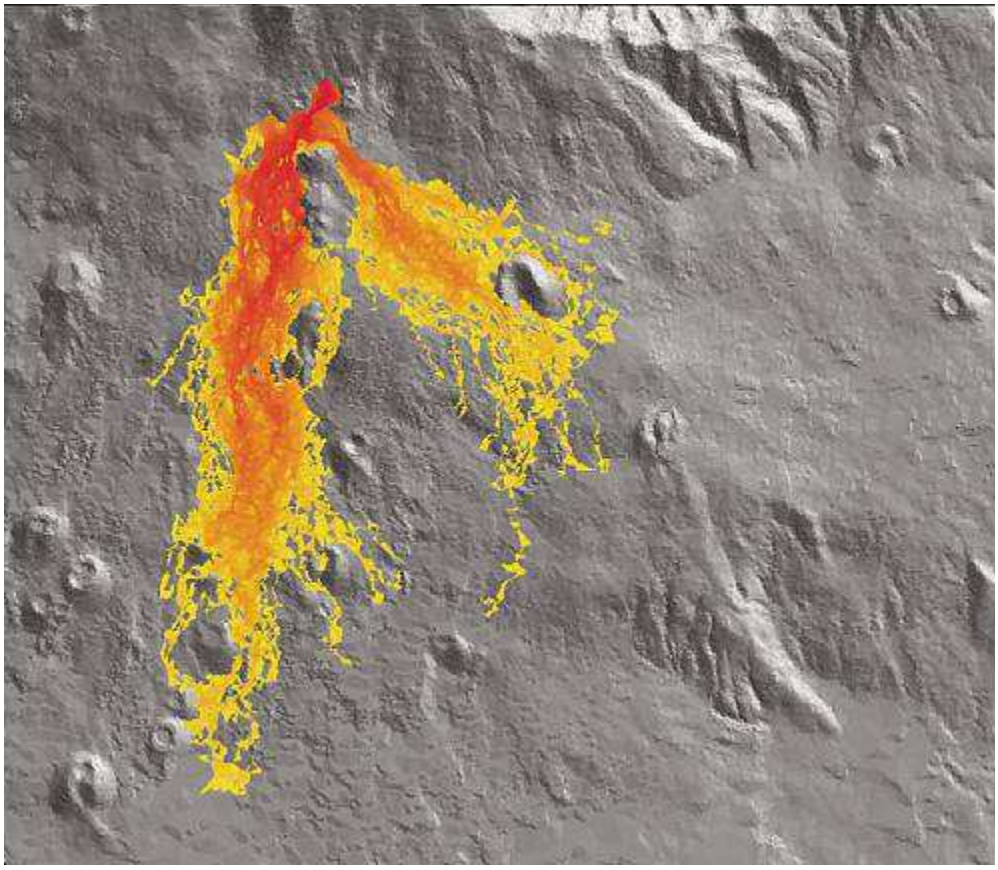

FIG. 36. Simulation results of Macedonio et al.'s probabilistic model [343] for the July 2001 Etna lava flow. A vent sited at 2100 m above sea level and a total number of 10 000 generated paths were considered. The color mapping is proportional to the number of times a path crosses a given area: yellow corresponds to once, while red corresponds to 10 000 times. From this simulation, two branches are evident: the first (in N-S direction), with a higher probability, is well correlated with the observed lava flow, while the second flow in the S-E direction, with a lower probability, was not observed. Reproduced courtesy of the Geological Society of America [351].

Models based on flow front movement

Young and Wadge [352] and Wadge et al. [353] proposed a model for the simulation of the lava flow (FLOWFRONT) based on the behavior of lava front only, assuming implicitly the arrival of the lava to the front. During each iteration, a volume of lava in excess of a critical volume is distributed to its eight neighboring cells. Assuming a Bingham rheology, spreading is possible when lava thickness is large enough that the shear stress exceeds the yield strength on that slope. Once a cell has successfully distributed its excess lava, it becomes inactive during the next iteration [353]. This model does not account for the variation of the lava rheology with the temperature, but does permit variations in the effusion rate and the yield strength. The model was applied to the 1988–1989 Lonquimay, Chile, lava eruption. However, as noted by the authors, this application has raised serious reservations about a deterministic employment of this model. Better results were obtained by the same authors for lava flows at Etna when a probabilistic approach based on a Monte Carlo simulation was performed [353]. In the latter case the input parameters of the model were randomly varied according to previously computed probability density functions evaluated by using a multivariate analysis on historical records of past lava flows in the period 1763–1989.

Models based on lava residual

Another recent semi-empirical model, not intended to mimic the fluid dynamics of lava flow, was proposed by Connor et al. [11] and used to assess the potential for lava flows to inundate the ANPP site. As the only primary information available for Armenian lava flows was thicknesses, areas, lengths and volumes inferred by field observations, the model was guided by these measurable parameters and not directly concerned with lava flow rate or their fluid dynamic properties. The general purpose of the model is to determine whether inundation of the site could occur. The lava flow model requires a DEM of the region of interest. For the ANPP application, this region was represented by ninety meter shuttle radar topography mission (SRTM) data. In the application, lava was distributed from one 100 m^2 grid cell to its adjacent grid cells. This grid cell size limits the resolution of the lava flow. Within the DEM region, a new vent location was randomly selected based on the spatial density of monogenetic volcanoes within the Shamiram Plateau area (See Section 5.2). The model simulated a lava flow from the new vent location onto the surrounding topography. Lava was added incrementally to the DEM surface at the vent location until the total specified lava flow volume was reached. At each iteration, a volume of 10^5 m^3 was added to the grid cell at the location of the vent, then distributed over adjoining grid cells (given that a grid cell was 100 m^2, this corresponds to adding a total depth of 10 m to the vent cell at each iteration). The model assumes that each cell inundated by lava retains or accumulates a residual amount of lava. The residual must be retained in a cell before that cell will pass any lava to adjacent cells. This residual corresponds to the modal thickness of the lava flow (e.g. 4–15 m for lava flows in the case of the Shamiram Plateau). Lava may accumulate in any cell to amounts greater than this residual value if the topography is such that pooling of lava is possible. As flow thickness varies between lava flows, the residual value chosen for the flow model also varies from simulation to simulation. The term residual corresponds to the term adherence used by Wadge et al. [353] and Barca et al. [354], but in this case, residual lava does not depend on temperature or underlying topography, but rather, is used to maintain a modal lava flow thickness. A simple algorithm is used to distribute the lava from a source cell to each of its adjacent cells once the residual of lava has accumulated. Adjacent cells are defined as those cells directly north, south, east and west of a source cell. For ease of calculation, volumes are changed to thicknesses. Cells that receive lava are added to a list of 'active' cells to track relevant properties regarding

cell state, including: location within the DEM, current lava thickness, and initial elevation. Active cells have one parent cell, from which they receive lava, and neighbor cells which receive their excess lava. A cell becomes a neighbor only if its effective elevation (i.e. lava thickness plus original elevation) is less than its parent's effective elevation. If an active cell has neighbors, then its excess lava is distributed proportionally to each neighbor based on the effective elevation difference between the active cell and each of its neighbors. Lava distribution can be summarized with the following equation:

$$H_n = X_a D_n / D_T \tag{45}$$

where H_n refers to the lava thickness in meters received by a neighbor, X_a is the excess lava thickness an active cell has to give away, D_n is the difference in the effective elevation between an active cell and a neighboring cell, $D_n = E_a - E_n$, where E_a refers to the effective elevation of the active cell, and E_n refers to the effective elevation of an adjacent neighbor. The effective elevation, $E_a(E_n)$, is defined as the thickness of lava in a cell plus its original elevation from the DEM. D_T is the total elevation difference between an active cell and all of its adjacent neighbors, $1 - N$,

$$D_T = \sum_{n=1}^{N} D_n \tag{46}$$

Iterations continue until the total flow volume is depleted.

In order to test model validity against available geologic data from the region of application (i.e. near the ANPP), Connor et al. [11] compared measured thickness, area, and volume versus lava flow length for each observed and simulated lava flow. The areas and flow extents of the simulated lava flows compared reasonably with those of mapped lava flows. In particular the simulations reproduced the proper order of magnitudes for volume limited flows whereas showed a poorer performance for long effusion rate limited flows [11].

Intermediate models

Cellular Automata models

Formally, a cellular automata (CA) is a quadruple $A = (E_d, X, S, \sigma)$ where E_d is a set of cells identified by points with integer coordinates in a d dimensional Euclidean space, X is a set of vectors defining the neighbors of each cell, S is a finite set of states that each elementary automaton may assume, and σ is a deterministic transition function for the states S of a cell as a function of the states of the neighboring cells [354], [355]. CA models assume the space inhabited by lava flow may be partitioned in terms of discrete volume (cells) to which a set of parameters is associated: (i) cell elevation; (ii) lava thickness; (iii) lava temperature; and (iv) four (or six) lava fluxes to and from the neighboring cells. These parameters may vary as a consequence of an interaction with a neighboring cell, or because of an imposed global condition that affects all the cells simultaneously [354]. A set of rules is given for changing a given parameter at each time step. For example, the cell elevation remains unchanged until lava reaches a given temperature and solidifies, then the elevation of the cell is increased by the value of lava thickness inside the cell, and the lava thickness is reset to zero. Flows among the cells are allowed as a consequence of the different hydrostatic pressure of the lava among neighboring cells. Lava rheology is accounted for by introducing a minimum lava level below which no flow is possible. This minimum level (adherence parameter) is allowed to vary with the temperature according to an exponential law. Temperature also varies during lava cooling by thermal radiation [356]. A model based on the CA method for the simulation of lava flows

was first proposed by Crisci et al. [357] and then simplified by Barca et al. [358]. The model was applied to several lava flows at Mt Etna, for example for reproducing the 1986–1987 Etna lava flow field or also the 1991–1993 Etna lava flow [355]. An improvement of this 2D model, called SCIARA, uses hexagonal instead of square cells [359].

Another CA model proposed by Ishihara et al. [360], [361] assumes lava behaves like a Bingham fluid whose viscosity and yield strength depends on the temperature. The computational domain is divided into two dimensional square cells with fixed dimensions. During each time step the lava volume variation in each cell is computed as the sum of the mass flows across the cell boundaries. This ensures the continuity equation is satisfied at each time step. The mass flow rates across each boundary of the cell are computed as a function of the thickness and the physical parameters of lava in the given cell. The flow can propagate only after lava has reached a minimum critical thickness. This also acts as a limiting factor for the numerical diffusion. Moreover, an energy balance equation based on the radiative heat exchange is solved to account for lava temperature in each cell. The model employs a propagation rule to compute the mass flux across each cell boundary based on an analytical solution given by Dragoni et al. [362] for steady lava flow on an inclined plane. The most dramatic assumption is the flow rate between two cells does not depend on the difference of lava thickness inside the cells but it is only a function of the different topographic elevations between the two cells. This assumption strongly simplifies the computational algorithm by neglecting coupling effects among the cells and reduces the computational time. The model was applied to reconstruct the Sakurajima, Japan, 1914 effusive eruption, showing a reasonable agreement with the field data (i.e. areas and flow extents of mapped lava flows) in the first phases of the simulation. The CA method used by Miyamoto and Sasaki [363] represents an improvement of the Ishihara et al. model [360], [361]. In fact, the Miyamoto and Sasaki method [363] extends the applicability of the model to a flat or little inclined plane, considering the effects of self gravity and including a correction to strongly reduce the well known problem of mesh dependence in the CA method. Confidence in the code results was supported using data from the 1983 Miyakejima lava flow, which reproduced the areas and flow extents of mapped lava flows. A more recent code based on the same approach is MAGFLOW, which was used to reproduce some lava flows at Etna [364].

Semi-analytical models

Semi-analytical models were proposed in order to overcome the main intrinsic computational difficulties. FLOWGO [365] is a self adaptive numerical model that follows lava elements down an open channel. The basis of the model is the estimation of lava velocity as Bingham fluid flowing in a channel (i.e. using a semicircular or a very wide channel approximation depending on the local morphology). At each step in the calculation, heat loss and gain are calculated in order to determine their effects on lava rheology, although viscous heating effects that can decrease viscosity are neglected. Starting with some given initial conditions at the vent, new lava with temperature, crystallinity, rheology, and velocity calculated by the model is passed a unit length down channel and eventually stops if velocity is zero or the flow core has reached the solidus temperature. The model was applied and calibrated simulating flow fields at Mauna Loa, Kilauea, and Etna showing a satisfactory performance in reproducing the measured lava flow lengths and estimated lava temperatures [365].

The model can be used to analyse important factors determining how far a channel fed flow can extend, and assessing lava flow hazard. Although the model solves a quite advanced equation for the energy budget, the principal limitations of the code are intrinsically contained in the validity of the simple analytical solution for obtaining the velocity profile on which the model is based, actually valid in idealized conditions only.

Two dimensional models based on shallow layer approach

Costa and Macedonio [366] presented a model based on depth averaged equations obtained by integrating mass, momentum, and energy equations over the depth of fluid from the bottom up to the free surface. This approach is valid within the limit $H^2/L^2 << 1$, where H is the undisturbed fluid height and L the characteristic wave length scale in the flow direction. Costa and Macedonio [366] assumed lava to be an incompressible fluid and a hydrostatic pressure distribution, and solved numerically a set of equations for lava volume and momentum similar to those described in the Appendix. Because lava viscosity is strongly temperature dependent it was necessary to solve the equation for the energy conservation. They proposed a heuristic equation based on the depth averaged lava temperature accounting for terms describing the radiative exchange, the convective and conductive heat transfer, and the heat generated by viscous dissipation. Lava viscosity was assumed to depend on temperature following an exponential relationship:

$$\mu(T) = \mu_r e^{-b(T-T_r)} \tag{47}$$

where b is an appropriate rheological parameter and μ_r is the viscosity value at the reference temperature T_r. A convenient choice is $T_r = T_0$, with T_0 equal to the emission temperature at the vent. Within this model, the crystallization effect on viscosity is not explicitly considered, but is implicitly accounted for in estimating empirically the rheological parameters in EQ. (47). As an example of an application to real lava flows, Costa and Macedonio [366] simulated some lava flow events that occurred during the 1991–1993 Etna eruption. The model was able to reproduce semi-quantitatively the behavior of the real lava flows and the proper order of magnitude of the main quantities, such as lava thickness and lava temperature, showing good agreement with field observations. This approach appears to be a robust physical description and a good compromise between the full three dimensional description and the need to decrease the computational time. The good performance of the model substantiates the model as a potential approach to reliably forecast lava flow paths even though computational requirements are still too elevated for its use in a probabilistic analysis.

Complex models

Three dimensional models are based on the solution of the governing transport equations given by mass conservation, and momentum and energy balances. For the solution of such equations it is necessary to specify the proper initial and boundary conditions and to account for the complex rheological properties of magmas. These kinds of models can be usefully applied to simulate lava flow paths on restricted domains or to evaluate the effects of human intervention, such as lava diversion strategies (e.g. water spray) or presence of natural or artificial barriers (e.g. [367], [368]). However the resulting equations are highly nonlinear and their solution is a hard task. Moreover, a lava flow's non Newtonian lava behavior, the need to describe a free surface, and nonlinear boundary conditions in the energy equation (i.e. heat loss by radiation) all drastically increase the complexity of the problem. During lava cooling, levèes can form laterally, and the flow may exhibit regime transitions from pahoehoe

to ‘aa’ or blocky flow, which need different modeling. As a consequence, several simplifications are introduced in order to make the problem tractible.

The LavaSIM code [368] is an example of a 3D CFD model for lava flow simulation, which is based on the algorithm described in [369], [370]. Assuming lava to be an incompressible fluid with constant specific heat, LavaSIM solves a set of three dimensional equations for the transport of mass, momentum, and energy. LavaSIM accounts for three dimensional convection, solidification, magma temperature viscosity dependence, and minimum spreading thickness, and considers heat transfer due to cooling at the surface and bottom, and between solid and liquid lava, respectively. The model accurately formulates the boundary interface between melt and crust. Moreover LavaSIM deals with the free surface by associating an attribute to each mesh cell (i.e. convection or free surface). The convection cells are completely filled with lava melt or crust, whereas the free surface cells are only partially filled and represent the external boundaries of the flow. Heat and mass transfer associated with lava flow propagation is modeled by updating these mesh attributes. In the code formulation it is necessary to assume lava melt does not scatter into the atmosphere and the crust floats and moves only vertically (which does not fully reflect actual behavior). The stopping criterion is based on the minimum spreading thickness due to the non null lava yield stress. However, as main limitations, it is worth noting that LavaSIM governing equations are solved without considering explicitly temperature, composition, and crystal content dependence on viscosity, and average effective parameters are used and a stopping criterion is commonly imposed (i.e. when lava thickness becomes lower than a critical minimum value, local flow stops).The model was applied to simulate lava flows of Izu-Oshima 1986 and Etna 2001 eruptions [368], [371] and was able to reasonably reproduce the areas and flow extents of the mapped lava flows.

Currently, the high complexity of the dynamics of actual lava flows and the high computational costs of fully 3D CFD models prevents of using them for either practical real time hazard assessment or probabilistic analysis.

5.8.3.2.Probabilistic assessment

In the assessment of hazard associated with lava flows at NPP, for each capable volcano, in order to estimate the conditional probability of lava flow inundation given a future effusive eruption, the analysis usually considers:

1. The potential magnitude (e.g. mass discharge rate, areal extent, volume) of lava flows;

2. Vent locations and topography, and evolution with time if vent position changes as the eruption progresses;

3. The rheological properties of erupted lava (e.g. temperature, viscosity, thickness) and its evolution with time.

4. The eruptive scenario (e.g. individual lava flows, lava tubes, flow fields);

Depending on the available information and on the objectives of the hazard analysis either a deterministic or probabilistic hazard assessment (or both) can be carried out.

A probabilistic approach can account for a range of physical parameters considered in the analysis, and uncertainty in the location of future source vents. All volcanoes produce

variations in the characteristics of lava flows. Limitations in the completeness and accuracy in the geologic record of lava flows commonly occurs due to burial of past flows. A probabilistic assessment allows uncertainty in the geologic record, in addition to recognized variability, to be accounted for in the analysis.

A probabilistic approach commonly considers the locations of vents and the potential formation of new volcanic vents. The probabilistic approach should entail numerical modeling of lava flows and should proceed with numerical simulations for each capable volcano, accounting for a range of values for parameters that control flow length and thickness, using stochastic methods. In numerical simulations, vent location, topography, and select lava characteristics are key parameters that control the modeled lava flow emplacement. Probabilistic assessments use models of lava flows coupled with Monte Carlo simulations or other applicable simulation techniques. Empirical observations from the capable volcano and analogous volcanoes can be used to inform the probabilistic analysis. Lava flow hazard curves can be determined and combined to express the annual frequency of exceedance of different levels of lava flow incursion and lava thickness at the nuclear power plant. If uncertainty in the resulting hazard curves is expressed by confidence bounds, the basis for the selection of the reported confidence intervals should be documented.

Concerning the numerical code to adopt in order to carry out the simulations, it is suggested that at least a basic probabilistic model should be used that can be promptly fed by an exhaustive collection of field data (e.g. [11]). However, a first immediate screening to see if the site can be potentially susceptable to lava inundation can be obtained by using the maximum slope model that needs only a DEM as input (e.g. [372]).

5.8.3.3.Deterministic assessment

A deterministic assessment needs to assume the location of a future vent, which should be selected so that the resulting hazard is not underestimated for the site. Subsequently, the hazard assessment for lava flows should determine threshold values on the basis of the maximum credible length, areal extent, thickness, temperature and potential speed of lava flows that could reach the site. This can be achieved using data from other volcanoes from the geographical region, from analogous volcanoes, or from empirical or numerical models of lava flow emplacement. Some empirical models of lava flow emplacement rely on correlations between lava flow length and effusion rate, whereas others are volume limited. Topography along the path and at the site of the nuclear power plant should be considered. It is important to consider in the assessment the possibility of additonal vents opening, vent migration and propagation as fissures or new isolated vents located above a propagating dyke (eg. 2002 eruption of Nyiragongo [336]). This has the potential to greatly widen and complexify the potential lava flow inundation area. The uncertainties in the various parameters should be properly taken into account, so that there is confidence that the lava flow hazard has not been underestimated for the site. Similarly, the deterministic model can be used to develop a screening distance value for lava flow hazards, to supplement the site specific information developed for lava flow characteristics.

Concerning the numerical code to adopt, where an accurate DEM and further advanced information are available (e.g. past lava volume, lava thicknesses, effusion rates, lava composition, etc.), physical based models, if necessary, could be used to refine the analysis carried out using simpler models. Semi-analytical models like FLOWGO (or even models based on a shallow layer approach or cellular automata) can be used for such an analysis. Another potential use of physical based models is to evaluate effect of potential countermeasures that would be constructed to divert or delay (e.g. artificial barriers, guiding channels, water cooling [368]) the advance of the lava front. Such countermeasures have been successful in diverting lavas from the 1991–1993 Etna eruption [346], [347]. Nevertheless, lava flows have overcome such countermeasures in, for example, Etna, Hawaii, and Iceland.

5.8.3.4. Examples of evaluating potential hazards

As a practical example of lava flow hazard assessment here we will summarize the procedure employed by Connor et al. [11] to estimate lava flow hazard at the nuclear power plant site near Aragats, a Quaternary volcano in Armenia using a two stage process. Connor et al. [11] used a computer model based on lava residual to estimate the conditional probability that a lava flow will inundate a designated site area, given that an effusive eruption originates from a vent within the volcanic system of interest. In their hazard assessment, first, they sampled the location of the lava flow sources from a spatial density model of new, potentially eruptive vents (See Section 5.2). Second, they utilized a basic model, such as that based on lava residual described above, to simulate the effusion of lava from these vents using field measurements of thicknesses and volumes of previously erupted lava flows within an area encompassing the site of interest in order to estimate the model input. As the simulated lava flows follow the topography, a DEM was an essential input. Spatial distribution of past eruptive vents, the distribution of past lava flows within an area surrounding the site, and measurable lava flow features including thickness, length, volume, and area of previously erupted lava flows were used as input data to develop a probability model (See Section 5.2). Given these input data, Monte Carlo simulations generated many possible vent locations and many possible lava flows, from which the conditional probability of site inundation by lava flow, given the opening of a new vent, was estimated.

The ANPP site lies within a relatively dense volcanic cluster at the southern margin of the Shamiram Plateau (See FIG. 25). Lava flow hazard assessment is designed to assess the conditional probability that lava flows reach the boundary of the NPP site area, given an effusive eruption on the Shamiram Plateau. Lava flows on the Shamiram Plateau can be divided into two age groups, pre-ignimbrite lava flows that range in age from approximately 0.91–1.1 Ma, and post ignimbrite lava flows that cover the ignimbrites of Aragats volcano.The youngest small volume lava flows of the Shamiram Plateau are the Dashtakar group of cinder cones. Other large volume lava flows lie on the flanks of Aragats volcano, a 70 km diameter volcano located immediately north of the Shamiram Plateau.The youngest features of Aragats Volcano are large volume lava flows from two cinder cones, Tirinkatar (0.45 Ma) and Ashtarak (0.53 Ma). Lava flows of the Shamiram Plateau are typical of monogenetic fields, being of comparatively low volume, generally < 0.03 km^3, and short total length, generally < 5 km. The total volume of lava flows at Shamiram Plateau making up the plateau was estimated to be ≈ 11–24 km^3. This implies that hundreds of individual lava flows comprise the entire plateau. Mapped lava flows of the Shamiram Plateau are volume limited flows [338], [373], [374], trachyandesite to trachydacite in composition. Lengths range from 1.4 km, from Shamiram volcano, to 2.49 km from Blrashark volcano; volumes range from 3×10^{-3} km^3, from Karmratar volcano, to 2.3×10^{-2} km^3 from Atomakhumb volcano. Volume limited flows occur

when small batches of magma reach the surface and erupt for a brief period of time, forming lava flows associated with individual monogenetic centers. These eruptions often occur in pulses and, during the eruption, erupting vents may migrate a short distance (< 1 km). Each pulse of activity in the formation of the monogenetic center may produce a new individual lava flow, producing a flow field over time. The longest lava flows in these fields are generally those associated with the early stages of the eruption, when eruption rates are typically larger [373]. Within the Shamiram Plateau area, individual monogenetic centers have one (e.g. Shamiram volcano) to many (e.g. Blrashark volcano) individual lava flows. Longer lava flows are also found on Aragats volcano, especially higher on its flanks. These summit lavas comprise a thick sequence of trachyandesites and trachydacites having a total volume > 500 km^3. The most recent lava flows from the flanks of Aragats include Tirinkatar, which is separated into two individual trachybasalt flows each have volumes ≈ 0.5 km^3. The largest volume flank lava flows are part of the trachydacitic Cakhkasar lava flow of Pokr Bogutlu volcano, with a total volume ≈ 18 km^3, on the same order as the largest historical eruptions of lava flows worldwide [375]. These larger volume lava flows are effusion rate limited and the length of the lava flow is controlled by the effusion rate at the vent. The lengths of the Ashtarak and Tirinkatar-1 lava flows exceed 20 km. Based on comparison with observed historical eruptions, their effusion rates were likely on the order of 10–100 m^3 s^{-1} [337], [338], [373], [376]. Thus, although volume limited flows erupt on the Shamiram Plateau in the immediate vicinity of the site, effusion rate limited flows erupt at higher elevations on the flanks of Aragats volcano. Although it is conceivable that these larger volume flows may reach the site because of their great potential length, this event is less likely because their occurrence is so infrequent and the Shamiram plateau would likely act as a topographic barrier to these longer, larger flows preventing them to reach the ANPP site. Each class of lava flows, smaller volume limited flows and larger effusion rate limited flows, was considered separately when assessing lava flow hazard at the ANPP site.

The ninety meter SRTM data from CGIAR-CSI (the Consultative Group on International Agricultural Research-Consortium for Spatial Information) was used as a DEM. SRTM database was re-sampled at 100 m × 100 m grid spacing, using the mapping program GMT. In the model, lava was distributed from one 100 m^2 grid cell to its adjacent grid cells. Within the area of interest a new vent location was randomly selected based on aspatial density model previously calculate (See Section 5.2). The model based on lava residual method (See Section 5.4.3.1) simulated a flow of lava from this new vent location onto the surrounding topography. Volume limited lava flows of the Shamiram Plateau are generally < 5 km in length, with volumes on the order of $0.3–2.3 \times 10^{-2}$ km^3 (in agreement with compilations by Malin [376] and Pinkerton and Wilson [377]. Using empirical estimations of effusion rates (10–100 m^3 s^{-1}), an iteration adding a volume of 10^5 m^3 of lava corresponds to an elapsed time of 10^3–10^4s. Lava was distributed to adjacent cells only at each iteration, so the estimated effusion rate corresponds to flow front velocity on the order of 0.01–0.1 m s^{-1}, in reasonable agreement with observations of volume limited flow front velocities. For the case of the Shamiram Plateau, on the basis of the thicknesses of some volume limited lava flows measured, a residual value was chosen randomly from a distribution representing thickness of each simulated flow. The measured lava flows thicknesses were fit to a truncated normal distribution with a mean of 7 m, a standard deviation of 3 m, and truncated at a minimum flow thickness of 4 m and a maximum flow thickness of 15 m. The lava flow code randomly selected a residual value from this best fit distribution. Based on volumes of some lava flows measured within and surrounding the Shamiram Plateau, the lava flow code calculates a total volume from a randomly chosen value from a truncated $\log_{10}$ normal distribution with a mean of 7.2, a

standard deviation of 0.5, and truncated at 6 and 9 log units. This range favours eruptions with smaller volume flows, but also allows rarer, comparatively large volume flows.

Lava flow paths are significantly affected by the large variability in possible lava flow volumes, lava flow lengths, and complex topography. Many simulations were required to estimate the probability of site inundation by lava. A computing cluster was used to execute this large number of simulations. The boundary of the ANPP site was taken as a rectangular area, 2.6 km^2. For the purposes of the simulation, it was assumed that if a lava flow crosses this perimeter, the site is inundated by lava. The lava flow simulation was based on the eruption of one lava flow from each vent, although more than one lava flow may erupt during the course of formation and development of a single monogenetic volcano. For the ANPP site, the conditional probability of site inundation was sensitive to lava flow length, but insensitive to broadening of the lava flow field. Therefore, only one lava flow was simulated per eruptive vent. Nevertheless, for some sites the potential for broadening the area of inundation by successive flows may be an important factor.

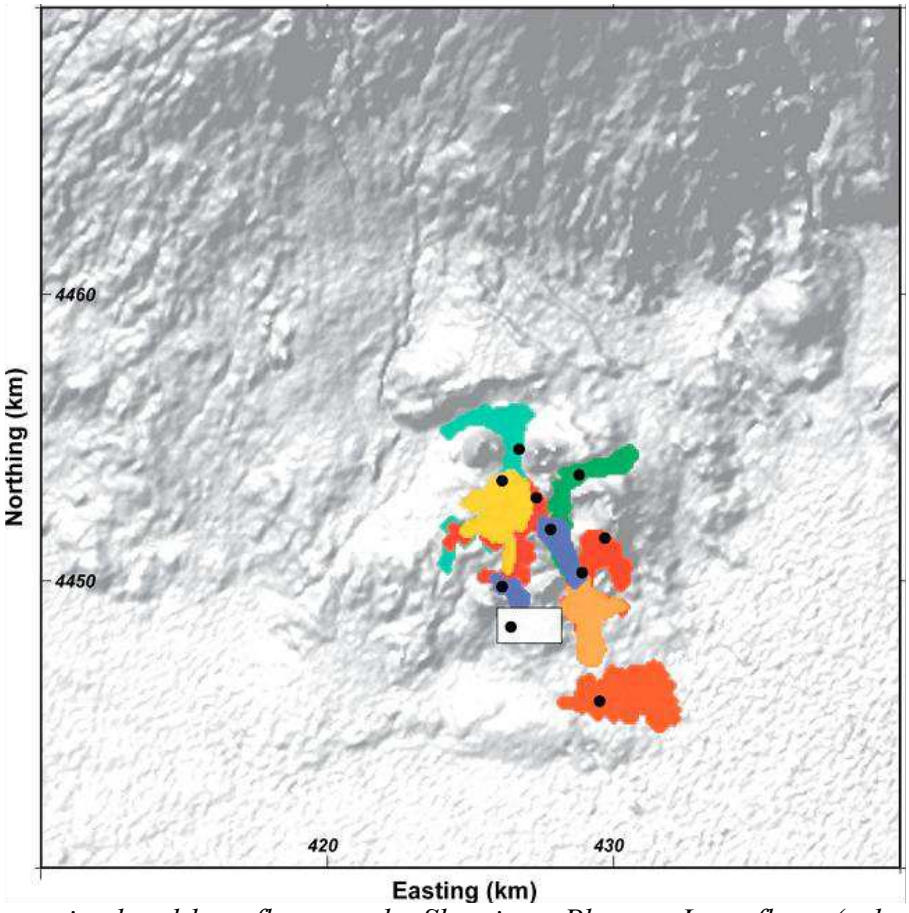

FIG. 37. Some simulated lava flows on the Shamiram Plateau. Lava flows (colored regions) are erupted from vents (black dots) that are randomly sampled from a spatial density model of vents on the Shamiram Plateau. Flow path follows the DEM. The site area is considered to be inundated if the lava flow intersects the white rectangle. In this example, two of the ten lava flows intersect the site and one vent falls with the site boundaries. Reproduced courtesy of the Ministry of Energy and Natural Resources of the Republic of Armenia [10].

A total of 10 000 simulations were executed in order to estimate the probability of lava flow inundation resulting from the formation of new monogenetic vents on the Shamiram Plateau. Out of 10 000 events, 2485 of the simulated flows crossed the perimeter of the site, or

24.9 % percent of the total number of simulations. Lava flows erupting from the central part of the Shamiram Plateau, up to 6 km north of the ANPP site, have a much greater potential of inundating the site area than lava flows originating from south, east, or west of the site. The central part of the Shamiram Plateau is the most likely location of future eruptions, based on the spatial density analysis. Substantial topographic barriers to the south, east, and west block lava flows from inundating the site from these directions, and the probability of vent formation in these locations is much lower.

Larger volume lava flows were simulated for flank eruptions of Aragats volcano. For these simulations a trachyandesite to trachybasalt composition was assumed. This flow regime mimics an effusion rate limited lava flows, with lava thicknesses (or lava residuals) ranging from approximately 6–9 m (similar, for example, to the Tirinkatar-1, Ashtarak, and Paros lava flows). The total volumes of these simulated flows range from approximately 0.5 km^3 to 0.87 km^3. An additional spatial density estimate was made to define the probability of future vent formation on the flanks of Aragats volcano (See Section 5.2) to assess the hazard of large volume, effusion rate limited flank lava flows. Since the details of these flank lava flows have been very poorly documented (only 5 have been classified by thickness, volume, and length) an accurate statistical analysis of these parameters was not considered. In this case, values for volume and thickness were randomly selected from those trachyandesite to trachybasalt flank flows that were measured in the field. Approximately 1000 flows were simulated. None of the simulated flows erupted on the flanks resulted in inundation of the ANPP site.These results appear credible, because the Shamiram Plateau creates an effective topographic barrier to < 10 m thick lava flows, diverting drainage of lava west or east of the plateau. Therefore, although Aragats lava flows are impressive in length and volume, the ANPP site is not likely to be inundated by long lava flows emitted from the flanks of Aragats volcano.

5.8.4. Summary

Lava flows are massive phenomena able to inundate areas at high temperature (typically > 800 °C), destroying structures or entombing them in meters of rock. Lava flows occasionally can travel up to hundreds of kilometers, and range in thickness from less than one meter to more than 100 meters. As indicated in TABLE 4, the effects from lava flows should be considered as part of the exclusion criteria of the site, since these effects appear to exceed the typical design basis of many structures, systems, and components that are important to safety. Considerable progress has been made in the understanding of the physics of lava flows and several approaches have improved our knowledge by trying to describe their complexities. However, at present a complete simulation of all the phenomena involved does not exist because not all relevant physical processes are completely understood. For these reasons, in order to simulate lava flows different models are commonly adopted, ranging from simple ‘maximum slope’ models aimed to guess the most likely flow path, to cellular automata models, two dimensional models based on the shallow layer approach, and, in some cases, more complex three dimensional models, able to estimate areas, flow extents, thickness, and temperatures of lava flows. Awareness of model uncertainty arising from poor parameter estimation, topographic resolution or mechanical understanding is critical to determine the appropriateness of these models for use in hazard assessment.

5.9. PYROCLASTIC DENSITY CURRENTS

5.9.1. Physical characteristics

Pyroclastic density currents (PDCs) are moving mixtures of particles and gas that flow across the ground, and originate in different ways and from various sources, during explosive eruptions or gravity driven collapse of domes. They mainly move under the effect of gravity and their mobility (i.e. distance travelled vs. difference in height from source and deposit) is greatly controlled by mass and height of generation (i.e. potential energy) and efficiency of conversion from potential to kinetic energy (e.g. loss of momentum due to frictional processes both within the current and at current edges). They may be short lived (i.e. highly unsteady) or relatively long lived (i.e. sustained unsteady to quasi steady) phenomena, driven by both magmatic or phreatomagmatic melt fragmentation (e.g. [378–380]). PDCs involve a spectrum between the dense and the dilute end members based on relative particle concentration [378]. Small volume (< 0.5 km^3) end member PDCs are a common volcanic phenomenon at active subduction zone volcanoes. These events, unlike large volume ignimbrite eruptions, are short lived, characterized by complex, gravity controlled, multi phase flow dynamics where the deposits generally consist of poorly sorted mixtures of decimeter to meter sized, dense to vesicular blocks set within an ash matrix (e.g. [378], [381]). Regardless of whether they are concentrated or diluted suspensions of gas and particles, PDCs consist of two essential and intergradational counterparts: an underflow and an overriding dilute ash cloud (e.g. [380], [382], [383]). The underflow is denser than the atmosphere and flows in direct contact with the ground. This underflow usually comprises a basal part dominated by particle–particle interaction overlaid by a turbulent part dominated by traction processes, which also is known as ash cloud surge (e.g. [378]). The ash cloud or co ignimbrite plume is less dense than atmosphere and lofts convectively [384], [385]. In contrast, the denser ground flow can have densities ranging from near atmospheric to hundreds of kg/m^3. The impacts of PDCs can be severe for obstacles in their flow paths as these flows can move at velocities as fast as hundreds of meters per second, commonly at temperatures more than 300 °C. As a result, dynamic pressures on order of kilopascals to hundreds of kilopascals can be produced by many PDCs, which are comparable to the overpressures created by nuclear explosions at similar distances from the source (e.g. [386]). Even relatively smaller volume PDCs (from VEI = 4 eruptions) can produce overpressures > 15 kPa and temperatures 200–300 °C within 6 km of the vent [387]. In addition, PDCs are destructive, owing to the momentum of the massive terrain enveloping mixture of hot lava blocks, ash and volcanic gas. PDC deposits are highly variable in bulk volume (< 0.1 to > 1000 km^3), runout distance (< 1 to > 100 km), deposit geometry and response to topography (channel confined to radially symmetrical), internal structure (massive through layered), degree of welding and chemical composition (mafic through felsic, often compositionally zoned). Deposits from larger volume (i.e. > 1 km^3) PDCs can exceed tens of meters in thickness tens of kilometres from the vent, including hot lava blocks up to several meters in diameter. Such massive deposits can greatly transform the landscape around the volcano, including river catchments and other complex topography over areas of several tens of square kilometres, and be subsequently remobilized to generate large volume lahars and major flooding events over several years after their emplacement. All types of PDCs (i.e. pyroclastic flows, surges and blasts) are known to surmount significant topographic features and to flow across large bodies of water (e.g. [388]). Interaction of PDCs with topography can significantly affect their dynamics including locally enhancing their dynamic pressures (e.g. [102]). Many properties of PDCs including, but not limited to, particle concentration, granulometry and componentry, bulk rheology and velocity are highly variable in both time (unsteadiness) and space (non uniformity).

5.9.2. Potential effects for nuclear installation

Pyroclastic density currents are usually lethal to humans because of high temperature and dynamic pressure, hot gases and missiles, and can ignite widespread fires that could affect nuclear installations. They commonly destroy or bury engineered structures in their path. For example, in Montserrat, PDCs that flowed into the capital city of Plymouth knocked down sturdy metal and concrete walls and single story concrete buildings, and devastated larger multi story buildings (e.g. [389]). The impact of PDCs depends primarily on two factors: (i) the initial conditions (e.g. volume, direction and generation mechanisms), and (ii) the physical characteristics of the PDCs (e.g. velocities, dynamic pressure, temperature, particle concentration, thickness). The morphology of the summit area and the topography across which PDCs move are also factors in controlling their potential distribution (e.g. inundated area and ability to surmount topographic barriers) and runout distances.

5.9.2.1.Consideration for siting

As indicated in TABLE 4, the effects from pyroclastic density currents should be considered as an exclusion criterion of the site [1]. The physical characteristics of PDCs indicate the impacts of these phenomena likely exceed common design bases for nuclear facilities. In addition, these impacts have not been analysed at a level of detail that would provide confidence that a safety related structures, systems, and components, and associated operations, could withstand the direct effects of a PDC impacting the installation. For comparison, peak positive overpressures of > 7 kPa ($\approx$ 1 atm) from potential nonvolcanic explosions occurring near United States nuclear power plants must be analysed in detail if the likelihood of such overpressures occurring is > 10^{-7} per year [390]. Structures, systems and components must be able to maintain their safety functions if such overpressures have the credible potential to reach the installation. Moreover, the range of possible energies of impacting particles from PDCs can be compared with impacts due to tornado borne projectiles (See Section 5.3). For example, NPPs in the United States consider the potential impacts of tornado generated projectiles ranging from a 2.5 cm diameter steel sphere traveling at $\approx$ 8 m s^{-1} to an automobile traveling at $\approx$ 40 m s^{-1} [186]. Nevertheless, such tornado generated impacts occur as transient events at ambient temperatures. PDC generated projectiles can occur at high temperatures with the potential for multiple impacts in a single event, which are significantly more severe conditions than envisioned for impacts from tornado generated projectiles.

5.9.2.2.Consideration for operations and emergency planning

Similar to lava flows, the potential for PDCs occurring at the site is generally considered a site exclusion criterion because of the extreme impacts on people and facilities from direct exposure to PDCs. PDCs also have the potential to affect facility operations from impacts on critical infrastructure located away from the site. For example, the electrical supply for the facility could be disrupted if PDCs destroyed transmission lines, leading to a potential station blackout condition. Ash and debris from PDCs flowing into water impoundments could disrupt water flow to the facility cooling system, for months to years after the eruption. Re-suspended ash from PDCs could have the same effects as ash falls on structures, systems, and components important to safety. In addition, the presence of PDCs near the site could restrict access of critical personnel to the site. Unlike lava flows, mitigation strategies have not been suggested to divert PDCs from a site. The ability of PDC to surmount hundreds of meters of topography and decouple the ground flow from the elutriated ash during transport presents significant challenges to any potential diversionary scheme.

5.9.3. How to evaluate effects

Many properties of pyroclastic density currents including, but not limited to, particle concentration, granulometry and componentry, bulk rheology and velocity are highly variable in both time (unsteadiness) and space (non uniformity). For example, in PDCs generated from lava dome collapses (i.e. block and ash flows), collapsing material progressively transforms from solid fractured lava, through coarse collapsing mega blocks, to highly fragmented, ash dominated material. In other cases, such as in the formation of small volume pumice flows, material progressively sediments from a collapsing but dilute mixture, eventually condensing to form ground hugging concentrated granular currents, which often show marked vertical and lateral segregation in terms of their high and low density components. Furthermore, the complexities associated with interpretation of field deposits, anticipation of inundation extents for given flow scenarios over specific terrain and our ability to effectively model these currents, are all essentially rooted in this unsteady, non uniform behavior. At present a complete simulation of all these phenomena, although possible in principle, does not exist, and current numerical models describe only a part of the observed phenomena. Moreover, numerical modeling of these events is complex and at present not all relevant physical processes are completely understood. For these reasons, in order to simulate PDCs, different simplified numerical models are commonly adopted, including the empirical energy cone model, semi-analytical 'basal friction' models, two dimensional models based on the shallow layer approach, and, in some cases, more sophisticated three dimensional models.

Surges arising from phreatomagmatic explosions represent a class of PDCs that are challenging to model in a hazards assessment. These surges arise from steam blasts that spew dilute mixtures of pulverized rock, magma, and gas, typically from new vents that form broad craters at ground level. Although there are numerous models that investigate the mechanics of phreatomagmatic surges (e.g. [391], [392]), these models have not been applied to numerical analysis of hazards.

5.9.3.1. Existing modeling approaches (hierarchy; advantages; limitations)

Basic models

An early modeling attempt was made by Sheridan [393] who developed the concept of an 'energy line' to model the emplacement of PDCs. In this type of model, the potential energy of the material erupted directly at the vent or at the top of the gas thrust column region is converted to kinetic energy as the material moves laterally away from the vent. During this movement kinetic energy is converted to friction and the flow stops when the energy line 'intersects' the topographic surface. The basal friction angle (φ) is a measure of the resistance to flow generated by a sliding avalanche at the contact with the underlying topography and is related to the tangent of the angle (α) connecting the top of the source area to the most distal part of the flow [394]:

$$\frac{\Delta H}{L} = \varphi = \tan \alpha \qquad (48)$$

where ΔH is the fall height and L is the horizontal distance travelled. The principal assumption of the energy line concept is that erupted material behaves as a gravity driven, cohesionless suspension of particles and gas with mass remaining constant [393]. By using digital topographic models of volcanoes, the energy line model was soon expanded into a three dimensional representation called the 'energy cone' model by sweeping the energy line

through a 360° arc [395], [396]. These friction models were equivalent to sliding block models, and were thought to potentially apply to virtually all pyroclastic flows [393]. A weakness of these models is that they assume straight line flow trajectories that pass through topographic obstacles, encompass the entire cone and ignore confining topography.

McEwen and Malin [397] developed the FLOW model to simulate pyroclastic flows, rockslide avalanches, lahars and the blast from the 1980 eruption of Mount St. Helens, Washington. The FLOW model calculates the velocity and simulated flow path of an event over a digital terrain model. The movement of the flow is determined by initial conditions, gravitational acceleration and resistance to motion. The latter is described by FLOW as Coulomb type, viscous or turbulent. This model takes a simplified approach to solving the complex physics driving such flows in nature. It is not based on conservation of mass and individual masses do not interact with one another. The authors also found that calculated flow velocities were too high, creating flow paths that responded poorly to topography.

Kover [398] developed this code further to produce the FLOW2D and FLOW3D models, respectively. The FLOW3D code is based on the generation of a DEM representing the topographic surface along which multiple sliding blocks move on a Triangulated Irregular Network (TIN) of elevations. The block trajectory is traced in small increments of time until it stops. The velocity and position of the block at each time step is recorded and can be plotted to show the trajectory and runout of a large number of blocks and to determine a rough estimation of the extent of the affected area. Resistance to flow in the model is calculated using the formula of Mellor [399] for snow avalanches:

$$\tau = a_0 + a_1 v + a_2 v_2 \tag{49}$$

where τ is the resistance to flow, v is the velocity, and a_0, a_1 and a_2 are parameters that represent the resistance due to basal friction, viscosity (or internal friction) and turbulence, respectively. Initial velocities may be input for blocks resulting from explosions or column collapse. The FLOW3D model has been used for risk assessment at several volcanoes (e.g. [400–402]). However, several limitations exist for this model, including that: (1) each block moves as if it is the only one traversing the slope, (2) the volumetric parameters (i.e. source volume, flow thickness, deposit thickness) are not included amongst either input or output data, (3) the equations for the conservation of mass are not used and (4) an accurate measurement of planimetric extent of a flow cannot be obtained from the output.

The model of Wadge et al. [403] added further complexity to the FLOW model to account for flow expansion as a result of atmospheric entrainment and sedimentation during downslope movement. The model is based on a two dimensional equivalent of the equation for the motion of the avalanche phase of the flow described by McEwen and Malin [397] and the dilute ash cloud surge is modeled following the approach of Bursik and Woods [404]. The path of the avalanche component of the flow then acts as the source for surge runout calculations to either side of the avalanche. Although this model more closely approximates the flow physics, five additional adjustable parameters are required for its implementation and equations for the conservation of mass as well as additional effects of internal pressure gradients in the flow are not included. Therefore, this model is regarded by its authors as an inverse modeling approach of simulating both the avalanche and surge components of dome collapse pyroclastic flows.

Widiwijayanti et al. [405] have developed a statistically constrained simulation model for block and ash flows (named PFz) to estimate potential areas of inundation by adapting

methodology from [406] for lahars (See Section 5.10). The predictive equations for block and ash flows are calibrated with data from several volcanoes and given by $A = (0.05\ to\ 0.1)V^{2/3}$, $B = (35\ to\ 40)V^{2/3}$, where A is cross sectional area of inundation, B is planimetric area and V is deposit volume. The proportionality coefficients were obtained from regression analyses and comparison of simulations to mapped deposits. The method embeds the predictive equations in a Geographical Information System (GIS) program coupled with DEM topography, using the LAHARZ program of Schilling [407]. Although the method is objective and reproducible, any PDC hazard zone so computed should be considered as an approximate guide only, due to uncertainties of the coefficients applicable to individual PDCs, the authenticity of DEM details, and the volume of future collapses. Multiple inundation zones, produced by simulations using a selected range of volumes, partly accommodate these uncertainties. These authors also proposed three different procedures for rapid estimation of surge limits, (1) by empirically examining the limits of pyroclastic surges associated with recent PDCs; (2) by simply using the standard LAHARZ/PFz approach, but with arbitrary large volumes and parameters adjusted such that the calculated lateral surge limits are similar on average to those surges observed historically; and (3) by following the approach of Wadge et al. [403] and Bursik and Woods [404], using a one dimensional hydraulic balance of sedimentation of clasts and entrainment of air away from the modeled PF basal avalanche source.

Intermediate models

Shallow layer models

A new class of models began with the work of Savage and Hutter [408] who introduced a consistent set of equations of motion for a translating, deforming granular mass based on a Coulomb frictional resistance term. Iverson and Denlinger [409] derived depth averaged, frame invariant equations for fluidized granular masses on three dimensional terrain and included the effect of interstitial fluid using a simple mixture theory approach. The general shallow layer depth averaged equations for the conservation of mass and momentum are described in Appendix. Recent studies by Heinrich et al. [410] on Montserrat and Le Friant et al. [411] on Montagne Pelée, Martinique, have shown that the emplacement of debris avalanches can be well modeled by a Coulomb type behavior law with a variable apparent basal friction angle [412].

The Titan2D computer program [413] is a freely available geophysical mass flow model, built on a depth averaged model for an incompressible Coulomb continuum, a shallow layer granular flow, based on the work of Savage and Hutter 427], Iverson [406], Iverson and Denlinger [409], Denlinger and Iverson [415] and Mangeney-Castlenau et al. [416]. It combines numerical simulations of a flow with digital elevation data of natural terrain supported by a GIS interface. The conservation equations for mass and momentum are solved with a Coulomb type friction term for the interactions between the grains of the media and between the granular material and the basal surface [417]. The model assumes that the flow starts as a dome shaped pile of material with user specified dimensions of height, width and thickness as well as the starting location coordinates. The two other input parameters are the internal friction angle and the basal or bed friction angle. The direct outputs are flow depth and momentum, which can be used to compute field observable variables at different locations and times during the flow, such as run up height, inundation area, velocity and time of flow. The version 2.0.1 of the Titan2D code allows the simulation of material that actively extrudes from

the ground at a specific rate over a specific period of time by using a combination of different piles and flux sources (i.e. multiple collapse events).

VolcFlow [418] and DAN3D [419] are other freely available geophysical mass flow model designed to simulate various granular flows. Like the Titan2D model, the codes are based on a depth averaged granular flow model and differ in the possibility to enter various user defined rheological behaviors (i.e. frictional, plastic, viscous and/or turbulent). Source conditions can also include shape, footprint, height, volume, position and initial velocity of a source of material or flux sources which add mass over a specified time period and area at a constant or varying rate. DAN3D can also account for varying vertical erosion rates along the flow path.

Although granular flow models simulate many aspects of small volume PDCs, other modelling approaches have been proposed. Several authors have assumed that some PDCs behave as Bingham fluids (e.g. [420–422]). However, this modelling assumption encounters problems when tested quantitatively (e.g. [397]). A separate line of reasoning was taken by authors assuming a constant resisting shear stress to flow spread [423], [424], which is considered by many to produce a better mechanical explanation for a number of PDCs. Results show that for a given type of flow, runout is controlled by a constant stress condition and not by a constant slope condition, as assumed by the Coulomb friction model where the shear stress is proportional to the normal stress. These contrasting views on the main flow regimes and rheological behavior that govern the dynamics of PDCs has led to the incorporation of different stress relationships into recent numerical models of PDCs, with the other terms used to define flow dynamics remaining the same for different flow types.

Cellular automata models

A cellular automata approach for PDCs uses the same numerical scheme described for lava flows (See Section 5.8). A new notion of CA was developed by Avolio et al. [425] as an empirical method for modeling macroscopic phenomena; its application to *PYR*, a CA model for simulating pyroclastic flows, generated *PYR2*, which permitted an improvement of the model and a more efficient implementation. However, *PYR2* does not consider the modeling mechanisms of the pyroclastic column formation or the granulometric composition of the deposit. *PYR2* was utilized for the 1991 eruption of Mt. Pinatubo in the Philippines islands and for the 1996 eruption of the Soufrière Hills at Montserrat Island. Results of the simulations were compared against measured deposit distributions.

Complex models

Multiphase flow models

The fact that any property of the PDC (e.g. particle concentration and velocities) sharply change with time (i.e. unsteadiness) and space (i.e. non uniformity, both vertically and horizontally) justifies a multiphase model approach. A multiphase approach is able to model the whole spectrum of volumetric grain concentrations, provided that a comprehensive rheological model is implemented in the algorithm and code. Multiphase flow models have been extensively tested through laboratory experiments and numerical simulations (e.g. [426–431]). Although these models can describe the sedimentation and aggradation of different particle classes, the limited vertical resolution of the computational grid (> 20 m) and the formulation of the adopted rheological model do not generally allow an adequate description of the granular basal component of the PDC, thus making these models more suited to the

simulation of particle sedimentation in shear flows at moderate particle concentrations of less than about 0.1 vol % (i.e. in kinetic to collisional flow regime).

An *ad-hoc* multiphase mathematical model [426] included a comprehensive unified stress tensor able to adequately describe stress within the flow for any of these regimes, and without imposing a priori what regime will dominate over the others:

$$T_s = P_s I + \tau_s = {}^{f}T + {}^{k/c}T \qquad (50)$$

where the total stress tensor of the solid phase, T_s, is the sum of the kinetic, collisional and frictional tensors, the superscript f stands for frictional and k/c for kinetic/collisional. Hence the solid pressure, P_s, and the viscous stress, τ_s, must encompass all the contributions from kinetic, collisional and frictional dissipations. To account for the whole spectrum of rheologies, the multiphase computer code GMFIX (Geophysical Multiphase Flow with Interphase Exchanges) has been devised, which can successfully simulate several pyroclastic phenomena and related eruptive processes [426], [432].

Another transient three dimensional multiphase flow model of pyroclastic dispersion has been proposed, in which solid particles are considered to be in dynamic equilibrium with the gas phase (e.g. [433]). In the applied Pyroclastic Dispersal Analysis Code (PDAC) [429], [433], [434] model, the fundamental processes governing explosive eruptions are expressed by the Eulerian multiphase transport laws of mass, momentum, and enthalpy of a gas pyroclast mixture formed by a continuous multicomponent gas phase and n solid particle phases representative of pyroclasts, with each phase characterized by size, density, specific heat, and thermal conductivity [426], [434], [435]. The transport equations are solved for each phase over the 3D spatial domain with prescribed boundary conditions by advancing time from assigned initial conditions. Model output provides, at each instant in time, the gas pressure, volume concentration, velocity, and temperature of each phase over the 3D domain. Mass balance equations do not account for gas phase transitions or mass transfer between particulate phases (e.g. via secondary fragmentation or aggregation). Free in out flow conditions are imposed at West, East, South, North and Top domain boundaries. At ground, the PDAC code imposes no slip (i.e. zero velocity) conditions. No solid mass outflow is allowed from bottom boundary, which is equivalent to avoiding particle deposition. Although this condition is conservative, it did not affect significantly the large scale dynamics of the flow, because the current rapidly decouples into a dense, basal layer and a dilute cloud. Although the basal layer controls the depositional features of the blast, the dynamics of the upper, dilute layer largely controls the runout distance and timing of the PDC emplacement.

5.9.3.2.Probabilistic assessment

A probabilistic approach should consider the probability of occurrence of pyroclastic density currents and should be calculated as a conditional probability of an eruption of a given intensity, multiplied by conditional probability distributions for: (a) occurrence of PDCs; (b) runouts of these phenomena; and (c) directivity effects. The value for conditional probability of PDCs should be representative of the physical properties of the magma, the dynamics of the eruption, including interaction with hydrothermal and groundwater systems, and the physics of flow spreading and diffusion. In many circumstances, the past frequency and nature of PDCs from the capable volcano, and from analogous volcanoes, can be used to refine the estimate. If uncertainty in the resulting hazard curves is expressed by confidence bounds, the basis for selection of the reported confidence levels should be documented.

Sheridan et al. [436] describe methodologies for quantifying the effect of the input data uncertainty in the use of the Titan2D code for geophysical mass flows in hazard analysis. In order to quantify the impact of these uncertainties on desired outputs, they used a variant of the polynomial chaos (PC) methodology, called polynomial chaos quadrature (PCQ), in which the input probability distribution function is approximated by an expansion in terms of a finite number of orthogonal polynomials. The method simplifies to intelligent sampling guided by the quadrature required to evaluate the appropriate integral. The approximation of the probability distribution can be computed with good accuracy at significantly less cost than a Monte Carlo sampling. This technique (as detailed in [437]) produces probabilistic hazard maps that are reproducible, incorporate current topography and source conditions, and are based on the principles of physics that are included in the Titan2D model.

5.9.3.3.Deterministic assessment

A deterministic assessment needs to assume the location of a future vent, which should be selected so that the resulting hazard is not underestimated for the site. Subsequently, the hazard assessment for PDCs should determine threshold values on the basis of the maximum credible length, areal extent, thickness, and potential speed of PDCs that could reach the site. This can be achieved using data from other volcanoes from the geographical region, from analogous volcanoes, or from empirical or numerical models of PDC emplacement. Some empirical models of PDC emplacement rely on correlations between flow length and effusion rate, whereas others are volume limited. Topography along the path and at the site of the nuclear power plant should be considered. The uncertainties in the various parameters should be properly taken into account, so that there is confidence that the PDC hazard has not been underestimated for the site. Similarly, the deterministic model can be used to develop a screening distance value for PDC hazards, to supplement the site specific information developed for PDC characteristics.

5.9.3.4.Examples of evaluating potential hazards

As a practical example of PDC hazard assessment at a nuclear power plant site, we will summarize the procedure employed by Volentik et al. [106] to estimate PDC hazard at the BNPP site near Mt. Natib, a Quaternary volcano in Philippines. Volentik et al. [106] considered a basic but widely used model (i.e. the energy cone model [393]) for the potential runout of PDCs to determine if the site lies within or beyond a screening distance value that is representative for such highly mobile flows. Essentially this model uses the height, H, from which PDCs originate, directly related to the potential energy of the flows, to estimate their runout, L, the horizontal distance the flows are likely to travel from their source. The ratio, H/L depends on the mobility of the PDC. Examples in the literature commonly range from H/L =0.2 for small flows, to H/L < 0.01for large volume, highly mobile PDCs (e.g. [438]).

The three gray shaded regions in FIG. 38 a represent possible areas inundated by pyroclastic flows originating from the collapse of a 100 m high dome on Mt. Natib. The different shaded regions represent areas inundated by pyroclastic flows of increasing potential energy, represented by the ratio of dome height to runout length: H/L = 0.2 (darkest gray area), H/L = 0.15 (medium gray area), H/L = 0.1 (light gray area). Uncertainty in the appropriate value of H/L results in uncertainty in the total runout of the flow. FIG. 38 left shows higher release heights (e.g. 1000 m above the caldera floor) associated with eruption column collapse and higher intensity eruptions. Shaded areas show inundation by pyroclastic density currents for H/L = 0.15 (closest to the vent, darkest shading), H/L = 0.1, and H/L = 0.075 (farthest

from the vent, lightest shading). For PDCs originating from dome building eruptions and from low volume explosive eruptions (< VEI 5), their analysis shows that the caldera wall will likely act as a topographic barrier for pyroclastic flows traveling toward the site from a central vent eruption of Mt. Natib. Such flows would have insufficient potential energy to overcome the 300–500 m high topographic barrier of the caldera wall and likely would be channelized toward the northwest, possibly exiting the caldera through a gap in the caldera wall (See FIG. 38). Therefore, assuming low volume explosive eruptions occur within the existing caldera, the site seems to be outside the screening distance for pyroclastic density currents released from such comparatively low lying sources within the caldera.

In the case of an explosive eruption of ≈VEI 5 or greater, or an eruption occurring from a new vent located on the southern flanks of the volcano, the energy cone model indicates that PDCs might reach the site. Flows associated with such eruptions often generate PDCs as a result of collapse of the eruption column or by boiling over of a particularly dense eruption column. In such circumstances, the potential energy of the flow may be sufficient to overcome topographic barriers approximately 500 m high, such as the caldera wall. Based on the energy cone model, a potential column collapse assumed to initiate at the top of the gas thrust region would need to originate at no more than 1 km elevation above the caldera floor. Once overcoming the southwest wall of the caldera, the topographic slope is such that the flow extends beyond the site area for $H/L < 0.15$ (See FIG. 38 right). Based on this simplified analysis, it appears that the BNPP site is located within the screening distance value of pyroclastic density currents for eruptions VEI 5 or greater. As is the case for tephra fallout, such flows could also generate voluminous lahars, which may have the potential to affect the site.

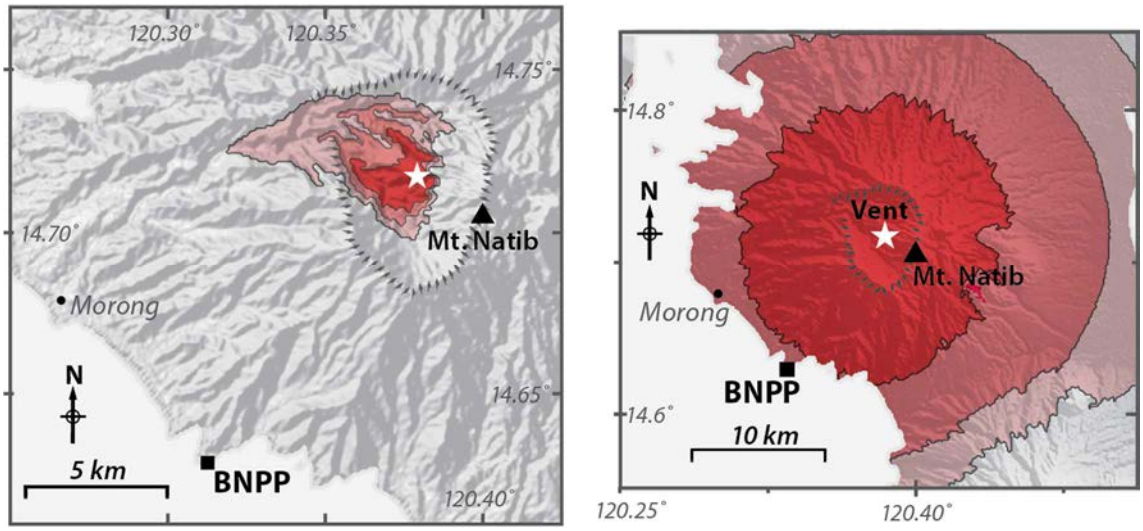

FIG. 38. Three potential pyroclastic flow runouts (red shaded areas) from the caldera floor of Mt. Natib, estimated using the energy cone model [106] from lava dome (left figure) and column collapse (right figure).

Volentik et al. [106] concluded that using more complex numerical models of PDCs might greatly improve this assessment and could be considered as part of a comprehensive hazard analysis for PDCs. The energy cone calculation strongly suggests such an assessment would be useful for understanding a range of PDC hazards for the BNPP site. In addition, a complete analysis of hazards also should consider the potential for new vent formation on the

flanks of Mt. Natib. As observed at other composite volcanoes, such vents might also be a source of PDCs that may create additional hazards at the site.

5.9.4. Summary

Pyroclastic density currents are moving mixtures of particles and gas that flow across the ground, and originate in different ways and from various sources, during explosive eruptions or gravity driven collapse of domes. The impacts of PDCs are very severe for obstacles in their flow paths as these flows can move at very high velocities (as fast as hundreds of meters per second), commonly at high temperatures (e.g. more than 300 °C). The impact of PDCs depends primarily on three factors: (i) the initial conditions (e.g. volume, source geometry, volatile content, direction and generation mechanisms), (ii) the physical characteristics of the PDCs (e.g. velocities, dynamic pressure, temperature, particle concentration, thickness); and (iii) the effects of topography along the flowpath. As indicated in TABLE 4, the effects from PDCs should be considered as part of the exclusion criteria of the site, since these effects appear to exceed the typical design basis of many structures, systems, and components that are important to safety. Considerable progress has been made in the understanding of the physics of PDC and several approaches have improved our knowledge by trying to describe their complexities. However, PDCs are complex multiphase fluids that significantly change in character during flow and, at present, not all relevant physical processes are completely understood. For these reasons, in order to simulate PDCs different simplified models are commonly adopted, including basic empirical models, semi-analytical 'basal friction' models, two dimensional models based on the shallow layer approach, and, in some cases, more complex multiphase three dimensional models. Awareness of model uncertainty arising from poor parameter estimation, topographic resolution or mechanical understanding is critical to determine the appropriateness of these models for use in hazard assessment.

5.10. LAHARIC FLOWS

5.10.1. Physical characteristics

As used in Vallance [439], 'Lahar' is an Indonesian term that corresponds to water saturated flow from a volcano (i.e. debris flow with > 50% sediment, transitional flow or hyperconcentrated flow with 20–50 % sediment and muddy streamflow with < 20 % sediment). At times, the term 'lahar' is used to denote only water saturated flows with > 20 vol % sediment, with 'banjir' used for lower concentration flows. Lahars can occur before (i.e. pre-eruptive lahars), during (i.e. syn eruptive lahars) or after (i.e. post eruptive lahars) volcanic eruptions or, less predictably, through other processes common to steep volcanic terrain when large masses of sediment, and water, sweep down and off volcano slopes incorporating additional sediment. Because lahars are water saturated, both liquid and solid interactions determine their unique behavior and distinguish them from other related phenomena common to volcanoes such as debris avalanches and floods. The rock fragments carried by lahars, ranging in diameter from order of 10^{-6} m to 10 m, make them especially destructive; abundant liquid contained in them allows them to flow over gentle gradients (slopes < 5 degrees) and can inundate areas far away from their sources with runouts of kilometers to > 100 km (e.g. [439]). Magnitude of lahars is most often characterized in terms of volume: relatively small lahars are the most frequent to occur, with volumes $\approx 10^3$–10^5 m^3, whereas the largest ones are rare, and have volumes > 10^8 m^3. Lahar genesis requires (1) an adequate water source; (2) abundant unconsolidated debris that typically includes pyroclastic flow and fall deposits, glacial drift, colluvium, soil, etc.; (3) steep slopes and substantial relief at the source; and (4) a triggering

mechanism. Water sources include pore or hydrothermal water, rapidly melted snow and ice, subglacially trapped water, crater or other lake water, and rainfall runoff (e.g. [439]). In tropical regions, they frequently occur during the rainy season. Lahars velocities can exceed 20 m s^{-1} on steep slopes but average velocities between 1–10 m/s are more common. Discharge rates of up to 10^5 m s^{-1} have been recorded in Iceland for jökulhlaups (floods resulting from subglacial eruptions of lavas) but peak discharges of < 10^3 m s^{-1} are more common for small to moderate lahars. Deposits up to 200 m thick have been identified [440] but average thicknesses generally range from a few centimeters (i.e. streamflow and hyperconcentrated flow deposits) to meters (i.e. debris flow deposits). Lahars can be hot (up to 100 °C) and commonly change character downstream. Flow transformation during transport involves periods of flow bulking (erosion and incorporation of secondary, exotic debris by lahars as they move downstream) and debulking (i.e. a process in which the lahar selectively deposits certain particles, owing to their size or density, as it moves downstream). Many properties of lahars including, but not limited to, particle concentration, granulometry and componentry, bulk rheology and velocity are highly variable in both time (i.e. unsteadiness) and space (i.e. non uniformity).

Pierson and Costa [441] and Scott et al. [442] refer to cohesive debris flows as those that have > 3 % of the total clay silt sand fraction and typically originate by removal of clay rich, hydrothermally altered debris. Pore pressures can build easily when clay content is high, so these flows are unusually mobile. In contrast, debris flows that contain less clay have lower pore pressures and are less mobile, unless they evolve by sedimentation into hyperconcentrated flows. They are mostly dominated by particle particle interactions (also known as 'granular temperature' [414], [443], [444]) and are also called non cohesive debris flows [439]. They can be classified as: (i) true grainflows, in which the interstitial fluid has a negligible effect on the physical state of the granular mass; and (ii) modified grainflows, in which the physical characteristics of the moving granular mass are modified by the intergranular fluid [445]. Primary particles in lahar deposits derive from contemporaneous eruptions or, in the case of avalanche induced lahar deposits, from the original avalanche mass; secondary particles derive from the erosion and incorporation of downstream volcaniclastic debris, alluvium, colluvium glacial drift, bedrock, etc. Particles found within lahar deposits can be monolithologic but are more commonly heterolithologic; they can be rounded to angular, but primary particles are usually subangular to angular. Deposits commonly exhibit vesicles in the matrix, which result from entrapment of air bubbles. Other common constituents include wood fragments, casts of wood fragments, and charcoal. Concentrations of coarse particles, especially low density particles such as pumice, are common at deposit tops.

5.10.2. Potential effects for nuclear installation

In addition to the impacts associated with ordinary flooding, lahars produce mechanical effects, owing to the mass of material involved (up to > 60 vol % particle concentration) and its velocity and therefore its erosive power and physical load. The occurrence and the effects of lahars can persist for periods ranging from months to decades following volcanic eruptions, as volcanic products such as pyroclastic density current and tephra fallout deposits are remobilized over time. In addition to the physical impacts associated with laharic flows, the large amount of suspended particles can adversely affect water circulation systems for nuclear facilities. These impacts include clogging of intakes and filters, and suspended sediment concentrations that exceed operational limits for pumps, seals, and valves.

5.10.2.1. Consideration for siting

As indicated in TABLE 4, the effects from volcanic debris flows, lahars and floods should be considered, in principle, a potential exclusion criterion for the site. This often is the case when a potential site could be inundated by future lahars. However, since their effects might be accommodated by site and plant layout, design, operation or site protective measures, an appropriate design basis might be determined for sites that are not significantly inundated. Early warning systems including rain gauges, flow sensors, low frequency seismic equipment or radios have been implemented at several active volcanoes (e.g. Japan, Indonesia, Philippines) and proved to be useful for emergency planning (e.g. [446–448]).

5.10.2.2. Consideration for operations and emergency planning

Although the potential for lahars occurring at the site is generally considered a site exclusion criterion, lahars also have the potential to affect facility operations from impacts on critical infrastructure located away from the site. For example, the electrical supply for the facility would be disrupted if lahars affected transmission lines, leading to a potential station blackout condition. Sediments and debris from lahars flowing into water impoundments could disrupt water flow to the facility cooling system and significantly increase suspended sediment loads, for months to years after the eruption. In addition, the presence of lahars near the site could restrict access of critical personnel to the site by disrupting transport networks.

In the days after the 18 May 1980 Mt. St. Helens eruption in Washington, U.S.A., sediments from debris flows unexpectedly migrated 8 km upstream from the point of entry in the Columbia River, to the location of the Trojan Nuclear Power Plant, Oregon [449]. The Trojan Plant was off line for refuelling prior to the eruption, thus, water intake systems and plant operations were not affected by these debris flow sediments. Although sediment deposits reached 12 m thickness in the main Columbia River channel near the Trojan NPP, intake systems for the facility withdrew water away from main river channel and suspended sediment loads remained within operational limits once the plant was restarted.

Hydroelectric power stations affected by lahar hazards have typically shutdown and opened spill gates on a precautionary basis [200]. The 156 MW Agoyan HEP facility, located 5 km east of the city of Baños in Ecuador, is occasionally exposed to lahars following heavy tephra fall in the Pastaza catchment of the dam [450]. Intake mechanisms such as wicket gates, turbine covers and blades are particularly at risk of abrasion from the tephra laden water. Severe pitting and scouring of the metallic components accelerate their degradation, and by 2010 four turbines had been replaced in the last 21 years [450]. To reduce the impacts from the intake of highly turbid water, Agoyan has a specially designed floodgate system in place so that the intake flow can be diverted away from generation components and directly flushed out into the river. When there is heavy rain, causing an increased risk of tephra laden floodwaters and lahars, the dam operators monitor water levels and turbidity, and activate the protective bypass system as required [450].

5.10.3. How to evaluate the effects

The hazard assessment for lahars and floods of volcanic origin for each capable volcano should consider: (a) The identification of potential source regions for volcanic debris and for water, including snowcaps and glaciers; (b) The potential magnitude and characteristics of the flow; (c) The potential for modification of the flow properties along the path, the sources of water and the topography between the source region and the nuclear power plant; (d) The frequency of such events in the past; (e) The meteorological data at the source region and along the potential path of such flows, especially for extreme events. The complexities associated with interpretation of field deposits, anticipation of inundation extents for given flow scenarios over specific terrain and our ability to effectively model these flows, are all essentially rooted in this unsteady, non uniform behavior. At present a complete simulation of all these phenomena, although possible in principle, does not exist, and current numerical models describe only a part of the observed phenomena. Moreover, numerical modeling of these events is complex and at present not all relevant physical processes are completely understood. Lahars are generally simulated with numerical models involving Navier–Stokes equations assuming different rheologies (e.g. Newtonian, Bingham, Bagnold, or Coulomb models, depending on flow behaviour). For these reasons, in order to simulate lahars, different simplified numerical models are commonly adopted, including empirical lahar inundation models, semi-analytical 'friction' models, two dimensional models based on the shallow layer approach, and, in some cases, more sophisticated multiphase models.

5.10.3.1. Existing modeling approaches

Basic models

A statistical model for lahars is the LAHARZ model, developed at the USGS [407]. LAHARZ model uses statistical descriptions of areas inundated by past mass flow events to forecast areas likely to be inundated by hypothetical future events. The forecasts are based on sets of statistically calibrated power law equations relating mass flow volume (V) to cross sectional areas (A) inundated by an average flow, such as:

$$A = cV^{2/3} \tag{51}$$

with c empirically determined by best fit. Data from past events are used also to calculate the standard error of the forecast considering the fact that the regression is based on an incomplete sample of the population of V and A values, providing explicit confidence limits.

In combination, a slope failure model for lahars has been developed by Iverson [451], and is based on the potential for gravitationally induced failure of the tephra deposit on the volcano slopes to trigger lahars. Iverson's model assumes that slope failure is described by a Coulomb failure criterion expressed as a yield condition:

$$|\tau| = c + \sigma_n tan\beta \tag{52}$$

where τ is shear stress, c is tephra cohesion, σ_n is normal stress (perpendicular to the slope) and β is the angle of internal friction. This Coulomb failure model can be expressed as a ratio of resistive and driving forces, known as the Factor of Safety:

$$FS = \frac{Resisting\ Force}{Driving\ Force} = \frac{c+\sigma_n \tan\beta}{|\tau|} \quad (53)$$

where $\tau = -Zy_t \sin\alpha$, $\sigma_n = Zy_t \cos\alpha$, with Z the layer thickness (here derived from estimates of potential tephra accumulation), y_t the total unit weight of the deposit per unit area and α the slope of the slip surface (pre-tephra deposition topography). It follows that:

$$FS = \frac{c}{Zy_t \sin\alpha} + \left(1 - \frac{y_w}{y_t}\right)\frac{\tan\beta}{\tan\alpha} \quad (54)$$

where y_w is the unit weight of water added to the deposit by rainfall. Slope failure occurs when $FS < 1$. Lahars will be generated primarily on steep slopes after deposition of tephra units that become saturated by water infiltration, greatly reducing the shear strength of these tephra layers [452]. This slope failure model for lahar generation is thus coupled to a tephra fallout model, and, assuming deposit saturation by infiltrating water, areas of likely slope failure ($FS <$ 1) can be inferred.

GIS Based Models

A range of models has been developed to simulate debris flows and floods within a GIS framework. Typically, these models take advantage of GIS capabilities in applying numerical codes to grid based data. As an example, *r.debrisflow* [453] was implemented using a 2.5D raster data model (i.e. the vertical dimension plays an important role, but is only quantified by attributes) and designed as a module for the open source GRASS GIS software. It combines physically based, deterministic modules and modules based on empirical relationships. In particular *r.debrisflow* couples a hydraulic model, a slope stability model, a sediment transport model, and a debris flow runout model:

- The deterministic hydraulic model distributes the water from precipitation or snow melt among vegetation interception, soil infiltration, and surface runoff. It then approximates the soil water status and the runoff variables;

- The deterministic slope stability model computes the 'factor of safety' for each cell, based on an infinite slope stability model, and identifies potential starting areas of debris flows;

- The sediment transport model, which is based on an empirical approach, provides an estimate for erosion and deposition by surface runoff, assesses the tendency of bedload rich runoff to develop into a debris flow;

- The debris flow runout model finally routes the debris flow downwards to the area of deposition, based on a two parameter friction model developed by Perla et al. [454] that was modified by Gamma [455] and applied by Wichmann [456] in a raster based GIS environment. The deterministic element of the approach is the velocity of the debris flow v (m s^{-1}) which is computed for each raster cell i:

$$v_i = \sqrt{\xi_i \left(\frac{M}{D}\right)_i (1 - e^{\eta_i}) + v_{i-1}^2 e^{\eta_i} \cos(\Delta\alpha_i)} \quad (55)$$

where M/D (m) is the mass to drag ratio of the debris flow, and v_{i-1} is the debris flow velocity of the previous cell. The factor ζ_i and the coefficient η_i are derived as follows:

$$\xi_i = g(\sin \alpha_i - \mu \cos \alpha_i) \quad (56)$$

$$\eta_i = \frac{-2L_i}{(M/D)_i} \quad (57)$$

where g is gravitational acceleration, α_i is local slope angle, μ is the dimensionless friction coefficient, and L (m) is slope length (cell size corrected for slope angle). $\Delta\alpha$ is the difference between the slope angle of the previous cell and the slope angle of the considered cell.

The modules are executed in a defined sequence for a user defined number of time steps during and after a rainfall or snow melt event. Slope stability and runout are computed at the end of the last time step. The slope stability model is only able to predict shallow translational slope failures in cohesionless soils. The two parameter friction model does not say anything about the patterns of particle entrainment and deposition. Instead of designing a more complex scheme like [456], simple thresholds of slope and velocity are used for delineating these processes in *r.debrisflow*, where entrainment as far down as to the wetting front is only assumed if both parameters are above the threshold, whilst deposition is assumed to take place only if both parameters are below the thresholds.

Intermediate models

Cellular automata models

A cellular automata approach for lahars uses a numerical scheme similar to that described for lava flows (See Section 5.8). A different methodology to approximately describe and model the main features of lahars is represented by Macroscopic Cellular Automata (MCA). MCA are an extension of classical cellular automata, developed for overcoming some of the limitation affecting conventional CA frames such as the modeling of large scale complex phenomena. Due to its particulate nature and local dynamics, MCA are very powerful in dealing with complex boundaries, incorporating of microscopic interactions, and parallelization of the algorithm. The MCA model SCIDDICA (SS2) [457] is suitable for the simulation of completely subaerial, completely subaqueous and combined subaerial subaqueous debris flows. Main features of a debris flow are accounted by the SS2 version such as erosion and deposition and triggering of secondary landslides along the path, presence of structures and buildings, run up effects and, in the case of coastal landslides, impulsive loss of matter (i.e. water and finer grains) and energy dissipation at water impact. Moreover, buoyancy effects, drag forces and peculiar mechanisms like hydroplaning are also modeled for submerged events. The last version of SCIDDICA (SS3) uses a better strategy to manage momentum that permits a better approximation of inertial effects that characterize some rapid debris flows [458]. A further improvement required to the SCIDDICA model would be the introduction of explicitly interactions between solid and fluid phases on the debris as the relevance of inner fluid pressures in the propagation of a debris flow has been demonstrated [414].

Shallow layer models

Assuming that thickness of the lahar is much smaller than its length, it is possible integrating the 3D mass and momentum balance equations in depth and obtaining the so called depth averaged continuum flow equations [408]. In this case changes in the mechanical behavior within the flow are ignored and the rheology of the flowing material is described using a single term describing the frictional stress at the interface between the flowing material and the surface of the bed path. The general shallow layer depth averaged equations for the conservation of mass and momentum are described in Appendix. Numerical codes like FLO-2D [459] and RASH3D [460], [461] are based on such an approach. As input this kind of codes need a pre-event DEM of the study area, the position of the source area of the debris flow, the magnitude of the triggered mass, and a parameterization of the frictional stress. In particular in FLO-2D rheology is modelled by a shear stress relationship written in slope form:

$$s_f = s_y + s_v + s_{td} \tag{58}$$

where s_f is the total friction slope and is equal to the sum of the yield slope (s_y), the viscous slope (s_v) and the turbulent dispersive slope (s_{td}) components. These can be written as:

$$s_f = \frac{\tau_y}{\gamma_m h} + \frac{K\eta V}{8\gamma_m h^2} + \frac{n_{td}^2 V^2}{h^{4/3}} \tag{59}$$

in which τ_y is yield strength, γ_m is the specific weight of the slurry, h is flow depth, K is an empirical resistance parameter, η is fluid viscosity, V is flow velocity and n_{td} is Mannings roughness coefficient. A quadratic solution to the slope friction equation is incorporated in FLO-2D. Of the above mentioned parameters, h and V are calculated by the model, K and n_{td} can be assumed from overland and channel flow resistance characteristics, leaving τ_y, γ_m and η as the parameters to be defined. These are linked to the flow sediment concentration (C_v). For γ_m the relationship is:

$$\gamma_m = \gamma + C_v(\gamma_s - \gamma) \tag{60}$$

where γ is the specific weight of water and γ_s the specific weight of the sediment, while for τ_y and η FLO-2D uses two empirical relationships deduced from field observations:

$$\tau_y = \alpha_2 e^{\beta_2 C_v} \tag{61}$$

$$\eta = \alpha_1 e^{\beta_1 C_v} \tag{62}$$

where α_i and β_i are coefficients defined by laboratory experiment [462]. The assessment of sediment concentration is therefore crucial when modeling with FLO-2D. Simple trials should be performed in the field in which water is gradually admixed with the deposit material until liquefaction is attained. The quantity of water added is used to calculate the volumetric sediment concentration with EQ. (57). The empirical coefficients α_1, β_1, α_2 and β_2 are subsequently determined from charts in which sediment concentration is plotted against yield strength and viscosity [463]. FLO-2D is data intensive and requires detailed fieldwork and laboratory analyses. This significantly lengthens model setup and preliminary results are obtained after some weeks.

Topographic data must be formatted according to specific requirements of FLO-2D. FLO-2D output includes inundation area and maximum and final values, as well as at user specified intervals of flow discharge, velocity, direction, depth and concentration.

A generalization of this approach accounting for liquid grain interaction was developed by Pitman and Le [464] who used a depth averaged, thin layer model that uses a derivation of the original Savage & Hutter equations [408] and the mixture model of Iverson [414] and Iverson & Denlinger [409]. The model considers a thin layer of granular material and interstitial fluid, each of constant specific density ρ_s and ρ_f, respectively, flowing over a smooth basal surface. The model does not consider any erosion of the base. From [465], mass conservation for the two constituent phases may be written as:

$$\left.\begin{array}{c} \partial_t \rho^s \varphi + \nabla \cdot (\rho^s \varphi v) = 0 \\ \partial_t \rho^f (1-\varphi) + \nabla \cdot (\rho^f (1-\varphi) u) = 0 \end{array}\right\} \quad (63)$$

where v and u denote the velocities of the solid and fluid constituents, respectively, and φ the solid volume fraction.

The momentum equations for the two species explicitly account for buoyancy effects, and take the form:

$$\left.\begin{array}{c} \rho^s \varphi (\partial_t v + (v \cdot \nabla) v) = -\nabla \cdot T^s - \varphi \nabla \cdot T^f + f + \rho^s \varphi g \\ \rho^f (1-\varphi)(\partial_t u + (u \cdot \nabla) u) = -(1-\varphi) \nabla \cdot T^f - f + \rho^f (1-\varphi) g \end{array}\right\} \quad (64)$$

where g is the gravitational acceleration, T^s and T^f are the solid and fluid stresses, respectively, and f includes all non buoyancy interaction forces of the fluid on the particle:

$$f = (1-\varphi)\beta(u-v) \quad (65)$$

where the leading factor of $(1-\varphi)$ accounts for the volume of the fluid acting on the entire particle phase and:

$$\beta = \frac{(\rho^s - \rho^f)\varphi g}{v_T (1-\varphi)^m} \quad (66)$$

is a phenomenological function based on the experimental results of [466], v_T is the terminal velocity of a typical solid particle falling in the fluid under gravity, and m is related to the Reynolds number of the flow. The model provides a rich enough description of solids and fluid flow and interaction while still being amenable to mathematical analysis. In particular, momentum equations for both fluid and solid phases are retained, providing equations for the velocities of both phases.

Complex models

Multiphase flow models

Martinez et al. [467] have developed a quasi three dimensional numerical model to simulate debris flows accounting for a continuum non Newtonian fluid phase (solved by the FLO-2D computational model) composed by water and fine sediments, and a non continuum phase (using the 3D Discrete Element Method) for large particles such as boulders. The model considers particle particle and wall particle collisions and the depth integrated stress terms, S_{fx}

and S_{fy}, depend on the rheological formulation used to model the flow. Their results show that when applied shear stresses are low, the Bingham formulation best simulate the stopping phase of the fluid. In the solid phase, spherical particles of different diameters are considered and their trajectories are tracked using Newton's second law. Forces on each particle are calculated at each time step, together with their acceleration, velocity and displacement.

Pudasaini [468] recently presented a new, generalized two phase debris flow model that employs the Mohr-Coulomb plasticity for the solid stress. The fluid stress is modeled as a solid volume fraction gradient enhanced non Newtonian viscous stress. The generalized momentum transfer includes viscous drag, buoyancy, and virtual mass. A new, generalized drag force (ranging from linear to quadratic) is proposed that covers both solid like and fluid like contributions. Strong coupling between the solid and the fluid momentum transfer leads to simultaneous deformation, mixing, and separation of the phases. Numerical results indicate that the model can adequately describe the complex dynamics of subaerial and submarine two phase debris flows, as well as particle laden and dispersive flows.

5.10.3.2. Probabilistic assessment

A probabilistic approach requires the numerical modeling of these flows using stochastic methods. Each capable volcano is assessed with a range of values for parameters that control flow geometry and/or dynamics. These parameters are estimated from field studies of previous lahars activity or from theoretical considerations. Output of these lahar models can be compared to field observations at the capable volcano, similar observations made at analogous volcanoes and/or laboratory experiments. The annual frequency of exceedance values for flow incursion at the site can then be expressed as hazard curves and uncertainties should be expressed by confidence bounds. The basis for the selection of the reported confidence intervals should also be documented.

5.10.3.3. Deterministic assessment

In deterministic methods, threshold values are defined on the basis of empirical observations of past lahar activity, analogous information from other volcanoes or numerical simulation of lahar emplacement. Decisions on site suitability and on the determination of the design basis are based upon whether or not these thresholds are exceeded. Threshold values that could be used for lahars assessment include maximum credible volume, runout distance and thickness of deposits for the site. A screening distance value can thus be defined for lahars beyond which they are not considered to be credible events. The uncertainties in the various parameters should be properly taken into account (i.e., consider whether such phenomena might result from secondary processes or scenarios that comprise complex sequences of events (e.g. lahars at Pinatubo)). Floods of volcanic origin should be evaluated in a manner consistent with the flood hazards assessment approach described in [469].

5.10.3.4. Examples of evaluating potential hazards

As a practical example of lahar hazard assessment at a nuclear power plant site, we will first summarize the procedure employed by Volentik et al. [106] to estimate potential lahar source regions at the BNPP site near Mt Natib, a Quaternary volcano in Philippines. Volentik et al. [106] focus on the coupled nature of tephra fallout and lahar generation by considering two empirical models, the first one being based on the potential for gravitationally induced failure

of the tephra deposit on the volcano slopes [451], and the second one based on the increase in water and sediment runoff as tephra accumulates [452], [470].

A Factor of Safety map (See FIG. 39 left) indicates zones of potential lahar generation, from where those flows may follow main drainages and inundate areas lower on the flanks of the volcano, similar to the screening distance calculation.

Results show that the potential lahar source region (See FIG. 39 left) covers an area of about 12 km^2 and the corresponding total volume of tephra deposit occurring on these steep slopes ($FS < 1$) is 1.7×10^7 m^3. Alternatively, Yamakoshi et al. [470] also found a positive, nonlinear correlation between tephra thickness and decreased infiltration, resulting in increased surface runoff that may trigger lahars with very low sediment load by volume (i.e. hyperconcentrated flows). In applying this alternative model, Volentik et al. [106] calculated a hazard curve for tephra accumulation in a specific area up slope of the site triggered by increased run off of surface water and tephra (See FIG. 39 right). For example, given an explosive eruption (VEI 5) of Mt. Natib, the TEPHRA2 model indicates that the probability of tephra exceeding 17 cm is 50 % (i.e. FIG. 33). For this thickness of tephra, using empirical observations on Miyakejima volcano, $\approx$25 % of rainfall will runoff into drainages, forming hyperconcentrated flows (See FIG. 39 right).

Volentik et al. [106] concluded that, despite near vent topographic barriers presented by the caldera wall, tephra dispersal can potentially result in flow paths for lahars toward the site vicinity, following the major drainages on Mt. Natib southern flanks (See FIG. 39 left),. The coupling of widespread tephra deposition on a particular flank of the volcano following an explosive eruption and modification of the nature of sedimentation on this flank is quite important to consider in estimation of screening distance values. Cumulatively, their results indicate that the BNPP site is within screening distance for lahars, given their potential volume and inundation areas. The geographic position of the BNPP site on Napot Point may protect the site from inundation by lahars but a comprehensive analysis of lahar flow paths with a high resolution DEM is required to validate this hypothesis.

Other examples of evaluation of potential lahar hazards in populated areas surrounding active volcanoes using intermediate models have been recently published in the literature. Procter et al. [471] compared modeled scenarios using the two phase version of Titan2D, run before the 18 March 2007 break out lahar of Ruapehu volcano, New Zealand, to inundation areas and travel times of the actual event at various key points down the volcano's flanks. Velocity and discharge predicted at a lahar deflection structure were up to 20 % less than those of the actual 2007 flow, but matched closely those of the largest 1995 lahar at this location. Predicted paths of flow, including sites of avulsion, correlated well with those in the March 2007 event. In addition the simulations predicted dynamic behavior, such as super elevation of flow in sharp valley bends and hydraulic ponding, which corresponds to real event measurements.

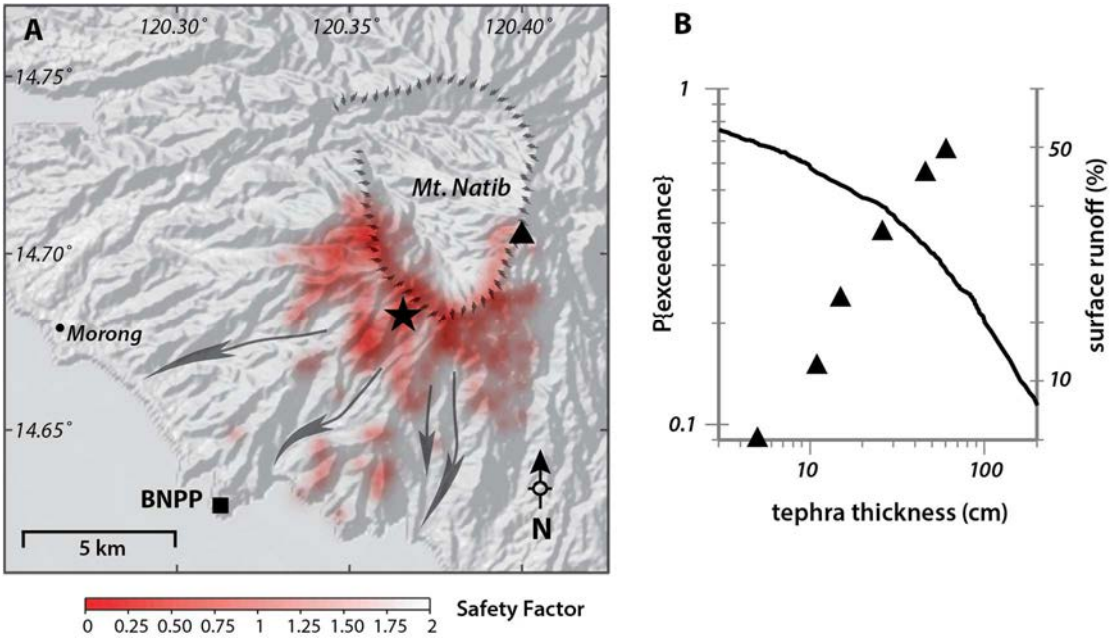

FIG. 39. Left: Potential lahar source regions (red shaded areas) resulting from a hypothetical VEI 5 eruption from Mt. Natib (wind blowing toward the site), identified as those areas where the Factor of Safety, FS, is ≤ 1. Arrows highlight main drainages on the SSW part of Mt. Natib where lahars have the potential to occur and affect the NPP site region. Black star indicates the location for the hazard curve shown in right figure. Right: Exceedance probability, based on the VEI 5 eruption used in left figure, and surface runoff % (100 × water and sediment runoff divided by the amount of rainfall) plotted as a function of tephra thickness. Surface runoff vs. tephra thickness values (solid triangles) for fine grained tephra on Miyakejima volcano (Japan), modified after [470].

Worni et al. [472] used lahar inundation depths, travel duration, and flow deposits to constrain the dimensions of the April 2007 event at Nevado del Huila, Colombia, and used the LAHARZ and FLO-2D model for comparisons. Measured hydrographs, geophone seismic sensor data and calculated peak discharges served as input data for the reconstruction of flow discharge rate and for calibration of the models. Based on their results of the 2007 lahar simulation, a deterministic approach using model lahar scenarios with volumes between 300 million and 1 billion m^3 allows an assessment of potential future events and related consequences for population centers downstream of Nevado del Huila.

5.10.4. Summary

'Lahar' typically corresponds to water saturated flows originating at a volcano and commonly can occur before, during or after pyroclastic volcanic eruptions. Additionally, lahars can form in steep volcanic terrains by slope failure and increase in volume by incorporating additional sediment during transport (bulking). Because lahars are water saturated, both liquid and solid interactions determine their unique behavior and Lahars are distinguished from other related phenomena common to volcanoes such as debris avalanches and floods due to the complex solid/liquid interactions that control their dynamics. Flow transformation during transport, involving periods of flow bulking and debulking, increases the complexities associated with interpretation of field deposits, anticipation of inundation extents for given flow scenarios over specific terrain and affects our ability to effectively model these flows. At present a complete simulation of all these phenomena, although possible in principle, does not

exist, and current numerical models describe only a part of the observed phenomena. Lahars are generally simulated with numerical models involving Navier–Stokes equations assuming different rheologies (e.g. Newtonian, Bingham, Bagnold, or Coulomb models), depending on flow behavior. For these reasons, in order to simulate lahars, different simplified numerical models are commonly adopted, including empirical lahar inundation models, semi-analytical 'friction' models, two dimensional models based on the shallow layer approach, and, in some cases, more sophisticated multiphase models. Lahar hazard assessments using a combination of these models and deterministic/probabilistic approaches have been commonly adopted for predicting potential future events.

5.11. DEBRIS AVALANCHES AND SECTOR COLLAPSE

5.11.1. Physical characteristics

A debris avalanche is a volcaniclastic, water unsaturated gravity driven flow that results from the sudden partial collapse of the unstable flanks of a volcanic edifice. Debris avalanches are composed of a chaotic, but locally coherent, mixture of rocks, soil and debris mixed with only minor amounts of liquid water, vapor, or ice. Debris avalanches can occur at volcanoes that have no signs of unrest, or might have been inactive for long periods of time, or during eruptions that do not directly involve magma, as well as during magmatic eruptions. Their formation is not necessarily dependent on having eruptive activity. Debris avalanches can travel several tens of kilometers before they stop. In contrast to laharic flows, which are water saturated, debris avalanches are water unsaturated flows, in which particles are maintained in suspension and transported as a result of viscous grain grain interactions rather than suspension in water. Hence, solid grain forces dominate the physics of avalanches [414]. As the moving debris rushes down a volcano and into river valleys, it incorporates water, snow, trees, buildings, and anything else in the way.

Debris avalanches form a debris avalanche deposit (DAD) that consists of a chaotic mixture ofcoherent blocks of varying sizes (up to decameters) surrounded by a matrix. The debris avalanche block facies consists of large fractured and deformed fragments mostly derived from the source volcano, which preserve original internal structures and textures. The debris avalanche matrix facies consists of a mixture of smaller volcanic fragments derived from various parts of the source volcano and mixed with a minor amount of exotic materials. DADs often can be traced to a horse shoe shaped steep walled structure representing the surface along which part of the edifice collapsed. DADs are characterized by an irregular hummocky topography consisting of numerous overlapping irregular shaped to conical and rounded hills rich in blocks separated by low lying areas and depressions. Characteristic textural features of DADs include the presence of: 1) deformed, stretched yet coherent avalanche blocks of varicolored hydrothermally altered material from the former interior of the edifice; and 2) angular fragments of rock that show a diagnostic jigsaw fit across fractures and which form clasts that have remained semi-coherent and have not totally disaggregated and mixed with the finer matrix material despite many kilometers of transport in the avalanche.

Avalanches with volumes greater than 10^6 m^3 are generally of long run out type. Long run out avalanches are emplaced in a catastrophic way, with observed or inferred velocities of 20–100 m s^{-1} [418]. Debris avalanches from composite volcanoes may exceed 10^{10} m^3, and associated deposits can extend more than 100 km from the volcano. Sometimes volcanic avalanches are hot (up to 100 °C).

Sector collapses originate debris avalanches, which are characterized by very different velocities of the mobilized mass, ranging from creep like movements like that at Valle del Bove, Etna Volcano, with velocity of $\approx 10^{-10}$ m s^{-1} [473], to catastrophic fast moving landslides like that at Mount St. Helens in 1980, with velocity of $\approx 10^2$ m s^{-1} [474]. Sector collapse events might recur just once or twice during the lifespan of a volcano, but in some cases repetitive collapse occurs repeatedly and can even be a characteristic behavior of a particular volcano (e.g. Soufrière of Guadeloupe [475], [476]). Volumes associated with flank failures of stratovolcanoes can range from 0.1 to > 100 km^3, posing a severe hazard both on the edifice flank itself and in downslope areas (e.g. [477]).

Large scale avalanches normally occur on steep volcanoes. Volcano collapse is typically produced by a combination of events rather than a single process [478]. They can be triggered by volcanic earthquakes, injection of magma and associated increases of porewater pressure within the volcano and loading by a growing dome (e.g. Soufrière Hills, Montserrat [479]), weakening of the volcanic edifice by tectonic processes, or chemical alteration of the rocks by hydrothermal or weathering effects [477], [478], [480–483]. It is possible that some collapses might have occurred without an evident triggering mechanism, due to gravitational instability of the edifice. Reid [482] suggested that heating from remote magma intrusion at depth can generate temporarily elevated pore fluid pressures that can destabilize the volcano edifice, but diffusion of heat through volcanoes takes years to decades while mechanically induced porewater increases bleed off within days. Mechanical pressurization induced by intrusions and compression of aquifers is a faster and more effective way to build pore pressure before it can bleed off [478], [481]. For example, at Krafla and Usu volcanoes, observed mechanically induced porewater pressure increases can be > 1 MPa, which can rise and dissipate within hours. As shown by the 1980 eruption of Mt. St. Helens, sector collapse resulting from magma intrusion into the edifice also resulted in a large explosive eruption as a pressurized magma intrusion that stagnated at shallow depth was suddenly decompressed by the collapse into a large laterally directed explosion or blast [474].

Lateral and vertical collapses appear to be less frequent in stratovolcanoes than in basaltic edifices. Gudmundsson [484] proposed that stratovolcanoes are tougher than basaltic edifices because they function as high toughness composite structures composed of layers with widely different elastic properties.

Large volume debris avalanches are common on the submerged flanks of ocean island volcanoes (e.g. Hawaiian Islands, Cape Verde Islands) and steep coastal cliffs can be caused by catastrophic debris avalanches that can even produce tsunamis (See Section 5.12).

Large scale debris avalanches, including sector collapse, represent a particular challenge in volcanic hazards assessment. A volcano may have a potential for future events, based on current topography and rock characteristics, yet had not experienced large debris avalanches in the past if such conditions did not occur in the past. Thus, the analysis can rarely assess large scale avalanche hazards through extrapolation from the record of past events. The assessment must rely on an understanding of the current and near term condition of the

volcanic system, with regards to its potential for future collapse events. For this reason, it is not possible to estimate the likelihood of future events based solely on the geologic record of past events, as only the current state of the edifice is indicative of the potential for a future collapse event. Certainly, external forcing agents (e.g. regional earthquake, extreme rainfall event) must also be considered in the edifice collapse assessment given the existence of unstable parts of the edifice.

5.11.2. Potential effects for nuclear installation

The effects from debris avalanches, landslides and slope failures on a volcanic system should be considered as part of the exclusion criteria of the site (See TABLE 4), because large volumes of flowing rock and mixed debris create physical loads on buildings and infrastructure that commonly exceed their design bases. In addition, debris avalanches and sector collapses affect relatively large areas and can destroy critical infrastructure around a nuclear facility, and disrupt the safe operation of the facility. Debris avalanches also can create atmospheric overpressures near the front of the flow, and, more importantly, significantly affect the water drainages and impoundments that are critical to the safe operation of a nuclear facility.

5.11.3. How to evaluate effects

Concerning hazard analyses for sector collapse, different approaches are commonly used. Typically these approaches rely on i) geological investigations of previous events [485], ii) comparison to analogous events at other volcanoes [486], and iii) modeling of the physical processes [477], [478], [482], [487]. Approaches i) and ii) are crucial for the hazard analysis, but conditions can change within a volcanic edifice, and mechanisms for future collapse events may differ significantly from past events. Physically based mechanical models, such as those used in approach iii), can be used for assessing and quantifying slope instability under a wide variety of conditions, and have been applied to reveal the importance of topography on the stability of volcanic edifices (e.g. [477], [482]). Such models, however, rely on assumptions about the internal structure that are difficult to determine. Also analogue models have been often used to simulate sector collapses of volcanoes (e.g. [488]).

The above approaches can help to estimate the potential collapse volumes involved in debris avalanches. However, modeling debris avalanche events is complex and at present not all relevant physical processes are completely understood. For these reasons, in order to simulate debris avalanches different simplified models are commonly adopted, including basic empirical models, semi-analytical ‘basal friction’ models, two dimensional models based on the shallow layer approach, and, in some cases, more complex three dimensional models.

5.11.3.1. Existing modeling approaches

Basic models

Models based on energy line concept

Similarly to pyroclastic density currents, a basic modelling attempt to model the emplacement of debris avalanches is based on the concept of an ‘energy line’ [10], [393]. In this type of model, the potential energy of the material released from some height on the volcano is converted to kinetic energy as the material moves laterally away from the source. During this movement kinetic energy is converted to friction and the flow stops when the energy line ‘intersects’ the topographic surface. The basal friction angle, φ (i.e. the ratio of fall

height, ΔH, and horizontal distance travelled, L) is a measure of the resistance to flow generated by a sliding avalanche at the contact with the underlying topography and is equal to the tangent of the angle (α) connecting the top of the source area to the most distal part of the flow [394]. The principal assumption of the energy line or energy cone concept is that flowing material behaves as a gravity driven, cohesionless suspension of particles and fluid with mass remaining constant [395], [396], [393]. A weakness of these models is that they assume straight line flow trajectories that pass through topographic obstacles, encompass the entire cone and ignore confining topography.

Basal friction models

One of the simplest approaches to determine the debris avalanche mobility is based on the estimation of the apparent coefficient of friction [489], that is the relationship between the drop height and the maximum runout of the flow. This parameter is largely used to describe the flow mobility, and is generally known that it increases as the mass increases [423]. The FLOW3D code [398], [490] is a flow path model based on this approach, and is used to simulate the trajectory of debris avalanches over digital topography. Simulation results give possible flow paths, velocity and maximum runout, but no information on the flow thickness and the lateral extension of the inundated areas. The model calculates the changes in velocity as the block slides across a 3D DEM. As input FLOW3D needs the three parameters describing basal friction, and the coordinates of the block. A similar approach has been used to model pyroclastic density currents and lahars (See Section 5.5 and Section 5.9). The model has several limitations, such as i) multiple sliding blocks do not interact with each other, ii) volumetric parameters (source volume, flow thickness, deposit thickness) are not included amongst either the input or output data, iii) conservation of mass is not used in the model, iv) an arbitrary flow termination mechanism has to be assumed (e.g. flow stops when the flow velocity reaches 0.1 m s^{-1} on a slope smaller than the critical value). Despite these limitations the FLOW3D model has been used in several debris avalanche hazard assessments (i.e. [490–492]).

Intermediate models

Shallow layer models

As computational resources are growing debris avalanche models based on the shallow layer approach are becoming more common for hazard assessment. These models abstract some of the physical processes that are not incorporated in basic models such as FLOW3D. The general shallow layer depth averaged equations solved by models of this category are similar to the equations described in the Appendix and are based on the conservation of mass and momentum in terms of the avalanche thickness, h, horizontal depth averaged flow velocity, (U, V), ground slope, α, retarding stress, T, bulk density of the avalanche, ρ, and Earth pressure coefficient (i.e. ratio of ground parallel to ground normal stress), k (e.g. [408], [418]). Generally, the retarding stress for granular material is function of the angle of dynamic friction between the avalanche and the ground surface, flow thickness and velocity [408], whereas k is a function of the internal angle of friction of the avalanche. However, Kelfoun and Druitt [418] showed that common parameterizations of the retarding stress are quite inadequate, and they found that the assumption of a constant retarding stress reproduce better field observations, with T in the range 50–100 kPa. Their constant retarding stress assumption was motivated by the earlier study of Dade and Huppert [423], who found that the field data for a large number of avalanches can be explained by an approximately constant retarding stress.

Assumption of a constant T is purely empirical and represents a crude approximation able to reproduce the first order behavior of avalanches. Most likely, the condition represents some average value of a retarding stress that varied with time during run out, consistent with Dade and Huppert results [423].

Kelfoun and Druitt [418] developed a model based on the assumption that avalanche slid on a thin basal layer, similar to the models of granular flows (e.g. [408], [410], [411], [413–415], [493]). As an application of the model, they simulated the Socompa avalanche in northern Chile [494], [495], an avalanche formed by gravitational collapse of the northwestern flank of the stratovolcano, that reached distance of about 40 km, covering 500 km^2, and leaving an amphitheater 12 km wide at its mouth and with cliffs 300–400 m high.

Another shallow layer model to simulate debris avalanches and flow based on a similar numerical abstraction is Titan2D [413], [417]. Titan2D is a code for incompressible Coulomb flow based on the model proposed by Savage and Hutter [408]. The conservation equations for mass and momentum are solved with a Coulomb type friction term at the basal interface [417].The model assumes that the debris avalanche or debris flow starts as an ellipsoidal pile of material with height, width and location specified by the user. The internal friction angle and the basal or bed friction angle have to be also specified. Titan2D includes the effects of erosion, variable basal friction angle keyed to different bed surface materials, and has a visualization platform for displaying the flows. Typically it is assumed the model stops when the flows cannot overcome the resistance forces acting on them.

Complex models

Three dimensional models

Reid et al. [477] presented a numerical model to analyse the three dimensional slope stability and quantifying both the relative stability of all parts of the edifice and the expected volumes subject to potential failure. Reid et al. method [477] considers the 3D materials underlying topography, defined by a DEM, and determines the least stable areas of an edifice and the potential failure volumes associated with these areas. Reid et al. model [477] use a 3D generalization of Bishop limit equilibrium analysis [496] that assumes that the average shear resistance τ, acting on a potential failure surface, is given by the Coulomb-Terzaghi failure rule:

$$\tau = c + (\sigma_n - u)\tan\phi \tag{67}$$

where c is cohesion, σ_n is the total normal stress acting on the failure surface, u is pore fluid pressure on the failure surface, and ϕ is the angle of internal friction. They assume that a fraction $1/F$ of the available shear strength (being F a factor of safety) resists the shear stress and the average resisting shear force at equilibrium, S, is:

$$S = \frac{1}{A}\int_A^0 \frac{\tau A}{F}\, dA \tag{68}$$

where A is the total failure surface area. To estimate the forces acting on each part of a potential failure surface, Reid et al. [477] assume a spherical failure surface with the solid failure domain divided into 3D vertical columns that are integrated using a DEM. Following their analysis, the overall factor of safety for dry material is:

$$F = \frac{\sum R[cA_c \cos\theta + W(1-r_u)\tan\phi]/m_a}{\sum W(R\sin\alpha + ke)} \quad (69)$$

where the sum is over all columns, $m_a = (F\cos\theta + \tan\phi\sin\alpha)/F$, R is the resisting force moment arm (i.e. equal to the failure surface radius), A_c is the area of the failure surface intersecting the column, W is the weight of the column above the failure surface, θ is the true dip of the failure surface, α is the apparent dip in the direction of slide movement, r_u is the pore pressure ratio, k is the horizontal pseudo acceleration from earthquake shaking expressed as a fraction of g, the magnitude of gravitational acceleration, and e is the horizontal driving force moment arm (i.e. equal to the vertical distance from the center of the column to the elevation of the axis of rotation). Asystematic search of all possible failure surfaces throughout the DEM is performed, using a computer code named SCOOPS, in order to find the trial failure surface with the lowest factor of safety (i.e. critical surface) affecting each section of the edifice.

Stratovolcano edifices are typically extremely heterogeneous, containing rocks or unconsolidated materials with a wide range in properties. However, uniform rock strength and density can also affect the location of the critical failure surface, and corresponding failure depth and volume. Thus, when material properties are unknown, the assumption of a homogeneous cone having a specified slope, can give useful insights on locations and volumes of potential collapses. Reid et al. [477] showed that the location of the critical failure surface is controlled by the dimensionless ratio:

$$\lambda = c/(\gamma H \tan\phi) \quad (70)$$

where H is the height of the cone, and γ is the total (rock plus fluid) unit weight. The effect of λ for the case of a homogeneous cone 1 km high with a slope angle of 25° is reported in FIG. 40, which illustrates how larger values of λ have deeper failure surfaces. FIG. 40 also illustrates effects of variations in slope morphology on stability and failure volumes, for a 1 km high uniform cone having λ = 0.05and different slope angles (20°, 30°, and 40°). Results show that steeper cones tend to be less stable, but the volumes associated with the critical failure surface decrease with increasing steepness.

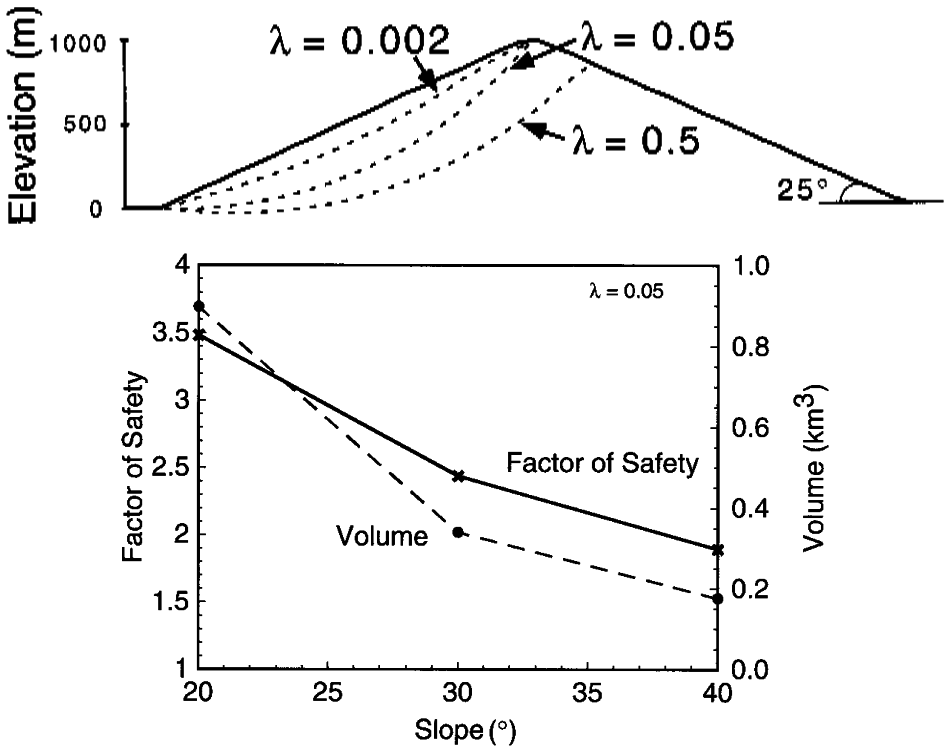

FIG. 40. Top figure: least stable failure surface in a homogeneous, 25°, symmetric cone for different values of λ (defined as the dimensionless ratio of cohesive to frictional strength); larger values of λ have deeper failure surfaces. Bottom figure: Changes in factor of safety and volume for the least stable failure surface in homogeneous symmetric cones having different slopes. Reproduced courtesy of American Geophysical Union [477].

The main conclusions of Reid et al. study [477] are that i) even in a homogeneous slope, material properties strongly influence the depth and volume of the least stable potential failure surface; ii) both the magnitude and spatial patterns of instability are influenced by the interaction of a potential failure surface with the 3D medium underlying topography and local ground surface slope direction may not necessarily predict the least stable movement direction.

Application of the Reid et al. model [477] to the Mount St. Helens morphology prior to the 1980 collapse provides estimates of potential future failure size and location. Because spatial variations in material properties were poorly known prior to collapse at Mount St. Helens, Reid et al. [477] initially assumed a strong, homogeneous, pre-collapse edifice with a dry, static, undeformed edifice topography. With these assumptions, the Reid et al. model [477] delineated the northwest flank of Mount St. Helens as the least stable region, although the north flank stability was within 5 % of the minimum. Although pore pressure and earthquake shaking effects can reduce the absolute edifice stability, dry, static conditions can be assumed for an initial hazard analysis scenario when geologic conditions within an edifice are not well known. Spatial variability in material properties can be incorporated if known. Using estimates of the conditions that existed two days prior to the Mt. St. Helens collapse, including deformed topography with a north flank bulge in combination with pore pressure and pseudo static earthquake shaking effects, Reid et al. [477] obtained good estimates of the actual failure location and volume.

Stratovolcano edifices can even collapse without magma intruding into the edifice, and typically these collapses are associated with shallow hydrothermal systems (e.g. [482]). Reid

[482] evaluated the efficacy of hydrothermally driven collapse using numerical models of heat and water flow. These results demonstrated that heating from a remote magma intrusion can temporarily elevate pore fluid pressures that can propagate upward into an overlying volcano edifice. These elevated pressures can modify effective stresses, destabilize the core, and cause hydrothermally driven collapse of an edifice. Because fluid pressurization can propagate rapidly (i.e. on order of months) threatening the mechanical stability of volcano edifices, detection would require intensive monitoring of pore fluid pressures or deformation in the edifice.

Voight and Elsworth [478] analysed conditions for failure of both oceanic volcanoes of shallow flank inclination and steeper composite terrestrial volcanoes. In their analysis they showed that structure and stratigraphy of individual volcano flanks are crucial for edifice stability. This relationship occurs because weak layers, fissured zones, and specific material properties control, in all cases, fluid pressurization and deformation. Magma intrusions can have an important role in driving downslope displacements and enhancing fluid pore pressure. Several mechanisms were identified including (a) mechanical influence in poroelastic media, (b) thermal influence, (c) retrograde boiling of magma chamber, (d) hydrothermal system overpressurization, and (e) vibrations associated with volcanic earthquakes. For shallow flank failure in presence of a magmastatic force only, stability is controlled mainly by material properties, lateral restraint, width of the failure block, and depth and angle of the basal failure plane. Where mechanically induced pore pressure is added to the static behaviour, magma intrusion rate and dyke extent is significant factors. Termal strain and thermally driven ground water can generate additional excess fluid pressure. All causes of volcano slope instability identified by Voight and Elsworth [478] are summarized in TABLE 8. Historic eruptions associated with major slope failure include those involving a magmatic component, identified as Bezamianny type, and those solely phreatic, know as Bandai type. For both types, hydrothermal processes may have a role in weakening the edifice materials, and in fluid pressurization.

Recently Borselli et al. [497] propose a new approach for assessing the degree of instability for flank collapse of volcanic edifices. The method combines three methodologies: i) slope stability by limit advanced equilibrium analysis of multiplesectors on the volcano using the code SSAP-4.0 (Slope Stability Analysis Software), which includes fluid internal overpressure, and rock mass strength criteria for local, stress state dependent, shear strength; ii) the analysis of relative mass volume deficit in the volcano structure, estimated using the VOLCANOFIT-2.0 software [497]; and iii) a statistical analysis of major flank debris avalanche ages, using stochastic arithmetic methods, and calculating the mean time of recurrence. The application of the new method to Colima volcano, Mexico, shows a significant deficit of volume in the W-SW quadrant of about 0.4 km^3. Moreover, considering the recurrence interval of major collapse events at Colima volcano, during the last 10 000 years, Borselli et al.'s analyses [497] gave a mean recurrence interval of 2698 years, with an uncertainty range of 180 years, and assessed the possibility of a flank collapse in the interval between 110 years and 345 years from the present.

Due to the complexity of all these processes involved in volcano sector collapse, any forward looking hazards assessment would need to consider the large degree of uncertainty in the source characteristics of potential future sector collapse from a capable volcano.

Distinct element models

Other approaches used to simulate debris avalanches are element based numerical models to investigate the rheological behavior and the mechanism of emplacement (e.g. [498]). Element based models describe the debris avalanche as a granular flow where each particle possesses its own material properties and interacts with its immediate neighbors or the basal boundary during emplacement (i.e. Distinct Element Model). Solution of the equations of motion at each time step allows for modeling of flowing particle assemblies [499]. Particle movement continues until all forces are balanced or completely dissipated by friction [499]. Particles may be bonded at their contacts to their immediate neighbors to create a fully bonded assembly. The bonds act as inter particle cement; if the strength of the bond is overcome, the bond breaks. Additionally, rigid wall elements (i.e. lines in two dimensions) can be present to constrain the particulate assembly or define model geometry. In a Distinct Element Model, material properties are attributed to individual particles and the bonds between their contacts and do not relate directly to typical real properties. Distinct Element Model simulations have been used to gain some insight into the geomechanical evolution of volcanic debris avalanches and the development of characteristic features in their deposits [498], [500], although they have still intrinsic limitations that prevent them to be applied for realistic real world hazard assessment. These limitations include difficulties in deriving parameters from real world data and an intensive computational approach that evaluates motion of each individual particle in the simulation.

TABLE 8. CAUSES OF VOLCANO COLLAPSE. MODIFIED AFTER VOIGHT AND ELSWORTH [478]

a) Inherent causes	1 Initial composition	
	2 Texture loose, porous, weak materials are slide prone	
	3 Bedding attitude relative to slope face	
	4 Layering sequences in relation to strength and permeability	
	5 Discontinuity systems faults, joints, dykes, bedding planes	
	6 Slope forming process history, movement history	
	7 Conditions of weathering and alteration	
	8 History of seismicity and seismic damage	
	9 Ambient (seasonal) groundwater conditions	
b) Causes that increase shear stress	1 Removal of lateral or underlying support of slopes	*i) Erosional processes*
		ii) Prior mass movements
		iii) Phreatic explosions near base of slope
	2 Static load	*i) Natural deposition (river sedimentation, tephra, lava)*
		ii) Weight of water added by natural precipitation or by exsolved volatiles
		iii) Seepage pressure and joint water pressure
		iv) Magma pressure
		v) Swelling pressure in expansion clays
	3 Dynamic load	*i) Regional or local tectonic earthquakes*
		ii) Vibrations from volcanic earthquakes, eruptive processes
		iii) Vibrations from adjacent, rapidly moving landslides
	4 Increase of surface slope	*i) Magma intrusion deformation (cryptodomes)*
		ii) Regional tectonics (slow or episodic changes)
		iii) Slope changes due to depositional processes
c) Causes that reduces shear stress	1 Physicochem	*i) Hydrothermal alteration*
		ii) Softening of clays

	ical factors	*iii) Hydration of clays minerals*
		iv) Ion exchange of clays
		v) Weathering
		vi) Solution of grain cement
		vii) Decomposition of organic materials
		viii) Physicochemical fracturing
	2 Pore fluid pressure enhancement	*i) Heavy rainfall or rapid snowmelt*
		ii) Changes in groundwater flow regime
		iii) Pore pressure changes in aquifers
		iv) Thermal expansion of pore fluid due to frictional slip
		v) Vibration induced pore fluid pressure rise
		vi) Shear deformation induced pressure rise
		vii) Consolidation seepage induced by surcharge
		viii) Base level change in reservoirs, lakes or oceans
		ix) Flow boundary condition changes
		x) Enhanced glacier melting due to increased geothermal flux
	3 Changes in structure	*i) Disturbance, remoulding*
		ii) Particle reorientation due to slip or dynamic loading
		iii) Grain collapse in altered, weakened tephra deposits
		iv) Fracturing and loosening of valley walls, stress relief, etc
		v) Deep seated fracturing due to magma intrusions, stress relief, etc
		vi) Adjustments to groundwater flow path; slope drainage enhanced or impeded

5.11.3.2. Probabilistic assessment

Probabilistic assessment of volcano debris avalanches and sector collapses represent major challenges in hazard assessment. Unlike PDCs and lahars, the source term (i.e. edifice volume) that is mobilized during the event is a critical factor in estimating the potential for very long runout of volcano debris avalanches. Furthermore, the conditions that lead to the collapse of volcanoes are not completely understood. Some volcanoes never experience this type of collapse and rather are characterized by the slow erosion and degradation of the cone. Other volcanoes, such as Shivelich, Russia, and Mombacho, Nicaragua, experience multiple collapse events during their life cycle (e.g. [501]). Because these events are rare, no methods have been developed to forecast the occurrence of debris avalanches. For other cases, like Colima volcano, Mexico, physical mechanical models have been used to evaluate hazards from debris avalanches for, estimating the probability of flank collapse (e.g. [497]).

The hazard assessment for debris avalanches, landslides and slope failures for each capable volcano should consider:

1. The identification of potential source regions of these events including areas of potential instability considering also the influence of volcanic activity, material heterogeneity, hydrothermal groundwater systems, earthquake and extreme rainfall triggering, etc;

2. The potential magnitude (i.e. volume, areal extent, thickness) of these events;

3. The frequency of such events;

4. Their potential flow paths;

5. Associated phenomena such as laterally directed explosions, subsequent magmatic explosive eruptions producing PDCs and tephra dispersal (e.g. May 18 1980 Mount St. Helens eruption sequence)

Modifications of the flow properties along the path, as well as the topography from the source region to the nuclear power plant should be also considered, noting that topography may be altered during the eruption so that flow paths may be altered significantly. It is important to consider, for example, that DADs will fill pre-existing valleys and topographic depressions with thick debris which can block stream flow, cause secondary temporary lakes and lead to dam breakage and catastrophic flooding and laharic debris flows far downstream from the avalanche front.

5.11.3.3. Deterministic assessment

A deterministic approach should determine threshold values for the maximum credible volume, the runout distance and the thickness of avalanche deposits at the site using information collected from actual deposits from analogous volcanoes and avalanche flow emplacement models. A screening distance value can thus be defined for debris avalanches and other associated mass flows beyond which they are not thought to be credible events. Models such as Reid et al. [477] or Borselli et al. [497] might be used to explore maximum credible volume associated with a sector collapse. The uncertainties in the various parameters should be properly taken into account.

5.11.3.4. Examples of evaluating potential hazards

Ararat volcano, located near the ANPP, is a steep sided composite volcano that might have experienced debris avalanches in the past [12], [13]. The energy cone method [395], [393] was used by Connor et al. [10] to assess the possibility of large volume volcano debris avalanche from Ararat volcano reaching the ANPP site area. Connor et al. [10] assumed that the debris flow initiates at the top of Ararat volcano, approximately 5200 m. The maximum potential run out of a volcano debris avalanche is shown in FIG. 41 for H/L ratio of 0.07–0.1. Only the most energetic flows, those corresponding to very low H/L ratios, are capable of reaching the site. This H/L ratio corresponds to the most energetic flows ever documented (e.g. [502]), which occurred during the collapse of the entire volcano edifice. Thus, volcanic debris avalanches from Ararat volcano would only reach the site in the event of catastrophic failure of a large fraction of the edifice (sector collapse), likely as a result of magmatic intrusion, and if this flow is directed toward the ANPP site. Connor et al. [10] estimated a potential of this type of event to be low (annual probability < 10^{-7}), noting that, although volcano debris avalanches are documented for Ararat, there is no evidence of large scale volcano sector collapse.

5.11.4. Summary

Partial volcano sector collapses lead to the emplacement of gravity driven debris avalanches that consist of a rapidly moving chaotic masses rocks, soil and debris mixed with minor amounts of water or ice.They are characterized by very different velocities of the mobilized mass, ranging from creep like movements, with velocity of $\approx 10^{-10}$ m s^{-1} to catastrophic fast moving landslides, with velocity of $\approx 10^{2}$ m s^{-1}. Sector collapse events might recur one or twice during the lifespan of a volcano, or even occur repeatedly at particular volcanoes. Volumes associated to flank failures of stratovolcanoes can range from 0.1 to > 100 km^3, posing a severe hazard both on the edifice flank itself and in downslope areas. As indicated in TABLE 4, the effects from debris avalanches should be considered as part of the exclusion criteria of the site, since these effects appear to exceed the typical design basis of many structures, systems, and components that are important to safety. Considerable progress has been made in the understanding of the physics of sector collapse and debris avalanches and several approaches have improved our knowledge by trying to describe their complexities. However, at present, not all relevant physical processes involved in sector collapses and debris avalanches are completely understood. For these reasons, in order to simulate these events different simplified models are commonly adopted, including basic empirical models, semi-analytical ‘basal friction’ models, two dimensional models based on the shallow layer approach, and, in some cases, more complex three dimensional models. Awareness of model uncertainty arising from poor parameter estimation, topographic resolution or mechanical understanding is critical to determine the appropriateness of these models for use in hazard assessment.

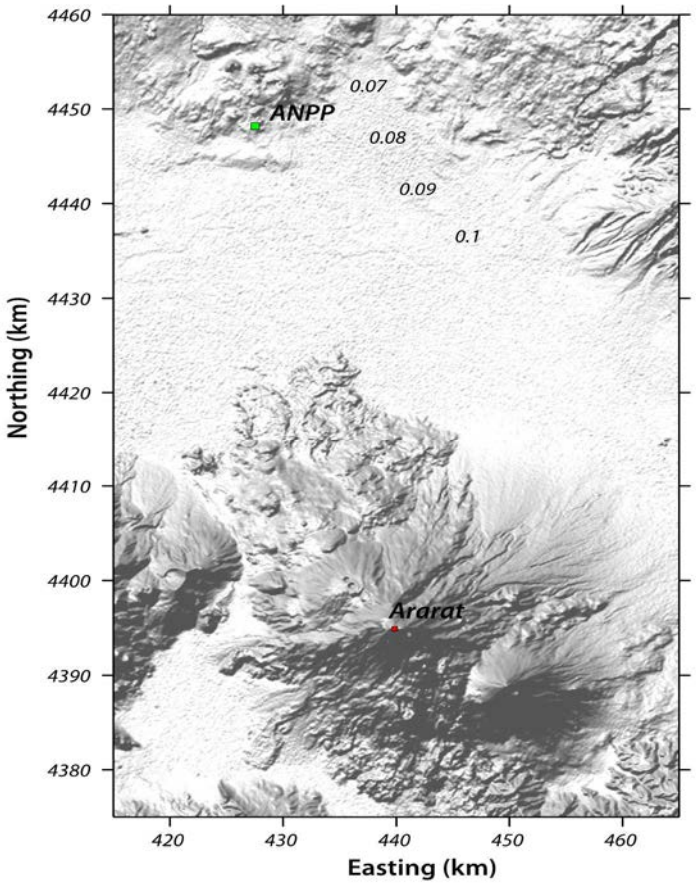

FIG. 41. The maximum potential run out of large volume volcanic debris avalanche from Ararat volcano is estimated using the energy cone method. Only debris avalanches with $\boldsymbol{H/L} < 0.075$ *are capable of reaching the ANPP site. Contour labels show* $\boldsymbol{H/L}$ *values for Ararat volcano. This corresponds to the most energetic types of volcano debris avalanches known, which only could occur as a result of sector collapse of the volcano. Reproduced courtesy of the Ministry of Energy and Natural Resources of the Republic of Armenia [10].*

5.12. VOLCANIC TSUNAMIS

5.12.1. Physical characteristics

Volcanic tsunamis and seiches can be generated when millions to hundred billions of m^3 of material enter large bodies of water. This mass movement can occur from submarine or subaerial landslides, lava flows, pyroclastic flows or debris avalanches. In addition, submarine eruption of volcanoes, caldera collapse, or volcanic earthquakes also can form volcanic tsunamis [503], [504]. Examples of some historical tsunamis that have been generated by these volcanic mechanisms are provided in TABLE 9.

TABLE 9. EXAMPLES OF SOME HISTORICAL VOLCANIC TSUNAMIS AND THEIR MAIN CHARACTERISTICS

Event	Year	Mechanism	Volume (km^3)	Max. runup (m)	References
Aniakchak, Alaska	3.5 ka	Pyroclastic flows	≈15	≈30	Waythomas and Watts [505]
Kikai, Japan	7.3 ka	Caldera collapse, pyroclastic flows	≈25	< 20	Maeno et al. [506]
Krakatau	1883	Submarine explosion, pyroclastic flow, caldera collapse	5–12	30–40	Maeno and Imamura [507]
Matavanu, Samoa	1906	Lava flow		3.5	Power and Downes [504]
Mount St. Helens	1980	Landslides/debris avalanches into Lake Spirit	2.5	200–400	Voight et al. [474], [508]
New Hebrides	1878	Volcanic earthquake		17	Power and Downes [504]
Ritter Island, Papua New Guinea	1888	Sector collapse	4–5	15	Ward and Day [509]
Soufrière Hills, Montserrat	1997	Landslides/debris avalanches	2–2.5	15	Heinrich et al. [410]
Soufrière Hills, Montserrat	2003	Dome collapse, Pyroclastic flows	0.2	15	Watt et al. [510]
Stromboli, Italy	2002	Volcanic landslide		11	Tinti et al. [511]
Unzen, Japan	1792	Sector collapse	0.3	20	Aida [512]

Note: Runups and Volumes Estimates are Uncertain.

Volcano edifices are typically unstable structures, thus, any such volcano located near water is a potential source of volcanic tsunamis. Edifice collapse can be triggered by volcanic eruptions or earthquakes and may lead to large displacement of the slopes, which, in turn, can generate tsunamis in proximal bodies of water. Massive amounts of rock also can abruptly enter large bodies of water during an eruption. Furthermore, volcano slopes can become unstable and collapse without warning or eruptive activity. Bathymetric surveys reveal that shield volcanoes in oceanic settings have been the sites of submarine debris avalanches (e.g. [513]). Underwater volcanic eruptions can also displace large volumes of water, from both slope collapse and the release of volcanic gases. Perhaps the most relevant volcanic tsunami associated with these types of source mechanisms is associated with the 1883 eruption of Krakatau volcano in the Sunda Strait. This event resulted in tsunami with maximum runup of approximately 30–40 m on Java and Sumatra, and caused tsunami damage reported as far as Western Australia and India. A total of 34 000 fatalities occurred in Indonesia as a result of the eruption, nearly all related to tsunamis. One lesson to draw from this event (See [503], [514], [515]) is that volcanic activity can result in complex sequences of events and multiple episodes of tsunami formation. Tsunamis during the 1883 Krakatau activity may be been generated by a variety of mechanisms, including collapse of the northern part of the volcanic island in to the Sunda Strait, pyroclastic flows entering the sea, and/or underwater explosion and caldera subsidence. These events occurred over several days and tsunamis appear to have been related to each of them.

For sites located near large bodies of water (e.g. see, lakes, reservoirs), tsunami and seiche hazards should normally be considered in the site assessment (i.e. [1]). For sites located in areas potentially affected by volcanic tsunamis and seiches consideration should be given to the potential for large volumes of rock from volcanic eruptions or unstable volcanic slopes to enter water bodies, as part of analysis of the potential distribution of tsunami sources.

TABLE 10. TSUNAMIGENIC PROCESSES ASSOCIATED WITH VOLCANISM (EXCLUDING SECTOR COLLAPSE) AND THE ORDER OF MAGNITUDE CHARACTERISTICS OF THE TSUNAMIS PRODUCED (FROM [519])

Mechanism	Source volume (km^3)	Wave height (m)	Period (min)	Travel distance (km)
Earthquakes	1–10	up to 17	10–40	<500
Submarine explosions	<1	1–6	1–10	<50
Pyroclastic flows	1–100	up to 25	1–40	<250
Caldera collapse	1–10	up to 15	short	<50
Avalanches of cold rock	<1	1–10	short	<50
Basal surges and shock waves	<1	up to 5	aperiodic	<10
Avalanches of hot rock	<1	small	short	<10
Lahars	<1	small	short	<50
Atmospheric phase coupling	?	small	15–40	>1000
Lava entering the sea	<1	very small	short	<10

Note: For some caldera collapse events, travel distances and source volumes might be factors of 2–10 higher, respectively, which are comparable to sector collapse events at, for example, Hawaii [521].

At present, tsunami and seiche hazards are commonly evaluated using deterministic numerical models, which consider the locations of potential sources, the volume and rate of mass flow, the source and characteristics of water displacement and the resulting propagation of waves on the basis of location specific bathymetry data. However, recently, a few studies used a more general probabilistic method for tsunami hazard assessment based on a Bayesian approach [516–518]. The approach has many pivotal features such as the integration of information derived from mathematical beliefs, instrumental measurements and historical data, the incorporationof both aleatory and epistemic uncertainties. The approach of Grezio et al. [516] also highlighted that aleatory uncertainty associated to the tsunami source may overcome other causes of uncertainty.

TABLE 10 summarizes the main tsunamigenic processes directly associated with volcanism, source volumes and tsunami characteristics obtained from a review of historical tsunamis generated by volcanic eruptions [515], [519].

5.12.2. Potential effects for nuclear installation

Considerations about hazards from volcanic tsunami and their impact on nuclear installations are the same as for non volcanic tsunami originated by earthquakes or landslides. Tsunami inundation is generally considered a site exclusion hazard [469], although for some sites tsunami might be considered as a design basis event.

5.12.3. How to evaluate effects

Here we summarize the existing approaches used to simulated volcanic tsunami processes.

5.12.3.1. Tsunamis generated by landslide

Landslides occurring on volcanic islands can reach the sea and trigger catastrophic tsunamis. These kinds of landslides are among the largest volume mass movements on Earth [520], [521] with deposits containing up to thousands of cubic kilometres of material [520]. If sufficiently large and rapid, such collapses could potentially generate wide tsunamis [522–524]. These tsunamis may represent a significant hazard from local to regional scale (e.g. [525–528]). However, for small size landslides, generated tsunamis are unlikely to maintain hazardous amplitudes on an ocean basin scale (e.g. [510]).

A useful dimensionless number is given by the landslide Froude number, F_r, that is the ratio of maximum landslide speed, v, to the linear shallow water wave speed, $c = (gh)^{1/2}$ where h is the water depth and g the acceleration due to gravity (e.g. [529–532]). If $F_r < 1$ (i.e. sub critical) then the tsunami propagates away from the source region faster than the landslide travels, and landslide motion may not increase the wave further. When $F_r = 1$, landslide and tsunami move together, allowing a large wave to form [532]. If $F_r > 1$ (super critical), wave generation becomes less efficient in the case of submarine landslides [527], [529], [532], whereas for subaerial landslides entering water the generated tsunamis can have very large waves [529]. For volcanic debris avalanche, available data [474], [502], [533] suggest that high impact velocities are easily possible, generating super critical tsunamis; for water depths less than 100 m, landslide velocities > 31 m s^{-1} would give $F_r > 1$. Landslide dynamics are not well constrained for large volcanic flank failures, but the most catastrophic scenario would be a landslide moving as a single, coherent body [418].

In order to simulate landslides generated tsunamis is necessary to properly describe the motion of the mass body as well as the consequent movement of the sea water, and their mutual continuous interaction. This problem is more difficult than simulation of earthquake generated tsunamis because in the latter case effects of the shock can incorporated straightforwardly in the hydrodynamic model by prescribing the proper initial conditions for the waves (i.e. the initial sea surface elevation is assumed to depend on the sea floor deformation) and there is no need to account for mutual interaction. Tinti et al. [511], [534–536] simulate the motion of the landslide using a numerical model based on a Lagrangian approach. The sliding mass is sliced in a set of N contiguous blocks that can change their shape but not their mass and volume during the motion. These blocks, that cannot separate from each other (i.e. the landslide is a continuous body) are subjected to internal forces of mutual interaction between neighboring contiguous blocks, and to external forces (i.e. the gravityand buoyancy), the Coulomb bottom friction and the resistance force, due to drag and shear stresses exerted by the ambient fluid. The model requires the specification of the slide surface. Though in principle the slide surface

cannot be known *a priori*, in practice an approximate evaluation of it can be often made on the basis of the topographic constraints considering the maximum slope gradient. Considering all the acting forces, the dynamical evolution of the landslide, which is determined by the motion of its constituent blocks, is computed at each time step along the slide profile. In order to increase the numerical accuracy, the time step size is larger when the mass moves slowly and smaller when the mass velocity is high.

Kelfoun et al. [537] used a two-fluid (i.e. seawater and landslide) numerical model to simulate the wave amplitudes and the propagation of tsunamis generated by a landslide. Both the landslides and seawater are simulated using the general shallow water equations of mass conservation and momentum balance. The landslide is simulated in terms of landslide thickness, density difference between landslide density and water density, landslide velocity, earth pressure coefficient (i.e. ratio of ground-parallel to ground-normal stress used with basal and internal friction angles), and gravity (See [418] and Section 5.10 for details). The main difficulty in modeling landslide propagation, using the Kelfoun et al. [537] approach, is to define the total retarding stress, T. Volcanic landslides exhibit a complex behavior that is at present impossible to describe physically in a robust way (See Section 5.10). Moreover, accurate description of submarine landslides would require accounting for processes that are not well understood due to the interaction between landslide and water involving mixing, dilution, water infiltration, and density variations. However, it is necessary to estimate the landslide rheology, which directly influences the characteristics of the tsunami. As a first order approach, T can be expressed as the sum of the drag between the landslide and water, T_{lw}, and of the stress between the landslide and the ground, T_{lg},. The first term, T_{lw}, is described in a way similar to the equation used by [511], as it is assumed to depend on the surface of the landslide in contact with the water and on the square of the relative velocity of the landslide with respect to the fluid. The second term is calculated as in [418], using the Mohr-Coulomb frictional law (See Section 5.10). The two sets of shallow layer equations (i.e. for water and landslide) are then calculated at the same time step accounting for their interaction. As an example of application of the model they simulated landslides from the eastern flank of Piton de la Fournaise volcano entering in the sea considering various possible volumes (from 0.5 to 10 km^3) and analysing the impact of the associated tsunamis.

5.12.3.2. Tsunamis generated by caldera collapse

Hazardous tsunamis can originate from caldera collapse during large explosive volcanic eruptions. The resulting sea level changes may create more potential energy for tsunami generation than the other possible volcanic mechanisms such as pyroclastic flows entering the sea or phreatomagmatic explosions (e.g. [538]). Tsunamis generated by caldera collapse are commonly simulated using a simple piston-like plunger model combined with asingle layer shallow water model (e.g. [507], [538]). Maeno and Imamura [538] assume that the topographic height of the collapsing area linearly decreases with time from the topography existing before collapse to the topography after collapse. They applied the model to examine tsunamis during a caldera formation at Kikai caldera in Japan [506] and to explore the most plausible mechanism of the tsunamis generated during the 1883 Krakatau eruption, Indonesia [507]. Geometrical changes were introduced using a time dependent still water depth in the collapsing area, $h(t)$, that is assumed falling either with a uniform velocity or following free fall conditions:

$$h(t) = h_{before} - t\left(h_{before} - h_{after}\right)/t_s \quad (71)$$

$$h(t) = h_{before} - 1/2gt^2 \quad (72)$$

where h_{before} and h_{after} denote respectively the still water depths before and after caldera collapse, t the time, t_s the duration of collapse, and g the gravitational acceleration.

Typically the duration of caldera collapses are not well constrained. For the case of the Kikai caldera, rapid collapse conditions with durations of few minutes to a few tens of minutes were able to generate the largest tsunamis [506] although the most plausible collapse duration was estimated to be longer than several hours [506], [538]. Caldera collapse speed, V_c, can be used to calculate the dimensionless collapse speed $V_c/\sqrt{gh}$. Computed maximum height of the tsunami is the largest when the dimensionless collapse speed $V_c/\sqrt{gh}$ is about 0.01, and the height substantially decreases with slower speeds (longer collapse durations). Simulations for Kikai caldera showed that when the collapse speed was high, the sea level rose rapidly, and a large tsunami was generated, because the large amount of seawater flowed into the collapsed area in a short time and the wave crest easily became higher than the original sea surface.

5.12.3.3. Tsunami generation by pyroclastic flows

Another mechanism able to generate tsunamis is given by a large discharge of a pyroclastic material into sea. Maeno and Imamura [507] simulate tsunamis generated by pyroclastic flows using an approach similar to that adopted by [537] for landslide generated tsunamis. In particular they consider a two layer shallow water models for two types of fluid, a dense type (DPF) and a light type (LPF). Shallow water equations of mass and momentum continuity in each layer are solved considering kinetic and dynamic conditions at the free surface and interfaces. Moreover, the model assumes a hydrostatic pressure distribution and negligible inter facial mixing, and uniform velocity and density and distributions, although a density change by particle sedimentation can eventually be significant with time. The two-layer model is used in the near-field, whereas a single-layer model is used in the far-field. A dense-type two-layer shallow water model is assumed for pyroclastic flows denser than seawater. In this case, dense pyroclasts are assumed to be the dominant components of the flow, which can therefore enter into seawater and travel along the slope. A light-type two-layer shallow water model is used for pyroclastic flows lighter than seawater. In this case, light pumice and ash are assumed to be the dominant components of the flow, and they thus travel over the sea surface. Maeno and Imamura [507] applied their model to simulate the tsunamis generated during the 1883 Krakatau eruption. Volume of 5 to 20 km^3 of pyroclastic flow with densities of 900 to 1500 kg m^{-3} and average discharge rates of 10^6 to 10^8 m^3 s^{-1} were examined. Simulation results suggest that a pyroclastic flow entering sea, with a volume larger than 5 km^3 and an average discharge rate of about 10^7 m^3 s^{-1}, would be the most plausible mechanism for the tsunamis generation.

Waythomas and Watts [505] evaluated tsunami generation by pyroclastic flow using an example from Aniakchak volcano in Alaska. They modeled a pyroclastic debris flow entering the ocean characterized by a volume V, maximum velocity U, width w, and duration t_0. The characteristic mass flux per unit width into the ocean can be written as $Q = V/(wt_0)$. Considering the local water depth d, a maximum tsunami amplitude h and a characteristic wavelength l_0 were estimated using the semiempirical equations of Walder et al. [539] implemented in the software named TOPICS. Their results suggest that about 25–30% of a volume > 50 km^3 of pyroclastic flow volume entered the ocean north of Aniakchak caldera.

5.12.3.4. Tsunamis generated by phreatomagmatic explosions

Tsunamis can be generated by underwater explosions (e.g. [503], [540–542]). If the explosion occurs in shallow water (i.e. if $d_w/W^{1/3} < 1$ being d_w the depth of explosion crater and W the explosion energy in pounds of TNT), it may be associated with a wave generation process [543]. The near-surface explosion might produce a water crater and even expose the seafloor to the atmosphere. After reaching its maximum size, the water crater collapses and, under the influence of gravity, the water flows inward onto the crater, analogous to a dam break problem. The initial water elevation is assumed to have a crater shape with a watery rim, and an empirical relationship between the explosion energy E and initial wave height η_i is used (e.g. [542]):

$$\eta_i = 0.024E^{0.24} \tag{73}$$

The crater shape is typically described by an empirical formula (e.g. [544]):

$$\begin{cases} \eta(r) = \eta_i \left[2\left(\frac{r}{R}\right)^2 - 1 \right] & \text{for } r \le R \\ \eta(r) = 0 & \text{for } r > R \end{cases} \tag{74}$$

where R is the initial water crater radius, and r denotes the distance from the source point. Concerning the relation between the initial water source radius and the explosion energy, Le Mehaute and Wang [544] provides an empirical relationship valid for shallow water conditions suggesting a power law dependence:

$$R = 10\, W^{0.30} \tag{75}$$

whereas, when the water reaches the seafloor, a different correlation is given [544]:

$$R = 4.4\, W^{0.25} \tag{76}$$

where R is given in ft and W in lbs of TNT equivalent (1 lb of TNT $\cong 1.9 \times 10^6$ J). A similar method was also used by [542] to analyse a tsunami induced by a phreatomagmatic explosion at Karymskoye Lake ($E = 10^{12}$ J) reproducing satisfactorily the wave characteristics. The EQ. (73) was assumed to be valid even for larger scale explosions by [507], which investigated the possibility of tsunamis generated by a large-scale phreatomagmatic explosion during the 1883 Krakatau eruption. In this case, using the empirical relationship between crater size and explosion energy [545], the explosion energy needed to produce a large crater like the Krakatau caldera (2 to 3 km in radius) can be estimated to be 10^{16} to 10^{17} J, whereas the ratio $d_w/W^{1/3}$ can vary from 0.2 to 0.5. Therefore, a potential largest phreatomagmatic explosion may be associated with a shallow water wave generation process, in which the water, initially expelled upwards and outwards, can form a plume and a crater with a watery rim. For this kind of explosion energy, the time required to generate a watery rim is of the order of 1 to 10 seconds.

5.12.4. Summary

Volcanic tsunamis can be generated through different mechanisms such as landslides associated with submarine or subaerial volcano sector collapses, debris avalanches, rapid entering of voluminous lava flows or pyroclastic flows into the sea or large lakes, by submarine eruptions, caldera collapse, or by volcanic earthquakes. Different numerical approaches recently have been developed in order to assess the source term associated with each of these mechanisms for models describing tsunamis propagation and their effects. Awareness of model uncertainty arising from poor parameter estimation, topographic resolution, or mechanical understanding is critical to determine the appropriateness of these models for use in hazard assessment.

6. VOLCANO MONITORING

6.1. PURPOSE OF MONITORING

As discussed in the SSG-21 [1], a monitoring program is needed if a nuclear installation is planned for a site has potential hazards from volcanic phenomenon. For such sites, all capable volcanoes should be monitored for the lifetime of the proposed nuclear installation [1]. Thus, if a volcano monitoring program is not in place at the site suitability stage, such a program should be developed prior to the start of construction of the installation and should be maintained and kept up to date throughout the operational stage. A monitoring network aims at providing information, quantifying uncertainty, reducing uncertainty with respect to addressing five key questions when facing volcanic unrest: When, where, what/how, what magnitude and intensity, and what impact?

A monitoring program has several components and purposes:

- Inform the development of emergency plans and operational considerations (i.e. practicability of implementing mitigation measures versus likely alert times). Some hazards develop quickly, others slowly. Some are transient and others long lasting. Monitoring helps to establish the severity and time scales associated with various volcanic activities.

- Establish baseline for characteristics of volcanic system, in other words, what is ‘normal’ behaviour for the volcano. Long term estimates of magma volume versus time help to establish the size of potential eruptions (See also Section 4). Eruptions may be of various types and the likely effects differ. For example, eruptions may be effusive and produce mainly lava flows, or explosive and produce ash clouds. It is assumed that readers are familiar with geologic characterization of volcanoes as discussed in IAEA (See Section 8.3 of the SSG-21 [1]) and Section 3 of this document.

- Monitoring for changes. Volcanoes may differ substantially in their details, so changes in character may be relative rather than absolute. A fundamental task of monitoring is to evaluate continually the on going status and the evolution of activity. Monitoring helps to evaluate the physical basis for observed changes in activity.

- Determining if changes affect the likelihood of a potentially hazardous event. Through case histories, the scientific community has experience with evaluating changes in

geophysical activity and estimating likely outcomes. This requires on going interpretation, and systematic and periodic evaluation of various data streams.

- Re-evaluating criteria for actions in response to elevated likelihoods of events. The new knowledge that is provided by monitoring forces new thinking about appropriate response actions. Response plans may be general; the specific characteristics of the activity revealed by monitoring will better resolve both spatial and temporal features of likely volcanic activity. This will allow updating of response plans.

Monitoring strategies are based on the occurrence of two types of phenomena. The first is forecasting based on magma and/or gas moving (e.g. ascent). Most eruptible magma is stored in a chamber at a depth of about 5–10 km. When the magma and gases begin to move upward, the depths of earthquakes may become shallower (rarely observed), new types of seismic events may occur, the centres of deformation become shallower and deformation may accelerate, and sources of heat or gases appear at the surface. The second type of phenomena is more closely related to rock or slope failure, and may include rock falls or landslides that trigger pyroclastic flows, dome collapses and related activity. These may be quite large and result in generation of ash clouds as well as the underlying flow events. From a monitoring perspective, quite different approaches are needed to evaluate these different types of activity because they are based on different physical processes.

A particular sequence of seismic events has been observed sufficiently often that it has been termed a generic volcanic earthquake swarm (See FIG. 42). Although this scenario illustrates a common sequence of seismic events that are likely associated with magma ascent, more complex and confusing patterns of activity and quiescence can be observed. Nevertheless, volcano tectonic (VT) events occur in increasing numbers above a recognized background rate, reflecting increasing stresses. The rates generally increase but fluctuations are also observed. Later, long period (LP) or low frequency (LF) events occur at shallower depths. These are followed by volcanic tremor, which typically increases in amplitude and duration in the days to hours before eruption. Just before eruption, a rapid increase in rate of VT events is commonly observed. The eruption itself is accompanied by strong volcanic tremor and/or explosion quakes. In the later stages of eruption deep VT events may occur as stresses readjust following magma withdrawal. Following eruption, the rates and sizes of all types of events gradually decline.

A fundamental problem in monitoring is that of distinguishing intrusions that will erupt versus intrusions that stall beneath the surface and not erupt [547], [548]. In both scenarios, pre-eruption magma movement is identified by monitoring instruments. Currently, there is no basis to distinguish between an intrusion that will erupt from one that will stall in the subsurface based on precursory observations. In addition, the subsurface movement of hydrothermal fluids also can produce signals that simulate magma movement. Thus, a likely outcome of monitoring is the detection of some intrusions or fluids that actually won't erupt, although this outcome can't be known until the movement ceases. Strictly speaking, these events would not be false alarms but rather real alarms, although this point may be lost on those involved. Intrusions to shallow depths, such as a few hundred meters, may trigger secondary effects such as landslides or sector collapse (cf. Section 5.10).

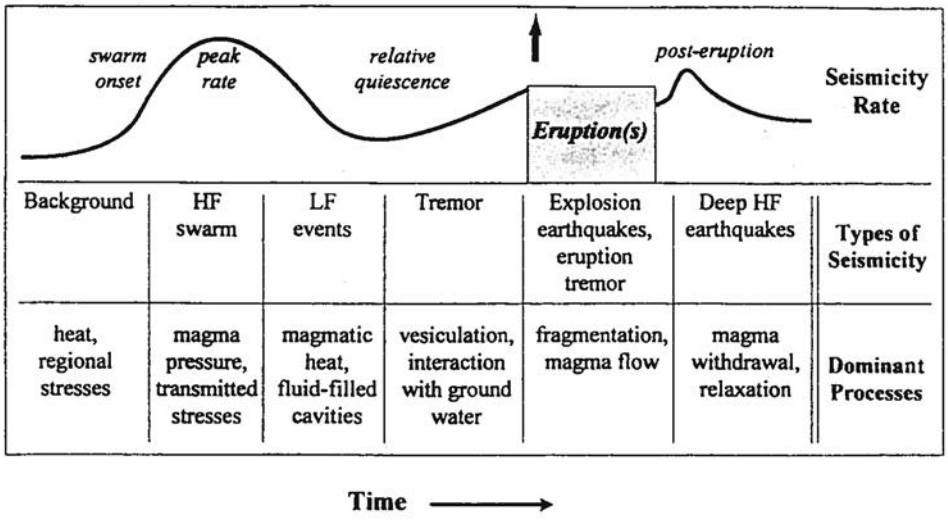

FIG. 42. Schematic of generic volcanic earthquake swarm model [546]. HF is high frequency events and LF is low frequency events. Reproduced courtesy of Springer Science+Business Media [546].

The subject of monitoring volcanoes is a broad subject and several books and hundreds of articles have been published. Among these are recent works by Scarpa and Tilling [549], Sigurdsson et al. [77], Mouginis-Mark et al. [550], Sparks [551], Voight and Sparks [552], Dzurisin [553], Zobin et al. [554], Crider et al. [555] and Moran et al. [547]. The present work is a brief overview of the subject focused on time scales, processes, instrumentation, and some elements of mitigation appropriate for the issue of nuclear installations located in the vicinity of capable volcanoes.

6.2. MONITORING TYPES

Monitoring a volcano requires continuous or periodic measurements of parameters that indicate the state of activity. Volcanoes are places where heat, molten rock (i.e. magma) and gases escape from the interior of the Earth into the atmosphere or onto the land surface. The parameters measured are those that indicate motion or change in state of magma, heat and gases either directly or indirectly. Modern methods include seismic, infrasound, deformation, gas and water or geochemical sampling, other geophysical methods such as magnetics or gravity, and thermal monitoring. Geological studies may also provide complementary information that helps the overall monitoring effort. Such studies include ash plume height and speed of rise, mass eruption rate from quantification of the erupted volumes, physical characteristics of erupted products, petrological monitoring and the tracking of magma ascent rate using the absence or presence and measurement of amphibole reaction rims, microtextural evidence for depressurization, degassing, undercooling, rheological jumps from matrix microlite studies, evidence of magma mixing, porosity or permeability changes of the magma, rate of explosion or pyroclastic flows, and spatial temporal variability of PDC runout distances. Here we emphasize contemporary geophysical techniques.

6.2.1. Seismic

Seismic monitoring employs a network of typically 6–8 seismometers located in an array on (if possible) and around the volcano at distances of several to 20 or so kilometres (e.g. [556]). Seismic events are of several types: HF events, LF events, explosions and volcanic tremor (See TABLE 11). Each volcano has a typical background rate of activity for events of each type. A fundamental purpose of seismic monitoring is to determine the background rates and associated variations such as day versus night, rainy versus dry season, etc. These background rates are of critical importance because they provide the baseline for normal activity, which is then compared with potential changes. The rates of activity may change when the state of stress changes, or when molten rock or gases move under the volcano.

TABLE 11. TYPES OF SEISMIC EVENTS AND TERMINOLOGY. Reproduced courtesy of Springer Science+Business Media [546]

This document	Minakami [557]	AVO*	Other names	Example (See FIG. 44)
High frequency HF	A type	Volcano tectonic VT	Short period	A
Low frequency LF	B type	Long period	Long coda event, tornillo	C,F, I, J
Mixed frequency	-	Hybrid	Medium frequency	B
Explosion quake	Explosion quake	Explosion	-	E
Volcanic tremor	Volcanic tremor	Volcanic tremor	Harmonic tremor, Spasmodic tremor	D,G,H,K

* Alaska Volcano Observatory

Seismic stations are typically deployed in a small network well distributed in azimuth and distance from the vent (See FIG. 43). Ideally stations are deployed in bedrock (which is rarely found at volcanoes) to achieve good coupling at sites removed from sources of noise such as roads, buildings, waterfalls, etc. Note these differ from seismic stations frequently deployed at a nuclear installation, whose purpose is to determine the level and frequency of shaking at the site. The purpose of the seismic stations on a volcano is to provide high quality data to determine the 3D velocity structure, details of sources, identification of unusual sources such as deep LP events, etc. Examples of waveforms (seismograms) of different types of events at volcanoes are shown in FIG. 44.

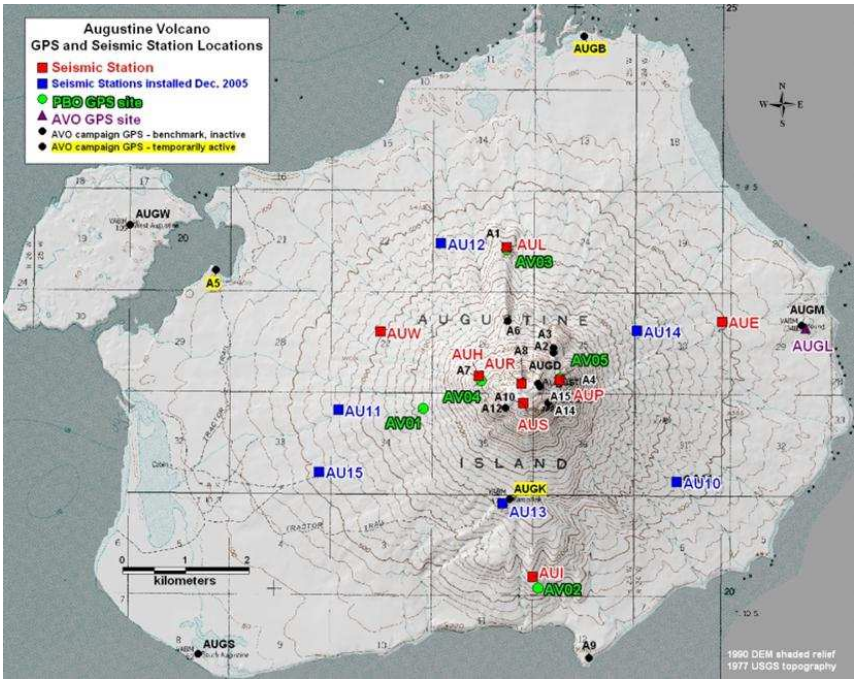

FIG. 43. Map of seismic and GPS stations on Augustine Volcano, Alaska. Figure courtesy of Alaska Volcano Observatory.

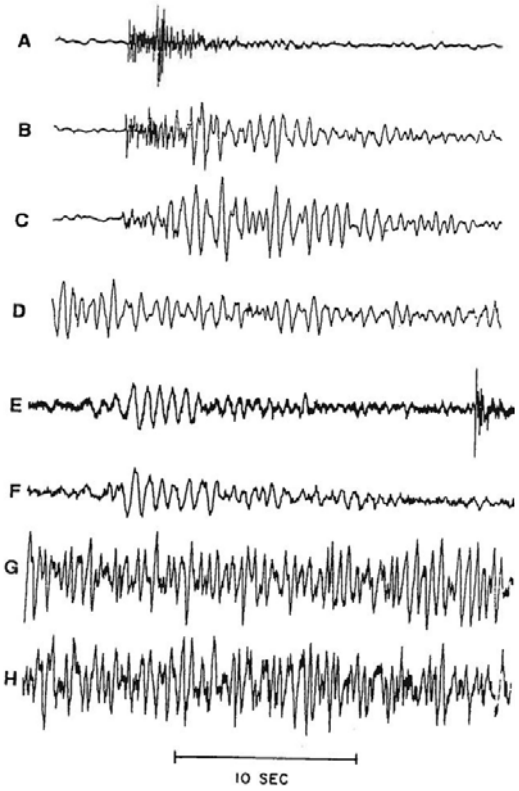

A. high frequency or volcano tectonic (VT) event, Redoubt
B. hybrid event, Redoubt
C. low frequency or long period (LP) event, Redoubt
D. volcanic tremor, Redoubt
E. explosion quake, Pavlof
F. low frequency or B type event, Pavlof
G. volcanic tremor, no eruption, Spurr
H. volcanic tremor, accompanying eruption, Spurr

FIG. 44. Examples of seismograms for different types of seismic events at Alaskan volcanoes. Reproduced courtesy of Springer Science+Business Media [546].

6.2.2. Infrasound

Infrasound signals are low frequency (< 20 Hz) sound waves. Typically the infrasound signal begins as soon as there is a flux of gases and tephra into the atmosphere, hence, such data are very useful to confirm unambiguously that an eruption is actually occurring. Depending on the pressure, infrasound may propagate as a shock wave at first (velocity faster than sound speed) then degrade into an acoustic wave as it spreads out geometrically. Acoustic speed in air is 331.4 m sec^{-1} at STP, increasing 0.59 m sec^{-1} per degree C temperature increase. Infrasound sensors are placed in a small array of 4–8 stations within a few hundred meters to 2 km of each other (See FIG. 45). The redundant sensors and low propagation speed allow the determination of back azimuth from the array to the source, so that such data are very useful in the case of multiple vents near each other. Ripepe et al. [558] show recent infrasound data from Soufrière Hills volcano.

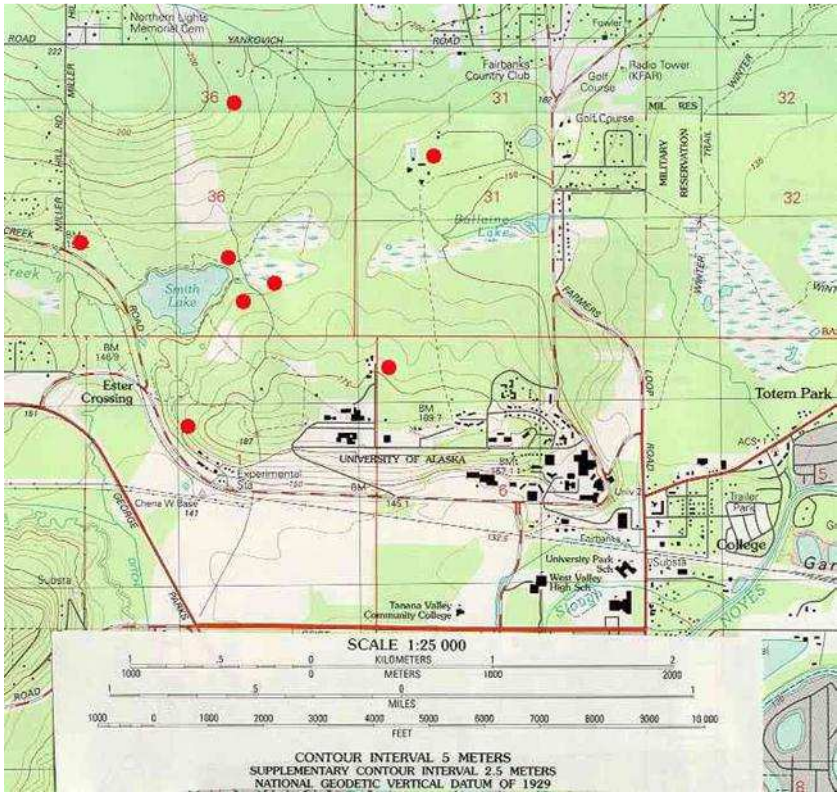

FIG. 45. An example of an infrasound array (red dots) at Fairbanks, Alaska. The aperture is 1.7 km. Figure courtesy of J. Olson.

6.2.3. Deformation

Deformation monitoring typically uses networks of at least 3–6 GPS instruments that are deployed in arrays around the volcano (See FIG. 43). Volcanoes typically inflate prior to eruptions, and GPS instruments measure the motion of the ground surface in response to magma intrusion at depth. Deformation modelling can help determine the depth and geometry of inflating magma bodies. In addition to GPS that provides continuous time series at specific points, other techniques produce complementary data that give a fuller picture of ground deformation. These include tiltmeters, dilatometers, and InSAR. Tiltmeters measure the tilt of the ground at a point. The instruments are often placed in shallow boreholes to reduce

meteorological noise and data are telemetered. Dilatometers are emplaced in deeper boreholes and measure volumetric strain that can accompany magma movement [559].

InSAR stands for Interferometric Synthetic Aperture Radar. This is a satellite or airborne based technique that has good spatial resolution but poor temporal resolution (11–24 days at present; TABLE 12). Images in the line of site of the satellite are compared when the orbits repeat (11–24 days) and interferograms are produced by comparing the phase differences of the recorded signals. InSAR data are complementary to GPS and tilt data. Electronic distance measurement (EDM) and geodetic levelling are two other techniques in common use at volcanoes [553].

TABLE 12. CHARACTERISTICS OF SELECTED REMOTE SENSING TECHNIQUES

Name/Acronym	Sensor	Repeat Interval	Spatial Resolution	Comments
ASTER	Advanced Spaceborne Thermal Emission and Reflection Radiometer	1 day (?)	15 m 30 m 90 m	VNIR (3 sensors) SWIR TIR satellite
AVHRR	Advanced Very High Resolution Radiometer	12 hours	LAC 1.1 km GAC 4.4 km	Polar orbiting; detects thermal anomalies and ash satellite
DOAS	Differential Optical Absorption Spectrometer	minutes	scanning	Ground based detects gas
ERS-1	European Radar Satellite	35 days	30 m; 80–100 km swath	Active radar; used for synthetic aperture radar
FLIR	Forward Looking Infrared Radiometer	minutes	1 m or less	Ground or aircraft based, detects thermal anomalies
GOES	Geostationary Operational Environmental Satellite	30 minutes	0.9 km (vis) 9.0 km (thermal)	Geostationary satellite
JERS-1 SAR	Japanese SAR	44 days	18 m; 75 km swath	Active radar; used for synthetic aperture radar
Landsat TM	Thematic Mapper	16 days	30 m	Satellite; 7 bands
OMI	Ozone Monitoring Instrument	1 day	13 × 25 km	Also detects SO_2 and aerosols
TOMS	Total Ozone Mapping Spectrometer	1 day	39 km	Also senses SO_2

6.2.4. Gas or water geochemical sampling

Magma contains dissolved gases of various compositions. These are generally in solution at depth (i.e. high pressure), but start to exsolve as magma moves to shallower depths (i.e. lower pressure). Monitoring programs often measure rates of gas and water output at fumaroles and hot springs, and also monitor temperatures and ratios of gases that have different solubilities. CO_2 is also monitored in soil gas on volcano flanks. If magma begins to ascend, typically CO_2 appears first (i.e. lower solubility) followed by SO_2 as the magma reaches shallower depths. Soil gases such as radon may increase as shallow fractures and pore spaces are altered. As with seismic and deformation monitoring, the same types of signals are observed during intrusion to shallow levels, thus an on going challenge is to increase the reliability of observations on time frames that are useful for decision making.

6.2.5. Thermal

In addition to monitoring gas fluxes and compositions at fumaroles and hot springs as above, monitoring programs also look for evidence of the edifice heating up. This may be caused by broad steaming of the ground driven by fluid convection or by conductive effects. These are potentially observed by ground based or remote sensing instruments (e.g. AVHRR, ASTER and FLIR). TABLE 12 gives summary information these various techniques. Edifice wide thermal precursors to eruptions are almost never observed. However, temperature increases at individual fumaroles or in crater lakes are observed before some eruptions.

6.2.6. Other geophysical techniques

When the ground surface moves, there is fundamental ambiguity about the cause, which may be rock squeezing, opening of cracks, or intrusion of water or magma. Gravity measurements can help verify mass injection and can help determine the cause by establishing the density. The magnetic properties of rock change with temperature and with (conductive) fluids moving through pore spaces, thus magnetic measurements can indicate changes in temperature or fluid flow at depth.

Both are generally done on as needed basis rather than continuously. Magneto tellurics (MT) and self potential are two electrical techniques that help determine presence and properties of magma and hot fluids. Many of these techniques apply tomography (e.g. Nicollin et al. [560]); these may extend beyond monitoring per se and may best be accomplished by invitation to the academic or commercial communities. Another promising new technique is muon imaging [561–564]. Examples of various data types and techniques are given in the case study summaries below.

As a general rule, the monitoring information is considered better or more reliable when phenomena show on several different types of instruments. This is a simple and effective use of redundancy that helps to reduce possible artefacts in the data.

6.3. EXAMPLES OF MONITORING USED IN HAZARDS FORECASTING

Here we give examples of the precursory and accompanying geophysical signals associated with four recent volcanic eruptions. These illustrate the rates of change and the timescales of increases of different types of unrest as measured at various monitoring instruments. Note that these can be quite variable, from a few hours to many months. Part of the differences in time scales may be caused by the presence of different processes. For example,

swarms of shallow earthquakes that persist for hours to a few days generally are indicative of discrete pulses of magma injection. In contrast, swarms of deeper earthquakes that persist for weeks to months generally represent brittle failure in surrounding country rocks as magma pressure increases beneath a volcano. Both swarm types are indicative of magma intrusion, but it may not be possible to distinguish these different types of swarms early in an unrest sequence. The examples chosen happen to be in Alaska but the trends identified are common to many volcanoes worldwide.

6.3.1. Augustine 2006

Augustine Volcano, Alaska, began to erupt January 14, 2006 following an 8.5 month long earthquake swarm, inflation of the edifice, and increased steaming [565]. The earthquake swarm intensified in the 10 hours immediately preceding the eruption. A series of strong explosive eruptions from January 14–28 produced ash columns from 4 to 14 km (See FIG. 46). Each was accompanied by strong seismic and infrasound signals (See FIG. 47) as well as lightning in the ascending plumes [275], [283]. Ash clouds were tracked for many hours in AVHRR satellite images (See FIG. 48). Following the explosive phase, dome growth occurred for several months and persistent small ash clouds were produced. Numerous rock falls produced secondary deposits and accompanying clouds; these were recorded on low light cameras. Two previous eruptions of Augustine, in 1976 and 1986, had similar precursory seismic sequences (8.5 and 9 months, respectively) as well as similar eruptions including both explosive (4–18 days) and dome growth (several months) stages. The close similarities suggest that Augustine has typical or characteristic eruptive activity. Thus a useful background investigation is to determine the parameters of typical eruptions at candidate volcanoes.

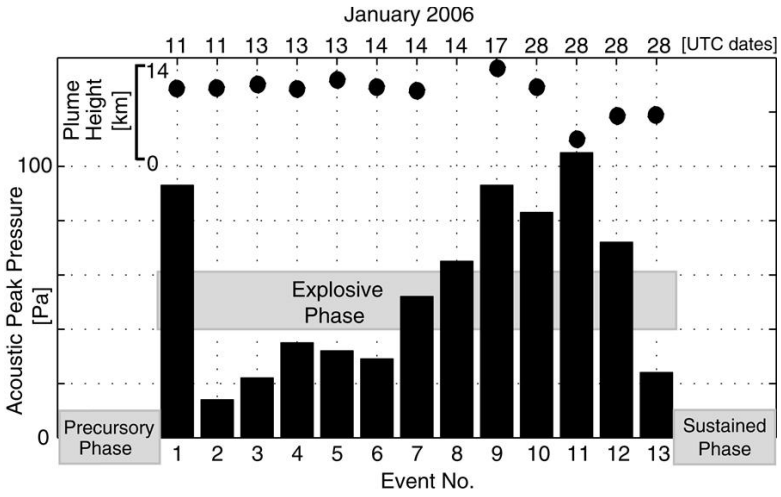

FIG. 46. Infrasound and plume height data from Augustine 2006 eruption. Reproduced courtesy of American Geophysical Union [566].

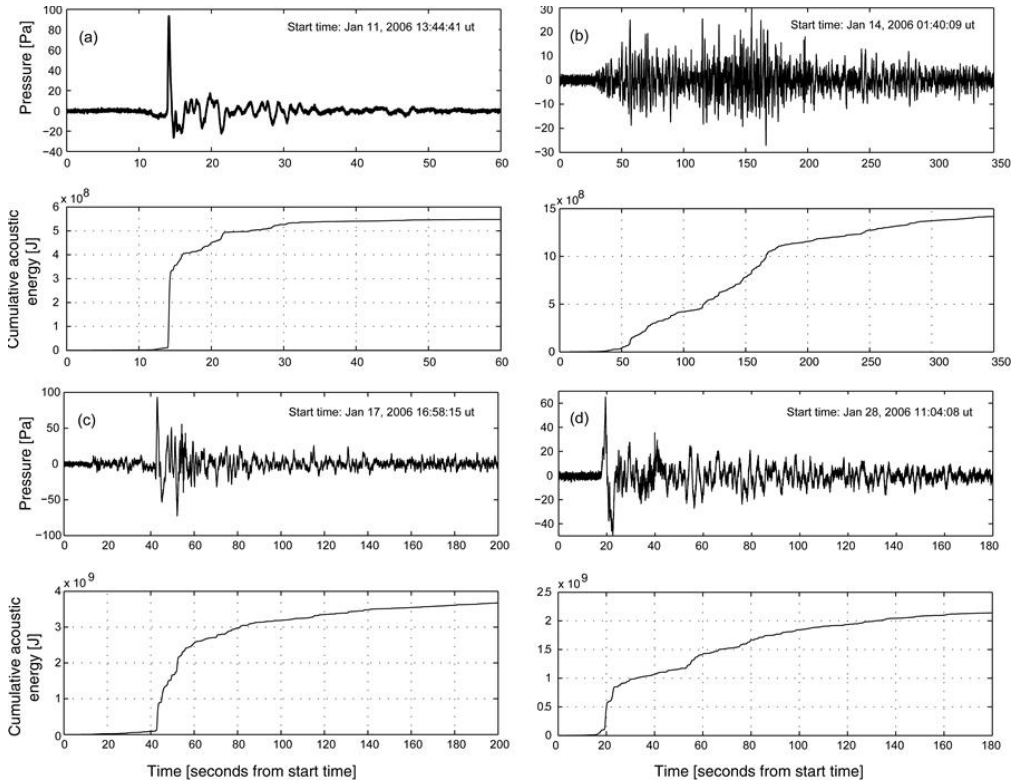

FIG. 47. Infrasound waveforms and cumulative energies from Augustine 2006 eruption. Reproduced courtesy of American Geophysical Union [566].

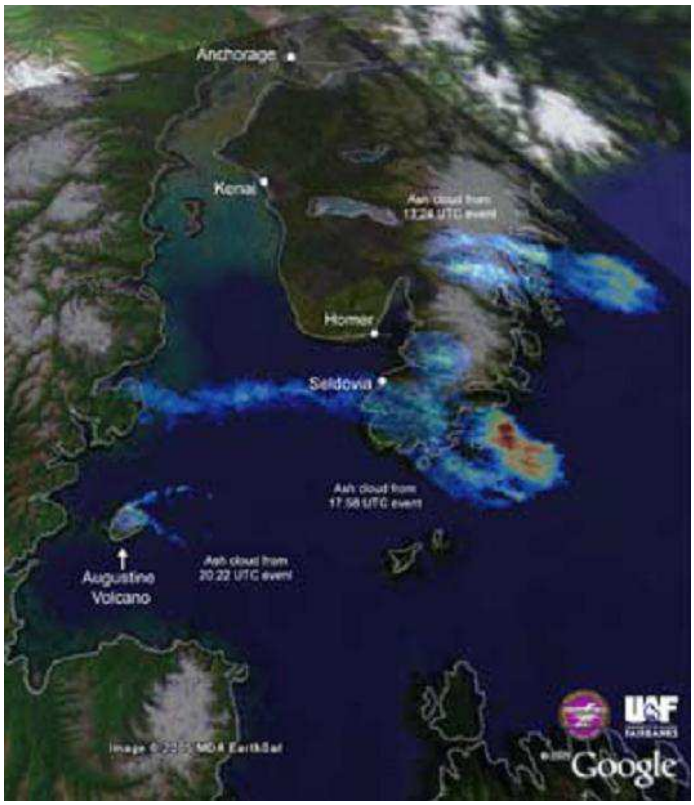

FIG. 48. AVHRR data from Augustine 2006 eruption. Figure courtesy of J. Dehn.

6.3.2. Pavlof 2007

Pavlof Volcano, Alaska, erupted in August 2007 following a 1–2 day swarm of low frequency earthquakes [567]. This volcano, which has an open vent and deep magma source, does not generally show a build up of VT earthquakes and shallow deformation has not been observed. The eruption lasted 5 weeks with continuous seismicity (See FIG. 49) and emission of ash and steam clouds, with several pulses of the ash column reaching 10 km (See FIG. 50). Small explosions occurred as many as 14 times per minute. Satellite images showed both the ash clouds and a lava flow that began a few days after the eruption onset and slowly moved down the SE flank. The lava flow was imaged with FLIR (See FIG. 51) which enabled estimates of its length and width. The lava flow melted snow, causing lahars in channels of the southern flanks of the volcano.

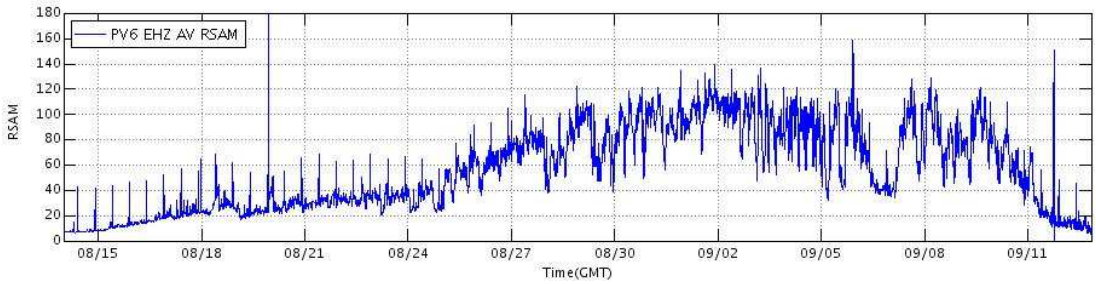

FIG. 49. RSAM data from Pavlof 2007 eruption. Sample interval is 10 minutes. Figure courtesy of Alaska Volcano Observatory.

FIG. 50. Steam and ash column from Pavlof 2007 eruption. Photo courtesy of C. Waythomas.

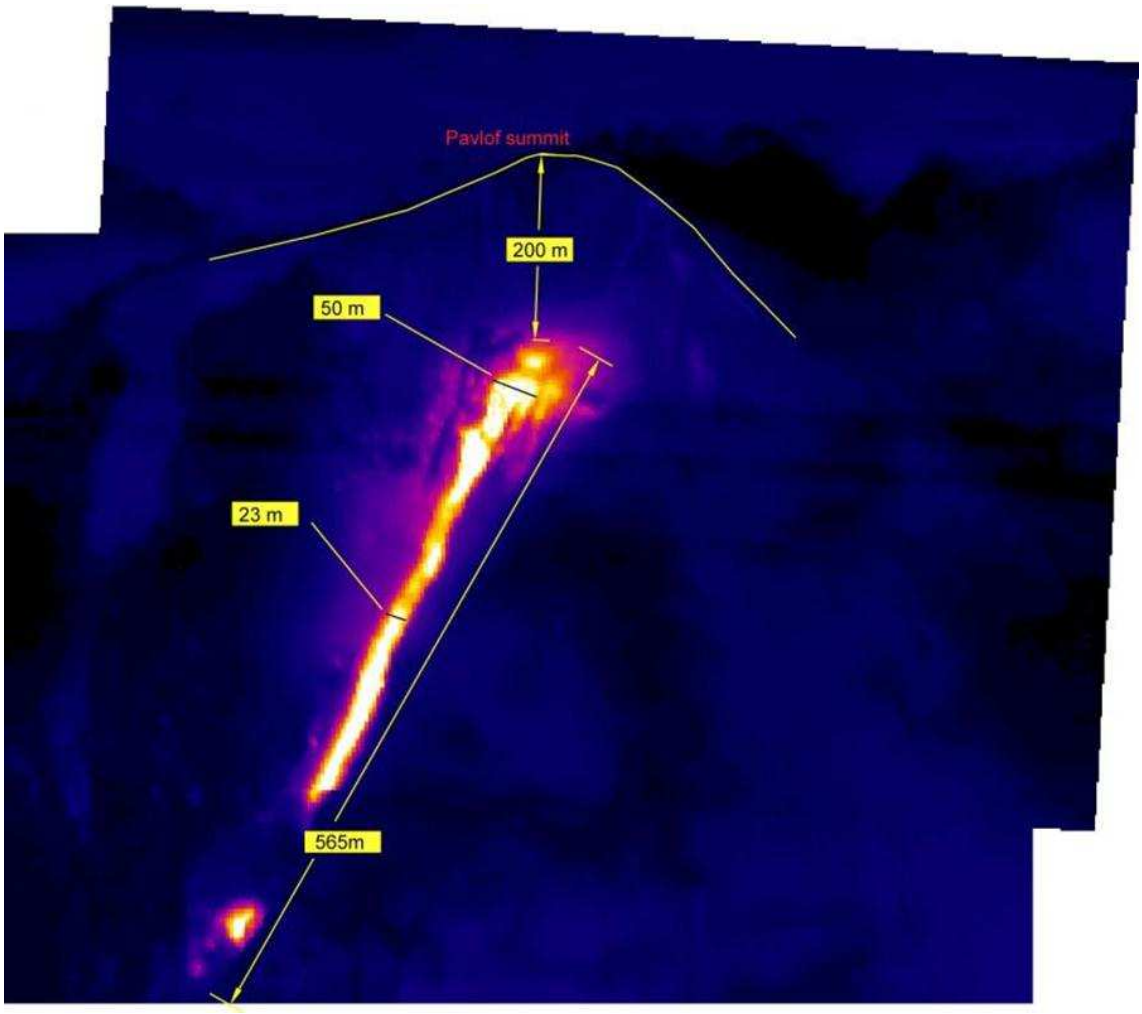

FIG. 51. FLIR data showing lava flow at Pavlof volcano, 2007. Figure courtesy of Alaska Volcano Observatory.

6.3.3. Okmok 2008

Okmok Volcano, Alaska, erupted on July 13, 2008 following a 5 hour long earthquake swarm that intensified approximately one hour before the eruption onset [568]. A new vent was opened at a location where no previous eruptions had occurred for 800 years. The eruption quickly formed an ash column to 16 km (See FIG. 52 b), and was sensed by several different satellites. The initial main phase lasted about 10 hours as determined from seismic and infrasound data (See FIG. 52 c). Later analyses of InSAR and GPS data showed deflation at the time of eruption (See FIG. 52 a) followed by inflation as the magma chamber began to refill. The eruption lasted five weeks with variable intensity.

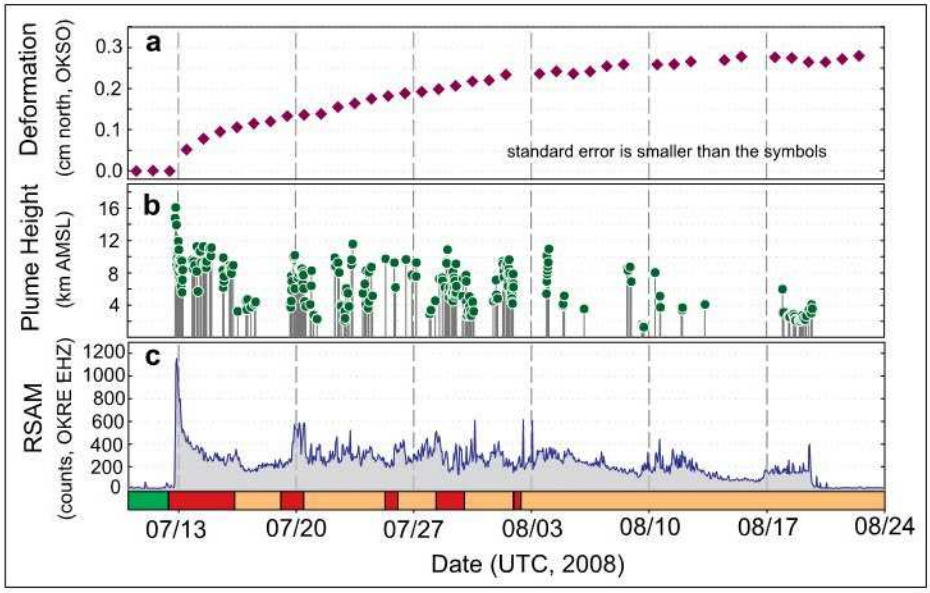

a) Deformation (up direction (N) corresponds to deflation) from GPS station OKSO
b) Plume height
c) Real Time Seismic Amplitude Measurement from station OKRE. Colour bar under c) shows level of concern colour code

FIG. 52. Summary monitoring data from Okmok 2008 eruption. Reproduced courtesy of American Geophysical Union [568].

6.3.4. Redoubt 2009

Redoubt volcano began to erupt explosively on March 23, 2009, following 2–3 months of gradually increasing precursors [569]. This was in sharp contrast to the precursors on the previous eruption in 1989, which began after just 23 hours of LP seismicity [570]. A series of explosive eruptions March 23–April 4, 2009 produced ash columns as high as 18 km (See FIG. 53). These ash clouds were detected in radar and satellite images but persisted only for several hours, likely because the clouds were very water rich and clumping of ash resulted in faster fall out. The explosive eruptions were accompanies by strong seismic and infrasound signals (See FIG. 53), and lightning that was especially prevalent when the ash clouds were more than 10 km high. Following the explosive phase, as at Augustine and many other volcanoes, a period of dome growth commenced, which lasted several months.

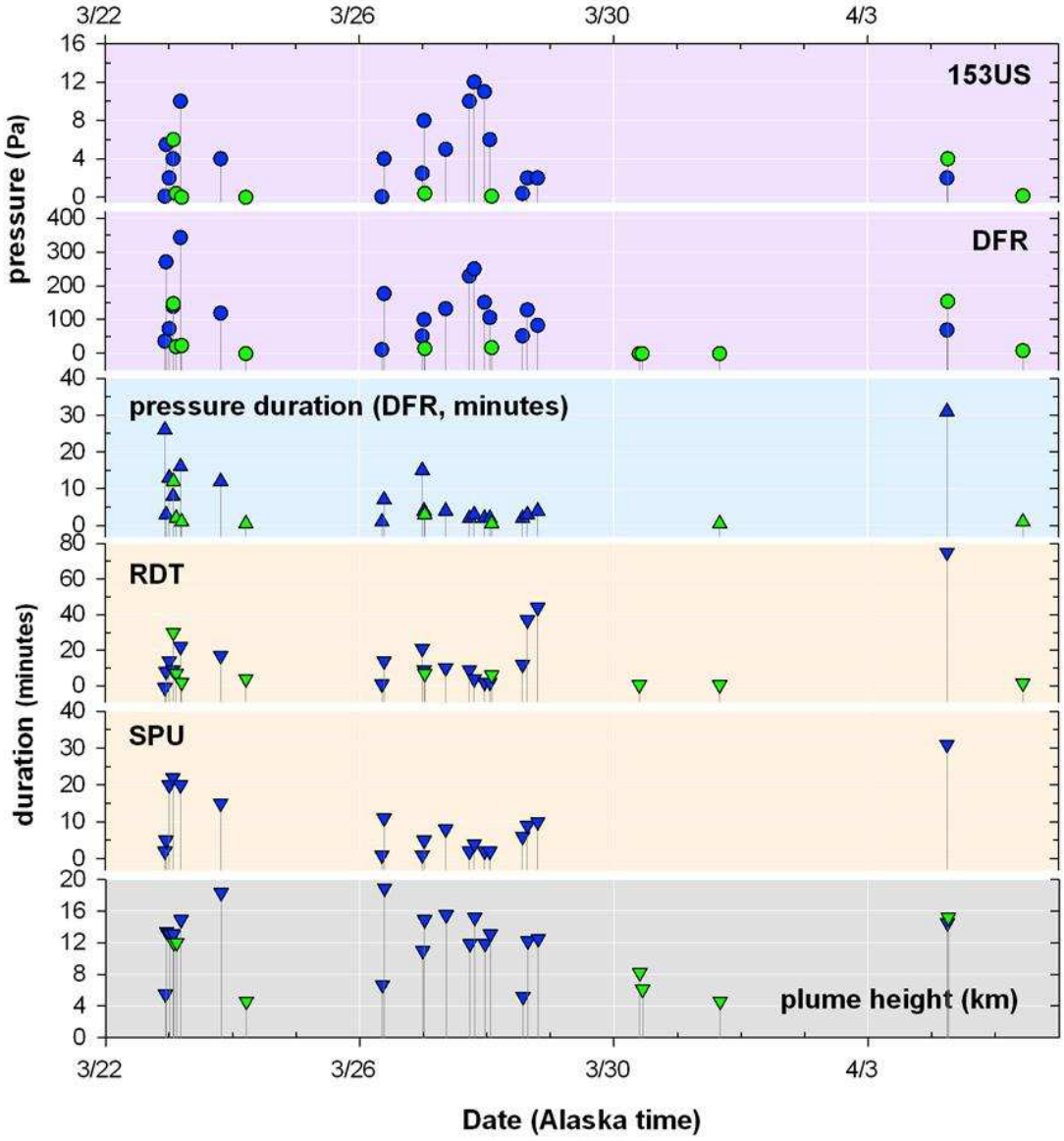

FIG. 53. Parameters of infrasound (i.e. pressure, top 3 panels) and seismic (i.e. duration, stations RDT and SPU), and plume height data from the Redoubt 2009 eruption. Blue symbols are 19 numbered events. Green symbols are re-analysis events. Figure courtesy of C. Nye.

TABLE 13 provides comparison data on the above eruptions and several other well known cases.

TABLE 13. COMPARISON OF PRECURSOR SEISMIC PARAMETERS FROM SELECTED CASE STUDIES

Volcano	Date m/d/y	VEI*	Earthquake Swarm Duration	Event type^	Precursor maximum M
Augustine	1/14/2006	3	8.5 mo.	H,L,T	1.6
Pavlof	8/14/2007	3	1.5 d	L	~1
Okmok	7/12/2008	4	5 h	H	1.5
Redoubt	3/23/2009	4	2–3 mo.	H,L,T	1.6
Mount St. Helens	5/18/1980	5	2 mo.	H,L,T	5.0
Pinatubo	6/15/1991	6	2–3 mo.	H,L,T	4.3
Galeras	1/14/1993	2	2 wk.	L	2.6

*Volcanic Explosivity Index; each increase of one unit corresponds to one order of magnitude increase in bulk tephra volume, along with higher ash columns and longer durations
^H – high frequency or volcano tectonic earthquakes
^L – low frequency or long period earthquakes
^T – volcanic tremor

6.3.5. General features of precursory activity

There are hundreds of such cases in the literature that present observations on precursory activity, including 1943 eruption of Paricutin, Mexico; 1975 and 2012 eruptions of Tolbachik, Russia; and 2000 eruption of Hekla, Iceland. A particularly well studied recent case is from Soufrière Hill Volcano, Montserrat [559], [571]. There are also hundreds of cases of potential precursors that did not lead to eruptions. Newhall and Dzurisin [572] performed a comprehensive and systematic study of calderas and associated unrest that provides many useful examples of time scales and types of activity for a large worldwide sample of precursory volcanic activity.

From these examples and many others some generalizations can be made about precursory activity. Short duration precursors, on scale of hours to days, are typically associated with basaltic systems. Relative to silicic magmas, basaltic magmas have lower viscosity, lower amounts of dissolved gas, and ascend rapidly. Longer duration precursors, on scale of days to weeks or longer, are generally associated with more silicic magma systems. Silicic magmas generally are several orders of magnitude more viscous than basalt, have higher amounts of gases in solution, and ascend slower. The amount of dissolved gases is one of the principal factors affecting eruption explosivity, and the gas rich silicic magmas typically erupt explosively, mainly producing tephra. In contrast, gas poor basaltic systems typically erupt effusively, with the main eruptive products being lava flows.

Explosive basaltic eruptions are possible, however, (such as the initial phase of Okmok 2008, above) especially when the ascent rate is very high so that little gas loss occurs during ascent. Interactions of magma with groundwater may also affect explosivity. All of these factors need to be considered when interpreting monitoring data.

Monitoring data are useful to help answer the suite of questions that evolve during a protracted period of precursory activity. Initial questions include whether there is evidence of magmatic unrest, magma movement, or impending eruption. As shown above, most volcanoes show increasing seismicity, deformation, heating, and venting of steam or other gases during initial phases of unrest. Time scales for precursory activity can be hours to months, with days to weeks being most common. Second, as an eruption becomes more likely, questions change to location (i.e. existing or new vent; summit or flank), the likely type of activity, and when it will begin. The typical time scale for this increase in activity is days. Third, if an eruption occurs, monitoring questions address the assessment of current activity (time scale of minutes), likely effects, and how long the eruption will last (which is highly variable). Fourth, if eruptive activity declines or pauses, questions will be concerned with possible resumptions of activity or clear indications that the eruption is over (e.g. time scale weeks to months). Finally, when the eruption has ended, monitoring data can help address questions of the new normal or background states that may not be the same as prior states, and after effects of eruptions such as lahars, re-suspension of ash, or local slope failures. Knowledge and data generally allow affected communities to be better prepared for the next event, including improvements to the monitoring program, that can occur on time scales of years. Volcanic event trees or decision trees offer a useful framework for evaluating hazards in near real time during periods of unrest or eruption [132], [133].

Volcanoes that show historical signs of unrest or prior eruptions have the highest likelihoods of being monitored. By contrast, volcanoes with negligible activity, or even lacking Holocene or written historical activity such as Pinatubo (400–500 year repose prior to 1991 reawakening [573]), Chaiten (400 year repose prior to its 2008 activity [574], [114]), often lack instrumentation as not being perceived as a priority. Thus, limited information exists on how long it takes for a historically inactive volcano to increase activity that leads to eruption. A handful of historic examples suggest this period might be a month or two, such as El Chichón, 1981 (500 year repose, 1 month earthquake swarm [575]), Kasatochi (> 200 year repose, 6 week earthquake swarm [576]), and Paricutin, 1943 (no prior eruption at this vent location although an eruption in 1760's occurred in the same volcanic field; 7 week earthquake swarm at Paricutin [577]). However, there is great uncertainty and the variance may also be large.

Most of the discussion in this section has been concerned with identifying precursors to eruption. Another important function of monitoring is to be able to characterize eruptions in progress. Eruptions can have quite variable durations (minutes to months), so it is important to recognize evolving activity. When eruptions are under way, it is possible to track factors such as height of ash clouds, speed of lava flows, volume fluxes, etc. (See FIG. 49, FIG. 50, FIG. 51 and FIG. 52). The most intense phase of an eruption often occurs close to the beginning [578] but this is not always the case. Some volcanoes have their climactic activity near the end of long periods of unrest, and other may have several similar sized peaks in activity. Eruptions such as Montserrat that produce large lava domes can suffer repeated dome collapse events that produce ash clouds as well as ground hazards. The time intervals between such events can be quite irregular, and depend on magma supply rate and other factors. Once the eruption begins, monitoring will likely fall under the control and direction of national authorities, because an area much larger than a nuclear installation will be affected. Safety and operational

considerations at the nuclear installation will need to be guided by this information. For some volcanoes, eruptive activity can continue for years or longer, which requires long term maintenance and support of a monitoring network.

Monitoring data, once they exist, may need to be factored into revised hazards assessments. It is an on going task to determine the significance of various types of unrest. A change in the monitoring status of a volcano may require a change in hazards response or plans. This is because new data provide a basis for changing levels of concern. Another concern is how long an event (eruption or episode of unrest) will last; monitoring helps to identify the end or the beginning of the end and provides estimates of uncertainty. Monitoring data may also be combined with geological evidence to infer the likely type of activity, such as explosive or effusive, large or small, etc.

6.4. CONCLUSIONS

There are both benefits and limitations to monitoring volcanoes. The chief benefit is that interpretations and decisions are based on data, models, and knowledge rather than guessing time scales and processes. There is no standard approach for how to interpret monitoring information, yet experience has shown that monitoring efforts are effective to mitigate the effects of volcanic eruptions. Another benefit to monitoring is the ability to state that 'nothing unusual is happening'. This can greatly help to provide the appropriate level of concern and to reduce the effects of misinformation and rumours about unrest at a volcano. In general, data driven decision making can done on a rational basis, and the information is updatable. For example, modern observatories often provide hourly situation updates during crises.

Effective monitoring uses data from different types of instruments including seismic, infrasound, deformation, gas and water or geochemical sampling, other geophysical methods such as magnetics or gravity, and thermal monitoring, and complementary geological studies. Data need to be stored and displayed in real time. Modern volcano observatories record multi parametric data and observations in searchable databases and provide data on web sites that may be retrieved on demand. This is an effective strategy because it assures rapid dissemination of data and distributes the monitoring workload. A particular challenge with this strategy, though, is ensuring that all data are indexed to a common time stamp so that synchronous events can be identified accurately. In addition, darkness, weather conditions, and instrumentation malfunctions can create appreciable gaps in multi parametric data streams. Mitigation or response strategies that rely on signals from multiple data streams need to be sufficiently flexible so that decisions can still be made if individual data streams are interrupted.

At volcanoes, the location of hazard is known in general (i.e. on the volcano) however, monitoring can provide additional clues to pinpoint the location, such as whether the activity will occur at the summit or on the flank, or whether activity is likely from a new or existing vent. Because there are multiple processes occurring, there is often ambiguity and multiple interpretations of activity are possible. There are also many cases of unrest that do not lead to eruption, but monitoring provides a basis for interpretation. Some volcanic activity is forced or triggered by nearby or regional tectonic activity such as large earthquakes, hence monitoring needs to include regional context and observations. Key signals may be small or subtle, so data need to be continually analysed and reassessed. This requires a small permanent staff of well trained personnel; partnering with universities or government agencies is a low cost way to

broaden needed expertise. Many countries have learned that a monitoring program is most effective when advice and guidance from an independent committee of experts is provided. In countries where a government agency or university has a formal or legal mandate to monitor volcanoes and to give public warnings, the monitoring programme for a nuclear installation could be appropriately integrated with the national program.

In the present context, monitoring is an on going assessment of the state of the volcano. It can permit forecasting of the timescales of implementing mitigation actions, and assessing the level of activity. The present effort is not geared towards a specific prediction, which in the current state of knowledge would provide warnings of days at best.

7. CONCLUSION

Within the context of nuclear safety, volcanic eruptions are rare natural events. Nevertheless, the products of these eruptions can create hazards that warrant careful consideration for the siting, design or operation of a nuclear installation. The adoption of the SSG-21 [1] constitutes a basic framework for conducting a volcanic hazards assessment in a series of tractable stages. This TECDOC establishes the practicability of evaluating the requirements in SSG-21 [1] through a systematic volcanic hazards assessment. Although none of the models discussed in this TECDOC are viewed as unequivocally suitable for a volcanic hazards analysis (i.e. validated), these models are representative of the current state-of-the-science and provide a foundation for future work in developing an international consensus on volcanic hazards assessment methods.

As discussed in SSG-21 [1] and this TECDOC, the initial stage of any volcanic hazards assessment uses available information to characterize potential volcanic sources in the region of interest. This initial information is used to conduct screening analyses that determine if specific volcanic phenomena might reach a proposed site. Typically, these screening analyses use conservative estimates of the distances that volcanic phenomena could travel from potential sources, based on information from both the region around the site and from analogous volcanic systems. The decision to exclude certain volcanic phenomena from additional consideration carries a significant burden in demonstrating that such phenomena have a negligible potential to reach the site or affect safety.

Data needs are identified as part of the initial screening analyses. For many volcanic areas, published information will not have sufficient breadth or depth to support a robust hazards assessment. The data needed to support this assessment, such as field investigations, age determinations, and geophysical data, often requires appreciable time and resources to collect successfully. Without these data, the uncertainties in the resulting hazards assessment might not be able to support positive safety conclusions regarding siting, design, or operation of a proposed nuclear installation.

The next stage of the hazard analysis needs to consider only those volcanic phenomena that have a potential to affect the siting, design, or operation of a nuclear installation. Thus, the hazards assessment focuses on determining the recurrence rate of past events, and projecting these rates to estimates for the occurrence of future events. In addition to being rare events, evidence of many past volcanic eruptions is poorly preserved in the geologic record.

Determining uncertainties in the number and character of past events is an important consideration in the recurrence rate assessments.

At this stage in the hazards analysis, a tectono magmatic model of volcanism is needed. This tectono magmatic model integrates the volcanic and tectonic history of the region into one or several interpretations that explain how volcanic processes have operated through time. These interpretations (i.e. conceptual models) allow the analyst to evaluate if the timing or character of past events is a reliable indicator of future activity. Conversely, the analyst might determine that only a part of the past record is relevant to projections of future activity, or that previously absent phenomena (e.g. pyroclastic eruptions) should be considered in the hazards assessment. In any case, the development of a tectono magmatic model provides confidence that volcanic processes are understood sufficiently to allow meaningful extrapolations of future activity.

Models appear practicable for most of the volcanic phenomena that are relevant to a hazards assessment (i.e. [1]), with the exception of hydrothermal activity. These models range in complexity from relatively simple empirical or physics based approaches that are amenable to stochastic implementation, to highly coupled first principles approaches that tend to provide deterministic assessments. No single type of modelling approach in this TECDOC is deemed appropriate for a hazards assessment, and the analysis must select the approach that best represents the data and captures relevant uncertainties. In addition, new models continue to be developed and published, which might provide additional insights on potential hazards. Although all of the models discussed in this TECDOC have been published and have undergone some testing, none of the models have been tested at the full range of volcanic systems that might warrant consideration at the site of a nuclear installation. As a consequence, none of these models can be viewed today as generally accepted or unequivocally suitable for a hazards assessment at a potential nuclear installation. Drawing analogy from international experiences in seismic hazards assessment, future efforts in volcanic hazards assessment could benefit from rigorous testing and evaluation of numerical models, to develop consensus on generally acceptable methodologies for modelling and assessing volcanic hazards at nuclear installations.

In the interim, practical safety decisions will need to be made based on the results of existing techniques. For some locations, the potential for future volcanic hazards will be sufficiently clear to preclude development of the site as a nuclear installation. But for other sites, limitations in the precision and accuracy of available modelling techniques, along with a paucity of necessary data, may result in a hazards analysis with uncertainties that can support either development or exclusion of a site. If the decision is made to develop a site, then the design bases for the installation must consider the uncertainties in the underlying hazards assessment when evaluating the potential demands placed on safety systems. In addition to the physical magnitude of these demands, the duration of these demands may be significantly larger than commonly considered in nuclear installation design. Similar considerations would need to be given for operational planning in response to potential volcanic hazards.

Unlike seismic hazards, volcanic hazards rarely occur without warning. For sites with the potential for future volcanic hazards, capable volcanoes would need to be monitored for signs of potential activity. In addition, some non eruptive phenomena such as debris avalanches can occur in response to heavy rainfall or other external triggers. If present, these external triggers also would need to be included in the monitoring system. Early warning of potential volcanic activity is required if human activities are needed to mitigate impacts from volcanic

phenomena. Thus, a volcano monitoring system is important to safety, and will need to be designed and maintained at a level commensurate with other safety significant systems at a nuclear installation.

Volcanic hazards can be assessed systematically and traceably, and, in many instances, appear practicable to mitigate through appropriate design or operation of a nuclear installation. The rarity of volcanic events, however, can create a false sense of security about a site with no visible impacts from past events. The potential for future hazards cannot be assessed solely from the record of past volcanic activity, as many events will not be preserved in this record and volcanic systems commonly change in character through time. A systematic volcanic hazards assessment, as presented in this TECDOC and SSG-21 [1], promotes evaluation of these uncertainties and provides the basis needed to make decisions about the safety or acceptability of a nuclear installation site.

APPENDIX: GOVERNING EQUATIONS BASED ON THE SHALLOW LAYER APPROACH

Depth averaged flow models are based on the so called Shallow Water Equations (SWE), firstly introduced by De Saint Venant in 1864 and Boussinesq in 1872. This kind of equations has been generalized in order to describe a much larger class of phenomena. Nowadays, applications of models based on the Shallow Layer Approach (SLA) include a wide range of problems having important implications for hazard assessment such as floods (e.g. [579]), lahars (e.g. [458]), lava flows (e.g. [366]), debris avalanches (e.g. [418]), tsunamis propagation (e.g. [580]), etc.

The SLA models are based on depth averaged equations obtained by integrating mass, momentum, volume, and energy equations over the fluid depth, from the bottom up to the free surface. This approach is valid in the limit $H2/L2 \ll 1$, being H the undisturbed fluid height and L the characteristic wavelength scale in the flow direction. Commonly, the assumptions of hydrostatic pressure distribution, and of uniform or gradually varied flow are also made.

For incompressible homogeneous fluids mass equation is equivalent to volume conservation and the governing equations are (e.g. [408]):

$$\frac{\partial \mathrm{h}}{\partial \mathrm{t}} + \frac{\partial(\mathrm{h}\bar{\mathrm{u}})}{\partial \mathrm{x}} + \frac{\partial(\mathrm{h}\bar{\mathrm{v}})}{\partial \mathrm{y}} = 0 \tag{77}$$

$$\frac{\partial(\mathrm{h}\bar{\mathrm{v}})}{\partial \mathrm{t}} + \frac{\partial(\mathrm{h}\bar{\mathrm{u}}^2)}{\partial \mathrm{x}} + \frac{\partial(\mathrm{h}\bar{\mathrm{u}}\bar{\mathrm{v}})}{\partial \mathrm{y}} = \mathrm{gh}\sin\alpha_{\mathrm{x}} - \frac{\mathrm{k}}{2}\frac{\partial(\mathrm{gh}^2\cos\alpha)}{\partial \mathrm{x}} + \frac{\mathrm{T_x}}{\rho} \tag{78}$$

$$\frac{\partial(\mathrm{h}\bar{\mathrm{v}})}{\partial \mathrm{t}} + \frac{\partial(\mathrm{h}\bar{\mathrm{u}}\bar{\mathrm{v}})}{\partial \mathrm{x}} + \frac{\partial(\mathrm{h}\bar{\mathrm{v}}^2)}{\partial \mathrm{y}} = \mathrm{gh}\sin\alpha_{\mathrm{y}} - \frac{\mathrm{k}}{2}\frac{\partial(\mathrm{gh}^2\cos\alpha)}{\partial \mathrm{y}} + \frac{\mathrm{T_y}}{\rho} \tag{79}$$

where t denotes time, x and y the horizontal coordinates, h, denotes the fluid depth measured from the altitude of the terrain surface Z (bed), $\overline{u}$ and $\overline{v}$ are the depth averaged flow velocity components (e.g. $\overline{u}(x,y) = \frac{1}{h}\int_Z^{Z+h} u(x,y,z)dz$ with ux component of the local velocity, and similar for the y component, α denotes ground slope, T represents a retarding stress (i.e. a friction term), ρ is the fluid bulk density, k is Earth pressure coefficient (ratio of ground parallel to ground normal stress), and subscripts denote components in the x and y directions. EQ. (77) represents the conservation of mass, EQ. (78) and EQ. (79) the conservation of momentum in the x and y directions respectively.

As we mentioned above, the equation system EQ. (77)–EQ. (79) can be generalized in order to describe a larger number of phenomena using a similar approach. For example, in the case of lava flows the viscosity is strongly dependent on temperature, therefore it is necessary to solve the equation for the energy conservation and account for the coupling between the effective viscosity and the depth averaged temperature [366].

In the case of transport of dense gases, because gases cannot be assumed incompressible and because of air entrainment during their flow, it is necessary to account for these effects and a more general equation system (e.g. [323]) is obtained imposing:

i) conservation of the volume:

$$\frac{\partial h}{\partial t} + \frac{\partial h\bar{u}}{\partial x} + \frac{\partial h\bar{v}}{\partial y} = u_{entr} \tag{80}$$

ii) conservation of mass:

$$\frac{\partial h(\bar{\rho}-\rho_a)}{\partial t} + \frac{\partial h(\bar{\rho}-\rho_a)\bar{u}}{\partial x} + \frac{\partial h(\bar{\rho}-\rho_a)\bar{v}}{\partial y} = \rho_a u_{entr} \tag{81}$$

iii) two equations describing the balance of forces along x and y directions:

$$\frac{\partial h\bar{\rho}\bar{u}}{\partial t} + \frac{\partial h\bar{\rho}\bar{u}^2}{\partial x} + \frac{\partial h\bar{\rho}\bar{u}\bar{v}}{\partial y} + \frac{1}{2}S_1\frac{\partial g(\bar{\rho}-\rho_a)h^2}{\partial x} + S_1 g(\bar{\rho}-\rho_a)h\frac{\partial e}{\partial x} + \frac{1}{2}\rho C_D\bar{u}|\bar{u}| + V_x + k\rho_a\left(\frac{\partial}{\partial t} + u_a\frac{\partial}{\partial x} + v_a\frac{\partial}{\partial y}\right)[h(\bar{u}-u_a)] = u_{entr}\rho_a u_a \tag{82}$$

$$\frac{\partial h\bar{\rho}\bar{v}}{\partial t} + \frac{\partial h\bar{\rho}\bar{v}^2}{\partial y} + \frac{\partial h\bar{\rho}\bar{u}\bar{v}}{\partial x} + \frac{1}{2}S_1\frac{\partial g(\bar{\rho}-\rho_a)h^2}{\partial y} + S_1 g(\bar{\rho}-\rho_a)h\frac{\partial e}{\partial y} + \frac{1}{2}\rho C_D\bar{v}|\bar{u}| + V_y + k\rho_a\left(\frac{\partial}{\partial t} + u_a\frac{\partial}{\partial x} + v_a\frac{\partial}{\partial y}\right)[h(\bar{v}-v_a)] = u_{entr}\rho_a v_a \tag{83}$$

where u_{entr} the entrainment rate of air, $e = e(x,y)$ is the terrain elevation, u_a and v_a denote air velocity (wind), V_x and V_y indicate the components of turbulent shear stress exerted on the cloud, C_D is a skin friction coefficient, and k is a semi-empirical parameter.

REFERENCES

[1] INTERNATIONAL ATOMIC ENERGY AGENCY, Volcanic Hazards in Site Evaluation for Nuclear Installations, IAEA Specific Safety Guide No. SSG-21, IAEA, Vienna (2012).

[2] MCBIRNEY, A.R., GODOY, A., Notes on the IAEA guidelines for assessing volcanic hazards at nuclear facilities, Journal of Volcanology and Geothermal Research **126** (2003) 1–9.

[3] MATTHEWS, N.E., SMITH, V.C., COSTA, A., DURANT, A.J., PYLE, D.M., PEARCE, N.J., Ultra-distal tephra deposits from super-eruptions: examples from Toba, Indonesia and Taupo Volcanic Zone, New Zealand, Quaternary International **258** (2012) 54–79.

[4] ALFANO, F., BONADONNA, C., VOLENTIK, A.C.M., CONNOR, C.B., WATT, S.F., PYLE, D.M., CONNOR, L.J., Tephrastratigraphy and eruptive volume of the May, 2008, Chaitén eruption, Chile, Bulletin of Volcanology **73** 5 (2011) 613–630.

[5] MACHIDA, H., ARAI, F., Extensive ash falls in and around the Sea of Japan from large late Quaternary eruptions, Journal of Volcanology and Geothermal Research **18** 1 (1983) 151–164.

[6] ORSI, G., D'ANTONIO, M., DE VITA, S., GALLO, G., The Neapolitan Yellow Tuff, a large magnitude trachytic phreatoplinian eruption: eruptivedynamics, magma withdrawal and caldera collapse, Journal of Volcanology and Geothermal Research **53** (1992) 275–287.

[7] FISHER, R.V., ORSI, G., ORT, M., HEIKEN, G., Mobility of a large-volume pyroclastic flow - emplacement of the Campanian ignimbrite, Italy, Journal of Volcanology and Geothermal Research **56** 3 (1993) 205–220.

[8] GUICHARD, F., CAREY, S., ARTHUR, M.A., SIGURDSSON, H., ARNOLD, M., Tephra from the Minoan eruption of Santorini in sediments of the Black Sea, Nature **363** (1993) 610–612.

[9] DRIESSEN, J., MACDONALD, C.F., "The eruption of the Santorini volcano and its effects on Minoan Crete", The Archaeology of Geological Catastrophes, Geological Society Special Publication No. 171 (MCGUIRE, W.J., GRIFFITHS, D.R., HANCOCK, P.L., STEWART, I.S., Eds), Geological Society of London, London (2000) 81–93.

[10] CONNOR, C., CONNOR, L., HALAMA, R., MELIKSETIAN, K., SAVOV, I., Volcanic Hazard Assessment of the Armenia Nuclear Power Plant Site, Final Report, University of South Florida / Leeds University / GeoRisk and Institute of Geological Sciences of the Armenian National Academy of Sciences, Tampa, Florida / Leeds, England / Yerevan, Armenia (2011).

[11] CONNOR, L.J., CONNOR, C.B., MELIKSETIAN, K., SAVOV, I., Probabilistic approach to modeling lava flow inundation: a lava flow hazard assessment for a nuclear facility in Armenia, Journal of Applied Volcanology **1** (2012) 1–19.

[12] YILMAZ, Y., GUNER, Y., SAROGLU, F., Geology of the Quaternary volcanic centers of the east Anatolia, Journal of Volcanology and Geothermal Research **155** (1998) 338–345.

[13] KARAKHANIAN, A., DJRBASHIAN, R., TRIFONOV, V., PHILIP, H., ARAKELIAN, S., AVAGIAN, A., Holocene-historical volcanism and active faults as natural risk factors for Armenia and adjacent countries, Journal of Volcanology and Geothermal Research **113** (2002) 319–344.

[14] KARAKHANIAN, A., JRBASHYAN, R., TRIFONOV, V., PHILIP, H., ARAKELIAN, S., AVAGYAN, A., BAGHDASSARYAN, H., DAVTIAN, V.,

Historical volcanoes of Armenia and adjacent areas: What is revisited?, Journal of Volcanology and Geothermal Research **155** 3–4 (2006) 338–345.
[15] HAROUTIUNIAN, R.A., The historical volcanoes of Armenia and adjacent areas revisited, Journal of Volcanology and Geothermal Research **155** 3–4 (2006) 334–337.
[16] KARAKHANIAN, A., JRBASHYAN, R., TRIFONOV, V., PHILIP, H., ARAKELIAN, S., AVAGYAN, A., BAGHDASSARYAN, H., DAVTIAN, V., GHOUKASSYAN, Y., Volcanic hazards in the region of the Armenian nuclear power plant, Journal of Volcanology and Geothermal Research **126** 1–2 (2003) 31–62.
[17] INTERNATIONAL ATOMIC ENERGY AGENCY, Review mission to Armenia: Seismic safety site investigations of the Armenian NPP (4th follow-up SSRM), report to the Government of Armenia of May 28-June 2, 1995, TC Project ARM/9/002, IAEA, Vienna (1995).
[18] CHERNYSHEV, I.V., LEBEDEV, V.A., ARAKELYANTS, M.M., JRBASHYAN, R., GUKASYAN, Y.G., Geochronology of the Aragats volcanic center, Armenia: Evidence from K-Ar dating, Doklady Earth Sciences **384** 4 (2002) 393–398.
[19] WELLER, J.N., MARTIN, A.J., CONNOR, C.B., CONNOR, L.J., KARAKHANIAN, A., "Modelling the spatial distribution of volcanoes: An example from Armenia", IAV001 Statistics in Volcanology, Special Publications of IAVCEI (MADER, H.M., COLES, S.G., CONNOR, C.B., CONNOR, L.J., Eds), Geological Society of London, London (2006) 77–88.
[20] GHUKASYAN, Y.G., Petrography, mineralogical and geochemical features and history of the formation of the Aragats volcanic complex, PhD Thesis, Univ. of Gerogian (1985).
[21] JRBASHYAN, R.T., GHUKASYAN, Y.G., SHIRINIAN, K.G., SAYADIAN, Y.V., Special volcanological investigations in the region of the Armenian NPP, Technical report, Institute of Geological Sciences of the Armenian National Academy of Sciences, Yerevan (1995).
[22] KESKIN, M., PEARCE, J.A., MITCHELL, J.G., Volcano-stratigraphy and geochemistry of collision-related volcanism on the Erzurum-Kars Plateau, northeastern Turkey, Journal of Volcanology and Geothermal Research **85** 1–4 (1998) 355–404.
[23] CHAPMAN, N.A., "Tectonic events and nuclear facilities", Volcanic and Tectonic Hazard Assessment for Nuclear Facilities (Connor, C.B., Chapman, N.A., Connor, L.J., Eds), Cambridge University Press, Cambridge (2009) 1–23.
[24] CLOOS, M., "The nature of tectonic hazards", Volcanic and Tectonic Hazard Assessment for Nuclear Facilities (Connor, C.B., Chapman, N.A., Connor, L.J., Eds), Cambridge University Press, Cambridge (2009) 24–73.
[25] CONNOR, C.B., SPARKS, R.S., DIEZ, M., VOLENTIK, A.C., PEARSON, S.C., "The nature of volcanism", Volcanic and Tectonic Hazard Assessment for Nuclear Facilities (Connor, C.B., Chapman, N.A., Connor, L.J., Eds), Cambridge University Press, Cambridge (2009) 74–115.
[26] FARMER, G.L., PERRY, F.V., SEMKEN, S., CROWE, B., CURTIS, D., DEPAOLO, D.J., Isotopic evidence on the structure and origin of subcontinental lithospheric mantle in southern Nevada, Journal of Geophysical Research **94** B6 (1989) 7885–7898.
[27] SPERA, F.J., FOWLER, S.J., "Conceptual model for small-volume alkali basalt petrogenesis: Implications for volcanic hazards at the proposed Yucca Mountain nuclear waste repository," Volcanic and Tectonic Hazard Assessment for Nuclear Facilities (Connor, C.B., Chapman, N.A., Connor, L.J., Eds), Cambridge University Press, Cambridge (2009) 195–228.

[28] VALENTINE, G.A., PERRY, F.V., "Volcanic risk assessment at Yucca Mountain, NV, USA: integration of geophysics, geology, and modeling," Volcanic and Tectonic Hazard Assessment for Nuclear Facilities (Connor, C.B., Chapman, N.A., Connor, L.J., Eds), Cambridge University Press, Cambridge (2009) 452–480.
[29] KESKIN, M., Magma generation by slab steepening and breakoff beneath a subduction-accretion complex: An alternative model for collision-related volcanism in Eastern Anatolia, Turkey, Geophysical Research Letters **30** 24 (2003) 8046.
[30] LIU, J.Q., Volcanoes of China, Science Press, Beijing (1999).
[31] KONDO, H., "Regional-scale volcanology in support of site-specific investigations," Volcanic and Tectonic Hazard Assessment for Nuclear Facilities (Connor, C.B., Chapman, N.A., Connor, L.J., Eds), Cambridge University Press, Cambridge (2009) 307–325.
[32] CHAPMAN, N.A., APTED, M., BEAVAN, J., BERRYMAN, K., CLOOS, M., CONNOR, C., CONNOR, L., JAQUET, O., LITCHFIELD, N., MAHONY, S., SMITH, W., SPARKS, S., STIRLING, M., WALLACE, L., Development of Methodologies for the Identification of Volcanic Hazards to Potential HLW Reposiotry Sites in Japan, - The Tohoku Case Study -, NUMO-TR-08-03, Nuclear Waste Management Organization of Japan, Tokyo (2009).
[33] TAMURA, Y., TATSUMI, Y., ZHAO, D., KIDO, Y., SHUKUNO, H., Hot fingers in the mantle wedge: new insights into magma genesis in subduction zones, Earth and Planetary Science Letters **197** 1 (2002) 105–116.
[34] TAMURA, Y., "Some geochemical constraints on hot fingers in the mantle wedge: evidence from NE Japan", Intra-Oceanic Subduction Systems: Tectonic and Magmatic Processes, Geological Society Special Publication No. 219 (LARTER, R.D., LEAT, P.T., Eds), Geological Society of London, London (2003) 221–237.
[35] MARTIN, A.J., UMEDA, K., CONNOR, C.B., WELLER, J.N., ZHAO, D., TAKAHASHI, M., Modeling long-term volcanic hazards through Bayesian inference: An example from the Tohoku volcanic arc, Japan, Journal of Geophysical Research **109** B10 (2004) B10208.
[36] KIMURA, J.I., YOSHIDA, T., Contributions of slab fluid, mantle wedge and crust to the origin of Quaternary lavas in the NE Japan arc., Journal of Petrology **47** 11 (2006) 2185–2232.
[37] SHAW, H.R., Links between magma - tectonic rate balances, plutonism, and volcanism, Journal of Geophysical Research **90** B13 (1985) 11275–11288.
[38] MELNIK, O., SPARKS, R.S., Nonlinear dynamics of lava dome extrusion, Nature **402** 6757 (1999) 37–41.
[39] BLUNDY, J., CASHMAN, K., HUMPHREYS, M., Magma heating by decompression - driven crystallization beneath andesite volcanoes, Nature **443** 7107 (2006) 76–80.
[40] SCANDONE, R., CASHMAN, K.V., MALONE, S.D., Magma supply, magma ascent and the style of volcanic eruptions, Earth and Planetary Science Letters **253** 3 (2007) 513–529.
[41] DELIGNE, N.I., COLES, S.G., SPARKS, R.S., Recurrence rates of large explosive volcanic eruptions, Journal of Geophysical Research **115** B6 (2010) B06203.
[42] CASHMAN, K.V., SPARKS, R.S., How volcanoes work: A 25 year perspective, Geological Society of America Bulletin **125** 5–6 (2013) 664–690.
[43] PARDO, N., MACIAS, J.L., GIORDANO, G., CIANFARRA, P., AVELLÁN, D.R., BELLATRECCIA, F., The ~1245 yr BP Asososca maar eruption: The youngest event along the Nejapa - Miraflores volcanic fault, Western Managua, Nicaragua, Journal of Volcanology and Geothermal Research **184** 3 (2009) 292–312.

[44] AVELLÁN, D.R., MACÍAS, J.L., PARDO, N., SCOLAMACCHIA, T., RODRIGUEZ, D., Stratigraphy, geomorphology, geochemistry and hazard implications of the Nejapa Volcanic Field, western Managua, Nicaragua, Journal of Volcanology and Geothermal Research **213** (2012) 51–71.
[45] Chernyshev, I.V., Lebedev, V.A., Arakelyants, M.M., Jrbashyan, R.T., Ghukasyan, Y.G., Geochronology of the Aragats volcanic centre, Armenia: Evidence from K-Ar dating, Doklady Earth Sciences **184** (2002) 393–398.
[46] SUN, S.S., MCDONOUGH, W., "Chemical and isotopic systematics of oceanic basalts: implications for mantle composition and processes", Magmatism in the Ocean Basins, Geological Society Special Publication No. 42 (SAUNDERS, A.D., NORRY, M.J., Eds), Geological Society of London, London (1989) 313–345.
[47] PEARCE, J.A., "Role of the sub-continental lithosphere in magma genesis at active continental margins", Continental Basalts and Mantle Xenoliths, U.K, Shiva, Cheshire (2003) 230–249.
[48] MCDONOUGH, W.F., Partial melting of subducted oceanic crust and isolation of its residual eclogitic lithology, Philosophical Transactions: Physical Sciences and Engineering **335** 1638 (1991) 407–418.
[49] PEARCE, J.A., BENDER, J.F., DELONG, S.E., KIDD, W.S., LOW, P.J., GUNER, Y., SARGOLU, F., YILMAZ, Y., MOORBATH, S., MITCHELL, J.G., Genesis of collision volcanism in eastern Anatolia, Turkey, Journal of Volcanology and Geothermal Research **44** 1–2 (1990) 189–229.
[50] NOTSU, K.T., FUJITANI, T.U., MATSUDA, J., ERCAN, T., Geochemical features of collision-related volcanic rocks in central and eastern Turkey, Journal of Volcanology and Geothermal Research **64** 3–4 (1995) 171–192.
[51] KAHL, M., CHAKRABORTY, S., COSTA, F., POMPILIO, M., Dynamic plumbing system beneath volcanoes revealed by kinetic modeling, and the connection to monitoring data: An example from Mt. Etna, Earth and Planetary Science Letters **308** 1–2 (2011) 11–22.
[52] KAHL, M., CHAKRABORTY, S., COSTA, F., POMPILIO, M., LIUZZO, M., VICCARO, M., Compositionally zoned crystals and real-time degassing data reveal changes in magma transfer dynamics during the 2006 summit eruptions of Mt. Etna, Bulletin of Volcanology **75** (2013) 692.
[53] DRUITT, T.H., COSTA, F., DELOULE, E., DUNGAN, M., SCAILLET, B., Decadal to monthly timescales of magma transfer and reservoir growth at a caldera volcano, Nature **482** 7383 (2012) 77–80.
[54] COSTA, F., ANDREASTUTI, S., BOUVET DE MAISONNEUVE, C., PALLISTER, J.S., Petrological insights into the storage conditions, and magmatic processes that yielded the centennial 2010 Merapi explosive eruption, Journal of Volcanology and Geothermal Research **261** (2013) 209–235.
[55] LUHR, J.F., Petrology and geochemistry of the 1991 and 1998–1999 lava flows from Volcán de Colima, México: implications for the end of the current eruptive cycle, Journal of Volcanology and Geothermal Research **117** (2002) 169–194.
[56] WILCOX, R.E., Petrology of Parícutin Volcano, México, Geological Survey Bulletin **965C** (1954) 281–353.
[57] CASHMAN, K.V., TAGGERT, J.E., Petrologic monitoring of 1981 and 1982 eruptive products from Mount St. Helens, Science **221** (1983) 1385–1387.
[58] MELSON, W.G., Monitoring the 1980–1982 eruptions of Mount St. Helens: Compositions and abundances of glass, Science **221** (1983) 1387–1391.

[59] CAMUS, G., GOURGAUD, A., VINCENT, P.M., Petrologic evolution of Krakatau (Indonesia): implications for a future activity, Journal of Volcanology and Geothermal Research **33** (1987) 299–316.
[60] MCBIRNEY, A.R., TAYLOR, H.P., ARMSTRONG, R.L., Parícutin re-examined: A classic example of crustal assimilation in calc-alkaline magma, Contributions to Mineralogy and Petrology **95** 1 (1987) 4–20.
[61] REAGAN, M.K., GILL, J.C., MALAVASSI, E., GARCIA, M.O., Changes in magma composition at Arenal Volcano, Costa Rica, 1968–1985: Real-time monitoring of open-system differentiation, Bulletin of Volcanology **49** (1987) 415–434.
[62] LUHR, J.F., CARMICHAEL, I.S., Petrological monitoring of cyclical eruptive activity at Volcán Colima, México, Journal of Volcanology and Geothermal Research **42** (1990) 235–260.
[63] FEDOTOV, S.A., BALESTA, S.T., DVIGALO, V.N., RAZINA, A.A., FLEROV, G.B., CHIRKOV, A.M., "New Tolbachik volcanoes", Active Volcanoes of Kamchatka (FEDOTOV, S.A., MASURENKOV, Y.P., Eds), Nauka Publishers, Moscow (1991) 275–279.
[64] PALLISTER, J.S., HOBLITT, R.P., CRANDELL, D.R., MULLINEAUX, D.R., Helens a decade after the 1980 eruptions: Magmatic models, chemical cycles, and a revised hazards assessment, Bulletin of Volcanology **54** (1992) 126–146.
[65] PALLISTER, J.S., HOBLITT, R.P., MEEKER, G.P., KNIGHT, R.J., SIEMS, D.F., "Magma mixing at Mount Pinatubo: Petrographic and chemical evidence from the 1991 deposits", Fire and Mud: Eruptions and Lahars of Mount Pinatubo, Philippines (NEWHALL, C.G., PUNONGBAYAN, R.S., Eds), Philippine Institute of Volcanology and Seismology / University of Washington Press, Quezon City / Seattle,WA (1996) 687–731.
[66] CORSARO, R.A., CRISTOFOLINI, R., Origin and differentiation of recent basaltic magmas from Mount Etna, Contributions to Mineralogy and Petrology **57** (1996) 1–21.
[67] GAMBLE, J.A., WOOD, C.P., PRICE, R.C., SMITH, I.E., STEWART, R.B., WAIGHT, T., A fifty year perspective of magmatic evolution on Ruapehu Volcano, New Zealand: Verification of open system behaviour in an arc volcano, Earth and Planetary Science Letters **170** (1999) 301–314.
[68] HOBDEN, B.J., HOUGHTON, B.F., DAVIDSON, J.P., WEAVER, S.D., Small and short-lived magma batches at composite volcanoes: time windows at Tongariro volcano, New Zealand, Journal of the Geological Society **156** 5 (1999) 865–868.
[69] PIETRUSZKA, A.J., GARCIA, M.O., A Rapid Fluctuation in the Mantle Source and Melting History of Kilauea Volcano Inferred from the Geochemistry of its Historical Summit Lavas (1790–1982), Journal of Petrology **40** 8 (1999) 1321–1342.
[70] MARTEL, C., BOURDIER, J.L., PICHAVANT, M., TRAINEAU, H., Textures, water content and degassing of silicic andesites from recent plinian and dome-forming eruptions at Mount Pelee volcano (Martinique, Lesser Antilles arc), Journal of Volcanology and Geothermal Research **96** (2000) 191–206.
[71] BRETÓN, M., RAMÍREZ, J.J., NAVARRO, C., Summary of the historical eruptive activity of Volcán de Colima, México: 1519–2000, Journal of Volcanology and Geothermal Research **117** 1–2 (2002) 21–46.
[72] SAUCEDO, R., MACÍAS, J., GAVILANEZ, J., ARCE, J., KOMOROWSKI, J., GARDNER, J., VALDEZ-MORENO, G., Eyewitness, stratigraphy, chemistry, and eruptivedynamics of the 1913 Plinian eruption of Volcán de Cólima, México., Journal of Volcanology and Geothermal Research **101** (2010) 149–166.

[73] LUHR, J.F., CARMICHAEL, I.S., The Colima Volcanic Complex, México: Part I. Post-caldera andesites from Volcán Colima, Contributions to Mineralogy and Petrology **71** (1980) 343–372.
[74] LUHR, J.F., NAVARRO-OCHOA, C., SAVOV, I.P., Tephrochronology, petrology and geochemistry of Late-Holocene pyroclastic deposits from Volcán de Colima, Mexico, Journal of Volcanology and Geothermal Research **179** 1–4 (2010) 1–32.
[75] WOODS, A.W., KOYAGUCHI, T., Transitions between explosive and effusive eruptions of silicic magmas, Nature **370** (1994) 641–644.
[76] ROGGENSACK, K., HERVIG, R.L., MCKNIGHT, S.B., Williams, S.N., Explosive basaltic volcanism from Cerro Negro volcano: Influence of volatiles on eruptive style, Science **227** (1997) 1639–1642.
[77] SIGURDSSON, H., HOUGHTON, B., RYMER, H., STIX, J., MCNUTT, S., Encyclopedia of Volcanoes, 1st Edition, Academic Press, San Diego (1999).
[78] SCHMINCKE, H.U., Volcanism, Springer, Berlin (2005).
[79] PARFITT, L., WILSON, L., Fundamentals of Physical Volcanology, Wiley-Blackwell, London (2008).
[80] BEBBINGTON, M.S., LAI, C.D., Statistical analysis of New Zealand volcanic occurrence data, Journal of Volcanology and Geothermal Research **74** 1–2 (1996) 101–110.
[81] HILL, B.E., CONNOR, C.B., JARZEMBA, M.S., LA FEMINA, P.C., NAVARRO, M., STRAUCH, W., 1995 eruptions of Cerro Negro volcano, Nicaragua, and risk assessment for future eruptions, Geological Society of America Bulletin **110** 10 (1998) 1231–1241.
[82] CRONIN, S.J., BEBBINGTON, M., LAI, C., A probabilistic assessment of eruption recurrence on Taveuni volcano, Fiji, Bulletin of Volcanology **63** 4 (2001) 274–288.
[83] HO, C.H., Empirical recurrence rate time series for volcanism: Application to Avachinsky volcano, Russia, Journal of Volcanology and Geothermal Research **173** 1 (2008) 15–25.
[84] TURNER, M.B., CRONIN, S.J., BEBBINGTON, M.S., PLATZ, T., Developing probabilistic eruption forecasts for dormant volcanoes: a case study from Mt. Taranaki, New Zealand, Bulletin of Volcanology **70** 4 (2008) 507–515.
[85] MARZOCCHI, W., BEBBINGTON, M.S., Probabilistic eruption forecasting at short and long time scales, Bulletin of volcanology **74** 8 (2012) 1777–1805.
[86] HO, C.H., Nonhomogeneous Poisson model for volcanic eruptions, Mathematical Geology **23** 2 (1991) 167–173.
[87] HO, C.H., Risk assessment for the Yucca Mountain high-level nuclear waste repository site: estimation of volcanic disruption, Mathematical Geology **24** 4 (1992) 347–364.
[88] HO, C.H., SMITH, E.I., FEUERBACH, D.L., NAUMANN, T.R., Eruptive probability calculation for the Yucca Mountain site, USA: statistical estimation of recurrence rates, Bulletin of Volcanology **54** 1 (1991) 50–56.
[89] CROWE, B.M., MORLEY, R., WELLS, S., GEISSMAN, J., MCDONALD, E., MCFADDEN, L., PERRY, F.V., MURRELL, M., POTHS, J., FORMAN, S., "The Lathrop Wells volcanic center, status of field and geological studies," Proceedings of the Third International High-Level Radioactive Waste Management Conference, Los Alamos National Laboratory, Los Alamos, NM, (1992) LA-UR-92-534.
[90] CONNOR, C.B., HILL, B.E., Three nonhomogeneous Poisson models for the probability of basaltic volcanism: Application to the Yucca Mountain region, Journal of Geophysical Research **100** B6 (1995) 107–125.

[91] MARTIN, A., TAKAHASHI, M., UMEDA, K., YUSA, Y., Probabilistic methods for estimating the long-term spatial characteristics of monogenetic volcanoes in Japan, Acta Geophysica Polonica **51** 3 (2003) 271–291.
[92] BEBBINGTON, M., CRONIN, S.J., Spatio-temporal hazard estimation in the Auckland Volcanic Field, New Zealand, with a new event-order model, Bulletin of Volcanology **73** 1 (2011) 55–72.
[93] YAMAMOTO, T., Safety assessment of high-level nuclear waste disposal in Japan from the standpoint of geology, Synthesiology **4** 4 (2011) 200–208.
[94] INTERNATIONAL ATOMIC ENERGY AGENCY, External Events excluding Earthquake in the Design of Nuclear Power Plants, IAEA Safety Standards Series No. NS-G-1.5, IAEA, Vienna (2003).
[95] BEBBINGTON, M.S., Models for Temporal Volcanic Hazard, Statistics in Volcanology **1** (2013) 1–24.
[96] BACON, C.R., Time-predictable bimodal volcanism in the Coso Range, California, Geology **10** 2 (1982) 65–69.
[97] CONNOR, C.B., MCBIRNEY, A.R., FURLAN, C., "What is the probability of explosive eruption at a long-dormant volcano?", IAV001 Statistics in Volcanology, Special Publications of IAVCEI (MADER, H.M., COLES, S.G., CONNOR, C.B., CONNOR, L.J., Eds), Geological Society of London, London (2006) 39–48.
[98] MCBIRNEY, A.R., SERVA, L., GUERRA, M., CONNOR, C.B., Volcanic and seismic hazards at a proposed nuclear power site in central Java, Journal of Volcanology and Geothermal Research **126** 1 (2003) 11–30.
[99] DRUITT, T.H., MELLORS, R., PYLE, D.M., SPARKS, R.S., Explosive volcanism on Santorini, Greece, Geological Magazine **126** 2 (1989) 95–126.
[100] LUHR, J., CARMICHAEL, I., The Colima volcanic complex, Mexico, Contributions to Mineralogy and Petrolog **71** 4 (1980) 343–372.
[101] CONDIT, C.D., CONNOR, C.B., Recurrence rates of volcanism in basaltic volcanic fields: An example from the Springerville volcanic field, Arizona, Geological Society of America Bulletin **108** 10 (1996) 1225–1241.
[102] KOMOROWSKI, J.C., JENKINS, S., BAXTER, P.J., PICQUOUT, A., LAVIGNE, F., CHARBONNIER, S., GERTISSER, R., PREECE, K., CHOLIK, N., BUDI-SANTOSO, A., Paroxysmal dome explosion during the Merapi 2010 eruption: Processes and facies relationships of associated high-energy pyroclastic density currents, Journal of Volcanology and Geothermal Research **261** (2013) 260–294.
[103] CHARBONNIER, S.J., GERMA, A., CONNOR, C.B., GERTISSER, R., PREECE, K., KOMOROWSKI, J.C., LAVIGNE, F., CONNOR, L., "Evaluation of the impact of the 2010 pyroclastic density currents at Merapi volcano from high-resolution satellite imagery, field investigations and numerical simulations.", Journal of Volcanology and Geothermal Research **261** (2013) 295–315.
[104] EBASCO, Evidence substantiating the incredibility of volcanism on the west flank of mt. natib, and the assessment of volcanic hazards at the natib point, Response to the philippine atomic energy commission question 3., Philippine Atomic Energy Commission, Manila (1979).
[105] CABATO, M.J., RODOLFO, K.S., SIRINGAN, F.P., History of sedimentary infilling and faulting in Subic Bay, Philippines revealed in high-resolution seismic reflection profiles, Journal of Asian Earth Sciences **25** 6 (2005) 849–858.
[106] VOLENTIK, A.C., CONNOR, C.B., CONNOR, L.J., BONADONNA, C., "Aspects of volcanic hazards assessment for the Bataan nuclear power plant, Luzon Peninsula, Philippines", Volcanic and Tectonic Hazard Assessment for Nuclear Facilities

(Connor, C.B., Chapman, N.A., Connor, L.J., Eds), Cambridge University Press, Cambridge (2009) 229–256.
[107] LAGMAY, A.M., RODOLFO, R., CABRIA, H., SORIA, J., ZAMORA, P., ABON, C., LIT, C., LAPUS, M.R., PAGUICAN, E., BATO, M.G., TIU, G., OBILLE, E., PELLEJERA, N.E., FRANCISCO, P.C., ECO, R.N., AVISO, J., "Geological hazards of SW Natib volcano, site of the Bataan Nuclear Power Plant, the Philippines", Natural Hazards in the Asia–Pacific Region: Recent Advances and Emerging Concepts, Geological Society Special Publication No. 361 (TERRY, J.P., GOFF, J., Eds), Geological Society of London, London (2012) 151–169.
[108] KIYOSUGI, K., CONNOR, C.B., SPARKS, R.S., SIEBERT, H.S., TAKARADA, S., "How many explosive eruptions are missing from the geologic record? Analysis of the Quaternary record of large magnitude explosive eruptions in Japan", American Geophysical Union, Washington, DC, 2010 (abstract).
[109] NOWELL, D.A., JONES, M.C., PYLE, D.M., Episodic Quaternary volcanism in France and Germany, Journal of Quaternary Science **21** 6 (2006) 645–675.
[110] DZIERMA, Y., WEHRMANN, H., Eruption time series statistically examined: Probabilities of future eruptions at Villarrica and Llaima volcanoes, southern volcanic zone, Chile, Journal of Volcanology and Geothermal Research **193** 1 (2010) 82–92.
[111] PYLE, D.M., Forecasting sizes and repose times of future extreme volcanic events, Geology **26** 4 (1998) 367–370.
[112] SIMKIN, T., SIEBERT, L., "Earths volcanoes and eruptions: An overview", Encyclopedia of Volcanoes, 1st Edition (SIGURDSSON, H., HOUGHTON, B., RYMER, H., STIX, J., MCNUTT, S., Eds), Academic Press, San Diego (1999) 249–262.
[113] WATT, S.F., PYLE, D.M., MATHER, T.A., MARTIN, R.S., MATTHEWS, N.E., Fallout and distribution of volcanic ash over Argentina following the May 2008 explosive eruption of Chaitén, Chile, Journal of Geophysical Research **114** B4 (2009) B04207.
[114] LARA, L.E., MORENO, R., AMIGO, A., HOBLITT, R.P., PIERSON, T.C., Late Holocene history of Chaiten volcano: New evidence for a 17th Century eruption, Andean Geology **40** 2 (2013) 249–261.
[115] LE FRIANT, A., LOCK, E.J., HART, M.B., BOUDON, G., SPARKS, R.S., LENG, M.J., SMART, C.W., KOMOROWSKI, J.C., DEPLUS, C., FISHER, K., Late Pleistocene tephrochronology of marine sediments adjacent to Montserrat, Lesser Antilles volcanic arc., Journal of the Geological Society **165** (2008) 279–289.
[116] BOUDON, G., KOMOROWSKI, J.C., VILLEMANT, B., SEMET, M.P., A new scenario for the last magmatic eruption of La Soufrière de Guadeloupe (Lesser Antilles) in 1530 A.D.: evidence from stratigraphy, radiocarbon dating and magmatic evolution of erupted products, Journal of Volcanology and Geothermal Research **178** (2008) 474–490.
[117] KIYOSUGI, K., CONNOR, C.B., An algorithm for estimating recurrence rate of volcanic events accounting for uncertainties in the geologic record, Statistics in Volcanology (2013) (in press).
[118] VALENTINE, G.A., PERRY, F.V., Decreasing magmatic footprints of individual volcanoes in a waning basaltic field, Geophysical Research Letters **33** 14 (2006) L14305.
[119] VARLEY, N., JOHNSON, J., RUIZ, M., REYES, G., MARTIN, K., "Applying statistical analysis to understanding the dynamics of volcanic explosions", IAV001 Statistics in Volcanology, Special Publications of IAVCEI (MADER, H.M., COLES,

S.G., CONNOR, C.B., CONNOR, L.J., Eds), Geological Society of London, London (2006) 57–76.
[120] CONNOR, C.B., SPARKS, R.S. MASON, R.M., BONADONNA, C., YOUNG, S.R., Exploring links between physical and probabilistic models of volcanic eruptions: The Soufrıère Hills Volcano, Montserrat, Geophysical Research Letters **30** 13 (2003) 1701–1704.
[121] MENDOZA-ROSAS, A.T., DE LA CRUZ-REYNA, S., A statistical method linking geological and historical eruption time series for volcanic hazard estimations: applications to active polygenetic volcanoes, Journal of Volcanology and Geothermal Research **176** 2 (2008) 277–290.
[122] JAQUET, O., CARNIEL, R., "Estimation of volcanic hazards using geostatistical models", IAV001 Statistics in Volcanology, Special Publications of IAVCEI (MADER, H.M., COLES, S.G., CONNOR, C.B., CONNOR, L.J., Eds), Geological Society of London, London (2006) 89–103.
[123] JAQUET, O., CONNOR, C.B., CONNOR, L.J., Probabilistic methodology for long-term assessment of volcanic hazards, Nuclear technology **163** 1 (2008) 180–189.
[124] FLECK, R.J., TURRIN, B.D., SAWYER, D.A., WARREN, R.G., CHAMPION, D.E., HUDSON, M.R., MINOR, S.A., Age and character of basaltic rocks of the Yucca Mountain region, southern Nevada, Journal of Geophysical Research **101** B4 (1996) 8205–8227.
[125] TURRIN, B.D., CHAMPION, D., FLECK, R.J., $^{40}Ar/^{39}Ar$ age of the Lathrop Wells volcanic center, Yucca Mountain, Nevada, Science **253** 5020 (1991) 654–657.
[126] TURRIN, B.D., CHAMPION, D.E., FLECK, R.J., Measuring the age of the Lathrop Wells volcanic center at Yucca Mountain: Response to comment on $^{40}Ar/^{39}Ar$ age of the Lathrop Wells volcanic center, Yucca Mountain, Nevada, Science **257** 5069 (1992) 556–558.
[127] PERRY, F.V., BOWKER, L.M., "Petrologic and geochemical constraints on basaltic volcanism in the Great Basin", Volcanic Hazard Assessment for the Yucca Mountain Project, LA-13478, Los Alamos National Laboratory, Los Alamos, NM (1998) 554.
[128] HEIZLER, M.T., PERRY, F.V., CROWE, B.M., PETERS, L., APPELT, R., The age of Lathrop Wells volcanic center: An 40Ar/39Ar dating investigation, Journal of Geophysical Research **104** B1 (1999) 767–804.
[129] POTHS, J., PERRY, F.V., CROWE, B.M., ^{3}He surface exposure ages at the Lathrop Wells, NV, volcanic center, Los Alamos National Laboratory, Los Alamos, NM (1994).
[130] ZREDA, M.G., PHILLIPS, F.M., KUBIK, P.W., SHARMA, P., ELMORE, D., Cosmogenic ^{36}Cl dating of a young basaltic eruption complex, Lathrop Wells, Nevada, Geology **21** 1 (1993) 57–60.
[131] CHERNYSHEV, I., LEBEDEV, V., ARAKELYANTS, M., K-Ar dating of Quaternary volcanics: methodology and interpretation of results, Petrology **14** (2006) 62–80.
[132] NEWHALL, C.G., HOBLITT, R.P., Constructing event trees for volcanic crises, Bulletin of Volcanology **64** (2002) 3–20.
[133] NERI, A., ASPINALL, W.P., CIONI, R., BERTAGNINI, A., BAXTER, P.J., ZUCCARO, G., ANDRONICO, D., COLE, P.D., ESPOSTI ONGARO, T., HINCKS, T.K., MACEDONIO, G., PAPALE, P., ROSI, M., SANTACROCE, R., WOO, R., Developing an event tree for probabilistic hazard and risk assessment at Vesuvius, Journal of Volcanology and Geothermal Research **178** (2008) 397–415.

[134] LEWIS-KENNEDY, C.B., LANGE, R.A., HALL, C.M., DELGADO-GRANADOS, H., The eruptive history of the Tequila volcanic field, western Mexico: ages, volumes and relative proportions of lava types, Bulletin Volcanologique **67** (2005) 391–414.
[135] BAXTER, P.J., NERI, A., BLONG, R., Evaluating explosive eruption risk at European volcanoes, Journal of Volcanology and Geothermal Research **178** 3 (2008) 5–9.
[136] BUDNITZ, R.J., APOSTOLAKIS, G., BOORE, D.M., CLUFF, L.S., COPPERSMITH, K.J., CORNELL, C.A., MORRIS, R.A., Recommendations for Probabilistic Seismic Hazard Analysis: Guidance on Uncertainty and Use of Experts, Vol. 2, NUREG/CR-6372 / UCRL-ID- 122160, NRC / LLNL, Washington, DC / LLNL, Livermore, CA (1997).
[137] ABRAHAMSON, N.A., COPPERSMITH, K.J., KOLLER, M., ROTH, P., SPRECHER, C., TORO, G.R., YOUNGS, R., Probabilistic Seismic Hazard Analysis for Swiss Nuclear Power Plant Sites (PEGASOS project), Final Report, Nationale Genossenschaft für die Lagerung radioaktiver Abfälle, Wettingen, Switzerland (2004).
[138] COPPERSMITH, K.J., SALOMONE, L.A., FULLER, C.W., GLASER, L.L., HANSON, K.L., HARTLEB, R.D., LETTIS, W.R., LINDVALL, S.C., MCDUFFIE, S.M., MCGUIRE, R.K., STIREWALT, G.L., TORO, G.R., YOUNGS, R.R., SLAYTER, D.L., BOZKURT, S.B., CUMBEST, R.J., FALERO, V.M., PERMAN, R.C., SHUMWAY, A.M., SYMS, F.H., TUTTLE, M.P., Central and Eastern United States Seismic Source Characterization for Nuclear Facilities, NUREG-2115 / DOE/NE-0140 / EPRI 1021097, NRC / DOE / EPRI, Washington DC / Washington DC / Palo Alto, CA (2012)
[139] ORESKES, N., SCHRADER-FRECHETTE, K., BELITZ, K., Verification, validation, and confirmation of numerical models in the Earth Sciences, Science **263** 5147 (1994) 641–646.
[140] HILL, B.E., ASPINALL, W.P., CONNOR, C.B., GODOY, A.R., "Recommendations for assessing volcanic hazards at sites of nuclear installations", Volcanic and Tectonic Hazard Assessment for Nuclear Facilities (Connor, C.B., Chapman, N.A., Connor, L.J., Eds), Cambridge University Press, Cambridge (2009) 566–5592.
[141] FEDOTOV, S.A. (Eds), The Great Tolbachik Fissure Eruption: Geological and Geophysical Data, 1975–1976, Nauka, Moscow (1984) (in Russian).
[142] CROWE, B.M., JOHNSON, M.E., BECKMAN, R.J., Calculation of the probability of volcanic disruption of a high-level radioactive waste repository in southern Nevada, USA, Radioactive Waste Management **3** (1982) 167–190.
[143] CONNOR, C.B., STAMATAKOS, J.A., FERRILL, D.A., HILL, B.E., OFOEGBU, G.I., CONWAY, M.F., SAGAR, B., TRAPP, J., Geologic factors controlling patterns of small-volume basaltic volcanism: Application to a volcanic hazards assessment at Yucca Mountain, Nevada, Journal of Geophysical Research **105** 1 (2000) 417–432.
[144] KUNTZ, M.A., CHAMPION, D.E., SPIKER, E.C., LEFEBVRE, R.H., Contrasting magma types and steady-state, volume-predictable, basaltic volcanism along the Great Rift, Idaho, Geological Society of America Bulletin **97** 5 (1986) 579–594.
[145] WETMORE, P.H., HUGHES, S.S., CONNOR, L.J., CAPLINGER, M.L., "Spatial distribution of eruptive centers about the Idaho National Laboratory," Volcanic and Tectonic Hazard Assessment for Nuclear Facilities (Connor, C.B., Chapman, N.A., Connor, L.J., Eds), Cambridge University Press, Cambridge (2009) 385–405.
[146] CAPPELLO, A., VICARI, A., DEL NEGRO, C., Retrospective validation of a lava flow hazard map for Mount Etna volcano, Annals of Geophysics **54** 5 (2011) 634–640.

[147] FUJITA, E., KOZONO, T., UEDA, H., KOHNO, Y., YOSHIOKA, S., TODA, T., KIKUCHI, A., IDA, Y., Stress field change around the Mount Fuji volcano magma system caused by the Tohoku megathrust earthquake, Japan, Bulletin of Volcanology **75** (2013) 1–14.
[148] KIYOSUGI, K., CONNOR, C.B., ZHAO, D., CONNOR, L.J., TANAKA, K., Relationships between volcano distribution, crustal structure, and P-wave tomography: an example from the Abu Monogenetic Volcano Group, SW Japan, Bulletin of volcanology **72** 3 (2010) 331–340.
[149] KIYOSUGI, K., CONNOR, C.B., WETMORE, P.H., FERWERDA, B.P., GERMA, A.M., CONNOR, L.J., HINTZ, A.R., Relationship between dike and volcanic conduit distribution in a highly eroded monogenetic volcanic field: San Rafael, Utah, USA, Geology **40** 8 (2012) 695–698.
[150] MARSH, B.D., Island arc development: some observations, experiments, and speculations, Journal of Geology **87** (1979) 687–713.
[151] BREMOND D'ARS, J., JAUPART, C., SPARKS, R.S., Distribution of volcanoes in active margins, Journal of Geophysical Research **100** B10 (1995) 20421–20432.
[152] CONNOR, C.B., CONDIT, C.D., CRUMPLER, L.S., AUBELE, J.C., Evidence of regional structural controls on vent distribution, Springerville volcanic field, Arizona, Journal of Geophysical Research **97** (1992) 349–359.
[153] LUTZ, T.M., GUTMANN, J.T., An improved method of determining alignments of point-like features and its implications for the Pinacate volcanic field, Mexico, Journal of Geophysical Research **100** 17 (1995) 659–670.
[154] CONDER, J.A., WIENS, D.A., MORRIS, J., On the decompression melting structure at volcanic arcs and back-arc spreading centers, Geophysical Research Letters **29** 15 (2002) 17-1–17-4.
[155] DIGGLE, P.J., A kernel method for smoothing point process data, Applied Statistics **34** (1985) 138–147.
[156] DIGGLE, P., MARRON, J.S., Equivalence of smoothing parameter selectors in density and intensity estimation, Journal of the American Statistical Association **83** 403 (1988) 793–800.
[157] GATRELL, A.C., BAILEY, T.C., DIGGLE, P.J., ROWLINGSON, B.S., Spatial point pattern analysis and its application in geographical epidemiology, Transactions of the Institute of British geographers **21** (1996) 256–274.
[158] CONNOR, C.B., LANE-MAGSINO, S., STAMATAKOS, J.A., MARTIN, R.H., LAFEMINA, P.C., HILL, B.E., LIEBER, S., Magnetic surveys help reassess volcanic hazards at Yucca Mountain, Nevada, Eos, Transactions American Geophysical Union **78** 7 (1997) 73–78.
[159] SILVERMAN, B.W., Weak and strong uniform consistency of the kernel estimate of a density and its derivatives, The Annals of Statistics **6** 1 (1978) 177–184.
[160] SILVERMAN, B.W., Density Estimation for Statistics and Data Analysis, Chapman and Hall, New York (1986).
[161] WAND, M.P., JONES, M.C., Kernel Density Estimation, Chapman and Hall, New York (1999).
[162] WOO, G., Kernel estimation methods for seismic hazard source modeling, Bulletin of the Seismological Society of America **86** (1996) 353–362.
[163] STOCK, C., SMITH, E.G., Adaptive kernel estimation and continuous probability representation of historical earthquake catalogs, Bulletin of the Seismological Society of America **92** 3 (2002) 904–912.
[164] DUONG, T., Kernel density estimation and kernel discriminant analysis for multivariate data in R, Journal of Statistical Software **21** 7 (2007) 1–16.

[165] DUONG, T., HAZELTON, M., Plug-in bandwidth matrices for bivariate kernel density estimation, Journal of Nonparametric Statistics **15** 1 (2003) 17–30.
[166] HALL, P., MARRON, J.S., PARK, B.U., Smoothed cross-validation, Probability Theory and Related Fields **92** 1 (1992) 1–20.
[167] HORNIK, K., R FAQ, Frequently Asked Questions on R, ISBN 3-901167-51-X (2003), http://www.mlb.co.jp/linux/science/R/doc/html/faq.html
[168] CONNOR, C.B., CONNOR, L.J., "Estimating spatial density with kernel methods", Volcanic and Tectonic Hazard Assessment for Nuclear Facilities (Connor, C.B., Chapman, N.A., Connor, L.J., Eds), Cambridge University Press, Cambridge (2009) 346–368.
[169] MAGILL, C., BLONG, R., Volcanic risk ranking for Auckland, New Zealand, I: Methodology and hazard investigation, Bulletin of Volcanology **67** 4 (2005) 331–339.
[170] FUDALI, R.F., MELSON, W.G., Ejecta velocities, magma chamber pressure and kinetic energy associated with the 1968 eruption of Arenal volcano, Bulletin of Volcanology **35** 2 (1972) 383–401.
[171] SELF, S., KIENLE, J., HUOT, J., UkinrekMaars, Alaska, II. Deposits and formation of the 1977 Craters, Journal of Volcanology and Geothermal Research **7** 1–2 (1980) 39–65.
[172] STEINBERG, G.S., LORENZ, V., External ballistic of volcanic explosions, Bulletin of Volcanology **46** 4 (1983) 333–348.
[173] WAITT, R.B., MASTIN, L.G., MILLER, T.P., "Ballistic showers during crater peak eruptions of Mount Spurr volcano, summer 1992", The 1992 Eruptions of Crater Peak Vent, Mount Spurr Volcano, Alaska, U.S. Geological Survey Bulletin 2139 (KEITH, T.E.C., Eds), United States Government Printing Office, Washington, WA (1995) 89–106.
[174] ALATORRE-IBARGÜENGOITIA, M.A., DELGADO-GRANADOS, H., Experimental determination of drag coefficient for volcanic materials: calibration and application of a model to Popocatépetl volcano (Mexico) ballistic projectiles, Geophysical Research Letters **33** 11 (2006) L11302.
[175] ALATORRE-IBARGÜENGOITIA, M.A., DELGADO-GRANADOS, H., DINGWELL, D.B., Hazard Map for Volcanic Ballistic Impacts at Popocatépetl Volcano (Mexico), Bulletin of Volcanology **74** 9 (2012) 2155–2169.
[176] FAGENTS, S.A., WILSON, L., Explosive volcanic eruptions - VII. The ranges of pyroclasts ejected in transient volcanic explosions, Geophysical Journal International **113** 2 (1993) 359–370.
[177] BOWER, S.M., WOODS, A.W., On the dispersal of clasts from volcanic craters during small explosive eruptions, Journal of Volcanology and Geothermal Research **73** 1–2 (1996) 19–32.
[178] BLONG, R.J., Volcanic Hazards: A Sourcebook on the Effects of Eruptions, Academic Press, Sydney (1984).
[179] ALATORRE IBARGÜENGOITIA, M.A., DELGADO GRANADOS, H., FARRAZ MONTES, I.A., Determination of hazard zones by ballistic products fall during volcanic explosions at Volcán de Fuego de Colima (Mexico), In: Neogene-Quaternary Continental Margin Volcanism: A perspective from Mexico, Geological Society of America, Special Paper **402** (2006) 209–216.
[180] GLOBAL VOLCANISM PROGRAM, Sakurajima, explosions remain frequent; tephra from one explosion damages houses and cars, Bulletin of the Global Volcanism Network **16** 6 (1991).

[181] GLOBAL VOLCANISM PROGRAM, Stromboli. Strong explosion on 5 April covers much of the summit in pyroclastic deposits, Bulletin of the Global Volcanism Network **28** 4 (2003).
[182] GLOBAL VOLCANISM PROGRAM, Masaya tourists experience a brief, bomb-charged 23 April 2001 explosion: no fatalities, Bulletin of the Global Volcanism Network **26** 4 (2001).
[183] DELGADO-GRANADOS, H., CÁRDENAS GONZÁLEZ, L., PIEDAD SÁNCHEZ, N., Sulfur dioxide emissions from Popocatépetl volcano (Mexico): case study of a high-emission rate, passively degassing erupting volcano, Journal of Volcanology and Geothermal Research **108** 1–4 (2001) 107–120.
[184] ZOBIN, V.M., LUHR, J.F., TARAN, Y.A., BRETÓN, M., CORTÉS, A., DE LA CRUZ-REYNA, S., DOMÍNGUEZ, T., GALINDO, I., GAVILANES, J.C., MUÑÍZ, J.J., NAVARRO, C., RAMÍREZ, J.J., REYES, G.A., URSÚA, M., VELASCO, J., ALATORRE, E., SANTIAGO, H., Overview of the 1997–2000 activity of Volcán de Colima, México, Journal of Volcanology and Geothermal Research **117** 1–2 (2001) 1–19.
[185] WARDMAN, J., SWORD-DANIELS, V., STEWART, C., WILSON, T., Impact assessment of the May 2010 eruption of Pacaya volcano, Guatemala, GNS Science Report, 2012/09, Institute of Geological and Nuclear Sciences Limited, Lower Hutt (2012).
[186] NUCLEAR REGULATORY COMMISSION, Design-Basis Tornado and Tornado Missiles for Nuclear Power Plants, Regulatory Guide 1.76, Revision 1, NRC, Washington, DC (2007).
[187] SHERWOOD, A.E., Effect of air drag on particles ejected during explosive cratering, Journal of Geophysical Research **72** 6 (1967) 1783–1791.
[188] WILSON, L., Explosive volcanic eruptions II. The atmospheric trajectories of pyroclasts, Geophysical Journal of the Royal Astronomical Society **30** (1972) 381–392.
[189] MASTIN, L.G., A simple calculator of ballistic trajectories for blocks ejected during volcanic eruptions, U.S. Geological Survey Open-File Report 01–45, USGS, Vancouver, WA (2001).
[190] DE' MICHIELI VITTURI, M., NERI, A., ESPOSTI ONGARO, T., LO SAVIO, S., BOSCHI, E., Lagrangian modeling of large volcanic particles: applica-tions to Vulcanian explosions, Journal of Geophysical Research **115** B8 (2010) B08206.
[191] VANDERKLUYSEN, L., HARRIS, A.J., KELFOUN, K., BONADONNA, C., RIPEPE, M., Bombs behaving badly: unexpected trajectories and cooling of volcanic projectiles, Bulletin of Volcanology **74** 8 (2012) 1849–1858.
[192] SPIELER, O., KENNEDY, B., KUEPPERS, U., DINGWELL, D.B., SCHEU, B., TADDEUCCI, J., The fragmentation threshold of pyroclastic rocks, Earth and Planetary Science Letters **226** (2004) 139–148.
[193] ALATORRE-IBARGÜENGOITIA, M.A., SCHEU, B., DINGWELL, D.B., DELGADO-GRANADOS, H., TADDEUCCI, J., Energy consumption by mag-matic fragmentation and pyroclast ejection during Vulcanian eruptions, Earth and Planetary Science Letters **291** (2010) 60–69.
[194] MACEDONIO, G., COSTA, A., Brief Communication: Rain effect on the load of tephra deposits, Natural Hazards and Earth System Sciences **12** 10 (2012) 1229–1233.
[195] HARRIS, D.M., ROSE, W.J., ROE, R., THOMPSON, M.R., "Radar observations of ash eruptions", The 1980 eruptions of Mount St. Helens, Washington (LIPMAN, P. W., MULLINEAUX, D. R., Eds), U.S. Geological Survey Professional Paper 1250, USGS, Reston, VA (1981) 323–333.

[196] DELMELLE, P., LAMBERT, M., DUFRÊNE, Y., GERIN, P., ÓSKARSSON, O., Gas/aerosol-ash interaction in volcanic plumes: new insights from surface analysis of fine ash particles, Earth and Planetary Science Letters **259** (2007) 159–170.
[197] WITHAM, C.S., OPPENHEIMER, C., HORWELL, C.J., Volcanic ash leachates: a review and recommendations for sampling methods, Journal of Volcanology and Geothermal Research **141** (2005) 299–326.
[198] JONES, M.T., GISLASON, S.R., Rapid releases of metal salts and nutrients following deposition of volcanic ash into aqueous environments, Geochimica et Cosmochimica Acta **72** 15 (2008) 3661–3680.
[199] WARDMAN, J.B., WILSON, T.M., BODGER, P.S., COLE, J.W., JOHNSTON, D., Investigating the electrical conductivity of volcanic ash and its effect on HV power systems, Physics and Chemistry of the Earth **45–46** (2012) 128–145.
[200] WARDMAN, J.B., WILSON, T.M., BODGER, P.S., COLE, J.W., STEWART, C., Potential impacts from tephra fall to electric power systems: a review and mitigation strategies, Bulletin of Volcanology **74** 10 (2012) 2221–2241.
[201] WILSON, T.M., STEWART, C., SWORD-DANIELS, V., LEONARD, G.S., JOHNSTON, D.M., COLE, J.W., WARDMAN, J.B., WILSON, G., BARNARD, S.T., Volcanic ash impacts on critical infrastructure, Physics and Chemistry of the Earth **45–46** (2012) 5–23.
[202] STEWART, C., PIZZOLON, L., WILSON, T., LEONARD, G., DEWAR, D., JOHNSTON, D., CRONIN, S., Can volcanic ash poison water supplies?, Integrated Environmental Assessment and Management **5** 4 (2009) 713–716.
[203] SPENCE, R.J., KELMAN, I., BAXTER, P.J., ZUCCARO. G., PETRAZZUOLI, S., Residential building and occupant vulnerability to tephra fall, Natural Hazards and Earth System Sciences **5** 4 (2005) 477–494.
[204] HANSELL, A.L., HORWELL, C.J., OPPENHEIMER, C., The health hazards of volcanoes and geothermal areas, Occupational and Environmental Medicine **63** 2 (2006) 149–156.
[205] HORWELL, C.J., BAXTER, P.J., The respiratory health hazards of volcanic ash: a review for volcanic risk mitigation, Bulletin of Volcanology **69** 1 (2006) 1–24.
[206] CRONIN, S.J., HEDLEY, M.J., NEALL, V.E., SMITH, R.G., Agronomic impact of tephra fallout from the 1995 and 1996 Ruapehu Volcano eruptions, New Zealand, Environmental Geology **34** 1 (1998) 21–30.
[207] MEREDITH, I.M., Sharing Experiences with Applying Coatings to Turbines, Hydro Review Worldwide Magazine (2007) 34–41.
[208] PYLE, D.M., The thickness, volume and grainsize of tephra fall deposits, Bulletin of Volcanology **51** 1 (1989) 1–15.
[209] FIERSTEIN, J., NATHENSON, M., Another look at the calculation of fallout tephra volumes, Bulletin of Volcanology **54** 2 (1992) 156–167.
[210] BONADONNA, C., HOUGHTON, B.F., Total grain-size distribution and volume of tephra-fall deposits, Bulletin of Volcanolog **67** 5 (2005) 441–456.
[211] GONZÁLEZ-MELLADO, A.O., DE LA CRUZ-REYNA, S., A simple semi-empirical approach to model thickness of ash-deposits for different eruption scenarios, Natural Hazards and Earth System Sciences **10** 11 (2010) 2241–2257.
[212] BONADONNA, C., COSTA, A., Estimating the volume of tephra deposits: A new simple strategy, Geology **40** 5 (2012) 415–418.
[213] PYLE, D.M., Assessment of the minimum volume of tephra fall deposits, Journal of Volcanology and Geothermal Research **69** 3 (1995) 379–382.
[214] SUZUKI, T., "A theoretical model for dispersion of tephra", Arc Volcanism: Physics and Tectonics, Terra Scientific Publishing, Tokyo (1983) 95–113.

[215] BARBERI, F., MACEDONIO, G., PARESCHI, M., SANTACROCE, R., Mapping the tephra fallout risk: an example from Vesuvius, Nature **344** (1990) 142–144.
[216] CONNOR, C.B., HILL, B.E., WINFREY, B., FRANKLIN, N.M., LA FEMINA, P.C., Estimation of volcanic hazards from tephra fallout, Natural Hazards Review **2** 1 (2001) 33–42.
[217] BONADONNA, C., MACEDONIO, G., SPARKS, R., "Numerical modelling of tephra fallout associated with dome collapses and Vulcanian explosions: application to hazard assessment on Montserrat", The Eruption of Soufrière Hills Volcano, Montserrat, from 1995 to 1999, Geological Society of London, Memoirs, Vol. 21 (DRUITT, T., KOKELAAR, B., Eds), Geological Society of London, London (2002) 517–537.
[218] BONADONNA, C., CONNOR, C.B., HOUGHTON, B.F., CONNOR, L.J., BYRNE, M., LAING, A., HINCKS, T., Probabilistic modeling of tephra dispersion: hazard assessment of a multi-phase eruption at Tarawera, New Zealand, Journal of Geophysical Research **110** B03 (2005) B03203.
[219] MACEDONIO, G., COSTA, A., LONGO, A., A computer model for volcanic ash fallout and assessment of subsequent hazard, Nature Geoscience **31** 7 (2005) 837–845.
[220] SPARKS, R.S.J, BURSIK, M.I., CAREY, S.N., GILBERT, J.S., GLAZE, L., SIGURDSSON, H., WOODS, A.W., Volcanic Plumes, John Wiley & Sons, New York, NY (1997).
[221] CONNOR, L.J., CONNOR, C.B., "Inversion is the key to dispersion: understanding eruption dynamics by inverting tephra fallout," IAV001 Statistics in Volcanology, Special Publications of IAVCEI (MADER, H.M., COLES, S.G., CONNOR, C.B., CONNOR, L.J., Eds), Geological Society of London, London (2006) 231–242.
[222] SCOLLO, S., TARANTOLA, S., BONADONNA, C., COLTELLI, M., SALTELLI, A., Sensitivity analysis and uncertainty estimation for tephra dispersal models, Journal of Geophysical Research **113** (2008) B06202-1–B06202-17.
[223] VOLENTIK, A.C., BONADONNA, C., CONNOR, C.B., CONNOR, L.J., ROSI, M., Modeling tephra dispersal in absence of wind: insights from the climactic phase of the 2450 BP Plinian eruption of Pululagua volcano (Ecuador), Journal of Volcanology and Geothermal Research **193** (2010) 117–136.
[224] WITHAM, C.S., HORT, M.C., POTTS, R., SERVRANCKX, R., HUSSON, P., BONNARDOT, F., Comparison of VAAC atmospheric dispersion models using the 1 November 2004 Grimsvötn eruption, Meteorological Applications **14** 1 (2007) 27–38.
[225] TANAKA, H.L., YAMAMOTO, K., Numerical simulation of volcanic plume dispersal from Usu Volcano in Japan on 31 March 2000 using PUFF model, Earth, Planets and Space **54** 7 (2002) 743–752.
[226] SCOLLO, S., PRESTIFILIPPO, M., SPATA, G., D'AGOSTINO, M., COLTELLI, M., Monitoring and forecasting Etna volcanic plumes, Natural Hazards and Earth System Sciences **9** 5 (2009) 1573–1585.
[227] RYALL, D.B., MARYON, R.H., Validation of the UK Met. Office's NAME model against the ETEX dataset, Atmospheric Environment **32** (1998) 4265–4276.
[228] JONES, A.R., THOMSON, D.J., HORT, M., DEVENISH, B., "The U.K. Met Office's next-generation atmospheric dispersion model, NAME III", Air Pollution Modeling and Its Application XVII (Proceedings of the 27th NATO/CCMS International Technical Meeting on Air Pollution Modelling and Its Application), Springer US, New York, NY (2007) 580–589.
[229] PEUCH, V.H., AMODEI, M., BARTHET, T., CATHALA, M.L., JOSSE, B., MICHOU, M., SIMON, P., MOCAGE, MOdèle de Chimie Atmosphérique à Grande

Echelle, Proceedings of Météo-France Workshop on Atmospheric Modelling (1999) 33–36.
[230] D'AMOURS, R., MALO, A., SERVRANCKX, R., BENSIMON, D., TRUDEL, S., GAUTHIER-BILODEAU, J.P., Application of the atmospheric Lagrangian particle dispersion model MLDP0 to the 2008 eruptions of Okmok and Kasatochi volcanoes, Journal of Geophysical Research **115** D2 (2010) D00L11.
[231] MATTHIAS, V., AULINGER, A., BIESER, J., CUESTA, J., GEYER, B., LANGMANN, B., SERIKOV, I., MATTIS, I., MINIKIN, A., MONA, L., QUANTE, M., SCHUMANN, U., WEINZIERL, B., The ash dispersion over Europe during the Eyjafjallajökull eruption - comparison of CMAQ simulations to remote sensing and air-borne in-situ observations, Atmospheric Environment **48** (2012) 184–194.
[232] ACKERMANN, I.J., HASS, H., MEMMESHEIMER, M., EBEL, A., BINKOWSKI, F.S., SHANKAR, U., Modal aerosol dynamics model for Europe: development and first applications, Atmospheric Environment **32** (1998) 2981–2999.
[233] COSTA, A., MACEDONIO, G., FOLCH, A., A three-dimensional Eulerian model for transport and deposition of volcanic ashes, Earth and Planetary Science Letters **241** 3–4 (2006) 634–647.
[234] FOLCH, A., COSTA, A., MACEDONIO, G., FALL3D: a computational model for transport and deposition of volcanic ash, Computers & Geosciences **35** (2009) 1334–1342.
[235] STOHL, A., HITTENBERGER, M., WOTAWA, G., Validation of the Lagrangian particle dispersion model FLEXPART against large scale tracer experiments, Atmospheric Environment **32** (1998) 4245–4264.
[236] DRAXLER, R.R., HESS, G.D., An overview of the HYSPLIT_4 modeling system of trajectories, dispersion, and deposition, Australian Meteorological Magazine **47** (1998) 295–308.
[237] SEARCY, C., DEAN, K.G., STRINGER, W., PUFF: a volcanic ash tracking and prediction model, Journal of Volcanology and Geothermal Research **80** (1998) 1–16.
[238] LANGMANN, B., VARGHESE, S., MARMER, E., VIGNATI, E., WILSON, J., STIER, P., O'DOWD, C., Aerosol distribution over Europe: a model evaluation study with detailed aerosol microphysics, Atmospheric Chemistry and Physics **8** (2008) 1591–1607.
[239] FOLCH, A., A review of tephra transport and dispersal models: Evolution, current status, and future perspectives, Journal of Volcanology and Geothermal Research **235–236** (2012) 96–15.
[240] SCHWAIGER, H.F., DENLINGER, R.P., MASTIN, L.G., Ash3d: A finite-volume, conservative numerical model for ash transport and tephra deposition, Journal of Geophysical Research **117** B4 (2012) B04204.
[241] BARSOTTI, S., NERI, A., SCIRE, S., The VOL-CALPUFF model for atmospheric ash dispersal: 1. Approach and physical formulation, Journal of Geophysical Research **113** B3 (2008) B03208.
[242] BARSOTTI, S., NERI, A., The VOL-CALPUFF model for atmospheric ash dispersal: 2. Application to the weak Mount Etna plume of July 2001, Journal of Geophysical Research **113** B3 (2008) B03209.
[243] COSTA, A., FOLCH, A., MACEDONIO, G., A model for wet aggregation of ash particles in volcanic plumes and clouds: 1. theoretical formulation, Journal of Geophysical Research **115** B9 (2010) B09201.
[244] BURSIK, M., Effect of wind on the rise height of volcanic plumes, Geophysical Research Letters **18** (2001) 3621–3624.

[245] MASTIN, L.G., GUFFANTI, M., SERVRANCKX, R., WEBLEY, P., BARSOTTI, S., DEAN, K., DURANT, A., EWERT, J.W., NERI, A., ROSE, W.I., SCHNEIDER, D., SIEBERT, L., STUNDER, B., SWANSON, G., TUPPER, A., VOLENTIK, A., WAYTHOMAS, C.F., A multidisciplinary effort to assign realistic source parameters to models of volcanic ash-cloud transport and dispersion during eruptions, Journal of Volcanology and Geothermal Research **186** (2009) 1–2 10–21.
[246] CORRADINI, S., MERUCCI, L., FOLCH, A., Volcanic ash cloud properties: comparison between MODIS satellite retrievals and FALL3D transport model, IEEE Geoscience and Remote Sensing Letters **8** 2 (2011) 242–252.
[247] MACEDONIO, G., COSTA, A., FOLCH, A., Ash fallout scenarios at Vesuvius: numerical simulations and implications for hazard assessment, Journal of Volcanology and Geothermal Research **178** 3 (2008) 366–377.
[248] SCOLLO, S., FOLCH, A., COSTA, A., A parametric and comparative study of different tephra fallout models, Journal of Volcanology and Geothermal Research **176** 2 (2008) 199–211.
[249] FOLCH, A., COSTA, A., BASART, S., Validation of the FALL3D ash dispersion model using observations of the 2010 Eyjafjallajökull volcanic ash clouds, Atmospheric Environment **48** (2012) 165–183.
[250] SELF, S., RAMPINO, M.R., NEWTON, M.S., WOLFF, J.A., Volcanolog- ical study of the great Tambora eruption of 1815, Geology **12** (1984) 659–663.
[251] SELF, S., GERTISSER, R., THORDARSON, T., RAMPINO, M.R., WOLFF, J.A., Magma volume, volatile emissions, and stratospheric aerosols from the 1815 eruption of Tambora, Geophysical Research Letters **31** 20 (2004) L20608.
[252] SIGURDSSON, H., CAREY, S., Plinian and co-ignimbrite tephra fall from the 1815 eruption of Tambora volcano, Bulletin of Volcanology **51** (1989) 243–270.
[253] LAVIGNE, F., DEGEAI, J.P., KOMOROWSKI, J.C., GUILLET,, S., ROBERT, V., LAHITTE, P., OPPENHEIMER, C., STOFFEL, M., VIDAL, C.M., PRATOMO, S.I., WASSMER, P., HAJDAS, I., SRI HADMOKO, D., DE BÉLIZAL, E., Source of the great A.D. 1257 mystery eruption unveiled, Samalas volcano, Rinjani Volcanic Complex, Indonesia, Proceedings of the National Academy of Sciences of the United States of America **110** 42 (2013) 16742–16747.
[254] KALNAY, E., KANAMITSU, M., KISTLER, R., COLLINS, W., DEAVEN, D., GANDIN, L., IREDELL, M., SAHA, S., WHITE, G., WOOLLEN, J., ZHU, Y., LEETMAA, A., REYNOLDS, R., The NCEP/NCAR 40-year reanalysis project, Bulletin of the American Meteorological Society **77** 3 (1996) 437–470.
[255] SULPIZIO, R., FOLCH, A., COSTA, A., SCAINI, C., DELLINO, P., Hazard assessment of far-range volcanic ash dispersal from a violent Strombolian eruption at Somma-Vesuvius volcano, Naples, Italy: implications on civil aviation, Bulletin of Volcanology **74** 9 (2012) 2205–2218.
[256] NEWHALL, C.G., SELF, S., The Volcanic Explosivity Index (VEI): An Estimate of Explosive Magnitude for Historical Volcanism, Journal of Geophysical Research **87** C2 (1982) 1231–1238.
[257] FIERSTEIN, J., HOUGHTON, B.F., WILSON, C.J., HILDRETH, W., Complexities of Plinian fall deposition at vent: an example from the 1912 Novarupta eruption (Alaksa), Journal of Volcanology and Geothermal Research **76** (1997) 215–227.
[258] KOYAGUCHI, T., OHNO, M., Reconstruction of eruption column dynamics on the basis of grain size of tephra fall deposits: 2. Application to the Pinatubo 1991 eruption, Journal of Geophysical Research **106** (2001) 6513–6534.

[259] COSTA, A., DELL'ERBA, F., DI VITO, M.A., ISAIA, R., MACEDONIO, G., ORSI, G., PFEIFFER, T., Tephra fallout hazard assessment at the Campi Flegrei caldera (Italy), Bulletin of Volcanology **71** (2009) 259–273.
[260] SCAINI, C., FOLCH, A., NAVARRO, M., Tephra hazard assessment at Concepción Volca- no, Nicaragua, Journal of Volcanology and Geothermal Research **219–220** (2012) 41–51.
[261] KOYAGUCHI, T., "Volume estimation of tephra-fall deposits from the June 15, 1991, eruption of Mount Pinatubo by theoretical and geological methods", Fire and Mud: Eruptions and Lahars of Mount Pinatubo, Philippines (NEWHALL, C.G., PUNONGBAYAN, R.S., Eds), University of Washington Press, Seattle, WA (1996) 583–600.
[262] PALADIO-MELOSANTOS, M.L.O., SOLIDUM, R.U., SCOTT, W.E., QUIAMBAO, R.B., UMBAL, J.V., RODOLFO, K.S., TUBIANOSA, B.S., DELOS REYES, P.J., ALONSO, R.A., RUELO, H.B., "Tephra falls of the 1991 eruptions of Mount Pinatubo", Fire and Mud: Eruptions and Lahars of Mount Pinatubo, Philippines (NEWHALL, C.G., PUNONGBAYAN, R.S., Eds), University of Washington Press, Seattle, WA (1996) 513–535.
[263] SIMKIN, T., SIEBERT, L., Volcanoes of the World, Geoscience Press, Tucson (1994).
[264] NAIRN, I.A., Atmospheric shock waves and condensation clouds from Ngauruhoe explosive eruptions, Nature **259** (1976) 190–192.
[265] JOHNSON, J.B., ASTER, R.C., KYLE, P.R., Volcanic eruptions observed with infrasound, Geophysical Research Letters **31** 14 (2004) L14604.
[266] MCNUTT, S.R., THOMPSON, G., WEST, M.E., FEE, D., STIHLER, S., CLARK, E., Local seismic and infrasound observations of the 2009 explosive eruptions of Redoubt Volcano, Alaska, Journal of Volcanology and Geothermal Research **259** (2013) 63–76.
[267] BEHNKE, S.A., THOMAS, R.J., MCNUTT, S.R., SCHNEIDER, D.J., KREHBIEL, P.R., RISON, W., EDENS, H.E., Observations of Volcanic Lightning during the 2009 Eruption of Redoubt Volcano, Journal of Volcanology and Geothermal Research **259** (2011) 214–234.
[268] JAMES, M.R., WILSON, L., LANE, S.J., GILBERT, J.S., MATHER, T.A., HARRISON, R.G., MARTIN, R.S., Electrical charging of volcanic plume, Space Science Reviews **137** 1–4 (2008) 399–418.
[269] LANE, S.J., GILBERT, J.S., Electric potential gradient changes during explosive activity at Sakurajima Volcano, Japan, Bulletin of Volcanology **54** (1992) 590–594.
[270] LANE, S.J., GILBERT, J.S., KEMP, A.J., "Electrical and chemical properties of eruption plumes at Sakurajima volcano, Japan", 8th Report of Geophysical and Geochemical Observations at Sakurajima Volcano, Sakurajima Volcanological Observatory, Kyoto University. Kyoto (1995) 105–127.
[271] JAMES, M.R., LANE, S.J., GILBERT, J.S., Special Volcanic plume monitoring using atmospheric electric potential gradients, Journal of the Geological Society **155** 4 (1998) 587–590.
[272] MIURA, T., KOYAGUCHI, T., TANAKA, Y., Atmospheric electric potential gradient measurements of ash clouds generated by pyroclastic flows at Unzen Volcano, Japan, Geophysical Research Letters **23** (1996) 1789.
[273] HOBLITT, R.P., An experiment to detect and locate lightning associated with eruptions of Redoubt volcano, Journal of Volcanology and Geothermal Research **62** (1994) 499–517.

[274] THOMAS, R.J., KREHBIEL, P.R., RISON, W., AULICH, G., EDENS, H., MCNUTT, S.R., TYTGAT, G., CLARK, E., Electrical activity during the 2006 Mount St. Augustine volcanic eruptions, Science **315** (2007) 1097.
[275] THOMAS, R.J., MCNUTT, S.R., KREHBIEL, P., RISON, W., AULICH, G., EDENS, H., TYTGAT, G., CLARK, E., "Lightning and electrical activity during the eruptions of Augustine volcano," The 2006 Eruption of Augustine Volcano, Alaska (POWER, J.A., COOMBS, M.L., FREYMUELLER, J.T., Eds), U.S. Geological Survey Professional Paper 1769, USGS, Reston, VA (2010) 579–608.
[276] WILLIAMS, E.R., MCNUTT, S.R., "Total water contents in volcanic eruption clouds and implications for electrification and lightning", Recent progress in lightning physics (PONTIKIS, C., Eds), Research Signpost Publishing, Kerala (2005) 81–93.
[277] MCNUTT, S.R., WILLIAMS, E.R., Volcanic Lightning: Global observations and constraints on source mechanisms, Bulletin of Volcanology **72** 10 (2010) 1153.
[278] BÜTTNER, R., ZIMANOWSKI, B., Physics of thermohydraulic explosions, Physical Review E **57** (1998) 5726–5729.
[279] ANDERSON, R., BJORNSSON, S., BLANCHARD, D.C., GATHMAN, S., HUGHES, J., JONASSON, S., MOORE, C.B., SURVILAS, H.J., VONNEGUT, B., Electricity in volcanic clouds, Science **148** (1965) 1179–1189.
[280] BROOK, M., MOORE, C.B., SIGURGEIRSSON, T., Lightning in volcanic clouds, Eos, Transactions American Geophysical Union **54** (1973) 701.
[281] ARASON, P., BENNETT, A.J., BURGIN, L.E., Charge mechanism of volcanic lightning revealed during the 2010 eruption of Eyjafjallajökull, Journal of Geophysical Research **116** B9 (2011) B00C03.
[282] MCNUTT, S.R., ARNOULT, K., SZUBERLA, C., OLSON, J.V., WILSON, C.R., Infrasound Studies of Alaskan Volcanoes, American Geophysical Union, Fall Meeting, 2010 (abstract #S11A-1933).
[283] MCNUTT, S., TYTGAT, G., ESTES, S., STIHLER, S., "A Parametric Study of the January 2006 Explosive Eruptions of Augustine Volcano, Alaska, using seismic, infrasonic, and lightning data", The 2006 Eruption of Augustine Volcano, Alaska (POWER, J.A., COOMBS, M.L., FREYMUELLER, J.T., Eds), U.S. Geological Survey Professional Paper 1769, USGS, Reston, VA (2010) 85–102.
[284] ARNOULT, K.M., OLSON, J.V., SZUBERLA, C.A., MCNUTT, S.R., GARCES, M.A., FEE, D., HEDLIN, M.A., Infrasound Observations of the 2008 Explosive Eruptions of Okmok and Kasatochi Volcanoes, Alaska, Journal of Geophysical Research **115** D2 (2010) D00L15.
[285] HAGERTY, M.T., SCHWARTZ, S.Y., GARCES, M.A., PROTTI, M., Analysis of seismic and acoustic observations at Arenal Volcano, Costa Rica, 1995–1997, Journal of Volcanology and Geothermal Research **101** (2000) 27–65.
[286] ROWE, C.A., ASTER, R.C., KYLE, P.R., DIBBLEB, R.R., SCHLUE, J.W., Seismic and acoustic observations at Mount Erebus Volcano, Ross Island, Antarctica, 1994–1998, Journal of Volcanology and Geothermal Research **101** 1–2 (2000) 105–128.
[287] JOHNSON, J.B., LEES, J.M., Plugs and chugs - Seismic and acoustic observations of degassing explosions at Karymsky, Russia and Sangay, Ecuador, Journal of Volcanology and Geothermal Research **101** 1–2 (2000) 67–82.
[288] FIRSTOV, P.P., KRAVCHENKO, N.M., Estimation of the amount of explosive gas released in volcanic eruptions using air waves, Journal of Volcanology and Seismology **17** (1996) 547–560.
[289] GARCÉS, M.A., HAGERTY, M.T., SCHWARTZ, S.Y., Magma acoustics and time-varying melt properties at Arenal Volcano, Costa Rica, Geophysical Research Letters **25** 13 (1998) 2293–2296.

[290] JOHNSON, J.B., ASTER, R.C., RUIZ, M.C., MALONEA, S.D., MCCHESNEYA, P.J., LEESD, J.M., KYLEB, P.R., Interpretation and utility of infrasonic records from erupting volcanoes, Journal of Volcanology and Geothermal Research **121** 1–2 (2003) 15–63.
[291] CAPLAN-AUERBACH, J., MCNUTT, S.R., New Insights into the 1999 Eruptions of Shishaldin Volcano Based on Acoustic Data, Bulletin of Volcanology **65** 6 (2003) 405–417.
[292] RIPEPE, M., MARCHETTI, E., Array tracking of infrasonic sources at Stromboli volcano, Geophysical Research Letters **29** 22 (2002) 2076.
[293] YAMASATO, H., Quantitative analysis of pyroclastic flows using infrasonic and seismic data at Unzen Volcano, Japan, Journal of Physics of the Earth **445** (1997) 397–416.
[294] EWING, P.D., KISNER, R.A., KORSAH, K., MOORE, M.R., WILGEN, J.B., WOOD, R.T., Technical Basis for Regulatory Guidance on Lightning Protection in Nuclear Power Plants, NUREG/CR-6866 / ORNL/TM-2001/140, NRC / ORNL, / Washingotn, DC / Oak Ridge, TN (2006).
[295] MAZZINI, A., SVENSEN, H., AKHMANOV, G.G., ALOISI, G., PLANKE, S., MALTHE-SØRENSSEN, A., ISTADI, B., Triggering and dynamic evolution of Lusi mud volcano, Indonesia, Earth and Planetary Science Letters **261** (2007) 375–388.
[296] RICHARDS, J.R., Report into the past, present, and future social impacts of Lumpur Sidoarjo, Humanitus Sidoarjo Fund, Melbourne (2011).
[297] DAVIES, R.J., MATHIAS, S.A., SWARBRICK, R.E., TINGAY, M.J., Probabilistic longevity estimate for the LUSI mud volcano, East Java, Journal of the Geological Society **168** 2 (2011) 517–523.
[298] RUDOLPH, M.L., KARLSTROM, L., MANGA, M., A prediction of the longevity of the Lusi mud eruption, Indonesia, Earth and Planetary Science Letters **308** (2011) 124–130.
[299] IZUMIYAMA, S., YAGITA, K., FURUSHIMA-SHIMOGAWARA, R., ASAKURA, T., KARASUDANI, T., ENDO, T., Occurrence and Distribution of Naegleria Species in Thermal Waters in Japan, The Journal of Eukaryotic Microbiology **50** 6 (2003) 514–515.
[300] INGEBRITSEN, S.E., GEIGER, S., HURWITZ, S., DRIESNER, T., Numerical simulation of magmatic hydrothermal systems, Reviews of Geophysics **48** 1 (2010) RG1002.
[301] PRUESS, K., The TOUGH codes - A family of simulation tools for multiphase flow and transport processes in permeable media, Vadose Zone Journal **3** (2004) 738–746.
[302] CHIODINI, G., BALDINI, A., BARBERI, F., CARAPEZZA, M.L., CARDELLINI, C., FRONDINI, F., GRANIERI, D., RANALDI, M., Carbon dioxide degassing at Latera caldera (Italy): Evidence of geothermal reservoir and evaluation of its potential energy, Journal of Geophysical Research **112** B12 (2007) B12204.
[303] CHIODINI, G., CALIRO, S., CARDELLINI, C., GRANIERI, D., AVINO, R., BALDINI, A., DONNINI, M., MINOPOLI, C., Long-term variations of the Campi Flegrei, Italy, volcanic system as revealed by the monitoring of hydrothermal activity, Journal of Geophysical Research **115** B3 (2010) B03205.
[304] TODESCO, M., RUTQVIST, J., CHIODINI, G., PRUESS, K., OLDENBURG, C.M., Modeling of recent volcanic episodes at Phlegrean Fields (Italy), Geothermics **33** 4 (2004) 531–547.
[305] TODESCO, M., Signals from the Campi Flegrei hydrothermal system: Role of a "magmatic" source of fluids, Journal of Geophysical Research **114** B5 (2009) B05201.

[306] GRANIERI, D., COSTA, A., MACEDONIO, G., CHIODINI, G., BISSON, M., Carbon dioxide in the city of Naples: contribution and effects of the volcanic source, Journal of Volcanology and Geothermal Research **260** (2013) 52–61.
[307] THORDARSON, T., SELF, S., Atmospheric and environmental effects of the 1783–1784 Laki eruption: A review and reassessment, Journal of Geophysical Research **108** D1 (2003) 4011.
[308] CENTERS FOR DISEASE CONTROL AND PREVENTION, NIOSH Pocket Guide to Chemical Hazards, CDC, Atlanta, GA (1997).
[309] BAXTER, P.J., KAPILA, M., MFONFU, D., Lake Nyos disaster, Cameroon, 1986: the medical effects of large scale emission of carbon dioxide?, British Medical Journal **298** (1989) 1437–1441.
[310] CLARKE, T., Taming Africa's killer lake, Nature **409** (2001) 554–555.
[311] COLE, I.S., MUSTER, T.J., AZMAT, N.S., VENKATRAMAN, M.S., COOK, A., Multiscale modelling of the corrosion of metals under atmospheric corrosion, Electrochimica Acta **56** 4 (2011) 1856–1865.
[312] WILLIS, G., DEARDOFF, J., A laboratory model of diffusion into the convective planetary boundary layer, Quarterly Journal of the Royal Meteorological Society **102** 432 (1976) 427–445.
[313] PASQUILL, F., SMITH, F.B., Atmospheric Diffusion (3rd Edition), John Wiley & Sons, Chichester (1983).
[314] BRIGGS, G., Analytical Parameterizations of Diffusion: The Convective Boundary Layer, Journal of Climate and Applied Meteorology **24** 11 (1985) 1167–1186.
[315] HINRICHSEN, K., Comparison of four analytical dis- persion models for near-surface release above a grass surface, Atmospheric Environment **20** (1986) 29–40.
[316] LIN, J., HILDEMANN, L., Analytical solutions of the atmospheric diffusion equation with multiple sources and height-dependent wind speed and eddy diffusivity, Atmospheric Environment **30** (1996) 239–254.
[317] NUCLEAR REGULATORY COMMISSION, Atmospheric Dispersion Models for Potential Accident Consequence Assessments at Nuclear Power Plants, Regulatory Guide 1.145-7, Revision 1, NRC, Washington, DC (1983).
[318] BLACKMORE, D., HERMAN, M., WOODWARD, J., Heavy gas dispersion models, Journal of Hazardous Materials **6** (1982) 107–128.
[319] ERMAK, D.L., User's manuals for SLAB: an atmospheric dispersion model for denser-then-air releases, UCRL-MA-105607, LLNL, Livermore, CA (1990).
[320] WITLOX, H., The HEGADAS model for ground-level heavy-gas dispersion - I. Steady-state model, Atmospheric Environment **28** 18 (1994) 2917–2932.
[321] SPICER, T., HAVENS, J., DEGADIS - DEnse GAs DISpersion Model, Technical Report EPA-450/4-89-0019, U.S. Environmental Protection Agency, San Rafael, CA (1989).
[322] COSTA, A., MACEDONIO, G., CHIODINI, G., Numerical model of gas dispersion emitted from volcanic sources, Annals of Geophysics **48** 4/5 (2005) 805–815.
[323] HANKIN, R.K., BRITTER, R.E., TWODEE: The Health and Safety Laboratory's shallow layer model for hea- vy gas dispersion. Part 1. Mathematical basis and physical assumptions, Journal of Hazardous Materials **66** 3 (1999) 211–226.
[324] HANKIN, R.K., BRITTER, R.E., TWODEE: The Health and Safety Laboratory's shallow layer model for heavy gas dispersion. Part 2. Outline and validation of the computa- tional scheme, Journal of Hazardous Materials **66** 3 (1999) 227–237.

[325] HANKIN, R.K., BRITTER, R.E., TWODEE: The Health and Safety Laboratory's shallow layer model for heavy gas dispersion. Part 3. Experimental validation (Thorney island), Journal of Hazardous Materials **66** 3 (1999) 239–261.
[326] VENETSANOS, A., BARTZIS, J., WURTZ, J., PAPAILIOU, D., DISPLAY-2: a two-dimensional shallow layer model for dense gas dispersion including complex features, Journal of Hazardous Materials **99** 2 (2003) 111–144.
[327] COSTA, A., CHIODINI, G., GRANIERI, D., FOLCH, A., HANKIN, R., CALIRO, S., AVINO, R., CARDELLINI, C., A shallow-layer model for heavy gas dispersion from natural sources: Application and hazard assessment at Caldara di Manziana, Italy, Geochemistry, Geophysics, Geosystems **9** 3 (2008) Q03002.
[328] CHIODINI, G., GRANIERI, D., AVINO, R., CALIRO, S., COSTA, A., MINOPOLI, C., VILARDO, G., Non-volcanic CO_2 Earth degassing: Case of Mefite d'Ansanto (southern Apennines), Italy, Geophysical Research Letters **37** 11 (2010) L11303.
[329] FOLCH, A., COSTA, A., HANKIN, R.K., A shallow layer model for dense gas dispersion on complex topography, Computers & Geosciences **35** 3 (2009) 667–674.
[330] DOUGLAS, S., KESSLER, R., User's Guide for the Urban Airshed Model, Volume III: User's Manual for the Diagnostic Wind Model, EPA-450/4-90-007C, U.S. Environmental Protection Agency, San Rafael, CA (1990).
[331] PONTIGGIA, M., DERUDI, M., BUSINI, V., ROTA, R., Hazardous gas dispersion: a CFD model accounting for atmospheric stability classes, Journal of Hazardous Materials **171** 1–3 (2009) 739–747.
[332] PONTIGGIA, M., DERUDI, M., ALBA, M., SCAIONI, M., ROTA, R., Hazardous gas releases in urban areas: Assessment of consequences through CFD modelling, Journal of Hazardous Materials **176** 1–3 (2010) 589–596.
[333] SKLAVOUNOS, S., RIGAS, F., Simulation of Coyote series trials - Part I: CFD estimation of non-isothermal LNG releases and comparison with box-model predictions, Chemical Engineering Science **61** 5 (2006) 1434–1443.
[334] MCBRIDE, M.A., REEVER, A.B., VANDERHEYDEN, M.D., LEA, C.J., ZHOU, X.X., Use of advanced techniques to model the dispersion of chlorine in complex terrain, Process Safety and Environmental Protection **79** 2 (2001) 89–102.
[335] STEVEN, R.H., BROWN, M.J., CAMELLI, F.E., CHAN, S.T., COIRIER, W.J., HANSEN, O.R., HUBER, A.H., KIM, S., REYNOLDS, R.M., Detailed Simulations of Atmospheric Flow and Dispersion in Downtown Manhattan: An Application of Five Computational Fluid Dynamics Models, Bulletin of the American Meteorological Society **87** 12 (2006) 1713–1726.
[336] KOMOROWSKI, J.C., TEDESCO, D., KASEREKA, M., ALLARD, P., PAPALE, P., VASELLI, O., DURIEUX, J., BAXTER, P., HALBWACHS, M., AKUMBE, M., BALUKU, B., BRIOLE, P., CIRABA, M., DUPIN, J.C., ETOY, O., GARCIN, D., HAMAGUCHI, H., HOULIÉ, N., KAVOTHA, K.S., LEMARCHAND, A., LOCKWOOD, J., LUKAYA, N., MAVONGA, G., DE MICHELE, M., MPORE, S., MUKAMBILWA, K., MUNYOLOLO, F., NEWHALL, C., RUCH, J., YALIRE,M., WAFULA, M., The January 2002 eruption - The January 2002 flank eruption of Nyiragongo Volcano (Democratic Republic of Congo): chronology, evidence for a tectonic rift trigger, and impact of lava flows on the city of Goma, Journal of the National Volcanicn Group of Italy **14** 1–2 (2002) / **15** (1–2) (2003) 27–62.
[337] WALKER, G.P., Lengths of Lava Flows, Philosophical Transactions of the Royal Society of London. Series A, Mathematical and Physical Sciences **274** (1973) 107–118.
[338] HARRIS, A.J., ROWLAND, S.K., "Controls on lava flow length", IAV002 Studies in Volcanology: The Legacy of George Walker (THORDARSON, T., SELF, S.,

LARSEN, G., ROWLAND, S.K., HOSKULDSSON, A., Eds), Geological Society of London, London (2009) 33–51.
[339] NUCLEAR REGULATORY COMMISSION, Environmental Impact Statement for the Proposed Idaho Spent Fuel Facility at the Idaho National Engineering and Environmental Laboratory in Butte County, NUREG-1773, NRC, Washington, DC (2004).
[340] GRIFFITHS, R., The dynamics of lava flows, Annual Review of Fluid Mechanics **32** (2000) 477–518.
[341] WYLIE, J., LISTER, J., The stability of straining flow with surface cooling and temperature-dependent viscosity, Journal of Fluid Mechanics **365** (1998) 369–381.
[342] COSTA, A., MACEDONIO, G., Viscous heating in fluids with temperature-dependent viscosity: implications for magma flows, Nonlinear Processes in Geophysics **10** 6 (2003) 545–555.
[343] MACEDONIO, G., PARESCHI, M.T., SANTACROCE, R., A simple model for lava hazard assessment: Mount Etna, paper presented at International Volcanological Congress, International Association of Volcanology and Chemistry of the Earth's Interior (IAVCEI), Mainz, 1990.
[344] GUEST, J., MURRAY, J., An analysis of hazard from the Mount Etna Volcano, Journal of the Geological Society of London **136** (1979) 347–354.
[345] VILLARI, L., RASÀ, R., CACCAMO, A., "Volcanic hazard at Mt. Etna (Sicily, Italy): Some insight from the geostructural pattern constraining flank eruptions," Proceeding of Kagoshima International Conference on Volcanoes (1988) 491–494.
[346] BARBERI, F., CARAPEZZA, M., VALENZA, M., VILLARI, L., The control of lava flow during the 1991–1992 eruption of Mt. Etna, Journal of Volcanology and Geothermal Research **56** (1993) 1–34.
[347] BARBERI, F., VILLARI, L., Volcano monitoring and civil protection problems during the 1991–1993 Etna eruption, Acta Vulcanologica **4** (1994) 157–165.
[348] DOBRAN, F., MACEDONIO, G., Lava modeling contributions of the Volcanic Simulation Group during the 1991–1992 eruption of Mt. Etna: Giardini, Pisa, Italy, Volcanic Simulation Group Report 92–7, Gruppo Nazionale per la Vulcanologia Consiglio Nazionale delle Ricerche (1992).
[349] FAVALLI, M., PARESCHI, M., NERI, A., ISOLA, I., Forecasting lava flow paths by a stochastic approach, Geophysical Research Letters **32** 3 (2005) L03305.
[350] FAVALLI, M., CHIRICO, G.D., PAPALE, P., PARESCHI, M.T., COLTELLI, M., LUCAYA, N., BOSCHI, E., Computer simulations of lava flow paths in the town of Goma, Nyiragongo volcano, Democratic Republic of Congo, Journal of Geophysical Research **111** B6 (2006) B06202.
[351] COSTA, A., MACEDONIO. G., Computational modeling of lava flows: A review, Geological Society of America Special Papers **396** (2005) 209–218.
[352] YOUNG, P., WADGE, G., FLOWFRONT: Simulation of a lava flow, Computers & Geosciences **16** 8 (1990) 1171–1191.
[353] WADGE, G., YOUNG, P., MCKENDRICK, I., Mapping lava flow hazard using computer simulation, Journal of Geophysical Research **99** B1 (1994) 489–504.
[354] BARCA, D., CRISCI, G.M., GREGORIO, S.D., NICOLETTA, F., Cellular automata for simulating lava flows: A method and examples of the Etnean eruptions, Transport Theory and Statistical Physics **23** (1994) 195–232.
[355] CANNATARO, M., DI GREGORIO, S., RONGO, R., SPATARO, W., SPEZZANO, S., TALIA, D., A parallel cellular automata environment on multicomputers for modeling and simulation, Parallel Computing **21** 5 (1995) 803–824.

[356] DI GREGORIO, S., SERRA, R., An empirical method for modelling and simulating some complex macroscopic phenomena by cellular automata, Future Generation Computer Systems **16** (1999) 259–271.
[357] CRISCI, G., DI GREGORIO, S., PINDARO, O., RANIERI, G., Lava flow simulation by a discrete cellular model: First implementation, International Journal of Modelling and Simulation **6** (1986) 137–140.
[358] BARCA, D., CRISCI, G., DI GREGORIO, S., NICOLETTA, F., Lava flow simulation by cellular automata: Pantelleria's examples, Proceedings of Internationa Applied Medelling and Simulation, Cairo, Egypt, Vol. 4 (1987) 9–15.
[359] CRISCI, G., RONGO, R., DI GREGORIO, S., SPATARO, W., The simulation model SCIARA: The 1991 and 2001 lava flows at Etna, Journal of Volcanology and Geothermal Research **132** (2004) 253–267.
[360] ISHIHARA, K., IGUCHI, M., AND KAMO, K., "Numerical simulation of lava flows at Sakurajima", Proceeding of Kagoshima International Conference on Volcanoes (1988) 479–482.
[361] ISHIHARA, K., IGUCHI, M., KAMO, K., "Numerical Simulation of Lava Flows on Some Volcanoes in Japan," Lava Flows and Domes, Springer, Berlin (1989) 174–207.
[362] DRAGONI, M., BONAFEDE, M., BOSCHI, E., Downslope flow models of a Bingham liquid: Implications for lava flows, Journal of Volcanology and Geothermal Research **30** (1986) 305–325.
[363] MIYAMOTO, H., SASAKI, S., Simulating lava flows by an improved cellular automata method, Computers & Geosciences **23** 3 (1997) 283–292.
[364] DEL NEGRO, C., FORTUNA, L., HERAULT, A., VICARI, A., Simulations of the 2004 lava flow at Etna volcano using the MAGFLOW cellular automata model, Bulletin of Volcanology **70** 7 (2008) 805–812.
[365] HARRIS, A.J., ROWLAND, S.K., FLOWGO: a kinematic thermo-rheological model for lava flowing in a channel, Bulletin of Volcanology **63** (2001) 20–44.
[366] COSTA, A., MACEDONIO, G., Numerical simulation of lava flows based on depth-averaged equations, Geophysical Research Letters **32** 5 (2005) L05304.
[367] MACEDONIO, G., LONGO, A., Lava flow in a channel with a bifurcation, Physics and Chemistry of the Earth **24** 11 (1999) 953–956.
[368] FUJITA, E., HIDAKA, M., GOTO, A., UMINO, S., Simulations of measures to control lava flows, Bulletin of Volcanology **71** (2009) 401–408.
[369] HIDAKA, M., UJITA, H., Verification for flow analysis capability in the model of three-dimensional natural convection with simultaneous spreading, melting and solidification for debris coolability analysis module in the severe accident analysis code 'SAMPSON', (I), Journal of Nuclear Science and Technology **38** 9 (2001) 745–756.
[370] HIDAKA, M., SATO, N., UJITA, H., Verification for flow analysis capability in the model of three-dimensional natural convection with simultaneous spreading, melting and solidification for debris coolability analysis module in the severe accident analysis code 'SAMPSON', (II), Journal of Nuclear Science and Technology **39** 5 (2002) 520–530.
[371] PROIETTI, C., COLTELLI, M., MARSELLA, M., FUJITA, E., A quantitative approach for evaluating lava flow simulation reliability: LavaSIM code applied to the 2001 Etna eruption, Geochemistry, Geophysics, Geosystems **10** 9 (2009) Q09003.
[372] CHIRICO, G.D., FAVALLI, M., PAPALE, P., BOSCHI, E., PARESCHI, M.T., Lava flow hazard at Nyiragongo volcano, D.R.C. 2. Hazard reduction in urban areas, Bulletin of Volcanology **71** 4 (2008) 375–387.

[373] KILBURN, C.J., LOPES, R.M., The growth of aa lava fields on Mt. Etna, Sicily, Journal of Geophysical Research **93** (1988) 722–759.
[374] STASIUK, M.V., JAUPART, C., Lava flow shapes and dimensions as reflections of magma system conditions, Journal of Volcanology and Geothermal Research **78** 1–2 (1997) 31–50.
[375] THORDARSON, T., SELF, S., The Laki (Skaftar fires) and Grimsvotn eruptions in 1783–85, Bulletin of Volcanology **55** (1993) 233–263.
[376] MALIN, M.C., Lengths of Hawaiian lava flows, Geology **8** (1980) 306–308.
[377] PINKERTON, H., WILSON, L., Factors controlling the lengths of channel-fed lava flows, Bulletin of Volcanology **56** (1994) 108–120.
[378] CAS, R.A.F., WRIGHT, J.V., Volcanic Successions: Modern and Ancient, Chapman & Hall, London (1987).
[379] CAREY, S.N., "Transport and deposition of tephra by pyroclastic flows and surges", Sedimentation in Volcanic Settings (FISHER, R.V., SMITH, G.A., Eds), Special Publications of SEPM, Vol. 45, Society for Sedimentary Geology, Tulsa, OK (1991) 39–57.
[380] BRANNEY, M.J., KOKELAAR, B.P., Pyroclastic Density Currents and the Sedimentation of Ignimbrites, Geological Society, London, Memoirs, Vol. 27, Geological Society of London, London (2002).
[381] DRUITT, T.H., "The eruption, transport and sedimentation of pyroclastic flows", The Physics of Volcanic Eruptions, Geological Society Special Publication No. 145 (GILBERT, J.S., SPARKS, R.S.J., Eds), Geological Society of London, London (1998) 147–200.
[382] FISHER, R.V., Mechanism of deposition from pyroclastic flows, American Journal of Science **264** (1996) 350–366.
[383] DADE, B.W., HUPPERT, H.E., Emplacement of the Taupo Ignimbrite by a dilute turbulent flow, Nature **381** (1996) 509–512.
[384] DOBRAN, F., NERI, A., MACEDONIO, G., Numerical simulations of collapsing volcanic columns, Journal of Geophysical Research **98** (1993) 4231–4259.
[385] SPARKS, R.S., GARDEWEG, M.C., CALDER, E.S., MATTHEWS, S.J., Erosion by pyroclastic flows on Lascar volcano. Chile, Bulletin of Volcanology **58** (1997) 557–565.
[386] VALENTINE, G.A., Damage to structures by pyroclastic flows and surges, inferred from nuclear weapons effects, Journal of Volcanology and Geothermal Research **87** (1998) 117–140.
[387] JENKINS, S., KOMOROWSKI, J.C., BAXTER, P.J., SPENCE, R., PICQUOUT, A., LAVIGNE, F., SURONO, The Merapi 2010 eruption: An interdisciplinary impact assessment methodology for studying pyroclastic density current dynamics, Journal of Volcanology and Geothermal Research **261** (2013) 260–294.
[388] VALENTINE, G.A., FISHER, R.V., "Pyroclastic surges and blasts", Encyclopedia of Volcanoes, 1st Edition (SIGURDSSON, H., HOUGHTON, B., RYMER, H., STIX, J., MCNUTT, S., Eds), Academic Press, San Diego (1999) 571–580.
[389] LOUGHLIN, S.C., CALDER, E.S., CLARKE, A., COLE, P.D., LUCKETT, R., MANGAN, M.T., PYLE, D.M., SPARKS, R.S., VOIGHT, B., WATTS, R.B., "Pyroclastic flows and surges generated by the 25 June 1997 dome collapse, Soufrière Hills Volcano, Montserrat," The Eruption of Soufrière Hills Volcano, Montserrat, from 1995 to 1999 (DRUITT, T.H., KOKELAAR, B.P., Eds), Geological Society, London, Memoirs, Vol. 21, Geological Society of London, Londao (2002) 191–210.

[390] NUCLEAR REGULATORY COMMISSION, Evaluations of Explosions Postulated to Occur on Transportation Routes Near Nuclear Power Plants, Regulatory Guide 1.91, Revision 1, NRC, Washington, DC (1978).
[391] WOHLETZ, K.H., SHERIDAN, M.F., A model of pyroclastic surge, Geological Society of America Special Papers **180** (1979) 177–194.
[392] ISHIMINE, Y., Numerical study of pyroclastic surges, Journal of Volcanology and Geothermal Research **139** (2005) 33–57.
[393] SHERIDAN, M.F., Emplacement of pyroclastic flows: A review, Geological Society of America Special Papers **180** (1979) 125–136.
[394] HEIM, A., Der Bergsturz von Elm, Zeitschrift der Deutschen Geologischen Gesellschaft **34** (1932) 74–115.
[395] MALIN, M.C., SHERIDAN, M.F., Computer-assisted mapping of pyroclastic surges, Science **217** (1982) 637–640.
[396] SHERIDAN, M.F., MALIN, M.C., Application of computer-assisted mapping to volcanic hazard evaluation of surge eruptions: Vulcano, Lipari and Vesuvius, Journal of Volcanology and Geothermal Research **17** (1983) 187–202.
[397] MCEWEN, A.S., MALIN, M.C., Dynamics of Mout St. Helens 1980 pyroclastic flows, rockslide-avalanche, lahars and blast, Journal of Volcanology and Geothermal Research **37** (1989) 205–231.
[398] KOVER, T.P., Application of a Digital Terrain Model for the Modeling of Volcanic Flows: A Tool for Volcanic Hazard Determination, State University New York at Buffalo, New York, NY (1995).
[399] MELLOR, M., "Dynamics of snow avalanches," Rockslides and avalanches, 1. Natural Phenomena, Elsevier Science, Amsterdam (1978) 753–792.
[400] HOOPER, D.M., MATTIOLI, G.S., Kinematic modeling of pyroclastic flows produced by gravitational dome collapse at Soufriere Hills Volcano, Montserrat, Natural Hazards **23** (2001) 65–86.
[401] SHERIDAN, M.F., HUBBARD, B., CARRASCO-NUŇEZ, G., SIEBE, C., Pyroclastic flow hazard at Volcán Citlaltépelt, Natural Hazards **33** (2004) 209–221.
[402] SAUCEDO, R., MACÍAS, J.L., SHERIDAN, M.F., BURSIK, M.I., KOMOROWSKI, J.C., Modeling of pyroclastic flows of Colima Volcano, Mexico: implications for hazard assessment, Journal of Volcanology and Geothermal Research **139** (2005) 103–115.
[403] WADGE, G., JACKSON, P., BOWER, S.M., Computer simulations of pyroclastic flows from dome collapse, Geophysical Research Letters **25** 19 (1998) 3677–3680.
[404] BURSIK, M.I., WOODS, A.W., The dynamics and thermodynamics of large ash flows, Bulletin of Volcanology **58** (1996) 175–193.
[405] WIDIWIJAYANTI, C., VOIGHT, B., HIDAYAT, D., SCHILLING, S.P., Objective rapid delineation of areas at risk from block-and-ash pyroclastic flows and surges, Bulletin of Volcanology **71** (2008) 687–703.
[406] IVERSON, R.M., SCHILLING, S.P., VALLANCE, J.W., Objective delineation of lahar inundation hazard zones, Geological Society of America Bulletin **110** (1998) 972–984.
[407] SCHILLING, S., LAHARZ: GIS programs for automated mapping of lahar-inundation hazard zones, USGS Numbered Series, Open-File Report 98–638, USGS, Vancouver, WA (1998).
[408] SAVAGE, S.B., HUTTER, K., The motion of a finite mass of granular material down a rough incline, Journal of Fluid Mechanics **199** (1989) 177–215.

[409] IVERSON, R.M., DENLINGER, R.P., Flow of variably fluidized granular masses across three dimensional terrain, I. Coulomb mixture theory, Journal of Geophysical Research **106** (2001) 537–552.
[410] HEINRICH, P., BOUDON, G., KOMOROWSKI, J.C., SPARKS, R.S., HERD, R., VOIGHT, B., Numerical simulation of the December 1997 debris avalanche in Montserrat, Geophysical Research Letters **28** 13 (2001) 2529–2532.
[411] LE FRIANT, A., BOUDON, G., KOMOROWSKI, J.C., HEINRICH, P., SEMET, M.P., Potential flank-collapse of Soufrière volcano, Guadeloupe, Lesser Antilles? Numerical simulation and Hazards, Natural Hazards **39** (2006) 381–393.
[412] POULIQUEN, O., Scaling laws in granular flows down rough inclined planes, Physics of Fluids **11** (1999) 542–548.
[413] PATRA, A.K., BAUER, A.C., NICHITA, C.C., PITMAN, E.B., SHERIDAN, M.F., BURSIK, M.I., RUPP, B., WEBBER, A., STINTON, A.J., NAMIKAWA, L.M., RENSCHLER, C.S., Parallel adaptive simulation of dry avalanches over natural terrain, Journal of Volcanology and Geothermal Research **139** (2005) 1–22.
[414] IVERSON, R.M., The physics of debris flows, Reviews of Geophysics **35** 3 (1997) 245–296.
[415] DENLINGER, R.P., IVERSON, R.M., Flow of variably fluidized granular material across three-dimensional terrain: 2. Numerical predictions and experimental tests, Journal of Geophysical Research **106** B1 (2001) 553–566.
[416] MANGENEY-CASTLENAU, A., VILOTTE, J.P., BRISTEAU, M.O., PERTHAME, B., BOUCHUT, F., SIMEONI, C., YERNEMI, S., Numerical modelling of avalanches based on Saint Venant equations using a kinetic scheme, Journal of Geophysical Research **108** B11 (2002) EPM 9–1.
[417] PITMAN, E.B., NICHITA, C.C., PATRA, A.K., BAUER, A., SHERIDAN, M.F., BURSIK, M.I., Computing granular avalanches and landslides, Physics of Fluids **15** 12 (2003) 3638–3646.
[418] KELFOUN, K., DRUITT, T.H., Numerical modeling of the emplacement of Socompa rock avalanche, Chile, Journal of Geophysical Research **110** B12 (2005) B12202.
[419] HUNGR, O., MCDOUGALL, S., Two numerical models for landslide dynamic analysis, Computers & Geosciences **35** 5 (2009) 978–992.
[420] SPARKS, R.S., Grain size variations in ignimbrites and implications for the transport of pyroclastic flows, Sedimentology **23** (1976) 147–188.
[421] FREUNDT, A., SCHMINCKE, H.U., Lithic-enriched segregation bodies in pyroclastic flow deposits of Laacher See volcano (East Eifel, Germany), Journal of Volcanology and Geothermal Research **25** (1985) 193–224.
[422] BATTAGLIA, M., On pyroclastic flow emplacement, Journal of Geophysical Research **98** B12 (1993) 22269–22272.
[423] DADE, W.B., HUPPERT, H.E., Long-runout rockfalls, Geology **26** (1998) 803–806.
[424] KELFOUN, K., SAMANIEGO, P., PALACIOS, P., BARBA, D., Testing the suitability of frictional behaviour for pyroclastic flow simulation by comparison with a well-constrained eruption at Tungurahua volcano (Ecuador), Bulletin of Volcanology **71** 9 (2009) 1057–1075.
[425] AVOLIO, M.V., CRISCI, G.M., DI GREGORIO, S., RONGO, R., SPATARO, W., D'AMBROSIO, D., Pyroclastic flows modelling using cellular automata, Computers & Geosciences **32** (2006) 897–911.
[426] DARTEVELLE, S., Numerical modeling of geophysical granular flows: 1. A comprehensive approach to granular rheologies and geophysical multiphase flows, Geochemistry Geophysics Geosystems **5** 8 (2004) Q08003.

[427] DARTEVELLE, S., VALENTINE, G.A., Transient multiphase processes during the explosive eruption of basalt through a geothermal borehole (Namafjall, Iceland, 1977) and implications for natural volcanic flows, Earth and Planetary Science Letters **262** (2007) 363–384.
[428] DUFEK, J., MANGA, M., In situ production of ash in pyroclastic flows, Journal of Geophysical Research **113** B9 (2008) B09207.
[429] ESPOSTI ONGARO, T., NERI, A., MENCONI, G., DE'MICHIELI VITTURI, M., MARIANELLI, P., CAVAZZONI, C., ERBACCI, G., BAXTER, P.J., Transient 3D numerical simulations of column collapse and pyroclastic density current scenarios at Vesuvius, Journal of Volcanology and Geothermal Research **178** 3 (2008) 378–396.
[430] ESPOSTI ONGARO, T., WIDIWIJAYANTI, C., CLARKE, A.B., VOIGHT, B., NERI, A., Multiphase-flow numerical modeling of the 18 May 1980 lateral blast at Mount St. Helens, USA, Geology **39** 6 (2011) 535–538.
[431] LEPORE, S., SCARPATI, C., New developments in the analysis of column-collapse pyroclastic density currents through numerical simulations of multiphase flows, Solid Earth **3** 1 (2012) 161–173.
[432] DARTEVELLE, S., ROSE, W.I., STIX, J., KELFOUN, K., VALLANCE, J.W., Numerical modeling of geophysical granular flows: 2. Computer simulations of plinian clouds and pyroclastic flows and surges, Geochemistry Geophysics Geosystems **5** 8 (2004) Q08004.
[433] ESPOSTI ONGARO, T., CAVAZZONI, C., ERBACCI, G., NERI, A., SALVETTI, M.V., A parallel multiphase flow code for the 3D simulation of explosive volcanic eruptions, Parallel Computing **33** 7–8 (2007) 541–560.
[434] NERI, A., ESPOSTI ONGARO, T., MACEDONIO, G., GIDASPOW, D., Multiparticle simulation of collapsing volcanic columns and pyroclastic flows, Journal of Geophysical Research **108** B24 (2003) ECV 4–1.
[435] DUFEK, J., BERGANTZ, G.W., Dynamics and deposits generated by the Kos Plateau Tuff eruption: Controls of basal particle loss on pyroclastic flow transport, Geochemistry Geophysics Geosystems **8** 12 (2007) Q12007.
[436] SHERIDAN, M.F., PATRA, A.K., DALBEY, K., HUBBARD, B., Robabilistic digital hazard maps for avalanches and massive pyroclastic flows using TITAN2D, Geological Society of America Special Paper **464** (2010) 281–292.
[437] DALBEY, K., PATRA, A.K., PITMAN, E.B., BURSIK, M.I., SHERIDAN, M.F., Input uncertainty propagation methods and hazard mapping of geophysical mass flows, Journal of Geophysical Research **113** B5 (2008) B05203.
[438] HAYASHI, J.N., SELF, S., A comparison of pyroclastic flow and debris avalanche mobility, Journal of Geophysical Research **97** (1992) 9063–9071.
[439] VALLANCE, J.W., "Lahars", Encyclopedia of Volcanoes, 1st Edition (SIGURDSSON, H., HOUGHTON, B., RYMER, H., STIX, J., MCNUTT, S., Eds), Academic Press, San Diego (1999) 601–616.
[440] VALLANCE, J.W., SCOTT, K.M., The Osceola mudflow from Mount Rainier: Sedimentology and hazard implications of a huge clay-rich debris flow, Geological Society of America Bulletin **109** (1997) 143–163.
[441] PIERSON, T.C., COSTA, J.E., A rheologic classification of subaerial sediment-water flows. Geological Society of America Reviews in Engineering, Geology **7** (1987) 1–12.
[442] SCOTT, K.M., VALLANCE, J.W., PRINGLE, P.T., Sedimentology, behavior, and hazards of debris flows at Mount Rainier, Washington, U.S. Geological Survey Professional Paper 1547, USGS, Reston, VA (1995).

[443] SAVAGE, S.B., “Granular flows down rough inclines - review and extension”, Mechanics of granular materials: new models and constitutive relations, Elsevier, Amsterdam (1983) 261–281.
[444] SAVAGE, S.B., The mechanics of rapid granular flows, Journal of Applied Mechanics **24** (1984) 289–366.
[445] IVERSON, R.M., VALLANCE, J.M., New views of granular mass flows, Geology **29** (2001) 115–118.
[446] MARCIAL, S.S., MELOSANTOS, A.A., HADLEY, K.C., LAHUSEN, R.G., MARSO, J., “Instrumental lahar monitoring at Mount Pinatubo”, Fire and Mud: Eruptions and Lahars of Mount Pinatubo, Philippines (NEWHALL, C.G., PUNONGBAYAN, R.S., Eds), University of Washington Press, Seattle, WA (1996) 1015–1022.
[447] LAVIGNE, F., THOURET, J.C., SUWA, H., VOIGHT, B., YOUNG, K., LAHUSEN, R., MARSO, J., SUMARYONO, A., SAYUDI, D.S., DEJEAN, M., Instrumental lahar monitoring atMerapi Volcano, Central Java, Indonesia, Journal of Volcanology and Geothermal Research **100** (2000) 457–478.
[448] DE BELIZAL, E., LAVIGNE, F., SRI HADMOKO, D., DEGEAI, J.P., DIPAYANA, G.A., MUTAQIN, B.W., MARFAI, M.A., COQUET, M., LE MAUFF, B., ROBIN, A.K., VIDAL, C., CHOLIK, N., AISYAH, N., Rain-triggered lahars following the 2010 eruption of Merapi volcano, Indonesia:A major risk, Journal of Volcanology and Geothermal Research **261** (2013) 330–347.
[449] SCHUSTER, R.L., “Effects of the eruptions on civil works and operations in the Pacific Northwest”, The 1980 eruptions of Mount St. Helens, Washington (LIPMAN, P. W., MULLINEAUX, D. R., Eds), U.S. Geological Survey Professional Paper 1250, USGS, Reston, VA (1981) 701–718.
[450] SWORD-DANIELS, V., WARDMAN, J., STEWART, C., WILSON, T., JOHNSTON, D., ROSSETTO, T., Infrastructure impacts, management and adaptations to eruptions at Volcán Tungurahua, Ecuador, 1999–2010, GNS Science Report, 2011/24, Institute of Geological and Nuclear Sciences Limited, Lower Hutt (2011).
[451] IVERSON, R.M., Landslide triggering by rain infiltration, Water Resources Research **36** 7 (2000) 1897–1910.
[452] DAAG, A.S., Modelling the erosion of pyroclastic flow deposits and the occurrences of lahars at Mt. Pinatubo, Philippines, ITC Dissertation number 104, Science and Earth Observation, Enschede (2003).
[453] MERGILI, M., SCHRATZ, K., OSTERMANN, A., FELLIN, W., Physically-based modelling of granular flows with Open Source GIS, Natural Hazards and Earth System Sciences **12** (2012) 187–200.
[454] PERLA, R., CHENG, T.T., MCCLUNG, D.M., A Two-Parameter Model of Snow Avalanche Motion, Journal of Glaciology **26** (1980) 197–207.
[455] GAMMA, P., dfwalk - Ein Murgang-Simulationsprogramm zur Gefahrenzonierung, vol. G66, Geographica Bernensia, Bern (2000).
[456] WICHMANN, V., Modellierung geomorphologischer prozesse in einem alpinen Einzugsgebiet. Abgrenzung und Klassifizierung der Wirkungsräume von Sturzprozessen und Muren mit einem GIS, Eichstätter Geographische Arbeiten **15** (2006) 231.
[457] AVOLIO, M.V., LUPIANO, V., MAZZANTI, P., DI GREGORIO, S., “Modelling combined subaerial-subaqueous flow-like landslides by Cellular Automata”, Cellular Automata, Lecture Notes in Computer ScienceVolume 5191, Springer, Berlin (2008) 329–336.

[458] AVOLIO, M.V., DI GREGORIO, S., LUPIANO, V., MAZZANTI, P., SCIDDICA-SS3: a new version of cellular automata model for simulating fast moving landslides, The Journal of Supercomputing **65** 2 (2013) 682–696.
[459] O'BRIEN, J.S., JULIEN, P.Y., FULLERTON, W.T., Two-dimensional water flood and mudflow simulation, Journal of Hydrologic Engineering **119** 2 (1993) 244–261.
[460] PIRULLI, M., Numerical modelling of landslide runout, a continuum mechanics approach, PhD Thesis, Politecnico di Torino (2005).
[461] PIRULLI, M., BRISTEAU, M.O., MANGENEY, A., SCAVIA, C., The effect of earth pressure coefficient on the runout of granular material, Environmental Modelling & Software **22** 10 (2007) 1437–1454.
[462] O'BRIEN, J.S., JULIEN, P.Y., Laboratory analysis of mudflow properties, Journal of Hydraulic Engineering **114** 8 (1988) 877–887.
[463] O'BRIEN, J.S., FULLERTON, W.T., "Simulation of Rio Grande floodplain inundation using Flo-2D", RMRS-P-7: Rio Grande ecosystems: linking land, water, and people. Toward a sustainable future for the Middle Rio Grande Basin. (FINCH, D.M., WHITNEY, J.C., KELLY, J.F., Eds), Rocky Mountain Research Station, Fort Collins, CO (1999) 52–60.
[464] PITMAN, E.B., LE, L., A two-fluid model for avalanche and debris flow, Philosophical Transactions of The Royal Society A: Mathematical, Physical and Engineering Sciences **363** (2005) 1573–1601.
[465] ANDERSON, T.B., JACKSON, R., A fluid mechanical description of fluidized beds: equations of motion, Industrial & Engineering Chemistry Research **6** 4 (1967) 527–539.
[466] RICHARDSON, J.F., ZAKI, W.N., Sedimentation and fluidization: part I, Transactions of the Institution of Chemical Engineers **32** (1954) 35–53.
[467] MARTINEZ, C.E., MIRALLES-WILLHELM, F., GARCIA-MARINEZ, R., "Quasi-three dimensional two-phase debris flow accounting for boulder transport", Italian Journal of Engineering Geology and Environment - Book, Sapienza Università Editrice university press, Rome (2011) 457–466.
[468] PUDASAINI, S.P., A general two-phase debris flow model, Journal of Geophysical Research **117** F3 (2012) F03010.
[469] INTERNATIONAL ATOMIC ENERGY AGENCY, Meteorological and Hydrological Hazards in Site Evaluation for Nuclear Installations, IAEA Safety Standards Series No. SSG-18, IAEA, Vienna (2011).
[470] YAMAKOSHI, T., DOI, Y., OSANAI, N., Post-eruption hydrology and sediment discharge at the Miyakejima volcano, Japan, Zeitschrift fur Geomorphologie **140** (2005) 55–72.
[471] PROCTER, J.N., CRONIN, S.J., SHERIDAN, M.F., Evaluation of Titan2D modelling forecasts for the 2007 Crater Lake break-out lahar, Mt. Ruapehu, New Zealand, Geomorphology **136** (2012) 95–105.
[472] WORNI, R., HUGGEL, C., STOFFEL, M., PULGARIN, B., Challenges of modeling current very large lahars at Nevadodel Huila Volcano, Colombia, Bulletin of Volcanology **74** (2012) 309–324.
[473] FROGER, J.L., MERLE, O., BRIOLE, P., Active spreading and regional extension at Mount Etna imaged by SAR interferometry, Earth and Planetary Science Letters **187** (2001) 245–258.
[474] VOIGHT, B., GLICKEN, H., JANDA, R.J., DOUGLAS, P.M., "Catastrophic rockslide avalanche of May 18", The 1980 eruptions of Mount St. Helens, Washington (LIPMAN, P. W., MULLINEAUX, D. R., Eds), U.S. Geological Survey Professional Paper 1250, USGS, Reston, VA (1981) 347–377.

[475] KOMOROWSKI, J.C., BOUDON, G., SEMET, M., BEAUDUCEL, F., ANT´ENOR-HABAZAC, C., BAZIN, S., HAMMOUYA, G., "Volcanic Hazard Atlas of the Lesser Antilles: Guadeloupe", Volcanic Hazard Atlas of the Lesser Antilles (LINDSAY, J.M., SMITH, A.L., ROOBOL, M.J., STASIUK, M.V., Eds), Seismic Research Centre, Tobago (2005) 65–102.
[476] KOMOROWSKI, J.C., NAVARRO, C., CORTÉS, A., SAUCEDO GIRÓN, R., GAVILANES, J.C., SIEBE, C., ESPINDOLA, J.M., RODRIGUEZ, S., "The Colima volcanic complex: Part I: Quaternary multiple debris-avalanche deposits, Part II: Historical pyroclastic sequences (1913, 1991, 1994)", IAVCEI General Assembly, Puerto Vallarta, Mexico, January 19–24, 1997, Fieldtrip Guidebook, Excursion 3 (1997).
[477] REID, M.E., CHRISTIAN, S.B., BRIEN, D.L., Gravitational stability of three-dimensional stratovolcano edifices, Journal of Geophysical Research **105** B3 (2000) 6043–6056.
[478] VOIGHT, B., ELSWORTH, D., Failure of volcano slopes, Geotechnique **47** 1 (1997) 1–31.
[479] VOIGHT, B., KOMOROWSKI, J.C., NORTON, G.E., BELOUSOV, A.B., BELOUSOVA, M., BOUDON, G., FRANCIS, P.W., FRANZ, W., HEINRICH, P., SPARKS, R.S., YOUNG, S.R., "The 1997 Boxing Day Sector Collapse and Debris Avalanche, Soufrière Hills Volcano, Montserrat", The Eruption of Soufrière Hills Volcano, Montserrat, from 1995 to 1999 (DRUITT, T.H., KOKELAAR, B.P., Eds), Geological Society, London, Memoirs, Vol. 21, Geological Society of London, Londao (2002) 363–407.
[480] DAY, S.J., "Hydrothermal pore fluid pressure and the stability of porous, permeable volcanoes", Volcano instability on the Earth and terrestrial planets, Geological Society Special Publication No. 110 (MCGUIRE, W.J., JONES, A.P., NEUBERG, J., Eds), Geological Society of London, London (1996) 77–93.
[481] ELSWORTH, D., VOIGHT, B., "Evaluation of volcano flank instability triggered by dyke intrusion", Volcano instability on the Earth and terrestrial planets, Geological Society Special Publication No. 110 (MCGUIRE, W.J., JONES, A.P., NEUBERG, J., Eds), Geological Society of London, London (1996) 45–53.
[482] REID, M.E., Massive collapse of volcano edifices triggered by hydrothermal pressurization, Geology **32** 5 (2004) 373–376.
[483] VAN WYK DE VRIES, B., KERLE, N., PETLEY, D., Sector collapse forming at Casita volcano, Nicaragua, Geology **28** (2000) 167–170.
[484] GUDMUNDSSON, A., Strengths and strain energies of volcanic edifices: implications for eruptions, collapse calderas, and landslides, Natural Hazards and Earth System Sciences **12** 7 (2012) 2241–2258.
[485] CRANDELL, D.R., MULLINEAUX, D.R., Technique and rationale ofvolcanic-hazards appraisals in the Cascade Range, north western United States, Environmental Geology **1** (1975) 23–32.
[486] SIEBERT, L., GLICKEN, H., UI, T., Volcanic hazards from Bezymianny- and Bandai-type eruptions, Bulletin of Volcanology **49** (1987) 435–459.
[487] VOIGHT, B., JANDA, R.J., GLICKEN, H., DOUGLASS, P.M., Nature and mechanics of the Mount St. Helens rockslide-avalanche of 18 May 1980, Geotechnique **33** (1983) 243–273.
[488] ACOCELLA, V., Modes of sector collapse of volcanic cones: Insights from analogue experiments, Journal of Geophysical Research **110** B2 (2005) B02205.
[489] HSU, K.J., Catastrophic debris stream (Sturzstroms) generated by rockfalls, Geological Society of America Bulletin **86** (1975) 129–140.

[490] SHERIDAN, M.F., STINTON, A.J., PATRA, A., PITMAN, E.B., BAUER, A., NICHITA, C.C., Evaluating TITAN2D mass-flow model using 1963 Little Tahoma Peak avalanches. Mount Rainier Washington, Journal of Volcanology and Geothermal Research **139** (2005) 89–102.
[491] MACÍAS VÁZQUEZ, J.L., CARRASCO NUÑEZ, G., DELGADO GRANADOS, H., MARTINN DEL POZZO, A.L., SIEBE GRABACH, C., HOBLITT, R.P., SHERIDAN, M.F., TILLING, R.I., Mapa de peligros del Volcán Popocatépetl, Universidad Nacional Autónoma de México, Instituto de Geofísica, Mexico (1995).
[492] CAPRA, L., NORINI, G., GROPPELLI, G., MACÍAS, J.L., ARCE, J.L., Volcanic hazard zonation of Nevado de Toluca Volcano, Journal of Volcanology and Geothermal Research **176** (2008) 469–484.
[493] SAVAGE, S.B., HUTTER, K., The dynamics of avalanches of granular materials from initiation to runout. Part I: Analysis, Acta Mechanica **86** 1–4 (1991) 201–223.
[494] FRANCIS, P.W., GARDEWEG, M., RAMIREZ, C.F., ROTHERY, D.A., Catastrophic debris avalanche deposit of Socompa volcano, northern Chile, Geology **13** (1985) 600–603.
[495] WADGE, G., FRANCIS, P.W., RAMIREZ, C.F., The Socompa collapse and avalanche event, Journal of Volcanology and Geothermal Research **66** (1995) 309–336.
[496] BISHOP, A.W., The use of slip circles in the stability analysis of slopes, Géotechnique **5** (1955) 7–17.
[497] BORSELLI, L., CAPRA, L., SAROCCHI, D., DE LA CRUZ-REYNA, S., Flank collapse scenarios at Volcán de Colima, Mexico: a relative instability analysis, Journal of Volcanology and Geothermal Research **208** (2011) 51–65.
[498] THOMPSON, N., BENNETT, M.R., PETFORD, N., Analyses of granular mass movement mechanics and deformation with distinct element numerical modelling: implications for large-scale rock and debris avalanches, Acta Geotechnica **4** (2009) 233–247.
[499] JING, L., STEPHANSSON, O., Fundamentals of Discrete Element Methods for Rock Engineering: Theory and Application, Development in Geotechnical Engineering, 85, Elsevier, Amsterdam (2007).
[500] THOMPSON, N., BENNETT, M.R., PETFORD, N., Development of characteristic volcanic debris avalanche deposit structures: New insight from distinct element simulations, Journal of Volcanology and Geothermal Research **192** (2010) 191–200.
[501] VAN WYK DE VRIES, B., FRANCIS, P.W., Catastrophic collapse at stratovolcanoes induced by gradual volcanic spreading, Nature **387** (1997) 387–390.
[502] STOOPES, G., SHERIDAN, M.F., Giant debris avalanches from the Colima Volcanic Complex, Mexico: Implications for long-runout landslides (>100 km) and hazard assessment, Geology **20** (1992) 299–302.
[503] NOMANBHOY, N., SATAKE, K., Generation mechanism of tsunamis from the 1883 Krakatau eruption, Geophysical Research Letters **22** (1995) 509–512.
[504] POWER, W., DOWNES, G., "Tsunami hazard assessment", Volcanic and Tectonic Hazard Assessment for Nuclear Facilities (Connor, C.B., Chapman, N.A., Connor, L.J., Eds), Cambridge University Press, Cambridge (2009) 276–306.
[505] WAYTHOMAS, C.F., WATTS, P., Numerical simulation of tsunami generation by pyroclastic flow at Aniakchak Volcano, Alaska, Geophysical Research Letters **30** 14 (2003) 51–54.
[506] MAENO, F., IMAMURA, F., TANIGUCHI, H. Numerical simulation of tsunamis generated by caldera collapse during the 7.3 ka Kikai eruption, Kyushu, Japan, Earth, Planets and Space **58** 8 (2006) 1013–1024.

[507] MAENO, F., IMAMURA, F., Tsunami generation by a rapid entrance of pyroclastic flow into the sea during the 1883 Krakatau eruption, Indonesia, Journal of Geophysical Research **116** B9 (2011) B09205.
[508] VOIGHT, B., JANDA, R., GLICKEN, H., DOUGLAS, P.M., Nature and mechanics of the Mount St Helens rockslide-avalanche of 18 May 1980, Géotechnique **33** 10 (1983) 243–273.
[509] WARD, S.N., DAY, S., Ritter Island Volcano - lateral collapse and the tsunami of 1888, Geophysical Journal International **154** 3 (2003) 891–902.
[510] WATT, S.F., TALLING, P.J., VARDY, M.E., HELLER, V., HÜHNERBACH, V., URLAUB, M., SARKAR, S., MASSON, D.G., HENSTOCK, T.J., MINSHULL, T.A., PAULATTO, M., LE FRIANT, A., LEBAS, E., BERNDT, C., CRUTCHLEY, G.J., KARSTENS, J., STINTON, A.J., MAENO, F., Combinations of volcanic-flank and seafloor-sediment failure offshore Montserrat and their implications for tsunami generation, Earth and Planetary Science Letters **319–320** (2012) 228–240.
[511] TINTI, S., PAGNONI, G., ZANIBONI, F., The landslides and tsunamis of the 30th of December 2002 in Stromboli analysed through numerical simulations, Bulletin of Volcanology **68** (2006) 462–479.
[512] AIDA, I., Numerical experiments of the tsunamis associated with the collapse of Mt. Matyuyama in 1792, Journal of the Seismological Society of Japan **28** (1975) 449–460.
[513] OEHLER, J.F., LABAZUY, P., LÉNAT, J.F., Recurrence of major flank landslides during the last 2 Ma history of Réunion Island, Bulletin of Volcanology **66** (2004) 585–598.
[514] SELF, S., RAMPINO, M.R., The 1883 eruption of Krakatau, Nature **294** (1981) 699–704.
[515] LATTER, J.H., Tsunamis of volcanic origin: summary of causes with particular reference to Krakatoa, 1883, Bulletin of Volcanology **44** (1981) 467–490.
[516] GREZIO, A., MARZOCCHI, W., SANDRI, L., GASPARINI, P., A Bayesian procedure for Probabilistic Tsunami Hazard Assessment, Natural Hazards **53** (2010) 159–174.
[517] GREZIO, A., MARZOCCHI, W., SANDRI, L., ARGNANI, A., GASPARINI, P., Probabilistic Tsunami Hazard Assessment for Messina Strait Area (Sicily - Italy), Natural Hazards **64** (2012) 329–358.
[518] GREZIO, A., GASPARINI, P., MARZOCCHI, W., PATERA, A., TINTI, S., Tsunami risk assessments in Messina, Sicily - Italy, Natural Hazards and Earth System Sciences **12** (2012) 1–13.
[519] DE LANGE, W.P., PRASETYA, G.S., HEALY, T.R., Modelling of tsunamis generated by pyroclastic flows (Ignimbrites), Natural Hazards **24** (2001) 251–266.
[520] MOORE, J.G., BRYAN, W.B., LUDWIG, K.R., Chaotic deposition by a giant wave, Molokai, Hawaii, Geological Society of America Bulletin **106** 7 (1994) 962–967.
[521] MASSON, D.G., WATTS, A.B., GEE, M.J., URGELES, R., MITCHELL, N.C., LE BAS, T.P., CANALS, M., Slope failures on the flanks of the western Canary Islands, Earth-Science Reviews **57** (2002) 1–35.
[522] LØVHOLT, F., PEDERSEN, G., GISLER, G., Oceanic propagation of a potential tsunami from the La Palma island, Journal of Geophysical Research **113** C9 (2008) C09026.
[523] WAYTHOMAS, C.F., WATTS, P., SHI, F., KIRBY, J.T., Pacific Basin tsunami hazards associated with mass flows in the Aleutian arc of Alaska, Quaternary Science Reviews **28** 11–12 (2009) 1006–1019.

[524] GIACHETTI, T., PARIS, R., KELFOUN, K., PEREZ-TORRADO, F.J., Numerical modelling of the tsunami triggered by the Güìmar debris avalanche, Tenerife (Canary Islands): Comparison with field-based data, Marine Geology **284** 1–4 (2011) 189–202.
[525] HEINRICH, P., GUIBOURG, S., MANGENEY, A., ROCHE, R., Numerical modeling of a landslide-generated tsunami following a potential explosion of the Montserrat Volcano, Physics and Chemistry of the Earth, Part A: Solid Earth and Geodesy **24** 2 (1999) 163–168.
[526] BARDET, J.P., SYNOLAKIS, C.E., DAVIES, H.L., IMAMURA, F., OKAL, E.A., Landslide Tsunamis: Recent Findings and Research Directions, Pure and Applied Geophysics **160** 10 (2003) 1793–1809.
[527] HARBITZ, C.B., LØVHOLT, F., PEDERSEN, G., MASSON, D.G., Mechanisms of tsunami generation by submarine landslides: a short review, Norwegian Journal of Geology **86** (2006) 255–264.
[528] HELLER, V., HAGER, W.H., Impulse product parameter in landslide generated impulse waves, Journal of Waterway, Port, Coastal, and Ocean Engineering **136** (2010) 145–155.
[529] FRITZ, H.M., HAGER, W.H., MINOR, H.E., Near field characteristics of landslide generated impulse waves, Journal of Waterway, Port, Coastal, and Ocean Engineering **130** (2004) 287–302.
[530] JIANG, L., LEBLOND, P.H., The coupling of a submarine slide and the surface waves which it generates, Journal of Geophysical Research **97** (1992) 12731–12744.
[531] PELINOVSKY, E., POPLAVSKY, A., Simplified model of tsunami generation by submarine landslides, Physics and Chemistry of the Earth **21** (1996) 13–17.
[532] WARD, S.N., Landslide tsunami, Journal of Geophysical Research **106** (2001) 11201–11215.
[533] UI, T., YAMAMOTO, H., SUZUKI-KAMATA, K., Characterization of debris avalanche deposits in Japan, Journal of Volcanology and Geothermal Research **29** (1986) 231–243.
[534] TINTI, S., BORTOLUCCI, E., VANNINI, C., A block-based theoretical model suited to gravitational sliding, Natural Hazards **16** (1997) l–28.
[535] TINTI, S., BORTOLUCCI, E., ROMAGNOLI, C., Computer simulations of tsunamis due to sector collapse at Stromboli, Italy, Journal of Volcanology and Geothermal Research **96** 1–2 (2000) 103–128.
[536] TINTI, S., CHIOCCI, F.L., ZANIBONI, F., PAGNONI, G., DE ALTERIIS, G., Numerical simulation of the tsunami generated by a past catastrophic landslide on the volcanic island of Ischia, Italy, Marine Geophysical Research **32** 1–2 (2011) 287–297.
[537] KELFOUN, K., GIACHETTI, T., LABAZUY, P., Landslide-generated tsunamis at Réunion Island, Journal of Geophysical Research **115** F4 (2010) F04012.
[538] MAENO, F., IMAMURA, F., Numerical investigations of tsunamis generated by pyroclastic flows from the Kikai caldera, Japan, Geophysical Research Letters **34** 23 (2007) L23303.
[539] WALDER, J.S., WATTS, P., SORENSEN, O.E., JANSSEN, K., Tsunamis generated by subaerial mass flows, Journal of Geophysical Research **108** B5 (2003) EPM 2–1.
[540] YOKOYAMA, I., A geophysical interpretation of the 1883 Krakatau eruption, Journal of Volcanology and Geothermal Research **9** (1981) 359–378.
[541] YOKOYAMA, I., A scenario of the 1883 Krakatau tsunam, Journal of Volcanology and Geothermal Research **34** (1987) 123–132.
[542] TORSVIK, T., PARIS, R., DIDENKULOVA, I., PELINOVSKY, E., BELOUSOV, A., BELOUSOVA, M., Numerical simulation of a tsunami event during the 1996

volcanic eruption in Karymskoye lake, Kamchatka, Russia, Natural Hazards and Earth System Sciences **10** (2010) 2359–2369.
[543] LE MEHAUTE, B., KHANGAONKAR, T., Generation and propagation of explosion generated waves in shallow water, Technical Report DNA-TR-92-40, Defense Nuclear Agency, Alexandria, VA (1992).
[544] LE MEHAUTE, B., WANG, S., Water Waves Generated by Underwater Explosion, Technical Report DNA-TR-94-128, Defense Nuclear Agency, Alexandria, VA (1996).
[545] SATO, H., TANIGUCHI, H., Relationship between crater size and ejecta volume of recent magmatic and phreato - magmatic eruptions: Implications for energy partitioning, Geophysical Research Letters **24** 3 (1997) 205–208.
[546] MCNUTT, S.R., "Seismic Monitoring and Eruption Forecasting of volcanoes: A Review of the State-of-the-Art and Case Histories", Monitoring and Mitigation of Volcano Hazards (SCARPA, R., TILLING, R.I., Eds), Springer, Berlin (1996) 99–146.
[547] MORAN, S.C., NEWHALL, C., ROMAN, D.C., Failed magmatic eruptions: Late-stage cessation of magma ascent, Bulletin of Volcanology **73** 2 (2011) 115–122.
[548] NEWHALL, C.G., "4.12 - Volcanology 101 for Seismologists", Treatise on Geophysics, Volume 4: Earthquake Seismology (SCHUBERT, G., KANAMORI, H., Eds), Elsevier Science, Amsterdam (2007) 351–388.
[549] SCARPA, R., TILLING, R.I., Monitoring and mitigation of volcano hazards, Springer, Berlin (1996).
[550] MOUGINIS-MARK, P.J., CRISP, J.A., FINK, J.H., Remote Sensing of Active Volcanism, Geophysical Monograph Series, Volume 116, American Geophysical Union, Washington, DC (2000).
[551] SPARKS, R.S., Forecasting Volcanic Eruptions, Earth and Planetary Science Letters **210** (2003) 1–15.
[552] VOIGHT, B., SPARKS, R.S.J., Introduction to special section on the Eruption of Soufrière Hills Volcano, Montserrat, the CALIPSO Project, and the SEA - CALIPSO Arc - Crust Imaging Experiment, Geophysical Research Letters **37** 19 (2010) L00E23.
[553] DZURISIN, D., Volcano Deformation: Geodetic Monitoring Techniques, Springer / Praxis Publishing, Berlin / Chichester (2006).
[554] ZOBIN, V.M., Complex Monitoring of Volcanic Activity: Methods and Results, Nova Science Publishers, New York, NY (2013).
[555] CRIDER, J.G., FRANK, D., MALONE, S.D., POLAND, M.P., WERNER, C., CAPLAN-AUERBACH, J., Magma at depth: A retrospective analysis of the 1975 unrest at Mount Baker, Washington, USA, Bulletin of Volcanology **73** (2011) 175–189.
[556] SHEPHERD, J.P., ASPINALL, W.P., Seismological studies of the Soufriere of St. Vincent, 1953–1979: Implications for volcanic surveillance in the Lesser Antilles, Journal of Volcanology and Geothermal Research **12** (1983) 37–55.
[557] MINAKAMI, T., Fundamental research for predicting volcanic eruptions (1) earthquakes and crustal deformations originating from volcanic activities, Bulletin of the Earthquake Research Institute **38** (1960) 497–544.
[558] RIPEPE, M., DE ANGELIS, S., LACANNA, G., VOIGHT, B., Observation of infrasonic and gravity waves at Soufrière Hills Volcano, Montserrat, Geophysical Research Letters **37** 19 (2010) L00E14.
[559] VOIGHT, B., LINDE, A.T., SACKS, I.S., MATTIOLI, G.S., SPARKS, R.S., ELSWORTH, D., HIDAYAT, D., Unprecedented pressure increase in deep magma

reservoir triggered by lava-dome collapse, Geophysical Research Letters **33** 3 (2006) L03312.
[560] NICOLLIN, F., GIBERT, D., BEAUDUCEL, F., BOUDON, G., KOMOROWSKI, J., Electrical tomography of La Soufrière of Guadeloupe Volcano: Field experiments, 1D inversion and qualitative interpretation, Earth and Planetary Science Letters **244** (2006) 709–724.
[561] LESPARRE, N., GIBERT, D., MARTEAU, J., DÉCLAIS, Y., CARBONE, D., GALICHET, E., Geophysical muon imaging: feasibility and limits, Geophysical Journal International **183** (2010) 1348–1361.
[562] LESPARRE, N., GIBERT, D., MARTEAU, J., KOMOROWSKI, J., NICOLLIN, F., COUTANT, O., Density Muon Radiography of La Soufrière of Guadeloupe: First Results and Comparison with Other Tomography Methods, Geophysical Journal International **190** (2012) 1008–1019.
[563] GIBERT, D., BEAUDUCEL, F., DÉLAIS, Y., LESPARRE, N., MARTEAU, J., NICOLLIN, F., TARANTOLA, A., Muon tomography: plans for observations in the Lesser Antilles, Earth Planets Space **62** (2010) 153–165.
[564] TANAKA, H., UCHIDA, T., TANAKA, M., SHINOHARA, H., TAIRA, H., Cosmic-ray muon imaging of magma in a conduit: degassing process of Satsuma Iwojima Volcano, Japan, Geophysical Research Letters **36** 1 (2009) L01304.
[565] POWER, J.A., COOMBS, M.L., FREYMUELLER, J.T., The 2006 Eruption of Augustine Volcano, Alaska, U.S. Geological Survey Professional Paper 1769, USGS, Reston, VA (2010).
[566] PETERSEN, T., DE ANGELIS, S., TYTGAT, G., MCNUTT, S., Local Infrasound Observations of Large Ash Explosions at Augustine Volcano, Alaska, During January 11–28, Geophysical Research Letters **33** (2006) L12303.
[567] WAYTHOMAS, C., MCNUTT, S., Spatter Construct, Ice Interaction and Lahar Generation: An Example from Pavlof Volcano, Alaska, Journal of Volcanology and Geothermal Research (2015) (in press).
[568] LARSEN, J., NEAL, C., WEBLEY, P., FREYMUELLER, J., HANEY, M., MCNUTT, S., SCHNEIDER, D., PREJEAN, S., SCHAEFER, J., WESSELS, R., Eruption of Alaska Volcano Breaks Historic Pattern, Eos, Transactions American Geophysical Union **90** (2009) 173–174.
[569] SCHAEFER, J.R., The 2009 Eruption of Redoubt Volcano, Alaska, Report of Investigations 2011–5, Alaska Division of Geological & Geophysical Surveys, Fairbanks, Alaska (2012).
[570] POWER, J., LAHR, J., PAGE, R., CHOUET, B., STEPHENS, C., HARLOW, D. MURRAY, T., DAVIES, J., Seismic evolution of the 1989–90 eruption sequence of Redoubt Volcano, Alaska, Journal of Volcanology and Geothermal Research **62** (1994) 69–94.
[571] DRUITT, T.H., KOKELAAR, B.P., The Eruption of Soufrière Hills Volcano, Montserrat: From 1995 to 1999, Geological Society, London, Memoirs, Vol. 21, Geological Society of London, London (2002).
[572] NEWHALL, C.G., DZURISIN, D., Historical unrest at large calderas of the world, U.S. Geological Survey Bulletin 1855, United States Government Printing Office, Washington, WA (1988).
[573] NEWHALL, C.G., PUNONGBAYAN, R.S., Fire and Mud: Eruptions and Lahars of Mount Pinatubo, Philippines, University of Washington Press, Seattle, WA (1996).
[574] WATT, S., PYLE, D., MATHER, T., Evidence of mid-to late-Holocene explosive rhyolitic eruptions from Chaitén Volcano, Chile, Andean Geology **40** 2 (2013) 216–226.

[575] ESPÍNDOLA, J., ZAMORA-CAMACHO, A., JIMÉNEZ, Z., Some aspects of the seismicity associated with the 1982 eruption of El Chichon Volcano, Chiapas, Mexico, Journal of Volcanology and Geothermal Research **73** 4 (2006) 367–374.
[576] RUPPERT, N., PREJEAN, S., HANSEN, R., Seismic swarm associated with the 2008 eruption of Kasatochi Volcano, Alaska: Earthquake locations and source parameters, Journal of Geophysical Research **116** B2 (2011) B00B07.
[577] LUHR, J.F., SIMKIN, T., Paricutin: the Volcano Born in a Mexican Cornfield, Geoscience Press, Phoenix, AZ (1993).
[578] SIEBERT, L., SIMKIN, T., KIMBERLY, P., Volcanoes of the World, Third Edition, University of California Press, Oakland, CA (2010).
[579] BURGUETE, J., GARCIA-NAVARRO, P., ALIOD, R., Numerical simulation of runoff from extreme rainfall events in a mountain water catchment, Natural Hazards and Earth System Sciences **2** (2002) 109–117.
[580] HEINRICH, P., PIATANESI, A., HEBERT, H., Numerical modelling of tsunami generation and propagation from submarine slumps: The 1998 Papua New Guinea event, Geophysical Journal International **145** (2001) 97–111.

ANNEX: REQUIRED DATA

The SSG-21 [A-1] presents a discussion of the data required to conduct a volcanic hazards assessment, so that appropriate investigations can be planned early in the site characterization. In this annex, additional information is presented to address key issues for data collection in greater detail than presented in SSG-21 [A-1]:

- Volcanological data to support specific hazards models; considerations for eroded/buried deposits.
- Precision and accuracy of age determinations.
- Accuracy of digital elevation models.
- Geochemical considerations.
- Geophysical data collection.
- Specific data needs for models discussed in Section 5 of this TECDOC.

A.1. VOLCANOLOGICAL DATA

The most critical information in any hazards assessment is the basic information on the geologic units that comprise the volcanic system. Essential information includes the physical characteristics of these units, their relative stratigraphic (i.e. age) relationships, and volumetric information. This information is collected through detailed field investigations that map the areal (and subsurface, if possible) extent of the units, evaluates how the characteristics of these units change with distance from the source vents, and collects physical sample for detailed characterization (e.g. geochronology, geochemistry).

It is of crucial importance the field data to correctly characterize eruptive products in fallout, flow and surge, debris avalanche, debris flow, blast (high energy pyroclastic density current or not) using tools and sets of common knowledge, such as the concept of lithofacies as introduced, for instance, by Branney and Kokelaar [A-2]. These are basically data needed to estimate magnitude and intensity of explosive eruptions. Another important issue is the distinction of juvenile and non juvenile products and the interpretation of the eruptive process after the distinction. Particular emphasis should be put in basic volcanological knowledge and analytical field and laboratory techniques that form the foundation of pyroclastic volcanology, because it is of prime importance in hazards assessment (e.g. [A-3–5]).

Once the eruptive history of a volcano has been reconstructed, the petrology of individual eruptions should be studied in detail. It is crucial to look within individual layers, and pumices or other pyroclastic rocks for evidence of magma mixing or evidences of magma ascent rate from diffusion and reaction rims on phenocrysts, and from melt inclusions in phenocrysts. Another important issue is to elucidate events of magma mixing and pre-eruption volatile contents of magma from the textural information in the pyroclasts (e. g. from X-ray tomography) that gives information about the dynamics of degassing, or about the intensity of shear along the conduit walls. This kind of details is relevant for hazards assessment.

A.2. CARTOGRAPHIC DATA

For most areas, a variety of geological, topographic, satellite and related data types are available. Topographic maps, digital elevation models (DEMs), satellite images and photographs are needed as base maps. Geologic maps and cross sections are designed to reveal features of the surface and subsurface, such as the distribution of volcanoes and volcanic products. Many of these maps are the end product of the accumulation of large amounts of data, interpretation, revision, and documentation of the study region. Therefore, such data are essential in order to develop consistent conceptual models of volcanism on a variety of scales.

A.2.1 Topographic base maps

A number of different types of maps are used as bases for presentation of geological data. Topographic maps are available at different scales depending on the region. Most nationally published maps are at scales 1:10 000, 1:20 000, 1:25 000, 1:50 000, 1:100 000, or 1:250 000. For regional studies 1:100 000 or 1:250 000 scales are appropriate, but for detailed regional work 1:50 000 maps are better, and for detailed geology of a NPP site 1:10 000 or 1:25 000 would be the best scales to work with.

A.3. DIGITAL ELEVATION MODELS

A digital elevation model is a 3D computer representation of the topography of the Earth's surface created from terrain elevation data. Digital elevation models are available, at least at regional scales, for everywhere on Earth. The terms: digital surface model (DSM), digital terrain model (DTM) and DEM are almost synonymous, but sometimes the different definitions and usage create some confusion. A DSM represents the Earth's surface and includes all objects on it. The DTM represents a ground surface with no objects on it such as buildings or trees. DEM is considered to include DSMs and DTMs, indicating height information without definition on the surface. Data captured with satellites or any airborne platform are DSMs in their origin (such as SRTM: Shuttle Radar Topography Mission; or ASTER GDEM: Advanced Spaceborne Thermal Emission and Reflection Radiometer Global Digital Elevation Model).

DEMs are generally used to convey information about regional tectonic setting and are used directly in many of the hazards models. DEMs are commonly derived directly from aerial imagery, or calculated from existing topographic maps. Both methods have limitations in resolution of the derived DEM, which must be thoroughly understood and documented. Typically available DEMs of 90 × 90 m grid resolution are inadequate for most flow hazard analyses, which require significantly finer resolutions. Consider that a higher resolution 10 × 10 m DEM often has uncertainties in the vertical resolution on the order of 10 m, which is comparable to the thickness of many modelled volcanic flows. Thus, reliance on a 10 × 10 m DEM for flow hazards analysis might introduce significant errors into the analysis of potential flow pathways.

The relative accuracy of DEMs can be evaluated also by comparison of DEMs from different sources (SRTM30, GTOPO30, SRTM3, digitisation of contour lines on topographic maps, etc.); provided the precision and accuracy of the sources can be determined. It might be important to apply also DEM verification with GPS measurements, if GPS data of sufficient precision can be obtained. Anyone attempting DEM verification with a GPS however, must also understand major uncertainty in GPS readings, especially in the vertical dimension. Good

examples of various methods of DEM accuracy assessment, comparison of DEMs obtained from various sources, and their verification using GPS measurements for Merapi volcano in Indonesia is available in Gerstenecker et al. [A-6] and for flat areas in Germany in Kleusberg and Klaedtke [A-7].

In addition to satellite based methods, lower altitude platforms are available for the production of DEMs. For example, airborne LIDAR and interferometric radar techniques (e.g. InSAR) can produce higher resolution DEMs that have greater precision and accuracy than satellite based methods. Ground based systems, such as total station surveys, also can produce high resolution DEMs. Nevertheless, few of these high resolution surveys are available for large areas, and such surveys often must be conducted for specific sites. Consequently, acquisition of adequate resolution and precision DEMs should occur early in the site investigation process.

A.3.1. Getting DEM's from satellite or airborne data

For hazards assessment the most widely used satellite imagery is ASTER, particularly, the available DEM. The InSAR (interferometric synthetic aperture radar) is a technique with a large potential to become a very powerful tool in the generation of digital elevation models using two or one passes of a radar satellite (i.e. RADARSAT-1, or SRTM instrumentation), obtaining a digital map tens of kilometres per side with a resolution as low as ten meters. The digital image correlation method can be applied with other stereoscopic pairs using two optical images acquired at different angles during the same pass of an aircraft or satellite (i. e. SPOT5 or ASTER). DEM's also can be obtained from ALOS satellite. High resolution DEM's can be produced using stereo satellite imagery and GPS ground control points on a specific target area. Increasing use of airborne LIDAR for DEM generation is becoming very popular. Satellite imagery also can be useful in the development of geologic maps, especially in the delineation of different soil or vegetation types.

A.3.2. Geographic information systems

A geographic information system (GIS) is a tool designed for capturing, storing, manipulating, analysing, managing, and presenting any type of geographic data. In a GIS database, technology is merged with cartography and statistical analysis. Any type of georeferenced data can be integrated in a GIS including geological, geophysical, geochemical, modelling data, etc.

Generally, a GIS is a custom designed tool, so a GIS constructed for a specific application is not necessarily compatible with another GIS. The spatial data infrastructure (SDI) is the most important part of a GIS. In order to use spatial data in a flexible and efficient way, it is necessary to set a framework of geographic data, metadata, users and tools, connected interactively through a data infrastructure (i.e. AnSDI). GIS applications allow users to create interactive queries, analyse spatial information, edit data in maps, and show the results.

The key index variable used by GIS for all information is the spatio temporal location. A GIS can reference any variable that can be located spatially and temporally.

Entering information into the system (data capture) represents a large consumption of time for the GIS users. There is a significant level of effort involved to construct a GIS. In addition to providing common framework for map data, it can be used for quality assurance

records for metadata from all relevant investigations. Both proprietary (e.g. ArcInfo) and open source (e.g. GRASS, QUANTUM GIS) software are available to meet this need.

A.3.3. Geologic maps

An increasing level of detail is needed as the investigation proceeds closer to the site. Regional scale geologic maps at 1:100 000 often provide adequate information for developing an understanding of regional tectono magmatic framework. However, map detail at scales of 1:50 000 or higher resolution are necessary to characterize individual volcanic centres, and develop the initial information for the hazards assessment. Often, mapping at scales of 1:25 000 or higher is necessary to develop the information needed to support the detailed hazards assessment.

Desirably, geologic maps can be accompanied with stratigraphic correlated cross sections, which are very important and usually integrated in maps although not always.

A.3.4. Tectonic/Structural maps

To emphasize the distribution of structural features a tectonic map should be prepared in order to depict the relationships between volcanoes and local structures. Volcanism patterns follow the distribution of the stress field at a certain geologic time so it is important to represent the faults and fractures in relation to the distribution of volcanoes and their products.

A.3.5. Uses of geologic maps in hazards assessment

The basic information available concerns the type of materials that will be encountered at or beneath the ground surface and rock structure. This information is valuable for the following purposes:

- Identification of natural hazards that may exist in any given area. This information is important in planning, design, and maintenance of engineering structures and in making environmental assessments. This identification depends on the characterization of the magmatic/eruptive processes that have occurred in the recent past of the region and the determination on the repetition of such events through time.

- Distribution of volcanic deposits is crucial to understand the dynamics of the eruptive processes in the site's region.

- Determination of volumetric features of the deposits in order to determine the magnitude of the past eruptions.

A.3.6. Hazards maps

Volcanic hazard is the probability or likelihood of a volcanic process occurring characterized by a certain magnitude. It can also be the probability of related products being distributed spatially or temporally or the probability to reach a maximum extent in a determined area. Thus, a hazard map highlights areas that can be affected or are vulnerable to a particular volcanic process. Volcanic hazards maps depict the probability or likelihood of occurrence of a certain process in an area, characterized by a certain magnitude; or the spatial distribution of the related products, or the maximum range of the products, or the maximum influence area of them, during the occurrence of a process of a given magnitude, or occurrence of certain process in a given interval of time.

Several concepts exist about presenting hazards, and so there are several types of hazards maps. In a volcanic hazards assessment for a particular nuclear installation site a relevant hazards map may not exit but, where one does, a review of the way it was elaborated conceived is essential if the recommendations of SSG-21 [A-1] guidelines are to be followed.

It is crucial to address volcanologic maps. This kind of maps cartographically represents data such as isopachs, isopleths, flow directions, eruptive lithofacies such as valley confined versus unconfined pyroclastic density currents, size of ballistics, number density of monogenetic vents. These maps depict physical volcanologic data and dynamic flow indicator data that, at a certain scale, represent fundamental information for the hazards assessment. A variety of volcanologic maps can exist, which show these data for different volcanoes in the study area. Among initial tasks would be, for instance, to make a synthesis of cumulated tephra thickness from different sources, and map the envelope of some threshold thickness considered important for the analysis. It is crucial to summarize these existing data or produce them from field studies as an input to models such as those described in Section 5. Typically, such maps can be associated with correlated stratigraphic sections, which can be used to develop time volume relationships and detailed interpretations of subsurface volcanic deposits.

A volcanologic map is different from a larger scale geologic map and is also different from a hazards map. This kind of map goes beyond the classical geologic map. Volcanologic maps identify, spatially and genetically, the different types of eruptive products. The process that governed the genesis and emplacement of these products is deciphered from field and laboratory analyses. The analyses reconstruct the deposits' spatio temporal sequence, grouping them in eruptive events and associating them with specific sources, dating the related events, and correlating them across a specific area. Examples of volcanologic maps are those of Etna [A-8], Soufrière of Guadeloupe [A-9], Katmai [A-10], Kilauea [A-11] and Piton de la Fournaise [A-12]. The techniques used in volcanology to accomplish these studies include the Streckeisen classification [A-13], [A-14], approaches for field evaluations (e.g. [A-3–5], [A-15]) and methods to process the field data (e.g. [A-16–19]).

A.4. PETROLOGICAL AND PETROGENIC DATA

One of the first questions to answer during the hazards evaluation at a nuclear installation, regarding the magmatic processes in the region, is which magmatic processes have occurred in the region in the recent geological past? Petrogenic studies of igneous rocks involve characterization of the source regions of the magmas, the conditions of partial melting, and the extent of subsequent modification of primary mantle derived magmas during transport and storage in crustal magma chambers. Such studies must be based on sound field

observations, involving careful mapping and sampling of the range of rock types exposed at a particular locality, and on a comprehensive knowledge of the petrography, major, minor and trace element and radiogenic and stable isotope geochemistry of the samples. Additionally, if the igneous activity is not recent, its age must be constrained, ideally by isotopic dating techniques. There are a few general features to look for when a hazards evaluation is made. The petrological characterization of the magmas erupted within a site's region is important in order to identify the kind of eruptive activity has occurred in the past and that may occur in the future.

A.4.1. Petrography

For the nomenclature of volcanic rocks, the QAPF (quartz alkali feldspar plagioclase feldespathoid) classification is one of the most used, based on modal proportions of constituent minerals [A-20], [A-21].

The chemical composition of the magma influences strongly the mineral composition and proportions so, it is important to determine the modes. The cooling history of the magma is reflected in the texture of the rock. Textures of mineral assemblages often reflect evidence of past magma mixing events, or repeated cycles of heating and cooling. Textures also can reflect periods of stagnation in the crust, or characteristics of rapid magma ascent from depth. Glass inclusions in larger minerals can preserve pre-eruption volatile contents and microanalyses of these help better understand the potential for explosive events. Textures also can reflect periods of stagnation in the crust, or characteristics of rapid magma ascent from depth.

It is important to determine petrographic features in the igneous rocks from the region surrounding a site during hazards assessment because the characteristics of minerals can provide important insights on magmatic processes.

A.4.2. Magma genesis in the region

It is generally accepted that partial melting of mantle material produces primary magmas of mafic or ultramafic composition in most tectonic settings, and that subsequent differentiation processes, including fractional crystallization, magma mixing and crustal contamination, are responsible for the generation of the wide compositional spectrum of igneous rocks. The geochemical characteristics of these primary magmas depend upon parameters such as the source composition and mineralogy and the depth and degree of partial melting; factors which may vary from one tectonic setting to another. Primary magmas appear to be generated within a very restricted depth range within the upper 100–200 km of the mantle, although in detail their precise depths of origin are poorly constrained.

In order to characterize magma series associated with specific tectonic settings a series of diagrams are useful tools, such as Harker diagrams. A Harker variation diagram of wt. % $Na_2O + K_2O$ versus wt. % SiO_2 provides a useful way of displaying the wide compositional range of terrestrial volcanic rocks and their nomenclature [A-22]. A simple diagram like this is suitable in the classification of igneous rocks as it makes direct use of their major element chemical composition, expressed in terms of weight percent constituent oxides. This classification diagram however, works well only for fresh rocks due to mobility of alkalis during weathering and metamorphism.

Volcanic rocks may be subdivided into members of two major magma series, alkalic and subalkalic. Each of these magma series contains rocks ranging in composition from mafic to felsic, and although the boundary between them is marked as a solid line it is actually

gradational. The compositional range of volcanic rocks may be regarded as a consequence of two fundamental processes, partial melting and fractional crystallization. These are not the only processes responsible for the compositional diversity of magmas but they are almost certainly the dominant ones.

Alumina is the second most abundant oxide in igneous rocks after silica. In general, the most abundant minerals occurring in igneous rocks are feldspars. Therefore, alumina saturation indicates an excess or lack of Al for making up the feldspars with three possibilities: peraluminous, metaluminous, and peralkaline.

It is important to distinguish source characteristics that are inherited by the primary partial melts at their depth of segregation from those arising from subsequent processes. Variations in the isotopic compositions of Sr, Nd and Pb provide important constraints on the structure and compositional heterogeneity of the upper mantle beneath the volcanoes of interest.

A.4.3. Major and trace element geochemistry, and isotopes

The most used feature to distinguish the igneous rocks is their chemical composition. A wide variety of instrumental techniques are commonly used for silicate rock analysis, permitting the determination of an extensive range of major and trace elements on a routine basis. X-ray fluorescence (XRF) is widely used for analysing rock samples for major elements (Na, Mg, Al, Si, P, K, Ca, Ti, Mn, Fe) and selected trace elements (Rb, Sr, Y, Nb, Zr, Cr, Ni, Cu, Zn, Ga, Ba, Pb, Th, U, La, Ce, Nd, Sm). Instrumental neutron activation analysis (INAA) is sometimes used for the analysis of specific trace elements (Sc, Co, Cr, Cs, Hf, Ta, Th, U) down to detection limits in the ppm and ppb range, and is especially useful for the analysis of the rare earth elements (La, Ce, Nd, Sm, Eu, Tb, Yb, Lu). Alternatively, isotope dilution mass spectrometry may be used to determine REE. Inductively coupled plasma (ICP) is also a technique currently applied to the analysis of geological materials.

None of the commonly used techniques can provide analyses of H_2O and CO_2 or the ratio of Fe^{2+}/Fe^{3+} in igneous rocks. Consequently, these must be determined independently by other methods, such as wet chemical analyses or measurements of glass inclusions trapped in phenocrysts.

A.4.4. Trace element geochemistry

The behaviour of trace elements during the evolution of magmas is expressed in terms of a partition coefficient (i.e. abundance between crystalline and liquid phases). Harker type variation diagrams may be plotted using trace elements instead of major element oxides and may be interpreted in a similar way. Highly incompatible trace elements such as Zr may be useful as an index of differentiation if SiO_2 or MgO are inappropriate.

In order to graphically compare REE (La, Ce, Pr, Nd, Pm, Sm, Eu, Gd, Tb, Dy, Ho, Er, Tm, Yb, Lu) abundances of different rocks, the Oddo-Harkins effect should be eliminated by normalizing the concentrations of individual REE in a rock to their abundances in reference materials, such as chondritic meteorites [A-23]. There are several variants of plots (spider diagrams) where the order of the elements plotted varies slightly, and different normalization constants have been adopted. For example, Wood [A-24] and Wood et al. [A-25] normalize to a hypothetical primordial mantle composition, whereas Thompson et al. [A-26] and Sun [A-27] normalize their data to chondritic abundances, with the exception of K and Rb. These diagrams

are essentially identical to each other except for the order of some of the elements. This is somewhat arbitrary, being designed to give a smooth pattern for average MORB [A-27].

Analytical error may be the source of many apparently spurious inflections in spider diagram patterns. However, once these effects have been taken into consideration, the peaks, troughs, slopes and curvature of the patterns may provide invaluable petrogenic information concerning crystal liquid equilibria.

A modified version of the spider diagram is most useful for comparing the trace element characteristics of different types of basalts. The sequence of elements plotted may be the same as that in a conventional spider diagram, or different (e.g. [A-28]). In this type of diagram the elements are divided into two groups based on their relative mobility in aqueous fluids. Sr, K, Rb and Ba are mobile and plot at the left of the pattern, while the remaining elements are immobile. The elements are arranged such that the incompatibility of the mobile and immobile elements increases from the outside to the centre of the pattern. Pearce considers that the shape of these patterns is not likely to be greatly changed by fractional crystallization or variable degrees of partial melting, and that they may consequently be used to discuss source characteristics. Such MORB normalized trace element variation diagrams are used to constrain mantle source's nature of subduction related basalts and continental flood basalts.

Partial melting of the upper mantle produces primary magmas. The composition of those magmas is not modified subsequently by differentiation processes (i.e. fractional crystallization, crustal contamination, magma mixing, liquid immiscibility and volatile loss). Such magmas encompass a variety of types including tholeiitic, calc alkaline and alkaline basalts. Clearly, it is of great petrogenic significance to be able to recognize primary magma compositions, as these are parental, giving rise through differentiation processes to more evolved (i.e. more silica rich) magma types.

A.4.5. Isotopes

Isotope geochemical studies are based on two groups of isotopes, radiogenic and stable. Radiogenic isotopic variations are caused by the radioactive decay of elements, whereas stable isotopic variations are the consequence of mass fractionation in chemical reactions. In general, mass fractionation effects are comparatively small, except for the lighter elements, O, H, C and S. The naturally occurring, long lived radioactive decay schemes of K, Rb, Sm, Th and U are critically important in establishing the chronology of magmatic events.

The importance of radiogenic isotopic variations is that they frequently survive the chemical fractionation events, which accompany the formation and evolution of magmas, as isotopes of the heavier elements are not separated from each other through crystal liquid equilibria. Thus, during partial melting, magma will inherit the isotopic composition of its source, and this will remain constant during subsequent fractional crystallization processes, provided that the magma does not become contaminated by interaction with isotopically distinct wall rocks or other batches of magma. As a consequence, estimates of the present day isotopic characteristics of the mantle source region of basaltic magmas may be obtained from studies of young oceanic volcanic rocks (MORB and ocean island basalt), which have not been significantly contaminated by crustal rocks en route to the surface.

Isotopes of the rare gases, particularly He, have proved to be useful tracers of the role of primordial mantle components in the petrogenesis of oceanic island basalts. Additionally,

cosmogenic radionuclides such as ^{10}Be are important as potential tracers of the role of subducted sediment in island arc and active continental margin magmatism.

The main isotopic series used in petrogenic and geochronologic studies are discussed briefly below:

A.4.5.1 Rb - Sr

The alkali metal Rb is an incompatible element during magma crystallization, and has two naturally occurring isotopes, ^{85}Rb and ^{87}Rb, of which ^{87}Rb is radioactive and decays to stable ^{87}Sr by beta emission. The naturally occurring isotopes of the alkali earth metal Sr are: ^{88}Sr, ^{87}Sr, ^{86}Sr and ^{84}Sr. The age and Rb/Sr ratio in a rock or mineral that contains Rb is governed by the precise isotopic composition of Sr.

The initial isotopic composition of Sr in volcanic rocks at the time of their formation can provide important information about the mantle sources from which the magmas originate, and the processes by which their chemical and isotopic compositions may be subsequently modified during ascent to the surface.

A.4.5.2 Sm - Nd

Samarium and neodymium are light REE, the concentrations of which in igneous rocks increase with increasing degree of differentiation, as they are incompatible. However, the Sm/Nd ratio decreases, as Nd is concentrated in the liquid relative to Sm during the course of fractional crystallization. A positive value of the epsilon parameter (ε_{Nd} [A-29]) implies that the magmas were formed from depleted mantle, whereas a negative value indicates that they were derived from enriched mantle sources that had a lower Sm/Nd than a chondritic uniform reservoir.

A.4.5.3 Combined Nd - Sr

Typical continental crustal rocks have lower Sm/Nd and therefore lower ^{143}Nd/^{144}Nd ratios (i.e, negative ε_{Nd} values) than those derived from the upper mantle. As a consequence, combined Nd–Sr isotopic studies potentially provide a powerful tracer for contamination of magmas by continental crustal rocks [A-30].

A.4.5.4. U - Th - Pb

Igneous rocks contain Pb, the isotopic composition of which reflects multistage histories, having evolved in systems with varying U/Pb and Th/Pb ratios for varying lengths of time. U and Th are both preferentially concentrated in silicate melts compared to Pb and, consequently, the U/Pb and Th/Pb ratios of crustal rocks are higher than those of the mantle. Additionally, U and Th are preferentially concentrated in upper crustal rocks and, consequently, the upper and lower crust may have distinctly different Pb isotope signatures. Thus, Pb isotopes may provide powerful constraints for the nature of crustal contaminants in continental volcanic suites.

A.4.5.5. U - series disequilibrium

The decay series arising from ^{238}U and ^{235}U contain radioactive isotopes of many different elements. Decay products from U may be separated from their parents and from each other during partial melting and subsequent fractional crystallization, because of their different geochemical properties. The resulting radioactive disequilibria may be used for dating over time periods ranging from a few tens of years to one million years [A-31]. Additionally, for young volcanic rocks, it may provide important information about the partial melting processes, and the time elapsed between the initial melting and subsequent extrusion of the lava [A-32]. The slope of the isochron begins to deviate detectably approximately 100 years after crystallization and approaches unity about 10^6 years after crystallization. Thus 10^3–10^6 years is the useful range of this geochronometer.

A.4.5.6. He isotopes

Basalts from the oceanic islands of Hawaii and Iceland have high $^3He/^4He$ ratios, which have been considered to reflect the involvement of relatively undegassed (i.e. primordial) mantle components in their petrogenesis [A-33], [A-34]. By contrast, basalts from the oceanic islands of Tristan da Cunha and Gough are characterized by low $^3He/^4He$ ratios of around 5, which may suggest the involvement of recycled source components.

A.4.5.7. Cosmogenic radionuclides: ^{10}Be

The identification of ^{10}Be in some recent subduction related lavas has been used to argue for the role of subducted oceanic sediments in their petrogenesis. However, because of its relatively short half life, the absence of ^{10}Be does not necessarily signify an absence of subducted sediment in the magma.

A.4.5.8. Oxygen

The isotopic composition of oxygen in young volcanic rocks has been used in conjunction with radiogenic isotopes of Sr, Nd and Pb to detect the contamination of basaltic magmas by crustal rocks [A-35], [A-36]. Compared to mantle derived magmas, the latter are enriched in ^{18}O and radiogenic ^{87}Sr, but depleted in radiogenic ^{143}Nd. As a consequence, addition of O, Sr and Nd from ancient silicic crustal components to basaltic magmas can cause positive correlations between $\delta\ ^{18}O$ and $^{87}Sr/^{86}Sr$ and negative correlations between $\delta^{18}O$ and $^{143}Nd/^{144}Nd$. However, the shape of the mixing curve may differ significantly depending upon the actual mechanism of contamination, which may be useful in petrogenic modelling.

A.5. QUATERNARY GEOCHRONOLOGY

A wide variety of geochronologic methods can be used to quantitatively and qualitatively estimate the age of rocks. All kinds of geological materials with ages from billions of years to historical records can be dated. However, for hazards assessment the interest is focused in the eruptive events occurring during the Quaternary period, which spans the last 2.6 million years [A-37]. As discussed in Section 4, particular attention is given to events that happened in the last 11,700 years (i.e. the Holocene Epoch [A-37]). In the following sub sections there is a description of the most useful dating methods when evaluating hazards to a site.

Although radiometric dating requires very careful laboratory work, its basic principle is simple: the rates at which various radioactive elements decay are known, and so the ratio of the radioactive element to the element into which it decays shows how long ago the radioactive element was incorporated into the rock. The challenge rests in determining if the system of interest has remained closed to the gain or loss of elements since its formation.

The methods mentioned below focus on age determinations of less than two million years, which are ages that are of most interest to the hazards assessment. In addition, some of these methods resolve ages within thousands of years, which can be a significant distinction at recently active volcanoes.

A.5.1. ^{14}C

Today, the majority of commercial radiocarbon laboratories utilize the gas counting (GC) method and liquid scintillation counting (LSC), which uses sample sizes >100 mg [A-38]. However, the recent development of the accelerator mass spectrometry method (AMS) of direct ^{14}C isotope counting [A-39–41] has the crucial advantage that < 100 mg sized samples are feasible for dating. The radiocarbon dating method is the technique most widely applied for dating events that occurred in the last 50 000 years or so.

This method is used to estimate the age of volcanic materials indirectly, in that organic material trapped in the volcanic deposit is analysed. It is the context in which the organic matter is found, related to the volcanic products, that makes this method so valuable in volcanology. It is important to notice that the best samples are not necessarily the largest samples. For instance, stumps included in laharic sequences might be trees that died long before the laharic event. In the case of pyroclastic density currents, the pyroclastic materials can char old dead trees. In these cases, the bark or outermost rings of a tree, or samples of tiny branches and burnt bushes provide the best ages.

It is worth mentioning that wood cannot be charred and preserved in pyroclastic deposits as well as charred. If possible, it is needed to date older and younger parts of the same large tree. Any populations of ^{14}C dates on a deposit will likely reflect the age distribution of the palaeo forest prior to its destruction by pyroclastic materials so it is not uncommon, depending on the longevity of the trees that were incorporated in the deposits, to have a spread of value. In addition, ^{14}C age dates need to be calibrated with other methods such as dendrochronology, because the non constant ratio of carbon isotopes in nature affects the dating [A-42], [A-43]. Also, a radiocarbon age need not be unique, and can have several ‘ages’ dependent on the curve of atmospheric ^{14}C through time [A-44].

A.5.2. $^{40}Ar/^{39}Ar$

$^{40}Ar/^{39}Ar$ ages allow estimating thermal histories of geologic materials. Theoretically, samples of any age can be accurately and precisely dated by the $^{40}Ar/^{39}Ar$ method, however, a minimum age of about 10–20 ka represents a practical limit for most deposits. Nevertheless, the eruption of Vesuvius of the year 79 AD has been dated by $^{40}Ar/^{39}Ar$ under highly favourable conditions [A-45], [A-46]. The age of formation, post formation thermal and alteration history can be obtained when applying this technique and along with other geochronologic techniques to various minerals within a single sample. In properly collected, irradiated and treated samples (i.e. high K bearing) age dating with $^{40}Ar/^{39}Ar$ is usually accurate within 1 to 2 percent.

Assumptions must be made when dating minerals in order to get age information for rocks. In geochronology with $^{40}Ar/^{39}Ar$ it is assumed that the rock retains all of its ^{40}Ar after cooling below the closing temperature and that this was properly sampled during analysis. Fresh unaltered samples are needed to carry out this dating method. Devitrification of aphyric volcanic rocks might be a problem but good dates can be achieved when using fresh whole rock. In the case of lava flows, whole rock dating renders the best results as compared with the dating of single concentrations of minerals (e.g. hornblende or biotite). In felsic rocks, sanidine can be used successfully to get young age determinations (on the order of tens of thousands of years).

A.5.3. K/Ar

Several assumptions must be accepted as true for a date to represent the true age of a rock [A-47]:

- In situ decay of ^{40}K produces the radiogenic argon that is eventually measured in the sample since the crystallization of the rock.
- Contamination of samples by absorption of non radiogenic ^{40}Ar from the atmosphere was avoided by careful handling.
- The place from where the sample was taken must be a closed system since the occurrence of the event whose date is under determination.

The technique is mainly applied for dating minerals and rocks over 100 000 years old. It is likely that not enough ^{40}Ar accumulated during shorter timescales, in order to be measured with accuracy.

A.5.4. U-series system

Quaternary sedimentary carbonate and silica, and fossils can be reliably dated using the U-series dating method. Although the interest is the dating of volcanic events, volcanic products may be interbedded with other kind of sedimentary deposits and other geological features that can be related with environmental changes, such as deglaciation and triggering of voluminous pyroclastic material in the Chilean Andes.

Using the U-Pb geochronology of igneous rocks, the age of emplacement of igneous rocks can be estimated using zircon or another high U mineral (e.g. monazite, allanite, rutile), or to evaluate the thermal history (e.g. sphene, apatite) of the rocks, particularly in conjunction with $^{40}Ar/^{39}Ar$ ages. Depending on the U-Pb isotopes used, dates can range from the Quaternary period to the age of the Earth.

Ion microprobe U-Pb dating of zircons using a sensitive high resolution ion microprobe–reverse geometry (SHRIMP RG) can achieve high resolution results. Zircons from rocks of the magma chamber walls at Mount Mazama, Oregon U.S.A., have been successfully dated in order to get the age of the rocks and the solidification time of the rocks with a high precision [A-48]. This and the SIMS U-Pb geochronology open new possibilities for dating young zircon bearing rocks [A-49].

A.5.5. Cosmogenic isotopes

The most frequently measured cosmogenic nuclides, produced when cosmic radiation hits ^{16}O and ^{28}Si, are ^{10}Be and ^{26}Al. Both can be utilized to measure how long geologic material on the surface has been exposed to cosmic radiation [A-50], [A-51]. The concentration ratio of these two nuclides can be utilized without further additional data, since both are decaying, to define the age when ^{10}Be and ^{26}Al were covered up by soil and shielded from any further cosmic radiation, which could typically be between 2 and 10 metres. Pleistocene ages often can be determined with this method, although Holocene ages can also be achieved [A-52], allowing for age determinations of events between thousands of years to a couple of million of years. To date surface rocks, ^{36}Cl nuclides are also measured. This method can also be used to obtain Pleistocene ages [A-53], [A-54].

A.5.6. Thermoluminescence

Thermoluminescence (TL) is a technique used for dating sediment and archaeological materials [A-55] with an age range of 1000 to 500 000 years. This technique is used on sediment grains with defects and impurities, which act as natural radiation dosimeters when buried. Part of the radioactive decay from K, U, Th, and Rb in the soil, and contributions from cosmic rays, are trapped in sediments through time. The longer the burial, the more absorbed dose is stored in the sediment; which is proportional to a glow curve of light obtained in response when the sample is heated or exposed to light from LEDs. Greater light doses indicate an older age. Almost any material heated above 500ºC is a candidate for TL dating. The method can be of use for dating volcanic material heating archaeological remains or sediments in relation with eruptive sequences.

A.5.7. Electron Spin Resonance

Electron Spin Resonance (ESR) is a dating method that measures radiation induced defects or trapped electrons' density in bone and calcite bearing materials. ESR measurements of a sample can be repeated several times because the method does not imply sample destruction [A-56].

This method can be useful for hazards assessment of a site when the datable materials are in close context to a particular volcanic deposit. In theory, the ESR age dating accuracy covers a range/period of some thousand years up to over a million years, but the ongoing uranium accumulation decreases the liability of ESR age assessments so that assessments of material older than 300 000 years will show higher uncertainties [A-56].

A.5.8. Varnish dating

Rock surfaces can be dated using the varnish dating method at places where people left pictorial remains [A-57]. This method implies small destruction of the sample. Using this method cobbles and exposed deposits in arid settings whose ages are within a range of several thousand to a few million sometime can be dated. This can be achieved with a new analytical method developed by Harrington and Whitney [A-58] determining the varnish cation ratio of a sample using a scanning electron microscope equipped with an energy dispersive X-ray analyser (EDAX). The age range of this method is early to late Pleistocene (thousands to a couple of million of years).

A.5.9. Fission track

Fission track analysis allows the determination of the thermal history of a sample. Fission tracks are preserved in minerals with a small content of uranium (i.e. apatite, sphene, and zircon). The spontaneous fission of ^{238}U present in the mineral produces these tracks [A-59]. In the case of apatite, all tracks disappear when a rock is heated above 120°C. Above ≈ 200° and ≈ 300°C zircon and sphene loose their tracks respectively. When a rock starts cooling the tracks also start to accumulate. In the case of volcanic rocks and shallow intrusions the cooling process is very fast, and so the ages determined by this method will indicate the date of the initiation of the cooling. The fission track method is one of the most successful methods that can be used for dating volcanic rocks, but the absence of sphene and zircon in many volcanic rocks limits its utility [A-60], [A-61]. The dating range is from 1 000 to 300 000 000 years.

A.5.10. Palaeomagnetism

Palaeomagnetism and archaeomagnetism rely on remnant magnetism. Volcanic rocks that cool rapidly record the direction and intensity of the local magnetic field once their temperature falls below the Curie temperature of magnetic and paramagnetic material. A geomagnetic polarity time scale has been calibrated using radiometric dating methods. Using the polarity time scale, an age range for a sample can be estimated using the polarities preserved in the rock. Paleomagnetic orientations are particularly useful in developing stratigraphic correlations, as rocks from the same eruptive event should have identical to nearly identical magnetic orientations. In order to determine the age of a sample, it is needed to know the approximate age of the sample using other dating methos such as K-Ar. This method helps to estimate the ages of volcanic rocks of almost any age within the Pleistocene and Holocene [A-62–66].

A.5.11. Tephrochronology

The characteristics of tephra (i.e. volcanic ash) such as mineralogy, morphology of glass shards, and the nature of other components present are used to establish the fingerprint that allow the correlation of tephra layers at several locations. It is necessary that the age of some of those layers needs to be determined in advance by any of the quantitative methods described above. Tephrochronologic studies are usually combined with other studies such as stratigraphic or magnetostratigraphic studies. The age range is normally between 300 000 and 500 000 years, the mean life of volcanic systems, central volcanoes however, may reach an age of over 2 million. Typically, a small tephrochronologic study requires the collection of ≈ 10 samples for examination, analysis and evaluation, but for a large study ≈ 100 samples may be required, as well as well as a longer time (> 1 year) for the study and process of the results [A-67], [A-68].

A.5.12. Tree ring

Dendrochronology can be extremely precise, sometimes allowing identification of the specific year a tree died. Dendrochronology has been used to correct or calibrate radiocarbon dates, which are designated by the abbreviation cal BP, or calibrated years before the present (i.e. before 1950). Worldwide tree ring sequences have been established during the last century; for instance, the Hohenheim Laboratory completed a 10 000 year sequence on oak

trees for central Europe [A-38], [A-69], [A-70]. Volcanologists use the tree ring data to also indirectly date the eruptive sequences in a region [A-71].

A.5.13. Palaeontological methods

Palaeontology seeks to map out how living things have changed through time. For volcanologists, known remains of living species may help to recognize the age of a deposit and the environment where volcanic products were deposited. A substantial obstacle to this aim is to define the age of fossils. Beds preserving fossils usually lack the materials needed for radiometric dating.

A.6. CLASSIFICATION OF VOLCANOES IN THE REGION

There are several schemes for the classification of volcanoes, some of them confusing because the classification schemes have been mixed with the eruptive styles of volcanoes and/or types of eruptions of volcanoes. A single volcano can be classified according to several schemes; the classification gives information about the behaviour of a single volcano or group of volcanoes in a region or the surrounding area where a NPP is located.

A.6.1. Classification of volcanoes according to their activity

The classification of volcanoes according to their range of past activity is always a matter of discussion. Some countries classify an active volcano as those that have had eruptive activity in historic time. However, this definition has a major problem: the history at several volcanic regions is very recent. Places such as Kamchatka and the Kurile Islands have a very short history in terms of human occupation so documentation of their activity becomes difficult. A better and more widely accepted definition of active volcanoes are those that have erupted within the Holocene period, since the end of the last glaciation 10 000 years before present.

Even the 10 000 year cut off poses some problems. If the limit for considering an active volcano is set at 10 000 years before present, another problem is that some countries (such as Japan, Indonesia or Chile) would struggle to give attention to the large number of active volcanoes within their territories. Geological studies show that some volcanoes can have eruptive activity for tens of thousands of years and have repose periods of hundreds of thousands of years as in the case of Tequila volcano in Mexico [A-72]. Very large volcanic systems like Toba and Yellowstone can also remain quiet for tens of thousands of years before erupting again [A-73], [A-74].

Szackacs [A-75] gives a phenomenological definition as: “A volcano should be considered active if its magmatic plumbing system is still working”. However, this definition implies the existence of a monitoring network in order to discriminate whether a volcano is active or not. Furthermore, even with a monitoring system, this task may not be achieved.

For volcanic hazards assessment, it is fundamental to recognize potentially active volcanoes. However, the most difficult task is to distinguish an active volcano or volcanic field from an extinct volcano or volcanic field. Therefore, a series of volcano stratigraphic studies accompanied by extensive dating work are very important to decide the possibility, or not, for reactivation of a volcanic system. Generally highly conservative assumptions about potential future activity are warranted.

A.6.2. Classification of volcanoes according to their tectonic setting

Identification of the tectonic setting to which an active volcano or group of volcanoes belongs is not a difficult task in general. However, some volcanoes typical of a certain type of tectonic environment coexist with another completely different one. This is true for several monogenetic volcanoes in Trans-Mexican volcanic arc; there are several small volcanoes that have an oceanic island basalt signature coexisting with the typical subduction type volcanoes of the arc [A-76–80]. This kind of apparent contradiction can lead to a misunderstanding of the origin of magmatism and, therefore, to a different view on the potential eruptive scenarios for the future.

A.6.3. Classification of volcanoes according to their chemical composition

The name given to a volcano according to a chemical classification scheme might not seem to be relevant at all. What is relevant, in fact, is the information the name brings with it. For instance, a felsic volcano is normally more explosive than a mafic volcano, and the related volcaniclastic products more abundant and widespread. So, for hazards evaluation, these names may indicate how well distributed the products of the different volcanoes might be. When reading the background literature of a region all these very general terms are very informative in order to plan fieldwork and a sampling campaign. And, as a consequence, hazards are associated with the compositional nature of the volcanoes (i. e. explosive vs. effusive processes).

However, this can drive to very broad generalizations. It is worth to note that there are many exceptions, e.g. huge mafic ignimbrites that swept large areas around Masaya, Taal, and other volcanoes [A-81].

A.6.4. Classification of volcanoes according to their genesis

The importance of classifying volcanoes properly during hazards assessment can be summarized as follows: for a polygenetic volcano the main questions are when and how the volcano will erupt? In the case of monogenetic volcanoes, the same questions remain but an additional question is, “where will the next volcanic activity take place?” The nature of the genetic lineage of a volcano indicates the kind of hazards assessment approach that it will be necessary to apply.

A.6.5. Classification of volcanoes according to their morphology

The proper morphological classification of a volcano has an importance in hazards assessment: by using a simple word regarding the volcano’s classification, a lot of implications for the genesis and processes occurring at the volcano are included. For instance, a scoria cone implies explosive activity mainly of Strombolian to violent Strombolian type. Similarly, a tuff cone, tuff ring and maar, besides the morphological connotation, imply hydro magmatic activity. Volcano morphology may be indicated in the geological literature at the time of reviewing the regional background of a site.

A.6.6. Classification of volcanoes according to their eruptive style

Classification of a volcano according to its eruptive styles does not imply the volcano might not erupt in a different way in the future or may not have erupted in a different way in the past. It is only a qualitative indication about the most common (or most recent) eruptive

behaviour the volcano has had in the past. For hazards assessment, this is important in a regional perspective because it allows setting the most common eruptive style within a region where a NPP facility is planned. If it has not been determined for a site, it should be determined at the first step.

A.7. GEOPHYSICAL INFORMATION

Geophysical information might not be used directly in the hazards modelling, but for the volcano tectonic framework it is nevertheless very useful. Recognition of scale is important, as large scale data are useful for the regional tectonic framework, whereas smaller scale, ground based surveys can be used to resolve individual features and buried structures (e.g. [A-82]). An important part for hazards assessment is the geophysical detection of buried volcanic features, which commonly can occur in basaltic volcanic fields located in subsiding or depositional basins.

A.7.1 Seismicity

A.7.1.1 Tectonic and volcanic earthquakes

Tectonic earthquakes reflect sudden slip (i.e. brittle fracture) along a fault plane. Analysis of waves at different seismic stations allows determination of where the rupture began, how much slip occurred, and the sense of slip. Similar to tectonic earthquakes, volcanic earthquakes are complex and diverse, and may exhibit very different frequency content from one volcano to another (or even within a volcano). Volcano tectonic earthquakes are from brittle rupture, but other types of volcanic earthquakes can include volumetric expansion or collapse. Soft, hydrothermally altered or hot rock, or even viscous magma, can fracture but produce lower frequency, less impulsive signals than tectonic earthquakes. Elevated pore water pressures can also be involved, especially in geothermal areas (e.g. [A-83–85]).

A.7.1.2. Taxonomy of volcanic signals

It is important to distinguish volcanic signals rather than volcanic earthquakes because some seismic signals have different characteristics than typical tectonic earthquakes. There are many possible classifications for volcanic signals; so, it is necessary to adapt a classification scheme to each volcano (or eruptive phase). This classification system is very important because some signals serve as precursors of an eruption. Some classifications are based on the waveform (i.e. time or frequency), or are based on the type of source mechanism [A-86–89]. Common volcanic seismic signals can be as follows:

A.7.1.3. Volcano tectonic earthquakes (VT)

Short period earthquakes result from cracking in an elastic medium, as for classical tectonic earthquakes, but occurring near a volcano and in relation to its activity. For instance, they may be generated as a response to a local change of the stress regime due to fluid movement (i.e. magma, water, gas). P and S waves are clear, usually with frequencies > 5 Hz, with no lengthy codas.

A.7.1.4. Long Period events: LPs

These signals are common at volcanoes, and are due to the presence of fluids (e.g. magma conduits, water, steam, gas and ash filled fissures). They result from resonance of a crack (i.e. fissure) or conduit induced by fluid pressure changes. They are characterized by relatively low frequencies. Some have a high frequency onset followed by quasi monochromatic oscillations with peak energy near 1.5 Hz, lasting 20 s or more.

A.7.1.5. Very Long Period events: VLPs

These signals are thought to reflect passage of magma or gas through a constriction.

A.7.1.6. Hybrid Events

These are events resulting from brittle faulting in zones of weakness intersecting, or nearby, a fluid filled crack. They are mixed events consisting of a high frequency onset and low frequency coda, mixed first motions, and a non dispersive harmonic wave train in coda. These signals may start as HF (high frequency) signals and continue with LF (low frequency) signals, or vice versa. They can be modified VTs due to paths in complex media (getting across a magma chamber for instance). If they are true hybrids (i.e. not modified VTs due to propagation effects), they are the result of two imbricated physical processes: fluid movement provoking rupture of cracks in its vicinity or a mixture of high frequency and low frequency signals. Hybrid events are common in association with viscous lava dome growth.

A.7.1.7. 'Tornillos'

Long period events with a screw shaped' coda; in some cases they appear to have S-waves. These are signals with a gradual decrease of the amplitude and can be long period or high frequency 'tornillos'.

A.7.1.8. Tremor (harmonic or not)

This is a continuous signal and sometimes very long (i.e. several minutes, hours, days). It can be harmonic (i.e. a low dominant frequency sine wave with smoothly varying amplitude) or spasmodic (i.e. a higher or more broadband frequency, pulsating, irregular signal), and sometimes harmonically related to the main frequency.

A.7.1.9. Explosions

Generally impulsive, high or low frequency, and may involve an air shock phase. Can also be emergent, if from strong, sustained jetting.

A.7.1.10. Rockfalls

Emergent, phase less, high frequency signals correlated with observed rockfalls or pyroclastic flows, often having a cigar shaped envelope.

Classification of volcanic earthquakes allows understanding the source of these signals, the mechanism of an eruption, and can sometimes be used to predict the evolution of an eruption. That is why it is very important to classify events at a volcano.

There are several common approaches to classifying volcanic earthquakes:

- Analyst classifications: Can detect subtle differences in event type, note events that do not fit within classification scheme; often do not do thorough analyses of events (i.e. classification by eye), can produce different results than another analyst.

- Automatic classifications: Consistent and systematic classification according to predefined rules; Analysis of critical parameters (e.g. frequency) for each event; may classify noise, fit unique events into a predefined (incorrect) category; and classification (or lack thereof) methods (Real time Seismic Amplitude Measurement (RSAM); or Spectral Seismic Amplitude Measurement (SSAM)).

The majority of information comes from very basic analyses: event classifications, event rates (by class), locations, magnitudes, and source mechanisms (Double-Couple FPS). Advanced analyses, often using broadband 3 component signals, include travel time inversions (i.e. tomography, relative relocations), and waveform analysis or modelling (i.e. multiplet analysis, moment tensor inversions, shear wave splitting analysis, ambient noise analysis, array processing).

A.7.2. Seismic profiles

Seismic profiles are made using seismic reflection, a method that allows to estimating subsurface properties using reflected seismic waves. This method uses explosives, air guns or seismic vibrator as controlled sources of seismic energy. Deconvolution, common midpoint stacking, and migration are the main seismic data processing methods.

At several regions, petroleum and mining explorations have produced seismic profiles that show the general structure in the vicinity of a proposed site. These profiles may be useful for understanding of basement structure and depth of the sedimentary and volcanic stratigraphic pile. Sometimes earthquake data allows a tomographic view of the structure beneath volcanoes [A-90].

A.7.3. Gravity data

Gravity investigations play an important role in the characterization of NPP sites. Usually sedimentary and volcanic rocks obscure the more complex pre-existing geology, and therefore obtaining information about subsurface rock geometry is critical to fully characterize the structure and water flow patterns in the area [A-91]. Both, seismic and gravity data have been used for long time to understand the structure beneath volcanic regions [A-92], [A-93].

More recently, gravity data is being used to detect magma movements within volcanic edifices such as Etna [A-94] and understand their structure [A-95]. There is some debate at some volcanoes as to whether people are detecting water movements, rather than magma (e.g. Campi Flegrei, Italy [A-96]).

A.7.4. Deformation data

A deformed volcano will have a different surface appearance which can provide important information about the processes ongoing deep inside the volcano. To detect and evaluate such deformations a network survey technique can be used based on data instruments that collect data in the volcano area over a period of time. Instruments include tiltmeters,

benchmarks measured with an Electronic Distance Meter, GPS, and borehole strainmeters. The collected data, together with the use of technologies such as InSAR (Interferometric Synthetic Aperture Radar) which are satellite based, can be utilized to gain a deeper knowledge of volcanoes and their potential danger, in order to enable timely warnings of upcoming eruptions [A-97–100].

A.7.5. Magnetic data

Another method to understand the regional structure at a potential site is through magnetic surveys and data. The geological surface can be assessed using magnetic mapping, looking especially at the spatial geometry of rock masses and existing folds and faults in the geological material, and the presence of water bodies or volcanic sedimentary deposits alienate bedrock. In addition, aeromagnetic data can be visualized in shades and colours by producing pseudo topography images. Magnetic anomalies will show as hills, ridges and valleys. Mathematical Modelling can reveal shapes, depths and geological details of rock bodies that cause anomalies [A-101], [A-102]. A better result of the structure can be obtained when aeromagnetic and gravity data are used together [A-103–105], and even better when using aeromagnetic data together with seismic data [A-106], [A-107].

A.7.6. Magnetotelluric data

Magnetotellurics (MT) is a geophysical method that allows imaging the subsurface using the natural variations at the surface of electrical and magnetic fields. Depth ranges from 300 m below ground when recording high frequencies, down to 10 000 m or deeper using long period soundings. MT has been used to study the distribution of silicate melts in mantle and crust [A-108]. MT applied for geothermal exploration has detected resistivity anomalies associated with productive geothermal structures including faults and the presence of a cap rock, allowing the estimation of the temperatures of geothermal reservoirs at varying depths in Japan and the Philippines [A-109], [A-110]. On a regional scale, the use of the MT method together with seismic refraction data can be very useful when determining the regional structure as in the case of the Cascades Range in the U.S.A. [A-111]. The identification of the presence of hydrothermal systems or magmas beneath a volcano is also a very important piece of information obtainable from MT surveys [A-112–114].

A.7.7. Resistivity profiles

The structure of a geothermal system can be studied using resistivity profiling [A-115–117]. Resistivity profiling can be very useful in locating the main tectonic faults and hydrogeologic trends at volcanoes by electrical resistivity measurements, accompanied by other sources of information such as soil CO_2 concentrations, temperature and self potential measurements along profiles. The data can be used to provide insights regarding the position of shallow aquifers and the extent of the hydrothermal system [A-118].

A.7.8. Paleomagnetic data

Measurements of anisotropy of magnetic susceptibility on volcanic rocks and its correlation with structural features (e.g. thickness and vesicle deformation fabric) of flow units can be used to determine the flow direction of lava flows and ignimbrites (e.g. [A-119], [A-120]). The degree of anisotropy may have a direct relationship to the viscosity of the lava, the morphology of the flows, or both. The degree of internal deformation of the lava flows is reflected in the shape of the magnetic susceptibility ellipsoid.

The application of this technique is useful for the determination of lava and pyroclastic flow directions and, thus, identification of the source for fissure related extrusions at monogenetic volcanic fields where the source is not known as well as identification of sources for ignimbrite sequences [A-121–123].

A.7.9. Monitoring databases

Several agencies and observatories carry out the surveillance of volcanoes around the globe. The institutions engaged in volcano monitoring are gathered in the World Organization of Volcano Observatories (WOVO).WOVO is currently assembling a volcano monitoring database called WOVOdat under the auspices of the Earth Observatory of Singapore and the Smithsonian National Museum of Natural History (http://www.wovodat.org/).This database is expected to include selected volcanic eruption parameters from the Smithsonian Institution compilation of historical and Holocene eruptions (http://www.volcano.si.edu/index.cfm). WOVOdat also includes monitoring data from the National Volcano database (GeoNet) of the GNS in New Zealand (http://www.gns.cri.nz/Home/Products/Databases/New-Zealand-Volcano-Database); the National Research Institute for Earth Science and Disaster Prevention database (http://www.bosai.go.jp/e/activities/database/), the Colima Volcano Database (http://www.geociencias.unam.mx/mexican_volcanoes/volcanoes/colima/index.php), and many other volcano observatories. Other databases with information on historical or prehistoric eruptions include LaMEVE (Large Magnitude Explosive Eruptions) of the Volcano Global Risk Identification and Analysis Project (VOGRIPA; http://www.bgs.ac.uk/vogripa/view/controller.cfc?method=lameve). The Global Volcano Model (GVM; http://www.globalvolcanomodel.org/) will be an umbrella for all of these databases.

A.7.10. Monitoring network / instrumentation

Monitoring networks around the world can be contacted or accessed through the links provided by WOVO (www.wovo.org). The International Association of Volcanology and Chemistry of the Earth's Interior (IAVCEI; http://www.iavcei.org/) is currently assembling a survey of monitoring capabilities around the world with the Volcano Monitoring Database (VOMODA), in collaboration with the Asociación Latinoamericana de Volcanología. This includes the instrumental facilities of Latin America so far, but is expected to be expanded in the coming years as a worldwide database on monitoring facilities worldwide.

REFERENCES TO ANNEX

[A-1] INTERNATIONAL ATOMIC ENERGY AGENCY, Volcanic Hazards in Site Evaluation for Nuclear Installations, IAEA Specific Safety Guide No. SSG-21, IAEA, Vienna (2012).

[A-2] BRANNEY, M.J., KOKELAAR, B.P., Pyroclastic Density Currents and the Sedimentation of Ignimbrites, Geological Society, London, Memoirs, Vol. 27, Geological Society of London, London (2002).

[A-3] CAS, R.A.F., WRIGHT, J.V., Volcanic Successions: Modern and Ancient, A Geological Approach to Processes, Products and Successions, Allen and Unwin, London (1987).

[A-4] FISHER, R., SCHMINCKE, H.U., Pyroclastic rocks, Springer, Berlin (1984).

[A-5] BONADONNA, C., CIONI, R., PISTOLESI, M., CONNOR, C., SCOLLO, S., PIOLI, L., Determination of the largest clast sizes of tephra deposits for the characterization of explosive eruptions: a study of the IAVCEI commission on tephra hazard modeling, Bulletin of Volcanology **75** (2013) 680.

[A-6] GERSTENECKER, C., LÄUFER, G., STEINECK, D., TIEDE, C., WROBEL, B., Validation of Digital Elevation Models around Merapi Volcano, Java, Indonesia, Natural Hazards and Earth System Sciences **5** (2005) 863–876.

[A-7] KLEUSBERG, A., KLAEDTKE, H.G., "Accuracy Assessment of a Digital Height Model Derived from Airborne Synthetic Aperture Radar Measurements", Photogrammetric Week '99 (FRITSCH, D., SPILLER, R., Eds), Wichmann Verlag, Heidelberg (1999) 139–143.

[A-8] BONACCORSO, A., CALVARI, S., COLTELLI, M., DEL NEGRO, C., FALSAPERLA, S., Mt. Etna: Volcano Laboratory, Geophysical Monograph Series, Volume 143, AGU, Washington, DC (2004).

[A-9] KOMOROWSKI, J.C., BOUDON, G., SEMET, M., SAMPER, A., QUIDELLEUR, X., COUDRET, E., VILLEMANT, B., LE FRIANT, A., BEAUDUCEL, F., HAMMOUYA, G., The eruptive history of Soufrière of Guadeloupe volcano in the last 100,000 years based on field, analytical, and bibliographic studies, EXPLORIS Deliverable D2.5 (2003).

[A-10] HILDRETH, W., FIERSTEIN, J., The Novarupta-Katmai Eruption of 1912 - Largest Eruption of the Twentieth Century: Centennial Perspectives, U.S. Geological Survey Professional Paper 1791, USGS, Reston, VA (2012).

[A-11] RHODES, J., LOCKWOOD, J., Mauna Loa revealed: structure, composition, history, and hazards, Geophysical Monograph Series, Volume 92, AGU, Washington, DC (2013).

[A-12] BACHELERY, P. LENAT, J.F., DI MURO, A., MICHON, L., Active Volcanoes of the Southwest Indian Ocean: Piton de la Fournaise and Karthala, Springer, Berlin (2014).

[A-13] STRECKEISEN, A., Classification and Nomenclature of Plutonic Rocks. Recommendations of the IUGS Subcommission on the Systematics of Igneous Rocks, Geologische Rundschau., Internationale Zeitschrift für Geologie **63** (1974) 773–785.

[A-14] STRECKEISEN, A., The IUGS Subcommission on the Systematics of Igneous Rocks. Classification and Nomenclature of Volcanic Rocks, Lamprophyres, Carbonatites and Melilite Rocks. Recommendations and Suggestions., Neues Jahrbuch für Mineralogie, Abhandlungen **141** (1978) 1–14.

[A-15] CRANDELL, D.R., BOOTH, B., KUSUMIDINATA, K., SHIMOZURU, D., WALKER, G.P.L, WESTERCAMP, D., Source-book for volcanic-hazards zonation, UNESCO, Paris (1984).

[A-16] WALKER, G., Explosive volcanic eruptions - a new classification scheme, Geologische Rundschau **62** 2 (1973) 431–446.
[A-17] CAREY, S., SPARKS, R.S.J., Quantitative models of the fallout and dispersal of tephra from volcanic eruption columns, Bulletin of Volcanology **48** (1986) 109–125.
[A-18] SPARKS, R., The dimensions and dynamics of volcanic eruption columns, Bulletin of Volcanology **48** (1986) 3–15.
[A-19] PYLE, D., "Sizes of volcanic eruptions", Encyclopedia of Volcanoes, 1st Edition (SIGURDSSON, H., HOUGHTON, B., RYMER, H., STIX, J., MCNUTT, S., Eds), Academic Press, San Diego (1999) 263–269.
[A-20] STRECKEISEN, A., Classification and nomenclature of igneous rocks. Final report of an inquiry, Neues Jahrbuch für Mineralogie, Abhandlungen **107** (1967) 144–204.
[A-21] STREKEISEN, A.L., Plutonic rocks. Classification and nomenclature recommended by the IUGS Subcommission on the systematics of igneous rocks, Geotimes **18** (1976) 26–30.
[A-22] LE BAS, M.J., LE MAITRE, R., STREKEISEN, A., ZANETTIN, B., IUGS Subcommission on the Systematics of Igneous Rocks, 1986, A Chemical Classification of Volcanic Rocks Based on the Total AlkalA-Silica Diagram, Journal of Petrology **27** 3 (1986) 745–750.
[A-23] NAKAMURA, N., Determination of REE, Ba, Fe, Mg, Na and K in carbonaceous and ordinary chondrites, Geochimica et Cosmochimica Acta **38** 5 (1974) 757–775.
[A-24] WOOD, D. A variably veined suboceanic upper mantle - Genetic significance for mid-ocean ridge basalts from geochemical evidence, Geology **7** (1979) 499–503.
[A-25] WOOD, D., TARNEY, J., VARET, J., SAUNDERS, A., BOUGAULT, H., GORON, J., TREUIL, M., CANN, R., Geochemistry of basalts drilled in the North Atlantic by IPOD Leg 49: Implications for mantle heterogeneity, Earth and Planetary Science Letters **42** (1979) 77–97.
[A-26] THOMPSON, R.N., MORRISON, M., HENDRY, G., PARRY, S., An assessment of the relative roles of crust and mantle in magma genesis, Philosophical Transactions of The Royal Society A: Mathematical, Physical and Engineering Sciences **310** 1514 (1984) 549–590.
[A-27] SUN, S.S., Lead isotopes study of young volcanic rocks from mid-ocean ridges, ocean islands and island arcs, Philosophical Transactions of The Royal Society A: Mathematical, Physical and Engineering Sciences, **297** 1431 (1980) 409–445.
[A-28] PEARCE, J.A., "Role of the sub-continental lithosphere in magma genesis at active continental margins", Continental Basalts and Mantle Xenoliths (HAWKESWORTH, C.J., Eds), Shiva Publications, Nanwitch, Shiva (1983) 230–249.
[A-29] DEPAOLO, D.J., WASSERBURG, G.J., Nd isotopic variations and petrogenetic models, Geophysical Research Letters **5** 3 (1976) 249–252.
[A-30] WHITE, W., HOFMANN, A., Sr and Nd isotope geochemistry of oceanic basalts and mantle evolution, Nature **296** 5860 (1982) 821–825.
[A-31] FAURE, G., Principles of Isotope Geology, 2nd edition, John Wiley & Sons, New York (1986).
[A-32] ALLÈGRE, C., CONDOMINES, M., Basalt Genesis and Mantle Structure Studied through Th-Isotopic Geochemistry, Nature **299** 5878 (1982) 21–24.
[A-33] ALLÈGRE, C., Th. Staudacher, and Ph. Sarda, Rare gas systematics: formation of the atmosphere, evolution and structure of the Earth's mantle, Earth and Planetary Science Letters **81** (1986) 127–150.
[A-34] ZINDLER, A., HART, S., Helium: problematic primordial signals, Earth and Planetary Science Letters **79** (1986) 1–8.

[A-35] JAMES, D., The combined use of oxygen and radiogenic isotopes as indicators of crustal contamination, Annual Review of Earth and Planetary Sciences **9** (1981) 311–344.
[A-36] KYSER, T.K., O'NEIL, R., CARMICHAEL, I.S.E., Genetic Relations Among Basic Lavas and Ultramafic Nodules: Evidence from Oxygen Isotope Compositions, Contributions to Mineralogy and Petrology **81** (1982) 88–102.
[A-37] COHEN, K.M., FINNEY, S.C., GIBBARD, P.L., FAN, J.X., The ICS International Chronostratigraphic Chart. Episodes 36 (2013 updated) 199–204.
[A-38] KROMER, B., Radiocarbon and dendrochronology, Dendrochronologia **27** (2009) 15–19.
[A-39] GOVE, H.E., "The history of AMS, its advantages over decay counting: applications and prospects", Radiocarbon after four decades: an interdisciplinary perspective (TAYLOR, E., LONG, A., KRA, R.S., Eds), Springer, Berlin (1992) 214–229.
[A-40] GOVE, H.E., From Hiroshima to the Iceman. The Development and Applications of Accelerator Mass Spectrometry, Institute of Physics Publishing, Bristol (1999).
[A-41] GOVE, H.E., Some comments on accelerator mass spectrometry, Radiocarbon **42** 1 (2000) 127–135.
[A-42] STUIVER, M., REIMER, P.J., BRAIZUNAS, T.F., High precision radiocarbon age calibration for terrestrial and marine samples, Radiocarbon **40** 3 (1998) 1127–1151.
[A-43] REIMER, P.J., BAILLIE, M.G., BARD, E., BAYLISS, A., BECK, J.V., BLACKWELL, B.G., BRONK RAMSEY, C., BUCK, C.E., BURR, G.C., EDWARDS, R.L., INTCAL09 and MARINE09 radiocarbon age calibration curves, 0–50,000 years CAL BP, Radiocarbon **51** 4 (2009) 1111–1150.
[A-44] MANNING, M.R., LOWE, D.C., MELHUISH, W.H., SPARKS, R.J., WALLACE, G., BRENNINKMEIJER, C.A., MCGILL, R.C., The use of radiocarbon measurements in atmospheric studies, Radiocarbon **32** 1 (1990) 37–58.
[A-45] RENNE, P., SHARP, W.D., DEINO, A.L., ORSI, G., CIVETTA, L., $^{40}Ar/^{39}Ar$ Dating into the Historical Realm: Calibration Against Pliny the Younger, Science **277** (1997) 1279–1280.
[A-46] LANPHERE, M., CHAMPION, D., MELLUSO, L., MORRA, V., PERROTTA, A., SCARPATI, C., TEDESCO, D., CALVERT, A., $^{40}Ar/^{39}Ar$ ages of the AD 79 eruption of Vesuvius, Italy, Bulletin of Volcanology **69** (2007) 259–263.
[A-47] MCDOUGALL, I., HARRISON, T.M., Geochronology and Thermochronology by the $^{40}Ar/^{39}Ar$ Method (2nd ed.), Oxford University Press, New York (1999).
[A-48] BACON, C.R., PERSING, H.M., WOODEN, J.L., IRELAND, T.R., Late Pleistocene granodiorite beneath Crater Lake caldera, Oregon, dated by ion microprobe, Geology **28** 5 (2000) 467–470.
[A-49] IRELAND, T.R., WILLIAMS, I.S., Considerations in zircon geochronology by SIMS, Reviews in mineralogy and geochemistry **53** 1 (2003) 215–241.
[A-50] BALCO, G., SHUSTER, D.L., ^{26}Al–^{10}Be–^{21}Ne burial dating, Earth and Planetary Science Letters **286** (2009) 570–575.
[A-51] GLASSNER, N.F., HUGHES, P.D., FENTON, C., SCHNABEL, C., ROTHER, H., ^{10}Be and ^{26}Al exposure-age dating of bedrock surfaces on the Aran ridge, Wales: evidence for a thick Welsh Ice Cap at the Last Glacial Maximum, Journal of Quaternary Science **27** 1 (2012) 97–104.
[A-52] SCHILDGEN, T., DETHIER, D.P., BIERMAN, P., CAFFEE, M., ^{26}Al and ^{10}Be dating of Late Pleistocene and Holocene fill terraces: A record of fluvial deposition and incisión, Colorado Front Range, Earth Surface Processes and Landforms **27** (2002) 773–787.

[A-53] PORTER, S.C., SWANSON, T.W., ^{36}Cl dating of the classic Pleistocene glacial record in the northeastern Cascade Range, Washington, American Journal of Science **308** (2008) 130–166.
[A-54] PHILLIPS, F.M., ZREDA, M.G., GOSSE, J.C., KLEIN, J., EVENSON, E.B., HALL, R.D., CHADWICK, O.A., SHARMA, P., Cosmogenic ^{36}Cl and ^{10}Be ages of Quaternary glacial and fluvial deposits of the Wind River Range, Wyoming, Geological Society of America Bulletin **109** 11 (1997) 1453–1463.
[A-55] RICHTER, D., Advantages and Limitations of Thermoluminescence Dating of Heated Flint from Paleolithic Sites, Geoarchaeology: An International Journal **22** 6 (2007) 671–683.
[A-56] SCHELLMANN, G., BEERTEN, K., RADTKE, U., Electron spin resonance (ESR) dating of Quaternary materials, Quaternary Science Journal **57** 1–2 (2008) 150–178.
[A-57] WATCHMAN, A., A review of the history of dating rock varnishes, Earth-Science Reviews **49** (2000) 261–277.
[A-58] HARRINGTON, C.D., WHITNEY, J.W., Scanning electron microscope method for rock-varnish dating, Geology **15** (1987) 967–970.
[A-59] WAGNER, G., VAN DEN HAUTE, P., Fission-Track Dating, Kluwer Academic Publishers, Dordrecht (1992).
[A-60] STERN, C.R., AMINI, H., CHARRIER, R., GODOY, E., HERVE, F., VARELA, J., Petrochemistry and age of rhyolitic pyroclastic flows which occur along the drainage valleys of the Rio Maipo and Rio Cachapoal (Chile) and the Rio Yaucha and Rio Papagayos (Argentina), Revista Geológica de Chile **23** (1984) 39–52.
[A-61] KOWALLIS, B.J., SWISHER III, C.C., CARRANZA-CASTAÑEDA, O., MILLER, W.E., TINGEY, D.G., Fission track and single-crystal ^{40}Ar/^{39}Ar laser-fusion ages from volcanic ash layers in fossil-bearing Pliocene sediments in central Mexico, Revista Mexicana de Ciencias Geológicas **15** 2 (1998) 157–160.
[A-62] HOLCOMB, R., CHAMPION, D., MCWILLIAMS, M., Dating recent Hawaiian lava flows using paleomagnetic secular variation, Geological Society of America Bulletin **97** 7 (1986) 829–839.
[A-63] MOCHIZUKI, N., TSUNAKAWA, H., SHIBUYA, H., TAGAMI, T., OZAWA, A., SMITH, I.E., Further K-Ar dating and paleomagnetic study of the Auckland geomagnetic excursions, Earth Planets Space **59** (2007) 755–761.
[A-64] CASSATA, W.S., SINGER, B.S., CASSIDY, J., Laschamp and Mono Lake geomagnetic excursions recorded in New Zealand, Earth and Planetary Science Letters **268** (2008) 76–88.
[A-65] LINDSAY, J., LEONARD, G., Age of the Auckland Volcanic Field, IESE Report 1-2009.02, Institute of Earth Science and Enginieering, Aotearoa (2009).
[A-66] MACIEL-PEÑA, R.A, GOGUITCHAICHVILI, A., GARDUÑO MONROY, V.H., RUIZ MARTINEZ, V.C., AGUILAR REYES, B., MORALES, J., ALVA-VALDIVIA, L., CABALLERO MIRANDA, C., URRUTIA-FUCUGAUCHI, J., Paleomagnetic and rock-magnetic survey of Brunhes lava flows from Tancitaro volcano, Mexico, Geofísica Internacional **48** 4 (2009) 375–384.
[A-67] LOWE, D., Tephrochronology and its application: a review, Quaternary Geochronology **6** (2011) 107–153.
[A-68] BALASCIO, N.L., WICKLER, S., NARMO, L.E., BRADLEY, R.C., Distal cryptotephra found in a Viking boathouse: the potential for tephrochronology in reconstructing the Iron Age in Norway, Journal of Archaeological Science **38** (2011) 934–941.

[A-69] BECKER, B., An 11,000-year German oak and pine dendrochronology for radiocarbon calibration, Radiocarbon **35** 1 (1993) 201–213.
[A-70] FRIEDRICH, M., REMMELE, S., KROMER, B., HOFMANN, J., SPURK, M., KAISER, K.F., ORCEL, C., KÜPPERS, M., The 12,460-year Hohenheim oak and pine tree-ring chronology from central Europe - a unique annual record for radiocarbon calibration and paleoenvironment reconstructions, Radiocarbon **46** 3 (2004) 1111–1122.
[A-71] SHEPPARD, P.R., ORT, M.H., ANDERSON, K.C., ELSON, M.D., VÁZQUEZ-SELEM, L., CLEMENS, A.W., LITTLE, N.C., SPEAKMAN, R.J., Multiple Dendrochronological Signals Indicate the Eruption of Parícutin Volcano, Michoacán, Mexico, Tree-Ring Research **64** 2 (2008) 87–108.
[A-72] LEWIS-KENNEDI, C.B., LANGE, R.A., HALL, C.M., DELGADO-GRANADOS, H., The eruptive history of the Tequila volcanic field, western Mexico: ages, volumes, and relative proportions of lava types, Bulletin of Volcanology **67** (2005) 391–414.
[A-73] MARK, D.F., PETRAGLIA, M., SMITH, V.C., MORGAN, L.E., BARFOD, D.N., ELLIS, B.S., PEARCE, N.J., PAL, J.N., KORISETTAR, R., A high-precision ^{40}Ar/^{39}Ar age for the Young Toba Tuff and dating of ultra-distal tephra: Forcing of Quaternary climate and implications for hominin occupation of India, Quaternary Geochronology **21** (2013) 90–103.
[A-74] CHRISTIANSEN, R.L., The Quaternary and Pliocene Yellowstone Plateau Volcanic Field of Wyoming, Idaho, and Montana, U.S. Geological Survey, Professional Paper 729-G, USGS, Reston, VA (2001).
[A-75] SZACKACS, A., Redefining active volcanoes: a discussion, Bulletin of Volcanology **56** (1994) 321–325.
[A-76] HASENAKA, T., CARMICHAEL, I.S., The Cinder Cones of Michoacán-Guanajuato, Central Mexico, Petrology and Chemistry, Journal of Petrology **28** 2 (1987) 241–269.
[A-77] LUHR, J.F., Extensional tectonics and the diverse primitive volcanic rocks in the western Mexican volcanic belt, The Canadian Mineralogist **35** (1997) 473–500.
[A-78] WALLACE, P., CARMICHAEL, I.S., Quaternary volcanism near the Valley of Mexico: implications for subduction zone magmatism and the effects of crustal thickness variations on primitive magma compositions, Contributions to Mineralogy and Petrology **135** (1999) 291–314.
[A-79] LANGE, R.A., CARMICHAEL, I.S., A potassic volcanic front in western Mexico: The lamprophyric and related lavas of San Sebastian, Geological Society of America Bulletin **103** (1991) 928–940.
[A-80] GÓMEZ-TUENA, A., LAGATTA, A., LANGMUIR, C., GOLDSTEIN, S., ORTEGA-GUTIÉRREZ, F., CARRASCO-NÚÑE, G., Temporal Control of Subduction Magmatism in the Eastern Trans-Mexican VolcanicBelt: Mantle Sources, Slab Contributions and Crustal Contamination, Geochemistry Geophysics Geosystems **4** 8 (2003) 8912.
[A-81] WILLIAMS, S.N., Plinian airfall deposits of basaltic composition, Geology **11** (1983) 211–214.
[A-82] COURTLAND, L.M., KRUSE, S.E., CONNOR, S.B., SAVOV, I.P., MARTIN, K.T., GPR investigation of tephra fallout, Cerro Negro volcano, Nicaragua: a method for constraining parameters used in tephra sedimentation models, Bulletin of Volcanology **74** (2012) 1409–1424.
[A-83] MCNUTT, S.R., "Seismic monitoring of volcanoes: A review of the state-of-the-art and recent trends", Monitoring and Mitigation of Volcano Hazards (SCARPA, R., TILLING, R.I., Eds), Springer, Berlin (1996) 99–146.

[A-84] CHOUET, B.A., Long-period volcano seismicity: its source and use in eruption forecasting, Nature **380** (1996) 309–316.
[A-85] ZOBIN, V.M., Introduction to Volcanic Seismology, Elsevier, Amsterdam (2003).
[A-86] MINAKAMI, T., "Seismology and volcanoes in Japan, Developments in Solid Earth Geophysics", Physical Volcanology (CIVETTA, L., GASPARINI, P., LUONGO, G., RAPOLLA, A., Eds), Elsevier, New York (1974) 1–27.
[A-87] LAHR, J.C., CHOUET, B.A., STEPHENS, C.D., POWER, J.A., PAGE, R.A., Earthquake classification, location, and error analysis in a volcanic environment: implications for the magmatic system of the 1989–1990 eruptions at Redoubt Volcano, Alaska, Journal of Volcanology and Geothermal Research **62** (1994) 137–151.
[A-88] CHOUET, B., "New methods and future trends in seismological volcano monitoring", Monitoring and Mitigation of Volcano Hazards (SCARPA, R., TILLING, R.I., Eds), Springer, Berlin (1996) 23–97.
[A-89] MILLER, A.D., STEWART, R.C., WHITE, R.A., LUCKETT, R., BAPTIE, B.J., ASPINALL, W.P., LATCHMAN, J.L., LYNCH, L.L., VOIGHT, B., Seismicity associated with dome growth and collapse at the Soufriere Hills Volcano, Montserrat, Geophysical Research Letters **25** 18 (1998) 3401–3404.
[A-90] LEES, J., CROSSON, R.S., Tomographic Inversion for Three-Dimensional Velocity Structure at Mount St. Helens Using Earthquake Data, Journal of Geophysical Research **94** B5 (1989) 5716–5728.
[A-91] SNYDER, D.B., CARR, W.J., Interpretation of Gravity Data in a Complex Volcano-Tectonic Setting, Southwestern Nevada, Journal of Geophysical Research **89** B12 (1984) 10193–10206.
[A-92] BOSSHARD, E., MACFARLANE, D.J., Crustal Structure of the Western Canary Islands from Seismic Refraction and Gravity Data, Journal of Geophysical Research **75** 26 (1970) 4901–4918.
[A-93] BERRINO, G., CORRADO, G., RICCARDI, U., Sea gravity data in the Gulf of Naples: a contribution to delineating the structural pattern of the Vesuvian area, Journal of Volcanology and Geothermal Research **82** (1998) 139–150.
[A-94] RYMER, H., CASSIDY, J., LOCKE, C.A., MURRAY, J.B., Magma movements in Etna volcano associated with the major 1991–1993 lava eruption: evidence from gravity and deformation, Bulletin of Volcanology **57** (1995) 451–461.
[A-95] WILLIAMS-JONES, G., RYMER, H., ROTHERY, D.A., Gravity changes and passive SO2 degassing at the Masaya caldera complex, Nicaragua, Journal of Volcanology and Geothermal Research **123** (2003) 137–160.
[A-96] DE NATALE, G., TROISE, C., PINGUE, F., MASTROLORENZO, G., PAPPALARDO, L., BATTAGLIA, M., BOSCHI, E., The Campi Flegrei caldera: unrest mechanisms and hazards, Geological Society: Special Publications **269** (2006) 25–45.
[A-97] TRYGGVASON, E., Multiple magma reservoirs in a rift zone volcano: ground deformation and magma transport during the September 1984 eruption of Krafla, Iceland, Journal of Volcanology and Geothermal Research **28** (1986) 1–44.
[A-98] DZURISIN, D., A comprehensive approach to monitoring volcano deformation as a window on the eruption cycle, Reviews of Geophysics **41** 1 (2003) 1–1.
[A-99] HOOPER, A., ZEBKER, H., SEGALL, P., KAMPES, B., A new method for measuring deformation on volcanoes and other natural terrains using InSAR persistent scatterers, Geophysical Research Letters **31** 23 (2004) L23611.
[A-100] HAUTMANN, S., GOTTSMANN, J., SPARKS, R.S., COSTA, A., MELNIK, O., VOIGHT, B., Modelling ground deformation caused by oscillating overpressure in a

dyke conduit at Soufrière Hills Volcano, Montserrat, Tectonophysics **471** (2009) 87–95.
[A-101] SUTHERLAND, R., Basement geology and tectonic development of the greater New Zealand region: an interpretation from regional magnetic data, Tectonophysics **308** (1999) 341–362.
[A-102] PAOLETTI, V., SECOMANDI, M., FEDI, M., FLORIO, G., RAPOLLA, A., The integration of magnetic data in the Neapolitan volcanic district, Geosphere **1** (2005) 85–96.
[A-103] RAPOLLA, A., FEDI, M., FIUME, M.G., Crustal structure of the Ischia-Phlegrean geothermal fields, near Naples, Italy, from gravity and aeromagnetic data, Geophysical Journal **97** (1989) 409–419.
[A-104] ARAÑA, V., CAMACHO, A.G., GARCIA, A., MONTESINOS, F.G., BLANCO, I., VIEIRA, R., FELPETO, A., Internal structure of Tenerife (Canary Islands) based on gravity, aeromagnetic and volcanological data, Journal of Volcanology and Geothermal Research **103** (2000) 43–64.
[A-105] GRAUCH, V.J., KELLER, G.R., "Gravity and aeromagnetic expression of tectonic and volcanic elements of the southern San Luis Basin, New Mexico and Colorado", New Mexico Geological Society Guidebook, 55th Field Conference, Geology of the Taos Region, New Mexico Geological Society, Albuquerque (2004) 230–243.
[A-106] SMITH, R.B., SHUEY, R.T., PELTON, J.R., BAILEY, J.P., Yellowstone Hot Spot: Contemporary Tectonics and Crustal Properties From Earthquake and Aeromagnetic Data, Journal of Geophysical Research **82** 26 (1977) 3665–3676.
[A-107] BISCHKE, R.E., SUPPE, J., DEL PILAR, R., A new branch of the Philippine fault system as observed from aeromagnetic and seismic data, Tectonophysics **183** (1990) 243–264.
[A-108] SCHMOLDT, J.P., ALAN G., J., HOGG, C., ROSELL, O., PICASSO- Phase I: MT Investigation of the Betic-Rif mountain system. Comparison of actual robust processing algorithms, IAGA WG 1.2 on Electromagnetic Induction in the Earth, 19th Workshop, Beijing, China, October 23–29, 2008, Beijing, 2008 (expanded abstruct).
[A-109] YU, G., STRACK, K.M., ALLEGAR, N., GUNNARSSON, A., TULINIUS, H., HE, L., HE, Z., Characterizing a geothermal reservoir using broadband 2-D MT survey in Theistareykir, Iceland, SEG Las Vegas 2008 Annual Meeting, Las Vegas, 2008 (expanded abstruct).
[A-110] ASSAUE, H., KOIKE, K., YOSHINAGA, T., TAKAKURA, S., Magnetotelluric resistivity modeling for 3D characterization of geothermal reservoirs in the Western side of Mt. Aso, SW Japan, Journal of Applied Geophysics **58** (2005) 296–312.
[A-111] STANLEY, W.D., MOONEY, W.D., FUIS, G.S., Deep Crustal Structure of the Cascade Range and Surrounding Regions From Seismic Refraction and Magnetotelluric Data, Journal of Geophysical Research **95** BI2 (1990) 19419–19438.
[A-112] OGAWA, Y., MATSUSHIMA, N., OSHIMA, H., TAKAKURA, S., UTSUGI, M., HIRANO, K., IGARASHI, M., DOI, T., A resistivity cross-section of Usu volcano, Hokkaido, Japan, by audiomagnetotelluric soundings, Earth Planets Space **50** (1998) 339–346.
[A-113] TROIANO, A., PETRILLO, Z., DI GIUSEPPE, M.G., BALASCO, M., DIAFERIA, I., DI FIORE, B., SINISCALCHI, A., PATELLA, D., About the shallow resistivity structure of Vesuvius volcano, Annals of Geophysics **51** 1 (2008) 181–189.
[A-114] HILL, G., CALDWELL, T.G., HEISE, W., CHERTKOFF, D.G., BIBBY, H.M., BURGESS, M.K., CULL, J.P., CAS, R.A.F., Distribution of melt beneath Mount St Helens and Mount Adams inferred from magnetotelluric data, Nature Geoscience **2** (2009) 785–790.

[A-115] BIBBY, H.M., Electrical resistivity mapping in the Central Volcanic Region of New Zealand, New Zealand Journal of Geology and Geophysics **31** (1988) 259–214.
[A-116] BIBBY, H.M., CALDWELL, T.G., DAVEY, F.J., WEBB, T.H., Geophysical evidence on the structure of the Taupo Volcanic Zone and its hydrothermal circulation, Journal of Volcanology and Geothermal Research **68** (1995) 29–58.
[A-117] BIBBY, H.M., CALDWELL, T.G., RISK, G.F., Electrical resistivity image of the upper crust within the Taupo Volcanic Zone, New Zealand, Journal of Geophysical Research **103** B5 (1998) 9665–9680.
[A-118] REVIL, A., FINIZOLA, A., RICCI, T., DELCHER, E., PELTIER, A., BARDE-CABUSSON, S., AVARD, G., BAILLY, T., BENNATI, L., BYRDINA, S., COLONGE, J., DI GANGI, F., DOUILLET, G., LUPI, M., LETORT, J., TSANG HIN SUN, E., Hydrogeology of Stromboli volcano, Aeolian Islands (Italy) from the interpretation of resistivity tomograms, self-potential, soil temperature and soil CO2 concentration measurements, Geophysical Journal International **186** (2011) 1078–1094.
[A-119] CAÑON-TAPIA, E., WALKER, G.P., HERRERO-BERVERA, E., Magnetic fabric and flow direction in basaltic Pahoehoe lava of Xitle Volcano Mexico, Journal of Volcanology and Geothermal Research **65** (1995) 249–263.
[A-120] CAGNOLI, B., TARLING, D.H., The reliability of anisotropy of magnetic susceptibility (AMS) data as flow direction indicators in friable base surge and ignimbrite deposits: Italian examples, Journal of Volcanology and Geothermal Research **75** (1997) 309–320.
[A-121] ELWOOD, B.B., Estimates of flow direction for calc-alkaline welded tufts and paleomagnetic data reliability from anisotropy of magnetic susceptibility measurements: central San Juan Mountains, southwest Colorado, Earth and Planetary Science Letters **59** (1982) 303–314.
[A-122] PALMER, H.C., MACDONALD, W.D., Anisotropy of magnetic susceptibility in relation to source vents of ignimbrites: empirical observations, Tectonophysics **307** (1999) 207–218.
[A-123] MARTIN-HERNANDEZ, F., CAÑON-TAPIA, E., MATTEI, M., Magnetic anisotropy different scales, different parameters, different stories?, Tectonophysics **466** (2009) 1–2.

CONTRIBUTORS TO DRAFTING AND REVIEW

Aspinall, W.P.	Aspinall & Associates and Bristol University, United Kingdom
Charbonnier, S.	University of South Florida, United States of America
Connor, C. B.	University of South Florida, United States of America
Connor, L. J. C.	University of South Florida, United States of America
Costa, A.	Instituto Nazionale di Geofisica e Vulcanologia, Italy
Courtland, L. M.	University of South Florida, United States of America
Delgado Granados, H.	National Autonomous University of Mexico, Mexico
Godoy, A.	Consultant, Argentina
Hibino, K.	International Atomic Energy Agency (until August 2015)
Hill, B. E.	United States Nuclear Regulatory Commission, United States of America
Komorowski, J.C.	Institut de Physique du Globe de Paris, France
McNutt, S.	University of South Florida, United States of America
Meliksetian, K.	Armenian National Academy of Sciences, Armenia
Morita, S.	International Atomic Energy Agency
Nakada, S.	University of Tokyo, Japan
Newhall, C.	Nanyang Technological University, Singapore
Samaddar, S. K.	International Atomic Energy Agency (until August 2015)
Savov, I. P.	University of Leeds, United Kingdom
Self, S.	United States Nuclear Regulatory Commission, United States of America
Uchiyama, Y.	Consultant, Japan
Wilson, T.	University of Canterbury, New Zealand
Yamamoto, T.	National Institute of Advanced Industrial Science and Technology, Japan
Watanabe, K.	International Atomic Energy Agency

Consultants Meetings

Florida, United States of America: 13–14 October 2011

Vienna, Austria: 19–20 April 2012

Florida, United States of America: 12–14 September 2012

Colima, Mexico: 15–16 November 2012

Vienna, Austria: 4–5 April 2013

Kagoshima, Japan: 16–19 July 2013

Maryland, United States of America: 3–4 December 2013

IAEA
International Atomic Energy Agency

No. 24

ORDERING LOCALLY

In the following countries, IAEA priced publications may be purchased from the sources listed below or from major local booksellers.

Orders for unpriced publications should be made directly to the IAEA. The contact details are given at the end of this list.

BELGIUM
Jean de Lannoy
Avenue du Roi 202, 1190 Brussels, BELGIUM
Telephone: +32 2 5384 308 • Fax: +32 2 5380 841
Email: jean.de.lannoy@euronet.be • Web site: http://www.jean-de-lannoy.be

CANADA
Renouf Publishing Co. Ltd.
22-1010 Polytek Street, Ottawa, ON K1J 9J1, CANADA
Telephone: +1 613 745 2665 • Fax: +1 643 745 7660
Email: order@renoufbooks.com • Web site: http://www.renoufbooks.com

Bernan Associates
4501 Forbes Blvd., Suite 200, Lanham, MD 20706-4391, USA
Telephone: +1 800 865 3457 • Fax: +1 800 865 3450
Email: orders@bernan.com • Web site: http://www.bernan.com

CZECH REPUBLIC
Suweco CZ, s.r.o.
SESTUPNÁ 153/11, 162 00 Prague 6, CZECH REPUBLIC
Telephone: +420 242 459 205 • Fax: +420 284 821 646
Email: nakup@suweco.cz • Web site: http://www.suweco.cz

FRANCE
Form-Edit
5 rue Janssen, PO Box 25, 75921 Paris CEDEX, FRANCE
Telephone: +33 1 42 01 49 49 • Fax: +33 1 42 01 90 90
Email: fabien.boucard@formedit.fr • Web site: http://www.formedit.fr

Lavoisier SAS
14 rue de Provigny, 94236 Cachan CEDEX, FRANCE
Telephone: +33 1 47 40 67 00 • Fax: +33 1 47 40 67 02
Email: livres@lavoisier.fr • Web site: http://www.lavoisier.fr

L'Appel du livre
99 rue de Charonne, 75011 Paris, FRANCE
Telephone: +33 1 43 07 43 43 • Fax: +33 1 43 07 50 80
Email: livres@appeldulivre.fr • Web site: http://www.appeldulivre.fr

GERMANY
Goethe Buchhandlung Teubig GmbH
Schweitzer Fachinformationen
Willstätterstrasse 15, 40549 Düsseldorf, GERMANY
Telephone: +49 (0) 211 49 874 015 • Fax: +49 (0) 211 49 874 28
Email: kundenbetreuung.goethe@schweitzer-online.de • Web site: http://www.goethebuch.de

HUNGARY
Librotrade Ltd., Book Import
Pesti ut 237. 1173 Budapest, HUNGARY
Telephone: +36 1 254-0-269 • Fax: +36 1 254-0-274
Email: books@librotrade.hu • Web site: http://www.librotrade.hu

INDIA
Allied Publishers
1st Floor, Dubash House, 15, J.N. Heredi Marg, Ballard Estate, Mumbai 400001, INDIA
Telephone: +91 22 4212 6930/31/69 • Fax: +91 22 2261 7928
Email: alliedpl@vsnl.com • Web site: http://www.alliedpublishers.com

Bookwell
3/79 Nirankari, Delhi 110009, INDIA
Telephone: +91 11 2760 1283/4536
Email: bkwell@nde.vsnl.net.in • Web site: http://www.bookwellindia.com

ITALY
Libreria Scientifica "AEIOU"
Via Vincenzo Maria Coronelli 6, 20146 Milan, ITALY
Telephone: +39 02 48 95 45 52 • Fax: +39 02 48 95 45 48
Email: info@libreriaaeiou.eu • Web site: http://www.libreriaaeiou.eu

JAPAN
Maruzen-Yushodo Co., Ltd.
10-10, Yotsuyasakamachi, Shinjuku-ku, Tokyo 160-0002, JAPAN
Telephone: +81 3 4335 9312 • Fax: +81 3 4335 9364
Email: bookimport@maruzen.co.jp • Web site: http://maruzen.co.jp

RUSSIAN FEDERATION
Scientific and Engineering Centre for Nuclear and Radiation Safety
107140, Moscow, Malaya Krasnoselskaya st. 2/8, bld. 5, RUSSIAN FEDERATION
Telephone: +7 499 264 00 03 • Fax: +7 499 264 28 59
Email: secnrs@secnrs.ru • Web site: http://www.secnrs.ru

UNITED STATES OF AMERICA
Bernan Associates
4501 Forbes Blvd., Suite 200, Lanham, MD 20706-4391, USA
Telephone: +1 800 865 3457 • Fax: +1 800 865 3450
Email: orders@bernan.com • Web site: http://www.bernan.com

Renouf Publishing Co. Ltd.
812 Proctor Avenue, Ogdensburg, NY 13669-2205, USA
Telephone: +1 888 551 7470 • Fax: +1 888 551 7471
Email: orders@renoufbooks.com • Web site: http://www.renoufbooks.com

Orders for both priced and unpriced publications may be addressed directly to:

IAEA Publishing Section, Marketing and Sales Unit
International Atomic Energy Agency
Vienna International Centre, PO Box 100, 1400 Vienna, Austria
Telephone: +43 1 2600 22529 or 22530 • Fax: +43 1 2600 29302
Email: sales.publications@iaea.org • Web site: http://www.iaea.org/books

International Atomic Energy Agency
Vienna
ISBN 978–92–0–104916–2
ISSN 1011–4289